Advances
in Clinical and Experimental Medicine

WROCLAW
MEDICAL UNIVERSITY

Advances
in Clinical and Experimental Medicine

Advances
in Clinical and Experimental Medicine

Editorial Policy

Contents

Original and generic clopidogrel: A comparison of antiplatelet effects and active metabolite concentrations in patients without polymorphisms in the *ABCB1* gene and the allele variants CYPC19*2 and *3

Tomasz Wójcik[1,A–D], Paweł Szymkiewicz[1,A,B,D], Krzysztof Ściborski[1,A,B], Marceli Łukaszewski[2,B,C], Grzegorz Onisk[1,D], Andrzej Mysiak[1,E], Andrzej Gamian[3,C,E], Jerzy Wiśniewski[3,B], Tadeusz Dobosz[4,B,E], Arleta Lebioda[4,B], Anna Jonkisz[4,B], Marcin Protasiewicz[1,A,C–F]

[1] Department and Clinic of Cardiology, Wroclaw Medical University, Poland

[2] Department and Clinic of Anaesthesiology and Intensive Therapy, Wroclaw Medical University, Poland

[3] Department and Section of Biochemistry, Wroclaw Medical University, Poland

[4] Molecular Techniques Unit, Department of Forensic Medicine, Wroclaw Medical University, Poland

A – research concept and design; B – collection and/or assembly of data; C – data analysis and interpretation;
D – writing the article; E – critical revision of the article; F – final approval of the article

Abstract

Background. Ticagrelor and prasugrel are widely used as antiplatelet therapy after coronary angioplasty. However, there is a group of patients with indications for clopidogrel treatment. This population includes patients with chronic or acute coronary syndrome who are treated invasively and have contraindications to the use of novel antiplatelet drugs due to antithrombotic treatment (particularly with non-vitamin K antagonist oral anticoagulants). A wide range of generic forms of clopidogrel are available on the market. However, it is unclear whether they are as effective as the originator drug.

Objectives. In the current study, we aimed to assess the concentrations of the active metabolite of clopidogrel and its effect on platelet aggregation inhibition in patients receiving the originator drug in comparison with those receiving generic clopidogrel.

Materials and methods. We enrolled 22 healthy individuals without polymorphisms in the *ABCB1* gene and the allele variants *CYPC19*2* and *CYPC19*3*. All participants received a loading dose of clopidogrel (600 mg), followed by a maintenance dose of 75 mg for the next 3 days. On day 3, blood samples were obtained 1 h after drug administration to assess active metabolite concentrations using liquid chromatography with tandem mass spectrometry. In each participant, platelet aggregation was assessed with light transmission aggregometry after 5-μmol/L and 10-μmol/L adenosine diphosphate (ADP) stimulation. Assays were performed for the originator clopidogrel and 2 different generic groups.

Results. The mean ± standard deviation (SD) concentrations of active clopidogrel did not differ between the originator drug and 2 generic products with clopidogrel (12.7 ± 5 pg/μL compared to 13.0 ± 4 pg/μL compared to 14.4 ± 4 pg/μL). Platelet aggregation inhibition after stimulation with 5 μmol/L and 10 μmol/L ADP was similar for all preparations.

Conclusions. In comparison with original clopidogrel, the use of its generic form does not affect the blood concentrations of the active metabolite or its antiplatelet effect.

Key words: *ABCB1*, clopidogrel active metabolite, *CYPC19*2*, *CYPC19*3*, clopidogrel bioequivalence

Introduction

Although ticagrelor and prasugrel are increasingly widely used as antiplatelet therapy after coronary angioplasty, there is a large group of patients with indications for clopidogrel treatment. This population includes primarily symptomatic patients with chronic coronary syndrome and acute coronary syndrome (ACS), who are treated invasively, and who have contraindications to the use of novel antiplatelet drugs due to concomitant atrial fibrillation and antithrombotic treatment (particularly with non-vitamin K antagonist oral anticoagulants).[1,2] Several generic forms of clopidogrel are available on the market. However, it is unclear whether they are as effective in daily clinical practice as the originator drug. It has been shown that agreement between platelet function measurements is relatively poor in patients receiving original and generic clopidogrel bisulfate forms.[3] Thus, physicians may be cautious when routinely introducing generic clopidogrel bisulfate. On the other hand, risks of mortality, bleeding and drug discontinuation were not different between Plavix and generics.[4] The available evidence is therefore limited and does provide sufficient data on differences in efficacy or safety between branded and generic products.

Clopidogrel is a prodrug metabolized to its active form through complex biochemical processes in the liver.[5,6] Its absorption is regulated by glycoprotein P, a transport protein encoded by the *ABCB1* gene. Eight-five percent of the absorbed drug is transformed by carboxyl esterases into a major but inactive clopidogrel metabolite – a carboxylic acid derivative. Only 15% of the absorbed clopidogrel is transformed by cytochrome P450 (CYP) isoenzymes (*CYP2B6*, *CYP2C9*, *CYP2C19*, and *CYP3A4*) into a thiol metabolite, which is responsible for blocking adenosine diphosphate (ADP) binding to the platelet $P2Y_{12}$ receptor and ADP-induced platelet aggregation.

Objectives

In the current study, we aimed to assess the concentrations of clopidogrel active metabolite as well as its effect on platelet aggregation inhibition, in patients receiving the originator drug in comparison with those receiving generic clopidogrel. Active metabolite generation following clopidogrel administration is diminished by limited intestinal absorption (which may be influenced by the *ABCB1* gene polymorphism), as well as by functional variability in the activity of the CYP isoenzymes (which is influenced by single nucleotide polymorphisms (SNPs) in genes encoding the CYP isoenzymes).[7] Therefore, to exclude genetic variability that might affect drug concentration and activity, participants were assessed for the presence of the most common genetic polymorphisms that reduce the absorption (*ABCB1*) and activation (*CYPC19*2* and *CYPC19*3*) of clopidogrel.

Materials and methods

Study population

We enrolled 22 healthy, non-smoking participants, who provided written informed consent to be included in the study. The study protocol was approved by the bioethics committee of Wroclaw Medical University, Poland. None of the participants were carriers of polymorphisms in the *ABCB1* gene or the allele variants *CYPC19*2* or *CYPC19*3*. The study protocol was approved by the bioethics committee of Wroclaw Medical University, and it was also in line with the Helsinki Declaration.

Genetic studies

To identify genetic polymorphism, genetic material was extracted from 200 μL of whole-blood samples of each patient, using the High Pure PCR Template Preparation Kit (Roche Diagnostics, Warszawa, Poland). Using the ability of the DNA to bind with silica under certain conditions, the lysate was centrifuged in a mini-column containing the silica membrane, which was then rinsed twice with a washing buffer. Finally, a mini-column elution buffer was applied to the membrane to recover the purified DNA. Next, amplified polymerase chain reaction (PCR) was carried out with the use of 3 pairs of specific primers for *CYP2C19*3*, *ABCB1* (C3435C> T) and *CYP2C19*2*, as well as a Multiplex PCR Kit (Qiagen, Hilden, Germany), according to the manufacturer's instructions. A single nucleotide polymorphism of *CYP2C19*2*, *CYP2C19*3* and *ABCB1* was genotyped using a mini-sequencing technique, which is a modification of PCR. The SNaPshot Multiplex Kit (Applied Biosystems, Foster City, USA) was used for the analysis, according to the manufacturer's instructions. The mini-sequencing reaction was performed with specific primers designed to hybridize to the template, ending before the designated polymorphic site. Dideoxynucleotide triphosphates, or fluorescent-labeled terminators, were involved in the reaction. Product detection was performed with capillary electrophoresis, using a 3130 Genetic Analyzer (Applied Biosystems). The results were analyzed with the use of the GeneMapper ID v. 3.2 program (Applied Biosystems) against the internal GeneScan™ LIZ 120 standard.

Clopidogrel administration, blood collection and plasma preparation

At baseline, all participants received a loading dose of original clopidogrel (600 mg), followed by a maintenance dose of 75 mg for the next 3 days. On day 3, blood samples of 7.5 mL were drawn into collection tubes containing ethylenediaminetetraacetic potassium salt, to assess the concentrations of the drug active metabolite in patients' plasma. Samples were obtained 1 h after drug administration (C1h), taking into account the high active

metabolite concentration reported in previous pharmacokinetic studies.[7] Due to the irreversible nature of the receptor modification, subsequent clopidogrel preparations were analyzed after 1 week, which ensured a natural restoration of the platelet pool. In this crossover study, assays were performed separately for the originator drug – Plavix (Sanofi-Aventis, Paris, France) (P) and 2 different generic forms – Areplex (Adamed, Pieńków, Poland) (A) and Egitromb (Egis Pharmaceuticals, Budapest, Hungary) (E). Each subject received generic products and the reference product. All drugs contained clopidogrel bisulfate as the active substance.

Sample preparation

To stabilize the active clopidogrel metabolite, 2-bromo-3′-methoxyacetophenone (MPB) was added to the blood sample immediately after collection, in accordance with the procedure described by Takahashi et al.[8]

The MPB-derivatized clopidogrel active metabolite hydrochloride and [13C6]-clopidogrel carboxylic acid (internal standard) were purchased from Alsachim (Illkirch-Graffenstaden, France). Clopidogrel and clopidogrel carboxylic acid were obtained from the Pharmaceutical Research Institute (Warszawa, Poland). Liquid chromatography mass spectrometry (LC-MS) grade water, methanol, and acetonitrile were obtained from J.T. Baker (Deventer, the Netherlands). The formic acid (purity ≥98%), trichloroacetic acid (purity ≥99.5%) and MPB were purchased from Sigma-Aldrich (Poznań, Poland), while leucine-enkephalin was sourced from Waters (Warszawa, Poland).

Plasma concentrations of clopidogrel active metabolite hydrochloride, clopidogrel and clopidogrel carboxylic acid were quantified using stable-isotope dilution LC-MS, according to a modified method adapted from Karaźniewicz-Łada et al.[7] Briefly, a volume of 100 μL of either plasma sample or internal standard was combined with 20 μL of internal standard solution (500 pg/μL). Then, 400 μL of acetonitrile was added and vortexed for 5 min at 1100 rpm. After additional centrifugation, the supernatant was analyzed using LC with tandem MS (LC-MS/MS).

Liquid chromatography – tandem mass spectrometry

The LC-MS/MS analysis was conducted using the nano-ACQUITY UPLC system, combined with a Xevo G2 QT of mass spectrometer (Waters). The analyzed compounds were separated in the HSS C18 column with membrane inline filter (Waters). The column temperature was set at 45°C. Mobile phase A consisted of 0.1% formic acid in water, while mobile phase B consisted of 0.1% formic acid in acetonitrile with an increasing gradient. The total run time of the method was 4 min, with a flow rate of 45 μL/min.

Mass spectra for the analyzed compounds were acquired in positive ion mode electrospray ionization. Data acquisition was performed with MassLynx Software (Waters), using the characteristic precursor and product ions. A quantitative analysis was also performed using QuanLynx software (Waters). We considered a range of 80–125% as an acceptance interval criterion for the clopidogrel mean concentration ratio for each tested product. For the measurement of clopidogrel active metabolite, a previously known measurement method was used, which was subject to detailed validation.[7]

Platelet aggregation

For each participant, platelet aggregation was assessed on day 3 of treatment with each preparation. Blood samples were obtained from a venous cannula into 2 tubes containing 0.109 mol/L of trisodium citrate, and centrifuged at room temperature (800 × g for 15 min) to collect platelet-rich plasma. The sample was re-centrifuged at 2400 × g for 15 min, and platelet-poor plasma was collected. Platelet reactivity was assessed within 2 h of collection, with light transmission aggregometry as developed by Born,[9] using a single-channel Chrono Log 560CA lumi-aggregometer (Chrono-Log, Haverton, USA). A platelet-poor plasma sample with 100% light transmission was used as a reference. Next, consecutive platelet-rich plasma samples (light transmission, 0%) were placed in cuvettes and stimulated with adenosine diphosphate (ADP; 5 μmol/L and 10 μmol/L). The results were expressed as percentage of the maximum platelet aggregation (MPA) within 6 min. Calculations and platelet aggregation curves were performed using the dedicated Agro-Link software (Chrono-Log). All reagents and laboratory equipment were purchased from Biogenet (Piaseczno, Polska). They were stored and used according to the manufacturer's instructions.

Cut-off MPA values higher than 46% and 67% were used to identify the lack of response to stimulation with 5 μmol/L and 10 μmol/L ADP, respectively.

Statistical analysis

The statistical analyses were performed using the STATISTICA v. 9.0 PL program (StatSoft Inc., Tulsa, USA). The variance homogeneity of each quantitative variable was determined using Levene's test. To compare the quantitative variables between groups, a one-way analysis of variance (ANOVA) was used. All hypotheses were verified at the statistical significance level $p \leq 0.05$.

Results

Demographic and clinical features of participants are presented in Table 1. The genetic analysis revealed that none of the participants were carriers of genetic polymorphisms responsible for reduced clopidogrel absorption and metabolism.

Table 1. Study population characteristics

Parameter	Study cohort
Age [years]	32 ±6.5
Sex (F/M)	8/14
Diabetes	0
Hypertension	0
Smoking	0
Hemoglobin [g/dL]	12.3 ±1.3
White blood cells [10^3/µL]	7.3 ±0.4
Creatinine [mg/dL]	0.9 ±0.4
Creatinine clearance [mL/min]	106.7 ±11.2
Body mass [kg]	62.7 ±16.3
BMI	24.6 ±4.2

SI conversion factors: to convert creatinine to µmol/L, multiply by 88.4. F – female; M – male; BMI – body mass index. Data are presented as mean ± standard deviation (SD).

We did not find any significant differences in the C1h concentrations of active clopidogrel between different preparations, specifically 12.7 ±5 pg/µL in group P, compared to 13.0 ±4 pg/µL in group A and 14.4 ±4 pg/µL in group E. This data is presented in Fig. 1.

Mean platelet aggregation inhibition values were similar for all drugs, without any significant differences, both after stimulation with 5 µmol/L ADP and 10 µmol/L ADP. Aggregation data are shown in Table 2.
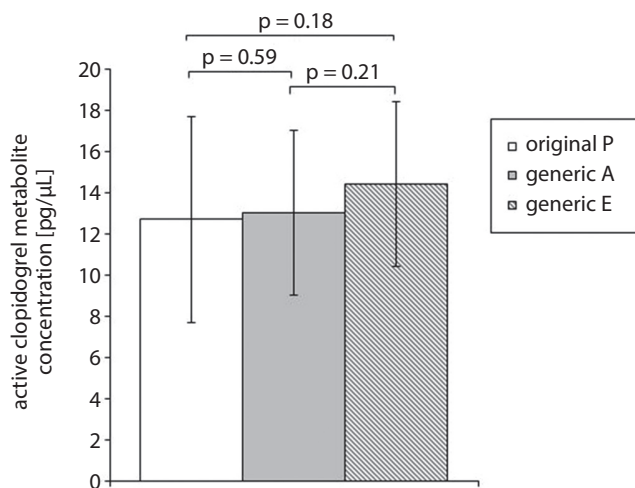
Fig. 1. Concentrations of clopidogrel active metabolite for original and generic drug

Table 2. Platelet aggregation values after ADP stimulation

Platelet aggregation	P	A	E
5-µmol/L ADP	34.5 ±9	35.0 ±7	36.6 ±8
10-µmol/L ADP	40.7 ±9	40.0 ±8	37.1 ±8

Data are presented as mean ± standard deviation (SD). ADP – adenosine diphosphate.

Discussion

Multiple lines of evidence suggest that insufficient active metabolite generation is the primary reason for variability in clopidogrel response and the lack of response where a negligible antiplatelet effect of clopidogrel is observed. High platelet reactivity to clopidogrel has been found to be associated with a significantly higher incidence of ischemic recurrence in patients undergoing percutaneous coronary intervention with stent implantation.[1,2,5] Therefore, the equal efficacy of generic drugs to that of the originator remains an important issue.

The cut-off values for defining clopidogrel non-responsiveness using aggregometry are often arbitrary.[10] The most important studies focusing on platelet activity used various concentrations of the P2Y$_{12}$ receptor inhibitor. The most common agonist in the largest studies was 5 µmol/L and 20 µmol/L ADP. In a group of 1069 patients with established chronic coronary syndrome undergoing percutaneous coronary intervention, Breet et al.[10] showed that an MPA of 42.9% or higher for 5 µmol/L ADP and of 64.5% or higher for 20 µmol/L ADP was associated with an increased risk of death, myocardial infarction, stent thrombosis, and ischemic stroke during a one-year follow-up. Gurbel et al.[11] reported a higher risk of cardiovascular events in a two-years follow-up in patients with an MPA higher than 46% and 59%, respectively. Cuisset et al.[12] revealed an elevated risk of stent thrombosis for an aggregation cut-off value higher than 67%. In 2010, Bonello et al.[13] published a consensus statement in which they proposed an ADP (5 µmol/L)-induced MPA of 46% as a cut-off value to identify high platelet reactivity. In our study, we accepted the recommended threshold of 46% for MPA induced by 5 µmol/L ADP, while for 10 µmol/L ADP, the cut-off value of more than 67% was used to identify an inadequate response to clopidogrel, as in the study by Cuisset et al.[12]

The quantitative assessment of the active form of clopidogrel in blood is a complex process, particularly due to the short half-life of the drug. High-performance liquid chromatography assays are not sensitive enough to measure clopidogrel levels in biological fluids after oral administration of therapeutic doses. The LC-MS/MS has been increasingly used because it can analyze test samples regardless of their purity in biological substances and measure drug concentrations in blood with high sensitivity and selectivity.[14,15] In our study, we used modified methods that allow for the stabilization of the active metabolite in blood.[8] The time of blood sampling, 1 h after drug administration, was chosen based on previous clopidogrel pharmacokinetic studies.[7] We decided to test each clopidogrel product after 1 week of treatment discontinuation, as it has been proven that complete recovery of platelet function can be seen 7 days after the last clopidogrel dose.[16]

We showed that the use of generic forms of clopidogrel does not significantly affect the blood concentrations of the active metabolite in healthy individuals with

the absence of the most common genetic polymorphisms (*ABCB1*, *CYPC19*2* and *CYPC19*3).* Moreover, none of our participants showed a lack of response to antiplatelet treatment, expressed as a low rate of platelet aggregation inhibition. Therefore, the original clopidogrel and the tested generic forms can be considered equivalent.

Our findings are in line with previous studies that revealed similar efficacy of the original and generic forms of clopidogrel in patients with ACS and chronic coronary syndrome.[17,18] However, other studies have reported contradictory results.[19,20] An Italian study evaluated 1579 patients with ACS and found that a significantly higher proportion of patients treated with clopidogrel base had high platelet reactivity when compared with original clopidogrel. However, it is important to note that clopidogrel base is a generic preparation that differs from original clopidogrel, which is formulated using clopidogrel bisulfate. In contrast, in our study, both generic and original clopidogrel contained the same salt.

Limitations

Our study has several limitations. First, the study group was relatively small, and we did not assess the presence of other polymorphisms and other variables that might have affected drug concentrations in blood. However, our results indicate that the generic preparations of clopidogrel bisulfate tested have similar efficacy to original clopidogrel and thus may be used in clinical practice.

Conclusions

In comparison with original clopidogrel, the use of its generic form does not affect the blood concentrations of the active metabolite or its antiplatelet effect.

ORCID iDs

Tomasz Wójcik https://orcid.org/0000-0001-9987-4872
Paweł Szymkiewicz https://orcid.org/0000-0002-8469-6871
Krzysztof Ściborski https://orcid.org/0000-0002-3922-2861
Marceli Łukaszewski https://orcid.org/0000-0002-4298-3178
Grzegorz Onisk https://orcid.org/0000-0003-4071-3163
Andrzej Mysiak https://orcid.org/0000-0002-4728-2565
Andrzej Gamian https://orcid.org/0000-0002-2206-6591
Jerzy Wiśniewski https://orcid.org/0000-0003-2831-7643
Tadeusz Dobosz https://orcid.org/0000-0003-0413-9109
Arleta Lebioda https://orcid.org/0000-0001-5802-2155
Anna Jonkisz https://orcid.org/0000-0001-6916-4212
Marcin Protasiewicz https://orcid.org/0000-0003-0253-0585

References

1. Gargiulo G, Goette A, Tijssen J, et al. Safety and efficacy outcomes of double vs. triple antithrombotic therapy in patients with atrial fibrillation following percutaneous coronary intervention: A systematic review and meta-analysis of non-vitamin K antagonist oral anticoagulant-based randomized clinical trials. *Eur Heart J.* 2019;40(46):3757–3767. doi:10.1093/eurheartj/ehz732
2. Neumann FJ, Sousa-Uva M, Ahlsson A, et al; ESC Scientific Document Group. 2018 ESC/EACTS guidelines on myocardial revascularization. *Eur Heart J.* 2019;40(2):87–165. doi:10.1093/eurheartj/ehy394
3. Jeong YH, Koh JS, Kang MK, et al. The impact of generic clopidogrel bisulfate on platelet inhibition in patients with coronary artery stents: Results of the ACCEL-GENERIC Study. *Korean J Inter Med.* 2010;25(2):154–161. doi:10.3904/kjim.2010.25.2.154
4. Caldeira D, Fernandes RM, Costa J, David C, Sampaio C, Ferreira JJ. Branded versus generic clopidogrel in cardiovascular diseases: A systematic review. *J Cardiovasc Pharmacol.* 2013;61(4):277–282. doi:10.1097/FJC.0b013e31827e5c60
5. Saiz-Rodríguez M, Belmonte C, Caniego JL, et al. Influence of CYP450 enzymes, CES1, PON1, ABCB1, and P2RY12 polymorphisms on clopidogrel response in patients subjected to a percutaneous neurointervention. *Clin Ther.* 2019;41(6):1199–1212.e2. doi:10.1016/j.clinthera.2019.04.037
6. Protasiewicz M, Szymkiewicz P, Kuliczkowski W, Mysiak A, Witkiewicz W. Modern antiplatelet therapy: Opportunities and risks. *Adv Clin Exp Med.* 2013;22(6):875–885. PMID:24431318
7. Karaźniewicz-Łada M, Danielak D, Burchardt P, et al. Clinical pharmacokinetics of clopidogrel and its metabolites in patients with cardiovascular diseases. *Clin Pharmacokinet.* 2014;53(2):155–164. doi:10.1007/s40262-013-0105-2
8. Takahashi M, Pang H, Kawabata K, Farid NA, Kurihara A. Quantitative determination of clopidogrel active metabolite in human plasma by LC-MS/MS. *J Pharm Biomed Anal.* 2008;48(4):1219–1224. doi:10.1016/j.jpba.2008.08.020
9. Born GV. Aggregation of blood platelets by adenosine diphosphate and its reversal. *Nature.* 1962;194:927–929. doi:10.1038/194927b0
10. Breet NJ, van Werkum JW, Bouman HJ, et al. Comparison of platelet function tests in predicting clinical outcome in patients undergoing coronary stent implantation. *JAMA.* 2010;303(8):754–762. doi:10.1001/jama.2010.181
11. Gurbel PA, Antonino MJ, Bliden KP, et al. Platelet reactivity to adenosine diphosphate and long-term ischemic event occurrence following percutaneous coronary intervention: A potential antiplatelet therapeutic target. *Platelets.* 2008;19(8):595–604. doi:10.1080/09537100802351065
12. Cuisset T, Frere C, Quilici J, et al. Predictive values of post-treatment adenosine diphosphate-induced aggregation and vasodilator-stimulated phosphoprotein index for stent thrombosis after acute coronary syndrome in clopidogrel-treated patients. *Am J Cardiol.* 2009;104(8):1078–1082. doi:10.1016/j.amjcard.2009.06.007
13. Bonello L, Tantry US, Marcucci R, et al; Working Group on High On-Treatment Platelet Reactivity. Consensus and future directions on the definition of high on-treatment platelet reactivity to adenosine diphosphate. *J Am Coll Cardiol.* 2010;56(12):919–933. doi:10.1016/j.jacc.2010.04.047
14. Peer CJ, Spencer SD, VanDenBerg DA, Pacanowski MA, Horenstein RB, Figg WD. A sensitive and rapid ultra HPLC-MS/MS method for the simultaneous detection of clopidogrel and its derivatized active thiol metabolite in human plasma. *J Chromatogr B Analyt Technol Biomed Life Sci.* 2012;880(1):132–139. doi:10.1016/j.jchromb.2011.11.029
15. Karaźniewicz-Łada M, Danielak D, Teżyk A, Zaba C, Tuffal G, Główka F. HPLC-MS/MS method for the simultaneous determination of clopidogrel, its carboxylic acid metabolite and derivatized isomers of thiol metabolite in clinical samples. *J Chromatogr B Analyt Technol Biomed Life Sci.* 2012;911:105–112. doi:10.1016/j.jchromb.2012.11.005
16. Weber AA, Braun M, Hohlfeld T, Schwippert B, Tschöpe D, Schrör K. Recovery of platelet function after discontinuation of clopidogrel treatment in healthy volunteers. *Br J Clin Pharmacol.* 2001;52(3):333–336. doi:10.1046/j.0306-5251.2001.01453.x
17. Ko DT, Krumholz HM, Tu JV, et al. Clinical outcomes of plavix and generic clopidogrel for patients hospitalized with an acute coronary syndrome. *Circ Cardiovasc Qual Outcomes.* 2018;11(3):11(3):e004194. doi:10.1161/CIRCOUTCOMES.117.004194
18. Hajizadeh R, Ghaffari S, Ziaee M, Shokouhi B, Separham A, Sarbakhsh P. In vitro inhibition of platelets aggregation with generic form of clopidogrel versus branded in patients with stable angina pectoris. *J Cardiovasc Thor Res.* 2017;9(4):191–195. doi:10.15171/jcvtr.2017.33
19. Marcucci R, Paniccia R, Gori AM, Gensini GF, Abbate R. Bioequivalence in the real world is a complex challenge: The case of clopidogrel. *J Am Coll Cardiol.* 2013;61(5):594–595. doi:10.1016/j.jacc.2012.10.020
20. Kovacic JC, Mehran R, Sweeny J, et al. Clustering of acute and subacute stent thrombosis related to the introduction of generic clopidogrel. *J Cardiovasc Pharmacol Ther.* 2014;19(2):201–208. doi:10.1177/1074248413510605

Clinical assessment and comparison of ACL reconstruction using synthetic graft (Neoligaments versus FiberTape)

Michał Barnaś[1,A–F], Maciej Kentel[1,A,C,E,F], Piotr Morasiewicz[2,A,E,F], Jarosław Witkowski[3,E,F], Paweł Reichert[4,A,D–F]

[1] Department of Orthopedics and Traumatology, eMKa Med Medical Centre, Wrocław, Poland

[2] Department of Orthopedic and Trauma Surgery, University Hospital in Opole, Institute of Medical Sciences, University of Opole, Poland

[3] Division of Sports Medicine, Department of Physiotherapy, Faculty of Health Sciences, Wroclaw Medical University, Poland

[4] Department of Trauma and Hand Surgery, Faculty of Medicine, Wroclaw Medical University, Poland

A – research concept and design; B – collection and/or assembly of data; C – data analysis and interpretation;
D – writing the article; E – critical revision of the article; F – final approval of the article

Abstract

Background. Due to the low potential for primary biological healing of the anterior cruciate ligament (ACL), the most popular approach is currently reconstruction using a graft. Recent research indicates that the technique of strengthening a damaged ligament with synthetic tapes (internal bracing) may be an alternative to reconstructive treatment, especially in cases of partial ACL damage.

Objectives. To compare and evaluate the possibility of using a synthetic graft (Neoligaments or FiberTape) to treat partial lesions of the ACL.

Materials and methods. This was a retrospective cohort study. Selected from a pool of 128 patients undergoing primary unilateral intra-articular ACL reconstruction due to partial lesion of the ACL, group I (Neoligaments) and group II (FiberTape) each included 30 patients. Range of motion (ROM), the Lachman test, the anterior drawer test and the pivot-shift test, the Lysholm Knee Scoring Scale, and International Knee Documentation Committee (IKDC) 2000 scale were used for assessment. Follow-up was carried out after 2 years.

Results. The knee joint regained anterior stability in both the subjective and objective assessments in all patients in both groups. The subjective results were respectively: in group I, 97.2 ±3.2 points on the Lysholm scale and 93.9 ±6.1 points on the IKDC 2000 scale; in group II, 96.1 ±4.9 points on the Lysholm scale and 93.2 ±6.8 points on the IKDC 2000 scale. Group comparison of the results of the IKDC 2000 scale, Lysholm Scale and ROM obtained postoperatively showed no statistically significant differences between groups.

Conclusions. Reconstruction of partial ACL lesions using a synthetic graft allows regained stability of the knee joint. The results of subjective assessment are comparable with the functional assessment results. The comparison between Neoligaments and FiberTape shows the same functional and objective results, although FiberTape is preferable from an economical perspective.

Key words: reconstruction, athletes, anterior cruciate ligament, primary repair, internal bracing

Background

An anterior cruciate ligament (ACL) tear is among the most frequent consequences of knee sprain, with a prevalence of approx. 1/3000.[1] In the USA, there are about 200,000 new cases annually.[2] An ACL tear is most frequently experienced by professional athletes. The athletes who practice sports such as skiing, football and basketball are at particularly high risk.[3] In a modern society, where physical culture is promoted, and, given the trend of regular involvement in physical activity as well as the increasing popularity of extreme sports, the number of patients presenting with ACL injuries is constantly growing.[4]

Untreated ACL tears result in a disturbed biomechanical balance of the knee joint, which leads to knee instability, increased susceptibility to future knee joint injuries and impairment of motion dynamics in the affected lower limb.[5] This translates directly into deterioration of athletic performance or, in certain sport disciplines, makes training impractical and even impossible.[6] More distant consequences include damaging other inner structures of the knee, namely the menisci and the articular cartilage, predisposing the development of arthritis. Given today's overarching trend of a healthy lifestyle and widespread efforts to maintain physical fitness, most patients wish to return to their routine training or hobbies and most often decide to undergo surgery shortly after learning about their diagnosis.[7]

Due to the low potential for primary biological ACL healing, reconstruction using a graft is now the most popular approach.[8–10] The latest studies show that, apart from reconstruction, especially in cases of partial damage, there is another alternative form of ACL tear treatment, namely, stabilization of the torn ligament with a synthetic graft, either polyethylene terephthalate tapes (Neoligaments, Leeds, UK) or FiberTape® (Arthrex, Warszawa, USA), which is referred to as internal bracing.[11–18]

The advantages of the internal bracing technique are reduced morbidity rate at the harvest site, a more rapid rehabilitation and postoperative recovery, lower incidence of postoperative arthrofibrosis, and lower level of postoperative pain.[19–21]

The parallel fibers provide a high degree of strength. The mesh is made of pure polyethylene terephthalate (PET), without any additions. It consists of repeating units of the monomer ethylene terephthalate ($C_{10}H_8O_4$). In this approach, the reinsertion procedure involves stabilization of the undamaged ACL structures, fixing the tape along the ligament. The tape strengthens the ligament and protects it against further tears.[22]

Objectives

The goal of the study was to assess, evaluate and compare the viability and opportunities for application of FiberTape compared to Neoligaments in partial ACL tears.

Materials and methods

This was a retrospective cohort study. The sample was made up of patients who had undergone primary ACL reconstruction, carried out at the Trauma and Orthopedics Department of eMKa Med Hospital in Wrocław, Poland. Out of 128 male patients admitted in 2015–2017 due to a partial lesion of the ACL involving anteromedial bundle damage, and undergoing primary unilateral intra-articular ACL reconstruction using restrictive inclusion and exclusion criteria, 60 patients qualified for the study. Group I consisted of 30 patients treated with Neoligaments, including 26 men and 4 women, aged 27.1 ±4.5 years. Group II involved 30 patients, including 26 men and 4 women, aged 31.3 ±11.8 years, treated with FiberTape.

The study was carried out according to the principles of the Helsinki Declaration, and approved by the Bioethics Committee of Wroclaw Medical University. Each participant was informed about the aim of the study and the applied approach, and each signed their informed consent for participation in the study. An additional goal of the assessment was to present the patient with the technique to be applied.

The ACL capacity was assessed using the 3 tests that are most often applied in clinical practice. The orthopedic assessment concerned the range of motion (ROM) in the knee joint and included the Lachman test, anterior drawer test and pivot-shift test. The assessment was combined with subjective evaluation based on the 2000 International Knee Documentation Committee (IKDC 2000) and Lysholm scales. Ultrasound and magnetic resonance imaging (MRI) were utilized for all patients who sustained knee joint injuries. The period of observation lasted 2 years. The first evaluated limb was a non-traumatic limb, to assess its range of motion and stability, and to familiarize the patient with the examination technique.

Postoperative controls took place on days 7, 14 and 28 after surgery. The examination was made 6, 12 and 24 months after surgery. Stitches were removed during the control procedure. Stress relief and use of the orthosis were recommended for a period of 3 weeks, increasing the range of flexion in the orthosis in a 30–60–90° schedule every 7 days. The ROM of the knee was measured bilaterally using a standard goniometer.[23] Anterior knee stability was evaluated manually using the Lachman test and anterior drawer test, according to the ligament examination section of the IKDC 2000 Knee Examination Form. The inter-limb difference in anterior tibial dislocation obtained from the Lachman test and anterior drawer test was rated as normal (0; 0–2 mm), nearly normal (1+; 3–5 mm), abnormal (2+; 6–10 mm), or severely abnormal (3+; >10 mm).[23] Anterolateral rotational knee stability was assessed manually with the pivot-shift test. The pivot-shift was considered negative when, according to the ligament examination section of the 2000 IKDC

Knee Examination Form, the anterolateral rotational dislocation of the tibia relative to the femur was equal in both lower limbs and positive when the difference between the limbs was rated as + (glide),++ (clunk) or +++ (gross).

Surgical technique

All the patients were operated on by the same team, using the same surgical technique and Neoligaments (Neoligaments) (Fig. 1) or FiberTape (Biomet) (Fig. 2) graft. It was fixed using Endobutton (Smith-Nephew, Watford, UK) on the femur and the interference screw, ComposiTCP30 (Biomet), on the tibia. It was prepared using the "outside-in" technique with the aimer device (Fig. 3–8).

Postoperative management

Each patient stayed in hospital for 24 h. After the removal of drains and changing dressings, the patient was verticalized under the control of rehabilitation. Next, the patient

moved using crutches and orthosis, allowing movement within the 0–30° range. How to perform isometric exercises correctly was demonstrated to the patient. Anti-clotting prophylaxis and oral antibiotic treatment were
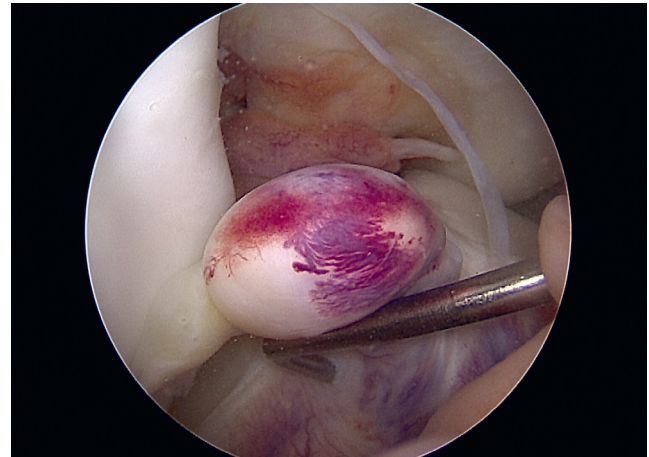
Fig. 3. Arthroscopic image. Right knee joint. View of partial rupture of the proximal stump of the anterior cruciate ligament
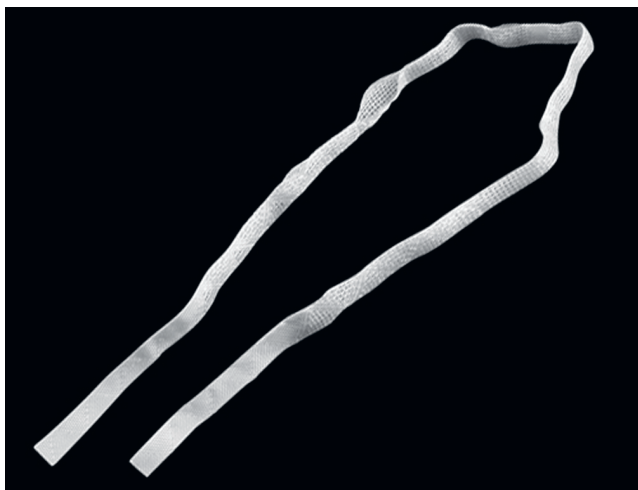
Fig. 1. Neoligaments
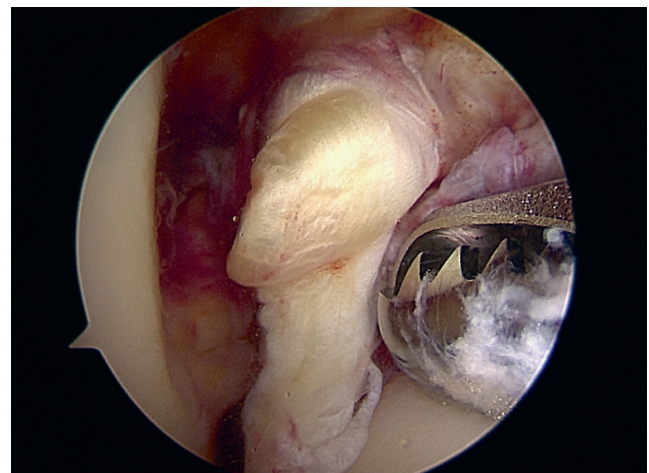
Fig. 4. Arthroscopic image. Right knee joint. View of the Endobutton and loop pull Neoligaments into the femoral canal
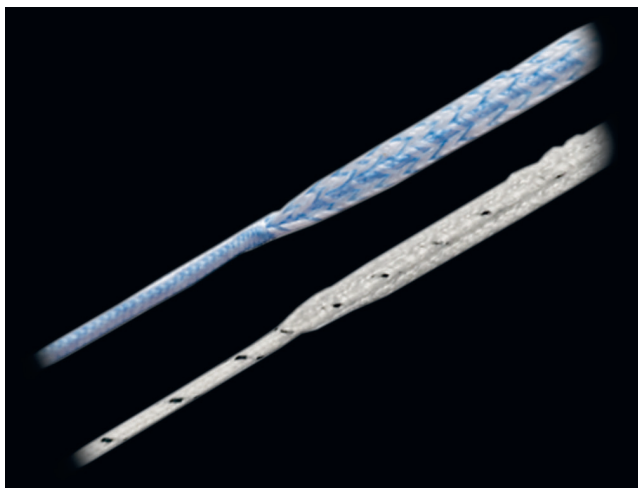
Fig. 2. FiberTape
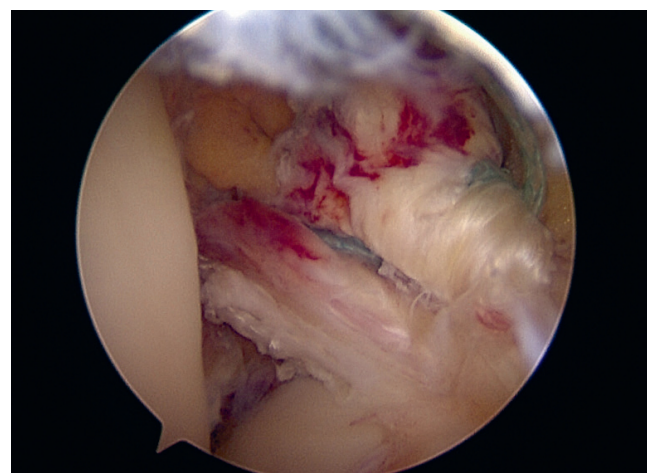
Fig. 5. Arthroscopic image. Right knee joint. View of fixed Neoligaments
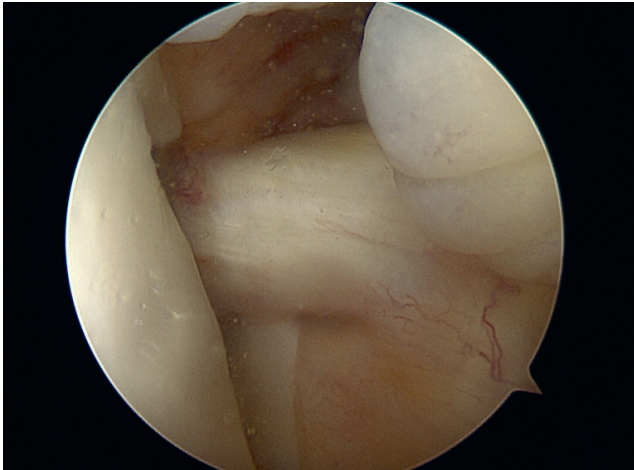
Fig. 6. Arthroscopic image. Right knee joint. View of partial rupture of the proximal stump of the anterior cruciate ligament
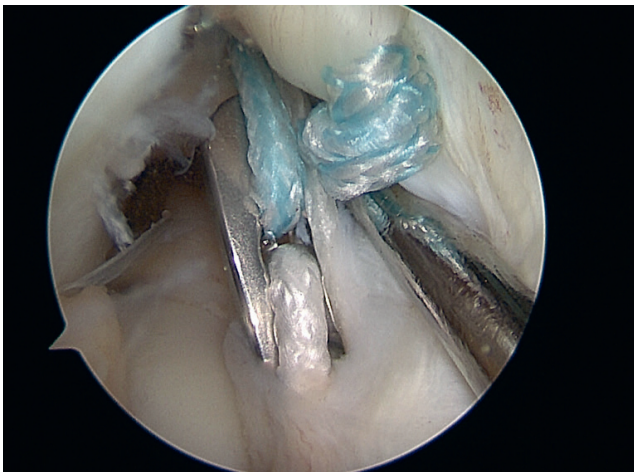
Fig. 7. Arthroscopic image. Right knee joint. View of FiberTape

Fig. 8. Arthroscopic image. Right knee joint. View of fixed FiberTape

applied. Weight release with crutches and orthosis were recommended within 3 weeks, as well as a gradual increase of flexion range in the orthosis, according to the 30°–60°–90° pattern every 7 days.

Statistical analyses

Statistical analyses were carried out using TIBCO Statistica™ (TIBCO Software Inc., Palo Alto, USA) and Microsoft Office Excel 365 Personal (Microsoft Corporation, Redmond, USA). As for characteristics of the studied sample and the analysis of the knee "giving way", as it is so-called, and the results of the Lachman test, anterior drawer test and pivot-shift test, the number of patients (n) who obtained a given result in each group was determined.

The arithmetic mean (x) and standard deviation (SD) were calculated for the following parameters: active extension and flexion range in both the operated and the uninvolved leg [°] and the total scores obtained from the Lysholm scale (n points) and IKDC 2000 questionnaire. Shapiro–Wilk tests were carried out to determine the normality of distribution for the studied parameters. Statistical significance was set at $p < 0.05$.

Choosing the type of transplant for each patient

After qualifying each patient for surgical treatment on the basis of the above diagnostics, and following their acceptance of this method of treatment, the choice of graft was discussed with the patient. The final decision as to the choice of the graft, after the operating physician presented the available options along with their pros and cons, was made by the patient.

Results

In group I, patients underwent primary unilateral internal bracing of ACL of the knee using Neoligaments. In group II, patients underwent primary unilateral internal bracing of ACL of the knee with FiberTape.

Clinical evaluation results

The results of the knee giving way, Lachman test, anterior drawer test, and pivot shift test are shown in Fig. 9 and Fig. 10 for both groups. Statistically significant results were found in all tests comparing preoperative examination
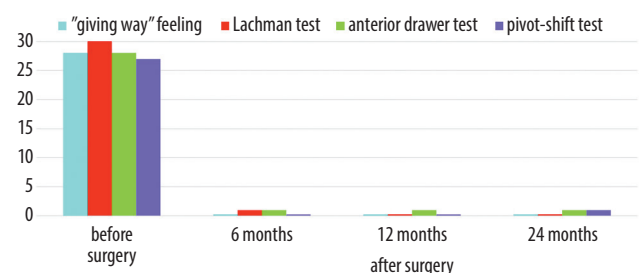
Fig. 9. Analysis of the results of so-called feelings of "giving way", Lachman test, anterior drawer test, and pivot-shift test in group I (Neoligaments) before surgery, and at 3, 6 and 24 months after surgery, respectively
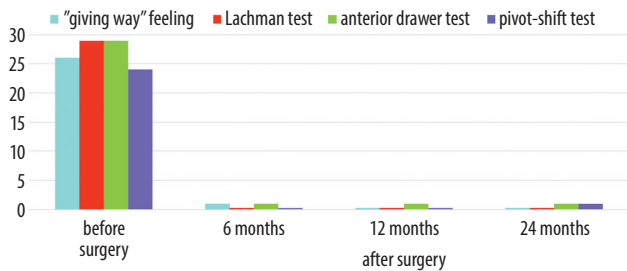
Fig. 10. Analysis of the results of so-called feelings of "giving way", Lachman test, anterior drawer test, and pivot-shift in group II (FiberTape) before surgery and at 3, 6 and 24 months after surgery, respectively

with examinations after 6, 12 and 24 months after surgery. No statistically significant differences were found when comparing results between groups 6, 12 and 24 months after reconstruction, and between groups over identical study periods. The statistical results were similar when comparing the range of motion between the operated and non-operated limb.

For group 1, the ROM of active knee extension before ACL reconstruction was statistically significantly lower (p ≤ 0.001) in the operated limb (x = 9.78 ±2.00°) when compared to the non-operated limb (x = 0.00 ±0.00°). Active starting extension range values for the operated limb in group I differed statistically significantly from measurements carried out subsequently (p ≤ 0.001; Table 1).

In group I, prior to surgery, the ROM of the active knee flexion in the operated limb (x = 111.32 ±8.32°) was significantly lower (p ≤ 0.001) than that in the non-operated limb (x = 129.19 ±5.81°), as well as at 6 months (p ≤ 0.001) and 12 months (p ≤ 0.001) following reconstruction. The ROM in the 24th month after reconstruction was lower than in the non-operated limb, but not significantly (p = 0.061),

and such a miniscule difference in obtained values should not be of clinical significance (Table 1).

For group II, prior to undergoing ACL reconstruction, ROM active extension in the operated limb (x = 4.07 ±2.08°) was statistically significantly lower (p ≤ 0.001) than in the non-operated limb (x = 0.00 ±0.00°). At 6, 12 and 24 months after surgery, the ROM of the operated limp was comparable to that of the non-operated limb (Table 1).

Prior to ACL reconstruction in group II, the ROM of active flexion in the operated limb (x = 111.33 ±10.82°) was also statistically significantly lower (p ≤ 0.001) than in the non-operated limb (x = 129.19 ±5.81°), and this remained the case at 6 and 12 months after the operation (Table 1).

The range of active extension movement in the operated limb in group I was significantly increased at 6 months after the reconstruction of the ACL, compared to the result obtained prior to the surgery (p ≤ 0.001). There was no significant change in the range of extension movement between 6 and 12 months after surgery, or between the results 12 and 24 months after surgery (Table 1).

The ROM active flexion in the operated limb in group I was significantly increased at 6 months after the reconstruction compared to the results obtained prior to surgery (p ≤ 0.001), and between 6 and 12 months after the reconstruction (p = 0.012). There was a slight decrease between 12 and 24 months, which was not a significant difference (Table 1).

The ROM of active extension in the operated limb in group II was significantly larger within 6 months following the ACL reconstruction in comparison to pre-reconstruction values. There were no significant changes in the operated limb values from 6 months to 24 months after surgery (Table 1).

Table 1. Comparative analysis values of the measurement of the active flexion and extension in the operated and non-operated limb in group I (Neoligaments) and group II (FiberTape) before reconstruction of the ACL, and at 6, 12 and 24 months after surgery

Variable	Group I			Group II		
	operated limb	non-operated limb	p-value	operated limb	non-operated limb	p-value
Extension [°]						
Before surgery	9.78 ±2.00	0.00 ±0.00	0.001	4.07 ±2.08	0.00 ±0.00	≤0.001
6 months after surgery	0.52 ±1.15	0.00 ±0.00	0.072	0.48 ±1.20	0.00 ±0.00	0.098
12 months after surgery	0.00 ±0.00	0.00 ±0.00	1.000	0.00 ±0.00	0.00 ±0.00	1.000
24 months after surgery	0.00 ±0.00	0.00 ±0.00	1.000	0.00 ±0.00	0.00 ±0.00	1.000
p-value	≤0.001	1.000	–	≤0.001	1.000	–
Flexion [°]						
Before surgery	111.32 ±8.32	129.19 ±5.81	≤0.001	111.33 ±10.82	129.19 ±5.81	≤0.001
6 months after surgery	121.94 ±10.46	129.19 ±5.81	≤0.001	114.50 ±16.10	129.19 ±5.81	≤0.001
12 months after surgery	123.55 ±5.80	129.19 ±5.81	≤0.001	124.00 ±7.36	129.19 ±5.81	≤0.001
24 months after surgery	126.23 ±2.75	129.19 ±5.81	0.061	127.61 ±6.16	129.19 ±5.81	0.119
p-value	≤0.001	1.000	–	≤0.001	1.000	–

Values expressed as the arithmetic mean and ± standard deviation (SD).

Comparison of the ROM of flexion in the operated limb in group II demonstrated a drastic, significant change in measurements (p ≤ 0.001) (Table 1).

Functional assessment results

Within 24 months of the reconstruction of the ACL, the average number of points obtained on the Lysholm group I scale was 95.70 ±4.25 points. In group II, patients obtained an average of 95.5 ±4.18 points over the same period since surgery (Fig. 11). A comparative analysis of the results of the functional assessment based on the Lysholm scale did not show statistically significant differences between the examined groups (p = 0.94).

Within 24 months of the reconstruction of the ACL, the average total number of points on the IKDC 2000 scale obtained in group I was 94.79 ±6.54 points. In group II, patients obtained an average of 94.81 ±5.63 points over the same period since surgery (Fig. 12). A comparative analysis of the results of the functional assessment did not show a statistically significant difference between the examined groups (p = 0.98).
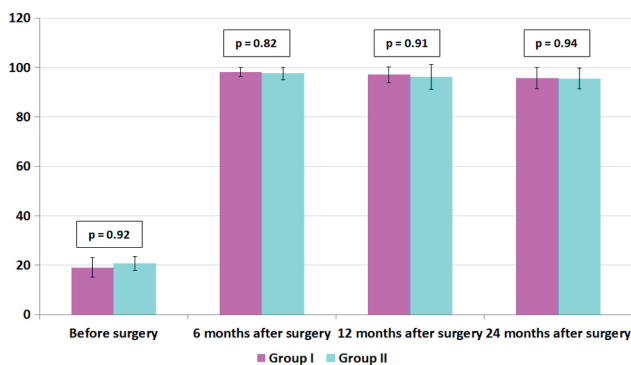
Fig. 11. Comparative analysis of the total number of points on the Lysholm scale obtained in group I (Neoligaments) and group II (FiberTape)
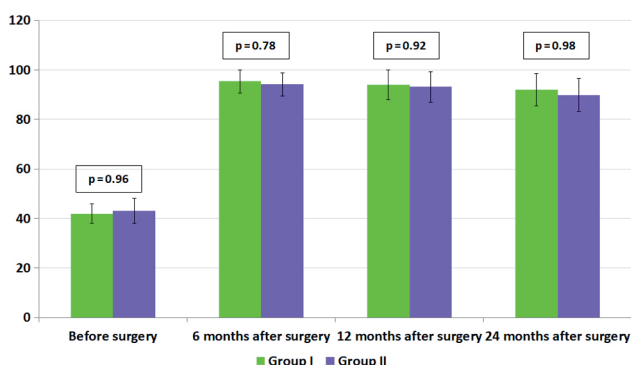
Fig. 12. Comparative analysis of the total number of points on the IKDC 2000 scale obtained in group I (Neoligaments) and group II (FiberTape)

Discussion

Numerous reports on ACL reconstruction draw different conclusions on the optimum term of surgical treatment, selection of graft and graft fixation approach, the way of preparing bone canals, or the choice of postoperative rehabilitation approach.[1,12,20,24] There are numerous advantages of using internal bracing techniques, and these are essential not only from the patient's perspective, but also from the perspective of a surgeon.[25] Firstly, the period of rehabilitation is truncated, and it is possible to increase the range of motion in the operated knee joint at an early stage.[20] It allows the maintenance of natural biomechanics and deep sensibility (contrary to reconstruction techniques with no correctly functioning proprioceptors in the autograft).[26] The pain experienced is not so intense, and there are fewer undesirable symptoms in comparison with the augmentation approach.

Our analysis of stability assessment in the knee joint using Lachman, anterior drawer and pivot-shift tests showed proper stability of the operated knee joint, much like in other reported studies.[27,28] No difference was found between the 12- and 24-month assessment results under the above-mentioned clinical conditions. The results of a subjective assessment carried out at 12 and 24 months after stabilizing the ACL using FiberTape were comparable to the results of the primary ACL reconstruction, as reported by other authors,[29] based on the Lysholm and IKDC 2000 scales.

Similarly, good subjective postoperative results after primary ACL reconstruction, using both allografts and autografts, are presented by other authors.[30,31] Some authors report better results based on the Lysholm and IKDC 2000 scales in patients operated on using internal bracing. Many authors emphasize that time is one of the most important factors contributing to patients' return to full physical fitness and ability where training continuation is concerned.[32]

Surgery is the initial phase of treatment and most convalescence time is dedicated to rehabilitation. However, it is the surgical technique which determines the duration and course of rehabilitation. As for the internal bracing technique, the authors emphasize the opportunity of a quick recovery.[33]

The promising results achieved show how the next generation of treatments will be utilized. In ligament diseases and discontinuity, a material is required that acts as a three-dimensional scaffold. Polytape is made of woven multifilament high-tenacity polyester fiber. The open-weave structure acts as a matrix and leaves space for tissue ingrowth. The parallel fibers provide a high degree of strength. The mesh is made of pure polyethylene terephthalate (PET), without any additions. Its physical properties are as follows: tensile strength 55–75 MPa; elastic limit 50–150%; glass transition temperature 67–81°C, with a softening point of 265°C. It is lightweight, strong and impact-resistant, as well as hygroscopic (absorbing water from its surroundings). Years of experience with similar polymers provide reproducible results. The infection rate is very low and recurrence is rare. Hypersensitivity to implant materials occurs infrequently. For these reasons, the use of the tape in tendon and muscle injury seems to be

safe. There is no data suggesting heterotopic ossification or muscle fibrosis.[22]

The use of polytape in ACL ligament ruptures is also promising. The technique is similar to what has been described above, similarly reproducible and not difficult. In the future, polytape may be applied in the reconstruction of other tendons, i.e., in the biceps brachii tendon or the Achilles tendon.

A final, very important issue is the full cost of this implant. As is apparent, the implant is more expensive than autograft. However, if both tapes are compared, there is a monumental difference between Neoligaments and FiberTape (depending on the country). As similar results are obtained in both cases, we recommend FiberTape as a cheaper, yet equivalent method to Neoligaments. Following promising clinical results, the use of polytapes in ligament surgery is very likely to gain popularity. The main limitation of most studies, however, is that there is only short-term follow-up of recovery. In the future, studies involving long-term follow up with patients that have undergone fully supervised physiotherapeutic procedures, and a comprehensive clinical and functional evaluation should be considered.

At present, there are a multitude of studies being conducted that focus on emphasizing genetic predisposition to cruciate ligament injuries. The ACL "suture" techniques need additional testing and studies, and require a greater amount of scientific material. Research on the application of stem cells, scaffolds, plasma rich in platelets, and xenografts are also breaking into new territory.[34,35] These present trends in the constant progression and evolution of ACL surgery will lead to a far more individualized method of operation and treatment.

Limitations

The main limitation of this study is the short-term follow-up. In the future, studies involving long-term follow-up with patients that have undergone anterior cruciate ligament reconstruction procedures and a comprehensive clinical and functional evaluation need to be taken into account. Additionally, the results should be referred to the control group, consisting of the patients after anterior cruciate ligament reconstruction using autogenous grafts.

Conclusions

Stabilizing the ACL using a synthetic graft with only partial damage enables the restoration of stability to the knee joint. The results of subjective assessment do not differentiate far from the functional assessment results. Comparing Neoligaments and FiberTape treatment shows the same functional and objective results; however, FiberTape is preferable from a price point of view.

ORCID iDs

Michał Barnaś ⬤ https://orcid.org/0000-0003-2148-844X
Maciej Kentel ⬤ https://orcid.org/0000-0002-7610-5410
Piotr Morasiewicz ⬤ https://orcid.org/0000-0002-7587-666X
Jarosław Witkowski ⬤ https://orcid.org/0000-0002-2754-1339
Paweł Reichert ⬤ https://orcid.org/0000-0002-0271-4950

References

1. Mall NA, Chalmers PN, Moric M, et al. Incidence and trends of anterior cruciate ligament reconstruction in the United States. *Am J Sports Med*. 2014;42(10):2363–2370. doi:10.1177/0363546514542796
2. Prodromos CC, Han Y, Rogowski J, Joyce B, Shi K. A meta-analysis of the incidence of anterior cruciate ligament tears as a function of gender, sport, and a knee injury-reduction regimen. *Arthroscopy*. 2007;23(12):1320–1325.e6. doi:10.1016/j.arthro.2007.07.003
3. Samuelsson K, Andersson D, Ahldén M, Fu FH, Musahl V, Karlsson J. Trends in surgeon preferences on anterior cruciate ligament reconstructive techniques. *Clin Sports Med*. 2013;32(1):111–126. doi:10.1016/j.csm.2012.08.011
4. Gobbi A, Francisco R. Factors affecting return to sports after anterior cruciate ligament reconstruction with patellar tendon and hamstring graft: A prospective clinical investigation. *Knee Surg Sports Traumatol Arthrosc*. 2006;14(10):1021–1028. doi:10.1007/s00167-006-0050-9
5. Czamara A, Królikowska A, Szuba Ł, Widuchowski W, Kentel M. Single- vs. double-bundle anterior cruciate ligament reconstruction: A new aspect of knee assessment during activities involving dynamic knee rotation. *J Strength Cond Res*. 2015;29(2):489–499. doi:10.1519/JSC.0000000000000638
6. Królikowska A, Sikorski Ł, Czamara A, Reichert P. Effects of postoperative physiotherapy supervision duration on clinical outcome, speed, and agility in males 8 months after anterior cruciate ligament reconstruction. *Med Sci Monit*. 2018;24:6823–6831. doi:10.12659/MSM.912162
7. Brophy RH, Schmitz L, Wright RW, et al. Return to play and future ACL injury risk after ACL reconstruction in soccer athletes from the Multicenter Orthopaedic Outcomes Network (MOON) group. *Am J Sports Med*. 2012;40(11):2517–2522. doi:10.1177/0363546512459476
8. Zeng C, Gao SG, Li H, et al. Autograft versus allograft in anterior cruciate ligament reconstruction: A meta-analysis of randomized controlled trials and systematic review of overlapping systematic reviews. *Arthroscopy*. 2016;32(1):153–163.e18. doi:10.1016/j.arthro.2015.07.027
9. Chen H, Chen B, Tie K, Fu Z, Chen L. Single-bundle versus double-bundle autologous anterior cruciate ligament reconstruction: A meta-analysis of randomized controlled trials at 5-year minimum follow-up. *J Orthop Surg Res*. 2018;13(1):50. doi:10.1186/s13018-018-0753-x
10. Murray MM. Current status and potential of primary ACL repair. *Clin Sports Med*. 2009;28(1):51–61. doi:10.1016/j.csm.2008.08.005
11. Jonkergouw A, van der List JP, DiFelice GS. Arthroscopic primary repair of proximal anterior cruciate ligament tears: Outcomes of the first 56 consecutive patients and the role of additional internal bracing. *Knee Surg Sports Traumatol Arthrosc*. 2019;27(1):21–28. doi:10.1007/s00167-018-5338-z
12. van Eck CF, Limpisvasti O, ElAttrache NS. Is there a role for internal bracing and repair of the anterior cruciate ligament? A systematic literature review. *Am J Sports Med*. 2018;46(9):2291–2298. doi:10.1177/0363546517717956
13. Bachmaier S, DiFelice GS, Sonnery-Cottet B, et al. Treatment of acute proximal anterior cruciate ligament tears-part 1: Gap formation and stabilization potential of repair techniques. *Orthop J Sports Med*. 2020;8(1):2325967119897421. doi:10.1177/2325967119897421
14. Bachmaier S, Smith PA, Bley J, Wijdicks CA. Independent suture tape reinforcement of small and standard diameter grafts for anterior cruciate ligament reconstruction: A biomechanical full construct model. *Arthroscopy*. 2018;34(2):490–499. doi:10.1016/j.arthro.2017.10.037
15. Heusdens CHW, Hopper GP, Dossche L, Roelant E, Mackay GM. Anterior cruciate ligament repair with independent suture tape reinforcement: A case series with 2-year follow-up. *Knee Surg Sports Traumatol Arthrosc*. 2019;27(1):60–67. doi:10.1007/s00167-018-5239-1
16. Kohl S, Evangelopoulos DS, Ahmad SS, et al. A novel technique, dynamic intraligamentary stabilization creates optimal conditions for primary ACL healing: A preliminary biomechanical study. *Knee*. 2014;21(2):477–480. doi:10.1016/j.knee.2013.11.003

17. Smith PA, Bozynski CC, Kuroki K, Henrich SM, Wijdicks CA, Cook JL. Intra-articular biocompatibility of multistranded, long-chain polyethylene suture tape in a canine ACL model. *J Knee Surg*. 2019;32(6): 525–531. doi:10.1055/s-0038-1655765

18. Gobbi A, Herman K, Grabowski R, Szwedowski D. Primary anterior cruciate ligament repair with hyaluronic scaffold and autogenous bone marrow aspirate augmentation in adolescents with open physes. *Arthrosc Tech*. 2019;8(12):e1561–e1568. doi:10.1016/j.eats.2019.08.016

19. Czamara A, Markowska I, Królikowska A, Szopa A, Domagalska-Szopa M. Kinematics of rotation in joints of the lower limbs and pelvis during gait: Early results-SB ACLR approach versus DB ACLR approach. *Biomed Res Int*. 2015;2015:707168. doi:10.1155/2015/707168

20. Królikowska A, Czamara A, Szuba L, et al. The effect of longer versus shorter duration of supervised physiotherapy after ACL reconstruction on the vertical jump landing limb symmetry. *Biomed Res Int*. 2018:7519467. doi: 10.1155/2018/7519467

21. Królikowska A, Sikorski Ł, Czamara A, Reichert P. Are the knee extensor and flexor muscles isokinetic parameters affected by the duration of postoperative physiotherapy supervision in patients eight months after ACL reconstruction with the use of semitendinosus and gracilis tendons autograft? *Acta Bioeng Biomech*. 2018;20(4):89–100. PMID:30520446

22. Navarro M, Michiardi A, Castaño O, Planell JA. Biomaterials in orthopaedics. *J R Soc Interface*. 2008;5(27):1137–1158. doi:10.1098/rsif.2008.0151

23. Wilson WT, Hopper GP, Byrne PA, MacKay GM. Anterior cruciate ligament repair with internal brace ligament augmentation. *Surg Technol Int*. 2016;29:273–278. PMID:27728954

24. Królikowska A, Reichert P, Czamara A, Krzemińska K. Peak torque angle of anterior cruciate ligament-reconstructed knee flexor muscles in patients with semitendinosus and gracilis autograft is shifted towards extension regardless of the postoperative duration of supervised physiotherapy. *PLoS One*. 2019;14(2):e0211825. doi:10.1371/journal.pone.0211825

25. DiFelice GS, van der List JP. Clinical outcomes of arthroscopic primary repair of proximal anterior cruciate ligament tears are maintained at mid-term follow-up. *Arthroscopy*. 2018;34(4):1085–1093. doi:10.1016/j.arthro.2017.10.028

26. Fleming BC, Carey JL, Spindler KP, Murray MM. Can suture repair of ACL transection restore normal anteroposterior laxity of the knee? An ex vivo study. *J Orthop Res*. 2008;26(11):1500–1505. doi:10.1002/jor.20690

27. van der List JP, DiFelice GS. Primary repair of the anterior cruciate ligament: A paradigm shift. *Surgeon*. 2017;15(3):161–168. doi:10.1016/j.surge.2016.09.006

28. Kandhari V, Vieira TD, Ouanezar H, et al. Clinical outcomes of arthroscopic primary anterior cruciate ligament repair: A systematic review from the Scientific Anterior Cruciate Ligament Network International Study Group. *Arthroscopy*. 2020;36(2):594–612. doi:10.1016/j.arthro.2019.09.021

29. Gobbi A, Whyte GP. Long-term outcomes of primary repair of the anterior cruciate ligament combined with biologic healing augmentation to treat incomplete tears. *Am J Sports Med*. 2018;46(14):3368–3377. doi:10.1177/0363546518805740

30. Hennings J. Primary anatomical repair of proximal acl ruptures with suture anchors: 1-year follow-up. *Orthop J Sports Med*. 2018;6(4 Suppl 2): 2325967118S00023. doi:10.1177/2325967118S00023

31. Kohl S, Evangelopoulos DS, Schär MO, Bieri K, Müller T, Ahmad SS. Dynamic intraligamentary stabilisation: Initial experience with treatment of acute ACL ruptures. *Bone Joint J*. 2016;98-B(6):793–798. doi:10.1302/0301-620X.98B6.35040

32. Murray MM, Kalish LA, Fleming BC, et al. Bridge-enhanced anterior cruciate ligament repair: Two-year results of a first-in-human study. *Orthop J Sports Med*. 2019;7(3):2325967118824356. doi:10.1177/2325967118824356

33. Murray MM, Magarian E, Zurakowski D, Fleming BC. Bone-to-bone fixation enhances functional healing of the porcine anterior cruciate ligament using a collagen-platelet composite. *Arthroscopy*. 2010;26 (9 Suppl):S49–S57. doi:10.1016/j.arthro.2009.12.017

34. Cieslik-Bielecka A, Reichert P, Skowronski R, et al. A new aspect of in vitro antimicrobial leukocyte- and platelet-rich plasma activity based on flow cytometry assessment. *Platelets*. 2019;30(6):728-736. doi:10.1080/09537104.2018.1513472

35. Gobbi A, Bathan L, Boldrini L. Primary repair combined with bone marrow stimulation in acute anterior cruciate ligament lesions: Results in a group of athletes. *Am J Sports Med*. 2009;37(3):571–578. doi:10.1177/0363546508327141

NF-κB1 -94del/del ATTG polymorphic variant maintains CLL at an early, mildest stage

Iwona Urbanowicz[1,A,B,D,F], Dariusz Wołowiec[2,A,E], Barbara Wysoczańska[3,B,C], Piotr Łacina[3,C], Anna Jonkisz[4,B,C], Wiesława Nahaczewska[1,B], Andrzej Tukiendorf[5,C], Iwona Bil-Lula[1,D,E], Katarzyna Bogunia-Kubik[3,E,F], Edyta Pawlak[6,C,D,F]

[1] Department of Clinical Chemistry, Department of Hematology, Wroclaw Medical University, Poland

[2] Department and Clinic of Hematology, Blood Neoplasms and Bone Marrow Transplantation, Wroclaw Medical University, Poland

[3] Laboratory of Clinical Immunogenetics and Pharmacogenetics, Hirszfeld Institute of Immunology and Experimental Therapy, The Polish Academy of Sciences, Wrocław, Poland

[4] Molecular Techniques Unit, Department of Forensic Medicine, Wroclaw Medical University, Poland

[5] Department of Social Medicine, Wroclaw Medical University, Poland

[6] Laboratory of Immunopathology, Department of Experimental Therapy, Hirszfeld Institute of Immunology and Experimental Therapy, Polish Academy of Sciences, Wrocław, Poland

A – research concept and design; B – collection and/or assembly of data; C – data analysis and interpretation;
D – writing the article; E – critical revision of the article; F – final approval of the article

Abstract

Background. NF-κB is an essential player in cancer biology, especially in tumor development, due to its constitutive activation, and because a four-base deletion (ATTG) in the *NF-κB1* promoter region at site -94, alters mRNA stability and regulates translation efficiency. This polymorphism is a good candidate risk marker and modulator of clinical course in chronic lymphocytic leukemia (CLL). As the effect of this *NF-κB1* gene polymorphism has not been studied in patients with CLL so far, the present study was undertaken to find out whether the *NF-κB1* promoter -94 ins/del ATTG polymorphism might be an essential genetic risk factor and/or modulatory disease player associated with CLL.

Objectives. The *NF-κB1* -94 ins/del ATTG (rs28362491) polymorphism was investigated as a potential CLL susceptibility and progression factor, along with demonstration of potential modulation of the stage of clinical disease based on Rai classification.

Materials and methods. The associations of *NF-κB1* -94 ins/del ATTG polymorphism with CLL and its clinical manifestation in 282 Polish individuals, including 156 CLL patients, were analyzed using polymerase chain reaction (PCR) with primers including a labeled forward primer, followed by capillary electrophoresis.

Results. A higher occurrence of the del/del homozygosity was observed among patients when compared to controls, resulting in an increase in CLL risk of more than twofold in patients carrying this homozygous genotype (OR = 2.23, p = 0.02, 95% CI = 1.14–4.37). Moreover, the del/del-positive patients more frequently presented the less aggressive disease phenotype (Rai 0), suggesting a low probability of progression to more advanced disease.

Conclusions. The *NF-κB1* -94 del/del genetic variant, although associated with increased risk of CLL disease, may be associated with maintenance of disease severity in the early, mildest stage. The likelihood of disease progression may increase as the frequency of wild-type (insertion) alleles for this polymorphism increases.

Key words: nuclear factor-κB, gene polymorphism, chronic lymphocytic leukemia, cancer risk factor

Introduction

Chronic lymphocytic leukemia (CLL) is the most common form of leukemia in the western world, with an incidence rate of 4–5/100,000. Multifactorial pathogenesis creates a complicated interaction network of internal (genetic and epigenetic) and external (for instance, microenvironmental and antigenic stimuli) factors engaged in the transformation, progression and evolution of CLL.[1] Most CLL cells are inert and are arrested in G0/G1 of the cell cycle, due to the inhibition of apoptosis associated with the increased expression of anti-apoptotic proteins from the BCL2 and IAP families, and the reduced expression of BAX and BAK, pro-apoptotic proteins from the BCL2 family. However, it is the progressive accumulation of tumor cells that ultimately leads to symptomatic disease. Chronic lymphocytic leukemia has a heterogeneous outcome, in which some patients progress rapidly and have short survival prognoses, whereas others have a more stable clinical course that may not need treatment for years. The most common staging systems for CLL are the Rai and Binet systems.[2–5] These systems define the following stages: 1) early stage (Rai 0, Binet A); 2) intermediate stage (Rai I/II, Binet B); and 3) advanced stage (Rai III/IV, Binet C). However, these systems are of limited prognostic value and the biological mechanisms involved in the clinical progression from early stages of patients with chronic lymphocytic leukemia are not well known.

Among the genetic factors related to CLL, the pleiotropic transcription factor nuclear factor-kappa B1 (NF-κB1; p105/p50), a potential key contributor to tumorigenesis in many types of cancer, plays an important role. This redox-sensitive transcription factor regulates a number of inflammatory genes, and is an essential player in the initiation and progression of pathogenesis of many autoimmune and inflammatory diseases[6–8] as well as a tumorigenesis promotor.[9] It regulates the transcription of a wide range of genes involved in the immune response, cell adhesion, differentiation, proliferation, angiogenesis, cellular stress reactions, tumorigenesis, and cell survival and apoptosis.[10] Specifically, the active form of the *NF-κB1* gene product, protein p50, can act as a transcription factor to regulate a target gene.[11,12]

Several investigators have reported the constitutive activation of NF-κB in various tumor cells and cell lines, such as in breast cancer,[13] colorectal cancer,[14,15] lung cancer,[16,17] pancreatic cancer,[18,19] melanoma,[11] and multiple myeloma.[20] Most importantly, the activation of the NF-κB pathway mediates CLL cell survival and is further emerging as a prognostic marker in CLL.[1,21]

NF-κB1 (Gene ID: 4790) is mapped to chromosome 4 locus 4q23-q24[22] (Fig. 1) and encodes the non-DNA-binding cytoplasmic molecule p105 and a DNA-binding protein corresponding to the N-terminus of p105-p50 (OMIM: 164011). This gene is composed of 24 exons and introns varying between 40,000 and 323 bp, spanning 156 kb (Fig. 1). Interindividual genetic variation is considered to be an important cancer risk and/or modulatory factor, and may impact the expression pattern encoded by the gene. Its location, molecular structure and genetic susceptibility have been extensively studied. Several variations have been described within the master regulator at the center of the *NF-κB1* gene, with special interest given to rs72696119 (C>G), rs28362491 (-94 ins/del ATTG), rs4648068 (A>G), and rs12509517 (G>C).
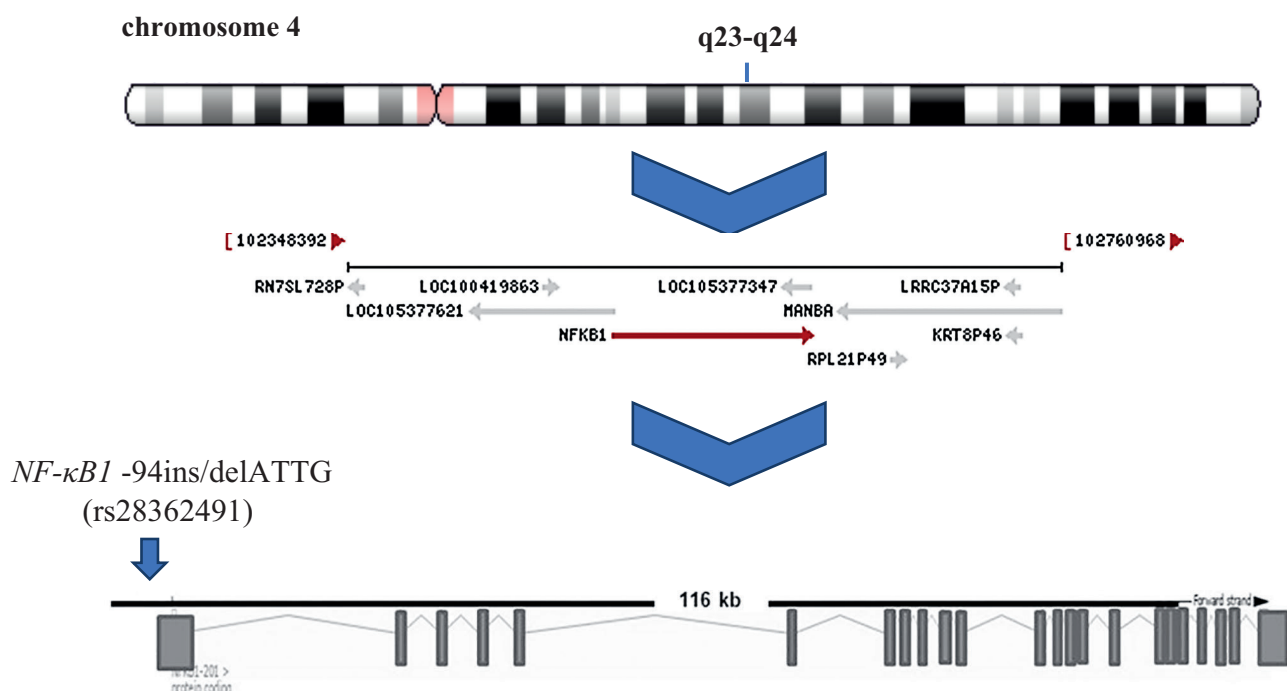
Fig. 1. *NF-κB1* chromosomal location and gene structure. *NF-κB1* promoter -94ins/delATTG (rs28362491) polymorphism location

A common insertion/deletion (-94 insertion/deletion ATTG, rs28362491), located between 2 putative key promoter regulatory elements (Fig. 1) (activator protein 1 and κB binding site), has a functional impact and is the most widely investigated.[20] This modification occurs between 2 important regulatory elements in the promoter region of the *NF-κB1* gene. The deletion of 4 bases (ATTG) reduces or prevents binding to nuclear proteins, and leads to lower transcript levels of the *NF-κB1* gene, thereby changing mRNA stability and regulating translation efficiency.[20]

Neither numerous case-control studies[23–27] nor several meta-analyses[28–34] have resolved the controversy of a potential association between the *NF-κB1* -94 ins/del ATTG promoter polymorphism and cancer risk.

Objectives

We undertook this study to find out whether the -94 ins/del ATTG polymorphism in the *NF-κB1* promoter might be an essential genetic risk factor and/or modulatory disease player associated with chronic lymphocytic leukemia.

Materials and methods

Patients and controls

The *NF-κB1* promoter -94 ins/del ATTG (rs28362491) polymorphism was determined in a group of 282 Polish individuals, including 156 patients with CLL diagnosed at the Department of Hematology, Wroclaw Medical University, Poland. Chronic lymphocytic leukemia was diagnosed according to defined clinical, morphological and immunological criteria. At the time of the study recruitment, all patients were untreated. Due to the availability of clinical data, the Rai classification was included for 144 patients. The clinical characteristics of the study group are shown in Table 1. One hundred and twenty-six age- and sex-matched healthy individuals that we previously genotyped[35] were included as a control group.

All procedures performed in studies involving human participants were in accordance with the ethical standards of the institutional and/or national research committee and with the Declaration of Helsinki (1975), as revised in 2008. The study was approved by the Wroclaw Medical University Ethics Committee. Informed consent was obtained from all individual participants included in the study.

Genotyping

DNA isolation

Genomic DNA from lymphocytes was isolated using a DNA extraction kit (NucleoSpin Blood; Macherey-Nagel GmbH & Co., KG, Düren, Germany) following the manufacturer's instructions.

Identification of -94 ins/del ATTG polymorphism (rs28362491) in the *NF-κB1* gene

The primer sequences for the DNA amplification reactions were designed based on information reported by Zhou et al.[11] and confirmed using the National Center for Biotechnology Information (NCBI) database (Table 2). The 5' end of the sense primer was labeled with TAMRA (Table 2).

Polymerase chain reaction (PCR) was carried out in a total volume of 10 μL. The reaction mixture contained 30 μg of genomic DNA, 0.1 μM each of sense primer (forward) (Metabion International AG, Planegg, Germany) and antisense primer (reverse) (Genomed S.A., Warszawa, Poland), 1 U Taq polymerase (EURX, Gdańsk, Poland), 1× PCR buffer (containing 15 mM $MgCl_2$) (EURX), and buffered dideoxynucleotide mixture (dNTP) containing 200 μM of each dNTP (Invitrogen, Life Technologies/Thermo Fisher Scientific, Foster City, USA). Amplifications were performed in a T100™ Thermal Cycler (Bio-Rad, Hercules, USA). The PCR cycling conditions were as follows: 95°C for 300 s, followed by 34 cycles of 94°C for 18 s, 64°C for 18 s, 72°C for 18 s, and 72°C for 600 s. Qualitative analysis of PCR products was based on electrophoresis in 2% agarose gel, visualized under ultraviolet light (UV).

Polymorphism analysis was performed using capillary electrophoresis using an Applied Biosystems® 3130 Genetic Analyzer, equipped with 3130 Series Data Collection Software v. 4 (Life Technologies/Thermo Fisher Scientific).

Table 1. Patient's characteristics

Patients		Value
Age [years]	median	70
	range	39–85
Gender	F/M	67/89
Stage of the disease (Rai)	0	59
	I	35
	II	28
	III	16
	IV	6

Table 2. Sequences of PCR primers for amplification of the *NF-κB1* gene fragment

Primers sequence	Amplicon [bp]	T_m [°C]	Product size [bp]*
F: 5'– TAMRA-TGG ACC GCA TGA CTC TAT CA' – 3' R: 5'– GGC TCT GGC TTC CTA GCA G – 3'	154/158	60	154/158

*capillary electrophoresis using Applied Biosystems 3130 Genetic Analyzer and POP-7™ polymer (Life Technologies/Thermo Fisher Scientific, Forster City, USA).

502

I. Urbanowicz et al. NF-κB1 polymorphism in CLL

Precise reading of the size of the tested fragments with accuracy to 1 bp was performed against GeneScan™ 500XL ROX™ dye Size Standard (Life Technologies/Thermo Fisher Scientific), which includes a mixture of fluorescently labeled DNA fragments of the following sizes: 35 bp, 50 bp, 75 bp, 100 bp, 139 bp, 150 bp, 160 bp, 200 bp, 300 bp, 340 bp, 350 bp, 400 bp, 450 bp, 490 bp, and 500 bp.

Statistical analyses

All genotypes were tested for deviations from Hardy–Weinberg equilibrium (HWE) using the χ^2 test. Allele and genotype association analyses were performed using dominant and recessive genetic models. Genotype and allele analyses were performed using SHEsis software (http://analysis.bio-x.cn/myAnalysis.php).

The odds ratio (OR) and 95% confidence intervals (95% CI) were calculated using the Simple Interactive Statistical Analysis platform (SISA, http://www.quantitativeskills.com/sisa/).

Differences were considered as statistically significant if the p-value was <0.05.

Results

Genotype distributions did not deviate from HWE, either in the patients or the controls in our cohort of Polish CLL patients (Table 3). A univariate analysis showed that patients with a recessive polymorphic homozygous *NF-κB1* -94 del/del variant (*NF-κB1* rs28362491) have a significantly modified risk of CLL. We observed that the del/del genotype of this polymorphism increased the risk

Table 3. Conformity of genotypic distribution of *NF-κB1* -94ins/del ATTG polymorphisms (rs28362491) with Hardy–Weinberg equilibrium in the group of patients with B-CLL and in the control group

Group	χ^2	p-value*
CCL patients	1.27	0.26
Control group	3.09	0.08

*Results of p > 0.05 were considered consistent with the Hardy–Weinberg equilibrium.

of the disease 2.23-fold (χ^2 = 5.63, p = 0.02, OR = 2.23, 95% CI = 1.14–4.37; Table 4).

Additional associative analysis of the -94 ins/del ATTG polymorphism (rs28362491) in the *NF-κB1* gene in CLL patients using Rai stage was carried out in a subset of 144 patients due to the limited availability of clinical data. The results are shown in Table 5. Patients with stages III and IV were analyzed together due to the small size of the groups. The CLL-prone recessive del/del genotype (χ^2 = 5.63, p = 0.02, OR = 2.23, 95% CI = 1.14–4.37) (Table 4) was the most frequent variant in CLL patients with Rai stage 0 (27.1% > 20% > 14.3% > 18.2%; Table 5).

Statistical analysis of the genotype distribution showed differences in genotype frequencies between patients with the following stages: 0 compared to I (χ^2 = 7.65, p = 0.02); I compared to II (χ^2 = 6.78, p = 0.03); 0 compared to control group (χ^2 = 8.00, p = 0.02); and I compared to control group (χ^2 = 7.65, p = 0.02). The ins/ins genotype may protect against progression of the disease, favoring maintenance in the initial stage (Rai 0). The recessive genotype had significantly different frequencies in the healthy group and the group of patients with the lowest clinical severity (Rai 0) (χ^2 = 7.58, p = 0.006, OR = 2.98, 95% CI = 1.34–6.62); The incidence of this genotype was the highest in the group with Rai 0.

Table 4. Associative analysis of -94ins/del ATTG polymorphism (rs28362491) in the *NF-κB1* gene in the CLL patients and the control group

Variable	CLL n (%)	Control group* n (%)	χ^2	p-value	OR	95% CI
Genotypes						
Ins/ins	52 (33.3)	43 (34.1)	reference			
Ins/del	70 (44.9)	69 (54.8)	0.43	0.51	0.84	0.50–1.42
Del/del	34 (21.8)	14 (11.1)	3.45	0.06	2.01	0.96–4.22
Alleles						
Ins	174 (55.8)	155 (61.5)	1.89	0.17	0.79	0.56–1.11
Del	138 (44.2)	97 (38.5)			1.27	0.90–1.78
Dominant model						
Ins/ins compared to del/del + ins/del	52 (33.3)	43 (34.1)	0.02	1.00	0.97	0.59–1.59
	104 (66.7)	83 (65.9)			1.04	0.63–1.70
Recessive model						
Del/del compared to ins/ins + ins/del	34 (21.8)	14 (11.1)	**5.63**	**0.02**	**2.23**	**1.14–4.37**
	122 (78.2)	112 (88.9)			**0.45**	**0.23–0.88**

Genotype: χ^2 = 6.07; p = 0.05. *published in: Bogunia-Kubik K, Wysoczańska B, Piątek D, Iwaszko M, Ciechomska M, Świerkot J. Significance of polymorphism and expression of miR-146a and NFkB1 genetic variants in patients with rheumatoid arthritis. *Arch Immunol Ther Exp (Warsz)*. 2016;64(Suppl 1):S131–S136. doi:10.1007/s00005-016-0443-5.[35] Statistically significant values are given in bold.

Table 5. Associative analysis of *NF-κB1* -94ins/del ATTG gene polymorphism (rs28362491) in the CLL patients depending on the Rai classification and in the control group

Variable	CLL				Control group* (E) n (%)	Group comparison	χ^2	p-value	OR	95% CI
	Rai 0 (A) n (%)	Rai I (B) n (%)	Rai II (C) n (%)	Rai III+IV (D) n (%)						
Genotypes										
Ins/ins	14 (23.7)	18 (51.4)	7 (25.0)	10 (45.5)	43 (34.1)	reference				
Ins/del	29 (49.2)	10 (28.6)	17 (60.7)	8 (36.4)	69 (54.8)	A:B	**6.90**	**0.009**	**0.27**	**0.10–0.73**
						A:C	0.08	0.77	1.17	0.40–3.48
						A:D	2.81	0.09	0.39	0.13–1.19
						A:E	0.46	0.50	1.29	0.61–2.71
						B:C	**6.39**	**0.01**	**4.37**	**1.36–14.11**
						B:D	0.35	0.55	1.44	0.43–4.83
						B:E	**6.11**	**0.01**	**0.35**	**0.15–0.82**
						C:D	2.97	0.08	0.33	0.09–1.19
						C:E	0.72	0.39	1.51	0.58–3.95
						D:E	1.89	0.17	0.50	0.18–1.36
Del/del	16 (27.1)	7 (20.0)	4 (14.3)	4 (18.2)	14 (11.1)	A:B	3.60	0.06	0.34	0.11–1.05
						A:C	0.37*	0.54*	0.36	0.12–2.07
						A:D	1.47*	0.23*	0.35	0.09–1.37
						A:E	**7.20**	**0.007**	**3.51**	**1.38–8.96**
						B:C	0.01*	1.00*	1.47	0.33–6.63
						B:D	0.11*	0.74*	1.03	0.24–4.39
						B:E	0.11	0.74	1.19	0.41–3.45
						C:D	0.00*	1.00*	0.70	0.13–3.79
						C:E	0.19*	0.66*	0.57	0.15–2.24
						D:E	0.001*	1.00*	1.23	0.33–4.54
Alleles										
Ins	57 (48.3)	46 (65.7)	31 (55.4)	28 (63.6)	155 (61.5)	A:B	**7.05**	**0.008**	**2.29**	**1.24–4.25**
						A:C	1.44	0.23	1.48	0.78–2.83
						A:D	**4.14**	**0.04**	**2.09**	**1.02–4.29**
						A:E	**8.05**	**0.005**	**0.52**	**0.33–0.82**
						B:C	1.40	0.24	0.65	0.31–1.33
						B:D	0.05	0.82	0.91	0.42–2.01
						B:E	0.41	0.52	1.20	0.69–2.09
						C:D	0.70	0.40	1.41	0.63–3.17
						C:E	0.73	0.39	0.78	0.43–1.39
						D:E	0.07	0.79	1.10	0.56–2.13
Del	61 (51.7)	24 (34.3)	25 (44.6)	16 (36.4)	97 (38.5)	A:B	**7.05**	**0.008**	**0.44**	**0.24–0.81**
						A:C	1.44	0.23	0.67	0.35–1.29
						A:D	**4.14**	**0.04**	**0.48**	**0.23–0.98**
						A:E	**8.05**	**0.005**	**1.91**	**1.22–3.00**
						B:C	1.40	0.24	1.55	0.75–3.18
						B:D	0.05	0.82	1.10	0.50–2.41
						B:E	0.41	0.52	0.83	0.48–1.45
						C:D	0.70	0.40	0.71	0.32–1.59
						C:E	0.73	0.39	1.29	0.72–2.31
						D:E	0.07	0.79	0.91	0.47–1.78

Discussion

NF-κB is an essential component of cancer biology, affecting proliferation, apoptosis, vascular regeneration, inflammation, and metastasis, as well as infiltration, especially in tumors with NF-κB constitutive activation, such as those with a hematopoietic origin. Regulation of over 200 different genes by NF-κB serves as the main signal for cell survival, participating in many stages of carcinogenesis and cancer cell resistance to chemo- and radiotherapy. This has therefore become an important target of associative research on cancer pathogenesis and autoimmune diseases.[11] A relationship between *NF-κB1* genetic polymorphism

and cancer risk has been identified, involving polymorphism variants rs72696119 (C>G), rs28362491 (-94 ins/del ATTG), rs4648068 (A>G), and rs12509517 (G>C). Among them, a common functional insertion/deletion polymorphism (-94 insertion/deletion ATTG, rs28362491), located between 2 putative key promoter regulatory elements, is the most frequently investigated genetic variant.

The connection between this polymorphism and cancer risk is inconsistently identified and appears to be divergent across different populations.[23–34] A stratified meta-analysis revealed that this polymorphism can exert ethnic- and cancer-specific effects on cancer risk,[28–34] but to fully establish these differences, further large-scale and

Table 5. Associative analysis of *NF-κB1* -94ins/del ATTG gene polymorphism (rs28362491) in the CLL patients depending on the Rai classification and in the control group – cont.

Variable	CLL				Control group* (E) n (%)	Group comparison	χ^2	p-value	OR	95% CI
	Rai 0 (A) n (%)	Rai I (B) n (%)	Rai II (C) n (%)	Rai III+IV (D) n (%)						
Dominant model										
Ins/ins compared to del/del + ins/del	14 (23.7)	18 (51.4)	7 (25.0)	10 (45.5)	43 (34.1)	A:B	**7.51**	**0.006**	**3.40**	**1.39–8.32**
						A:C	0.02	1.00	1.07	0.38–3.05
						A:D	3.63	0.06	2.68	0.96–7.51
						A:E	2.04	0.15	0.60	0.30–1.21
						B:C	**4.54**	**0.03**	**0.31**	**0.11–0.93**
						B:D	0.19	0.66	0.79	0.27–2.29
						B:E	3.48	0.06	2.04	0.96–4.36
						C:D	2.30	0.13	2.50	0.75–8.29
						C:E	0.87	0.35	0.64	0.25–1.63
						D:E	1.05	0.31	1.61	0.64–4.02
	45 (76.3)	17 (48.6)	21 (75.0)	12 (54.5)	83 (65.9)	A:B	**7.51**	**0.006**	**0.29**	**0.12–0.72**
						A:C	0.02	1.00	0.93	0.33–2.65
						A:D	3.63	0.06	0.37	0.13–1.05
						A:E	2.04	0.15	1.67	0.82–3.37
						B:C	**4.54**	**0.03**	**3.18**	**1.08–9.37**
						B:D	0.19	0.66	1.27	0.44–3.70
						B:E	3.48	0.06	0.49	0.23–1.04
						C:D	2.30	0.13	0.40	0.12–1.33
						C:E	0.87	0.35	1.55	0.61–3.94
						D:E	1.05	0.31	0.62	0.25–1.55
Recessive model										
Del/del compared to ins/ins + ins/del	16 (27.1)	7 (20.0)	4 (14.3)	4 (18.2)	14 (11.1)	A:B	0.60	0.44	0.67	0.25–1.84
						A:C	1.12*	0.29*	0.45	0.13–1.49
						A:D	0.29*	0.59*	0.60	0.18–2.04
						A:E	**7.58**	**0.006**	**2.98**	**1.34–6.62**
						B:C	0.07*	0.80*	0.67	0.17–2.56
						B:D	0.03*	0.86*	0.89	0.23–3.48
						B:E	1.91	0.17	2.00	0.74–5.42
						C:D	0.00*	1.00*	1.33	0.29–6.06
						C:E	0.02*	0.88*	1.33	0.40–4.41
						D:E	0.34*	0.56*	1.78	0.53–6.01
	43 (72.9)	28 (80.0)	24 (85.7)	18 (81.8)	112 (88.9)	A:B	0.60	0.44	1.49	0.54–4.08
						A:C	1.12*	0.29*	2.23	0.67–7.44
						A:D	0.29*	0.59*	1.67	0.49–5.71
						A:E	**7.58**	**0.006**	**0.34**	**0.15–0.75**
						B:C	0.07*	0.80*	1.50	0.39–5.75
						B:D	0.03*	0.86*	1.13	0.29–4.40
						B:E	1.91	0.17	0.50	0.18–1.36
						C:D	0.00*	1.00*	0.75	0.17–3.41
						C:E	0.02*	0.88*	0.75	0.23–2.48
						D:E	0.34*	0.56*	0.56	0.17–1.90

*control group: Bogunia-Kubik K, Wysoczańska B, Piątek D, Iwaszko M, Ciechomska M, Świerkot J. Significance of polymorphism and expression of miR-146a and NFkB1 genetic variants in patients with rheumatoid arthritis. *Arch Immunol Ther Exp (Warsz).* 2016;64(Suppl 1):S131–S136. doi:10.1007/s00005-016-0443-5. Statistically significant values are given in bold.

Genotype:

A:B $\chi^2_{df=2}$ = 7.65; p = 0.02   A:C $\chi^2_{df=2}$ = 1.85; p = 0.40   A:D $\chi^2_{df=2}$ = 3.64; p = 0.16   A:E $\chi^2_{df=2}$ = 8.00; p = 0.02

B:C $\chi^2_{df=2}$ = 6.78; p = 0.03   B:D $\chi^2_{df=2}$ = 0.38; p = 0.83   B:E $\chi^2_{df=2}$ = 7.65; p = 0.02

C:D $\chi^2_{df=2}$ = 3.09; p = 0.21   C:E $\chi^2_{df=2}$ = 0.93; p = 0.63

D:E $\chi^2_{df=2}$ = 2.66; p = 0.26

functional studies are necessary. There are several factors that may explain the occurrence of discrepancies in the results of the above studies, the most important of which are small sample sizes and diverse ethnicity, which affect the distribution of polymorphisms and environmental factors.

This genetic variant, consisting of the deletion of 4 nucleotides (ATTG) in the promoter region of the *NF-κB1* gene, reduces or completely prevents binding to nuclear proteins and leads to a reduction in the level of the *NF-κB1* gene transcript, thereby altering mRNA stability and regulating translation efficiency.[11] In bladder cancer, the presence of the del allele (ins/del + del/del genotype) reduces *NF-κB1* (p50) mRNA expression in tumor tissues.[26] Moreover, patients homozygous for the deletion possess a statistically higher risk of tumor recurrence than carriers with 1

or more insertion alleles in non-muscle invasive bladder cancer.[26]

Prior to this study, the potential role of the *NF-κB1* -94 ins/del ATTG (rs28362491) genetic polymorphism in the development and course of chronic lymphocytic leukemia had not been investigated. We have shown for the first time a significant impact of this genetic variation on CLL pathogenesis. A recessive polymorphic homozygous *NF-κB1* -94 del/del ATTG variant significantly modified the risk of CLL in our Polish CLL patients, increasing the disease risk 2.23-fold. Additionally, the CLL-prone recessive del/del genotype was the most frequent variant in CLL patients with Rai stage 0, so the del/del-positive patients more frequently presented with the less aggressive disease phenotype, suggesting a low probability of progression to more advanced disease. Although this is a variant associated with increased risk of CLL disease, it may also be associated with the maintenance of the disease in the early, mildest stage.

The enhanced expression and activity of p50 (NF-κB1)[20,36,37] as a result of this polymorphism may serve as an explanation for this phenomenon. The del allele is reportedly associated with the decreased promoter activity and enhanced NF-κB1 mRNA expression,[20,36,37] which might influence cancer development. As a transcription factor NF-κB component, p50 (NF-κB1) serves an important function in inhibiting cell apoptosis by modulating the expression levels of several survival genes (*Bcl-2* homologue A1, *PAI-2* and *IAP* gene family), which reveal the contribution of p50 (NF-κB1) signaling pathways to cellular proliferation by increasing IL-5, promoting MAPK phosphorylation and modulating cyclin D1 expression.[38] Consequently, the observed association between the *NF-κB1* -94 ins/del ATTG polymorphism and cancer risk can be explained by decoupling this genetic variation from its roles in apoptosis and cellular proliferation by modulating the expression of p50 (NF-κB1),[19,36,37] which is implicated through the mechanism described above.

Limitations

Our study has several limitations, including the study size, and further, well-designed studies with representative sample sizes are necessary to validate our findings. A comparative analysis of age, sex and other prognostic factors such as the mutation status of the gene encoding immunoglobulin heavy chains should be taken into account in order to prove that the *NF-κB1* promoter -94 ins/del ATTG polymorphism is a significant CLL risk and modulatory factor.
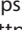
Therefore, firstly the relevant studies should be developed by increasing the sample size in both study groups. Second, comparative analysis of age, sex and other prognostic factors, such as mutation status of the gene encoding immunoglobulin heavy chains, should be considered.

Finally, we cannot exclude the possibility that the ATTG polymorphism of the *NF-κB1* -94ins/del promoter may be an important factor of both risk and modulating CLL; therefore, further well-designed studies with a representative sample size are needed to definitively elucidate the role of this polymorphism to confirm our findings.

Conclusions

We suggest that the del/del polymorphism genotype -94 ins/del ATTG (rs28362491) in the *NF-κB1* gene increases the risk of chronic lymphocytic leukemia. This may be associated with retardation of disease progression and maintenance at an early, mild stage. In populations with increased frequencies of wild-type (insertion) alleles for -94 ins/del ATTG polymorphism (rs28362491) in the *NF-κB1* gene, the probability of disease progression may be increased.

ORCID iDs

Iwona Urbanowicz https://orcid.org/0000-0002-9489-322X
Dariusz Wołowiec https://orcid.org/0000-0003-4081-5397
Barbara Wysoczańska https://orcid.org/0000-0002-2392-9002
Piotr Łacina https://orcid.org/0000-0002-9659-9403
Anna Jonkisz https://orcid.org/0000-0001-6916-4212
Wiesława Nahaczewska https://orcid.org/0000-0002-0356-9505
Andrzej Tukiendorf https://orcid.org/0000-0001-5278-989X
Iwona Bil-Lula https://orcid.org/0000-0002-2769-0166
Katarzyna Bogunia-Kubik https://orcid.org/0000-0001-9744-0376
Edyta Pawlak https://orcid.org/0000-0002-0386-7940

References

1. Montillo M, Hamblin T, Hallek M, Montserrat E, Morra E. Chronic lymphocytic leukemia: Novel prognostic factors and their relevance for risk-adapted therapeutic strategies. *Haematologica.* 2005;90(3): 391–399. PMID:15749671
2. Hallek M, Cheson BD, Catovsky D, et al. International Workshop on Chronic Lymphocytic Leukemia. Guidelines for the diagnosis and treatment of chronic lymphocytic leukemia: A report from the International Workshop on Chronic Lymphocytic Leukemia updating the National Cancer Institute–Working Group 1996 guidelines. *Blood.* 2008;111(12):5446–5456. doi:10.1182/blood-2007-06-093906
3. NCCN Clinical Practice Guidelines in Oncology. Chronic lymphocytic leukemia/small lymphocytic lymphoma, version 2.2019. National Comprehensive Cancer Network website. nccn.org/professionals/physician_gls/pdf/cll.pdf. Updated October 5, 2018. Accessed October 18, 2018.
4. Binet JL, Auquier A, Dighiero G, et al. A new prognostic classification of chronic lymphocytic leukemia derived from a multivariate survival analysis. *Cancer.* 1981;48(1):198–206. doi:10.1002/1097-0142(19810701)48:1<198::aid-cncr2820480131>3.0.co;2-v
5. Rai KR, Sawitsky A, Cronkite EP, Chanana AD, Levy RN, Pasternack BS. Clinical staging of chronic lymphocytic leukemia. *Blood.* 1975;46(2): 219–234. PMID:1139039
6. Chen F, Castranova V, Shi X, Demers LM. New insights into the role of nuclear factor-kappaB, a ubiquitous transcription factor in the initiation of diseases. *Clin Chem.* 1999;45(1):7–17. PMID:9895331
7. Ghosh S, May MJ, Kopp EB. NF-kappa B and Rel proteins: Evolutionarily conserved mediators of immune responses. *Ann Rev Immunol.* 1998;16:225–260. doi:10.1146/annurev.immunol.16.1.225
8. Valen G, Yan ZQ, Hansson GK. Nuclear factor kappa-B and the heart. *J Am Coll Cardiol.* 2001;38(2):307–314. doi:10.1016/s0735-1097(01)01377-8
9. Aggarwal BB. Nuclear factor-kappaB: The enemy within. *Cancer Cell.* 2004;6(3):203–208. doi:10.1016/j.ccr.2004.09.003
10. Beinke S, Ley SC. Functions of NF-κB1 and NF-κB2 in immune cell biology. *Biochem J.* 2004;382(Pt 2):393–409. doi:10.1042/BJ20040544

11. Zhou B, Rao L, Peng Y, et al. Functional polymorphism of the *NFKB1* gene promoter is related to the risk of dilated cardiomyopathy. *BMC Med Genet*. 2009;10:47. doi:10.1186/1471-2350-10-47

12. Pharoah PD, Dunning AM, Ponder BA. Association studies for finding cancer-susceptibility genetic variants. *Nat Rev Cancer* 2004;4(11): 850–860. doi:10.1038/nrc1476

13. Zhang Q, Lenardo MJ, Baltimore D. 30 years of NF-κB: A blossoming of relevance to human pathobiology. *Cell*. 2017;168(1–2):37–57. doi:10.1016/j.cell.2016.12.012

14. Hoesel B, Schmid JA. The complexity of NF-κB signaling in inflammation and cancer. *Mol Cancer*. 2013;12:86.doi:10.1186/1476-4598-12-86

15. Tian B, Nowak DE, Jamaluddin M, Wang S, Brasier AR. Identification of direct genomic targets downstream of the nuclear factor-κB transcription factor mediating tumor necrosis factor signaling. *J Biol Chem*. 2005;280(17):17435–17448. doi:10.1074/jbc.M500437200

16. Cilloni D, Martinelli G, Messa F, Baccarani M, Saglio G. Nuclear factor KB as a target for new drug development in myeloid malignancies. *Haematologica*. 2007;92(9):1224–1229. doi:10.3324/haematol.11199

17. Escarega RO, Fuentes A, Garcia-Carasco M, Gatica A, Zamora A. The transcription nuclear factor-kappa B and cancer. *Clin Oncol (R Coll Radiol)*. 2007;19(2):154–161. doi:10.1016/j.clon.2006.11.013

18. Hayden MS, Ghosh S. Signaling to NF-κB. *Genes Dev*. 2018;18(18): 2195–2224. doi:10.1101/gad.1228704

19. Gilmore TD, Herscovitch M. Inhibitors of NF-κB signaling: 785 and counting. *Oncogene*. 2006;25(51):6887–6899. doi:10.1038/sj.onc.120 9982

20. Karban AS, Okazaki T, Panhuysen CI, et al. Functional annotation of a novel NFKB1 promoter polymorphism that increases risk for ulcerative colitis. *Hum Mol Genet*. 2004;13(1):35–45. doi:10.1093/hmg/ddh008

21. Zhang S, Kipps TJ. The pathogenesis of chronic lymphocytic leukemia. *Annu Rev Pathol*. 2014;9:103–118. doi:10.1146/annurev-pathol-020712-163955

22. Mathew S, Murty VVVS, Dalla-Favera R, Chaganti RSK. Chromosomal localization of genes encoding the transcription factors, c-rel, NF-kappa-Bp50, NF-kappa-Bp65, and lyt-10 by fluorescence in situ hybridization. *Oncogene*. 1993;8(1):191–193. PMID:8423996

23. Cheng CW, Su JL, Lin CW, et al. Effects of *NFKB1* and *NFKBIA* gene polymorphisms on hepatocellular carcinoma susceptibility and clinico-pathological features. *PLoS One*. 2013;8(2):e56130. doi:10.1371/journal.pone.0056130

24. Lo SS, Chen JH, Wu CW, Lui WY. Functional polymorphism of *NFKB1* promoter may correlate to the susceptibility of gastric cancer in aged patients. *Surgery*. 2009;145(3):280–285. doi:10.1016/j.surg.2008.11.001

25. Lin SC, Liu CJ, Yeh WI, Lui MT, Chang KW, Chang CS. Functional polymorphism in *NFKB1* promoter is related to the risks of oral squamous cell carcinoma occurring on older male areca (betel) chewers. *Cancer Lett*. 2006;243(1):47–54. doi:10.1016/j.canlet.2005.11.019

26. Riemann K, Becker L, Struwe H, et al. No association of the *NFKB1* insertion/deletion promoter polymorphism with survival in colorectal and renal cell carcinoma as well as disease progression in B-cell chronic lymphocytic leukemia. *Pharmacogenet Genomics*. 2006;16(11): 783–788. doi:10.1097/01.fpc.0000230414.74726.f6

27. Lehnerdt GF, Bankfalvi A, Grehl S, et al. No association of the *NF-kappaB1*: 94ins/delATTG promoter polymorphism with relapse-free and overall survival in patients with squamous cell carcinomas of the head and neck region. *Int J Immunopathol Pharmacol*. 2008;21(4): 827–832. doi:10.1177/039463200802100407

28. Yang X, Li P, Tao J, et al. Association between *NFKB1* -94ins/del ATTG promoter polymorphism and cancer susceptibility: An updated meta-analysis. *Int J Genomics*. 2014;2014:612972. doi:10.1155/2014/612972

29. Xu L, Huang S, Chen W, Song Z, Cai S. *NFKB1* -94 insertion/deletion polymorphism and cancer risk: A metaanalysis. *Tumour Biol*. 2014;35: 5181–5187. doi:10.18632/oncotarget.14190

30. Nian X, Zhang W, Li L, Sun Y, Sun E, Han R. Meta-analysis of studies on the association between the *NF-kappaB1* -94ins/del ATTG promoter polymorphism and cancer. *Tumour Biol*. 2014;35:11921–11931. doi:10.1007/s13277-014-2470-3

31. Duan W, Wang E, Zhang F, Wang T, You X, Qiao B. Association between the *NFKB1*-94ins/del ATTG polymorphism and cancer risk: An updated meta-analysis. *Cancer Invest*. 2014;32(7):311–320. doi:10.3109/0735 7907.2014.911881

32. Zou YF, Yuan FL, Feng XL, et al. Association between *NFKB1* -94ins/delATTG promoter polymorphism and cancer risk: A meta-analysis. *Cancer Invest*. 2011;29:78–85. doi:10.3109/07357907.2010.535054

33. Wang X, Lu P, Xu L, et al. Updated meta-analysis of *NFkappaB1* -94ins/Delattg promoter polymorphism and cancer risk based on 19 case-control studies. *Asian Pac J Cancer Prev*. 2011;12:2479–2484.

34. Fu W, Zhuo ZJ, Chen YC, et al. *NFKB1* -94insertion/deletion ATTG polymorphism and cancer risk: Evidence from 50 case-control studies. *Oncotarget*. 2017;8(6):9806–9822. doi:10.18632/oncotarget.14190

35. Bogunia-Kubik K, Wysoczańska B, Piątek D, Iwaszko M, Ciechomska M, Świerkot J. Significance of polymorphism and expression miR-146a and *NFKB1* genetic variants in patients with rheumatoid arthritis. *Arch Immunol Ther Exp (Warsz)*. 2016;64(Suppl 1):131–136. doi:10.1007/s00005-016-0443-5

36. Li P, Gu J, Yang X, et al. Functional promoter -94 ins/del ATTGpolymorphism in *NFKB1* gene is associated with bladder cancer risk in a Chinese population. *PLoS ONE*. 2013;8(8):e71604. doi:10.1371/journal.pone.0071604

37. Riemann K, Becker L, Struwe H, Rübben H, Eisenhardt A, Siffert W. Insertion/deletion polymorphism in the promoter of *NFKB1* as a potential molecular marker for the risk of recurrence in superficial bladder cancer. *Int J Clin Pharmacol Ther*. 2007;45(8):423–430. doi:10.5414/cpp45423

38. Yang X, Li P, Tao J, et al. Association between *NFKB1* −94ins/del ATTG promoter polymorphism and cancer susceptibility: An updated meta-analysis. *Int J Plant Genom*. 2014;2014:612972. doi:10.1155/2014/612972

An insight into the promoter methylation of *PHF20L1* and the gene association with metastasis in breast cancer

Jose Alfredo Sierra-Ramirez[1,B,F], Emmanuel Seseña-Mendez[2,E,F],
Marycarmen Godinez-Victoria[1,B,F], Marta Elena Hernandez-Caballero[2,A,C–E]

[1] Medical School, Graduate Section, National Polytechnic Institute, Mexico City, Mexico

[2] Department of Biomedicine, Faculty of Medicine, Meritorious Autonomous University of Puebla (BUAP), Puebla, Mexico

A – research concept and design; B – collection and/or assembly of data; C – data analysis and interpretation;
D – writing the article; E – critical revision of the article; F – final approval of the article

Address for correspondence
Marta Elena Hernandez-Caballero
E-mail: ehdezc@yahoo.com

Abstract

Background. Plant homeodomain finger protein 20-like 1 (*PHF20L1*) is a protein reader involved in epigenetic regulation that binds monomethyl-lysine. An oncogenic function has been attributed to *PHF20L1* but its role in breast cancer (BC) is not clear.

Objectives. To explore *PHF20L1* promoter methylation and comprehensive bioinformatics analysis to improve understanding of the role of *PHF20L1* in BC.

Materials and methods. Seventy-four BC samples and 16 control samples were converted using sodium bisulfite treatment and analyzed with methylation-specific polymerase chain reaction (PCR). Bioinformatic analysis was performed in the BC dataset using The Cancer Genome Atlas (TCGA) trough data visualized and interpreted in the MEXPRESS website. Methylation, gene expression and survival evaluation were performed with R v. 4.0.2 software. Using multiple bioinformatic tools, we conducted a search for genes co-expressed with *PHF20L1*, analyzed its ontology and predicted associated miRNAs and miRNA-*PHF20L1* networks. The expression and prognostic value of *PHF20L1* and co-expressed genes were analyzed.

Results. We found demethylation in *PHF20L1* promoter in both BC samples and healthy tissues. Data mining with 241 patients demonstrated changes in methylation of promoter regions in basal-like and luminal A subtypes. Expression of the *PHF20L1* gene had a negative correlation with methylation. Twelve genes were co-expressed. *PHF20L1* is a target of miR96-5p, miR9-5p and miR182-5p, which are involved in proliferation and metastasis. *PHF20L1* gene expression was not associated with overall survival (OS), or relapse-free survival (RFS), but was associated with distant metastasis-free survival (DMFS).

Conclusions. Our findings showed differences in methylation of *PHF20L1* promoter region near TSS and upstream in BC subtypes; its overexpression impacted DMFS. We found that *PHF20L1* is targeted by miR96-5p, miR9-5p and miR182-5p, which are involved in proliferation and metastasis, and regulates genes engaged in processes such as alternative splicing.

Key words: metastasis, hypomethylation, *PHF20L1*, miRNA, promoter

Background

DNA mutations are the driving force for cancer initiation, progression and invasion. Nevertheless, accumulating evidence suggests that epigenetic modifications are also involved. In tumors at early stages, it is common to observe hypomethylation of DNA from tumor cells and hypermethylation of CpG islands of specific promoters, which has led to the suggestion that epigenetic dysregulation actually precedes tumor events before classic mutations.[1] Histone acetylation is an essential key for epigenetic regulation. Histone acetyltransferases (HATs) are responsible for transferring an acetyl group from acetyl-Co-A to the ε-amino of histone lysine residues.[2] They do not work in isolation but as part of a complex whose components are responsible for determining the lysine specificity.[3] In vivo, HATs require coactivators that determine which lysine will be acetylated and play a key role in a variety of cellular functions thanks to their various domains.[4,5] *PHF20L1* is part of the non-specific lethal (NLS) complex involved in histone acetylation and post-translational modification.[6] Located in the nucleoplasm and plasma membrane, *PHF20L1* has Tudor, MBT, Lys-rich, and zinc finger plant homeodomain (PHD) type domains (Uniprot KB-A8MW92). It is similar to the PHF20 homolog,[7] with which it maintains 33% homology, especially in the second PHD domain of PHF20, which shares 73% identity. Currently, its role and regulation are being revealed. It participates in avoiding SOX2 proteolysis[8] and regulates the degradation of methylated DNMT1.[9] *PHF20L1* is considered an oncogene[10] and has an important function in breast cancer (BC), which suggests that *PHF20L1* may have a role in cancer treatment.[5] MicroRNAs (miRNAs) are short noncoding RNA that regulate the expression of target genes and are associated with tumorigenesis, invasion and metastasis. An miRNA can regulate multiple genes that participate in the same biological pathway.[11]

The availability of cancer multi-omics databases allows us to decipher the genomic drivers of cancer, and the emergence of user-friendly tools to analyze and visualize a bulk of data is crucial to achieve the full potential of these datasets. In this study, we examined the *PHF20L1* promoter methylation through sodium bisulfite treatment and its participation in BC by analyzing expression in public gene datasets.

Objectives

We investigated PHF20L1 methylation and gene expression with an emphasis on its relationship with co-expressed genes, its contribution to survival (independently and with co-expressed genes), miRNAs that target it, and its involvement in cancer.

Materials and methods

Study subjects

Tissues from 80 confirmed BC cases and 16 healthy adjacent fresh tissue controls were collected in Hospital la Raza (Mexico City, Mexico). The study was approved by institutional ethical committees for research La Raza Hospital, Mexican Social Security Institute (IMSS), Mexico City, Mexico, and informed consent was obtained from all patients. All clinical data were collected from medical records. The state of disease was obtained based on pathological report.

DNA extraction

DNA from tissues was obtained with QIAamp DNA Micro Kit (Qiagen, Valencia USA). DNA concentration was measured using NanoDrop 8000 Spectrophotometer (Thermo Fisher Scientific, Waltham, USA).

Sodium bisulfite treatment and methylation-specific PCR (MSP)

DNA isolated from tissues was bisulfite-modified using EpiTect Bisulfite Kit (Qiagen, Frederick, USA) according to the manufacturer's protocol as previously described.[12] The CpG island from the promoter region was located using Eukaryotic Promoter Database tool (https://epd. epfl.ch/index.php). MSP primer pairs were designed using Methprimer software[13] to detect bisulfite-induced changes affecting unmethylated (U) and methylated (M) alleles. Primer sequences are as follows: *PHF20L1* (MF) 5'-TTAAGAATAATAAATAATGTTTTTCGT-3'; (MR) 5'-GTAACTCACGAAAATTAAACCCG-3'; (UF) 5'-AAGAATAATAAATAATGTTTTTTGT-3'; (UR) 5'-ATAACTCACAAAAATTAAACCCAAA-3'. The size of methylated polymerase chain reaction (PCR) products was 204 bp for methylated and 203 bp for unmethylated amplicon in *PHF20L1*. PCR for bisulfite-converted DNA was performed using EpiTect MSP Kit (Qiagen). Twenty nanograms of DNA, 10 µM of each primer and 2X Master mix MSP (Qiagen, Valencia USA) were combined in a final reaction volume of 10 µL. For methylated *PHF20L1*, cycle conditions were as follows: 95°C for 10 min, 1 cycle; 35 cycles (94°C for 15 s, 52°C for 30 s, 72°C for 30 s); and 72°C for 10 min, 1 cycle. For unmethylated *PHF20L1*, cycle conditions were as follows: 95°C for 10 min, 1 cycle; 35 cycles (94°C for 15 s, 50°C for 30 s, 72°C for 20 s); and 72°C for 10 min, 1 cycle. Each PCR assay included a methylation control, an unmethylated control and genomic DNA (EpiTect PCR Control DNA Set, Qiagen, USA). The PCR products were analyzed using 3.5% agarose gel electrophoresis.

Bioinformatic analysis of data in breast invasive carcinoma

We assessed the gene expression and methylation of *PHF20L1* in breast invasive carcinoma dataset using The Cancer Genome Atlas (TCGA) database (http://tcgaportal.org). Data were visualized and interpreted using MEXPRESS (https://www.mexpress.be/).

Methylation and RNA analysis

Methylation data of 561 BC samples were obtained through MEXPRESS for methylation assay.[14] MEXPRESS is an online user-friendly tool for the visualization and interpretation of TCGA data to assess expression, DNA methylation, and clinical data, as well as the relationships among them.[15] TCGA database was used for analyses of mRNA expression with R v. 4.0.2 (www.r-project.org).[14] Mean and standard deviation of parameters were used as descriptive statistics. Because data did not show normal distribution, a generalized linear model (GLM) of gamma distribution error was used (test analogous to a one-way analysis of variance (ANOVA)) in addition to Kruskal–Wallis analysis. Afterward, Tukey and Dunnet tests were performed with the multcomp[16] and FSA libraries.[17] All graphs were made with ggplot2[18] and ggsignif libraries.[19] An α value of 0.05 was used.

Co-expression analysis

Using ONCOMINE (https://www.oncomine.org), we analyzed pair-wise gene expression correlation (correlation ≥ 0.60). Database for Annotation, Visualization and Integrated Discovery (DAVID) v. 6.8 was used to perform gene ontology (GO) function analysis of co-expressed genes. In the GO analysis, the categories included were cellular component (CC) and molecular function (MF).

miRNAs analysis

miRNAs associated with *PHF20L1* were predicted using miRDB (http://mirdb.org/index.html)[20] and mirDIP (http://ophid.utoronto.ca/mirDIP/),[21] an online tool that provides 152 million human miRNA-target interactions. Our search was limited to high confidence (integrated score ≥ 0.90). Furthermore, to obtain a miRNA-*PHF20L1* network with co-expressed genes, we used miRNet (https://www.mirnet.ca.).[22]

Survival

We used R v. 4.0.2 software to determine survival probability with *PHF20L1* gene expression levels between TCGA BC samples. The patients samples were divided in 2 cohorts according to an expression cutoff of 3 (obtained using median value) and analized using the R package named survival.[23] Methylation compared to survival was evaluated using data only from cg with significant results in shorter-survival patients. To evaluate the global prognostic value of *PHF20L1* co-expressed genes, we used Kaplan–Meier plotter (http://kmplot.com), an online database of microarray datasets that assesses the effect of genes on survival in 5143 breast samples among other cancers,[24] and calculates hazard ratio (HR) with 95% confidence intervals (95% CIs) and log-rank p-values. Survival analyses play a central role in identifying potential genes as key genes and biomarkers.

Results

Methylation analysis

The promoter methylation status of the *PHF20L1* gene was examined in 74 sporadic BC tumors (6 patients did not have complete data) and 16 non-tumoral adjacent tissues from some of these same patients. The mean age of the patients was 54.1 ±11 years. The BC stage frequencies were as follows: stage II 39.0%, stage III 45.5% and stage IV 15.6%. The methylation assay using sodium bisulfite revealed no difference in *PHF20L1* promoter methylation status between cancer stages or in comparison to healthy tissues; all samples were demethylated (Fig. 1A). Through data mining of *PHF20L1* gene in the TCGA database with MEXPRESS tool, we analyzed DNA methylation (Infinium HumanMethylation450 microarray) in 241 patients with complete data. Eight promoter probes were analyzed. There was no significant difference regarding tumor stage (stage I 18%, stage II 58.5%, stage III 21.2%, and stage IV 2.3%) or histology type (data from 824 patients were used for this analysis). When we looked for differences between methylation and PAM50 BC molecular classification, we found differences with 2 probes: cg5307234 and cg27342122, of which cg27342122 corresponded to the region we analyzed (Fig. 1B). The luminal A subtype had more methylation and the basal-like subtype had less methylation in promoter region cg5307234 probe, while, the basal-like subtype showed hypomethylation in the promoter region of cg27342122 compared to the other subtypes (Fig. 1C,D).

HF20L1 gene expression

Due to the minimum amount of tissue for our analysis, it was not possible to obtain RNA. The *PHF20L1* gene expression was checked in TCGA BC samples that had subtype information available. We found that the mRNA expression level of *PHF20L1* was higher in the basal-like subtype (Fig. 2A). In addition, a negative correlation between DNA methylation and *PHF20L1* transcription was also observed (r = −0.19, p < 0.001) (Fig. 2B).
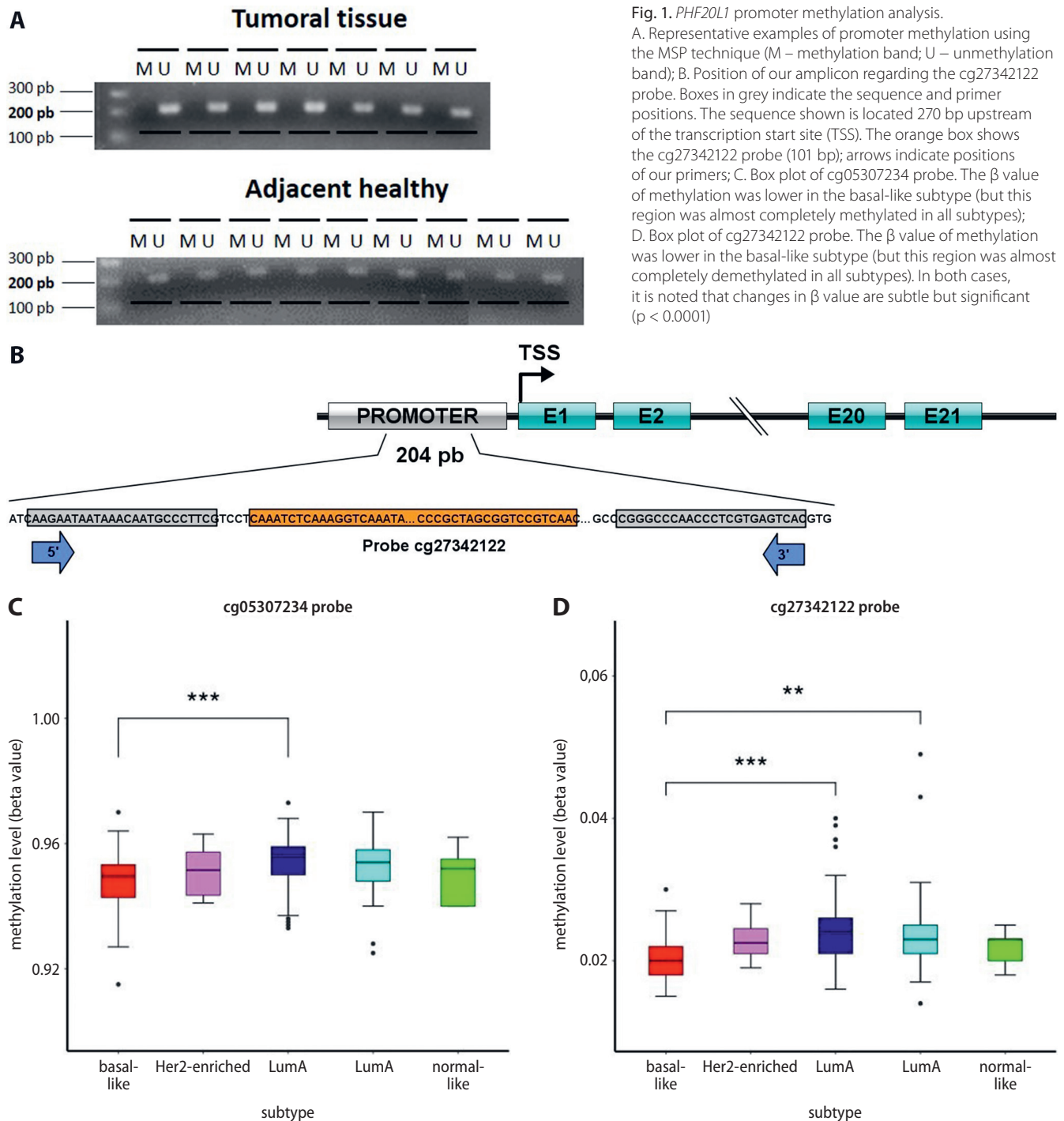
Fig. 1. *PHF20L1* promoter methylation analysis.
A. Representative examples of promoter methylation using the MSP technique (M – methylation band; U – unmethylation band); B. Position of our amplicon regarding the cg27342122 probe. Boxes in grey indicate the sequence and primer positions. The sequence shown is located 270 bp upstream of the transcription start site (TSS). The orange box shows the cg27342122 probe (101 bp); arrows indicate positions of our primers; C. Box plot of cg05307234 probe. The β value of methylation was lower in the basal-like subtype (but this region was almost completely methylated in all subtypes); D. Box plot of cg27342122 probe. The β value of methylation was lower in the basal-like subtype (but this region was almost completely demethylated in all subtypes). In both cases, it is noted that changes in β value are subtle but significant ($p < 0.0001$)

Co-expression analysis

Using the ONCOMINE database, we selected co-expression analysis in BC primary sites, using only female mRNA data. We found 12 genes co-expressed with *PHF20L1* across the BC dataset with a correlation value of ≥0.6. Co-expressed genes were clustered through gene ontology analysis using DAVID. The enrichment GO terms considered were CC and MF ontologies (Table 1). In the CC ontology, we obtained 3 GO categories involved with nucleus (7 genes), nucleoplasm (5 genes) and coiled coil (5 genes).

The other enrichment category MF comprised items related to alternative splicing (10 genes), splice variant (9 genes) and phosphoprotein (9 genes). Only clusters that had at least 5 genes were included.

miRNAs analysis

miRNAs have a role in post-transcriptional regulation of gene expression which leads to targeting of mRNAs for degradation and/or inhibition of translation. Furthermore, one miRNA can co-regulate several genes. Using mirDIP
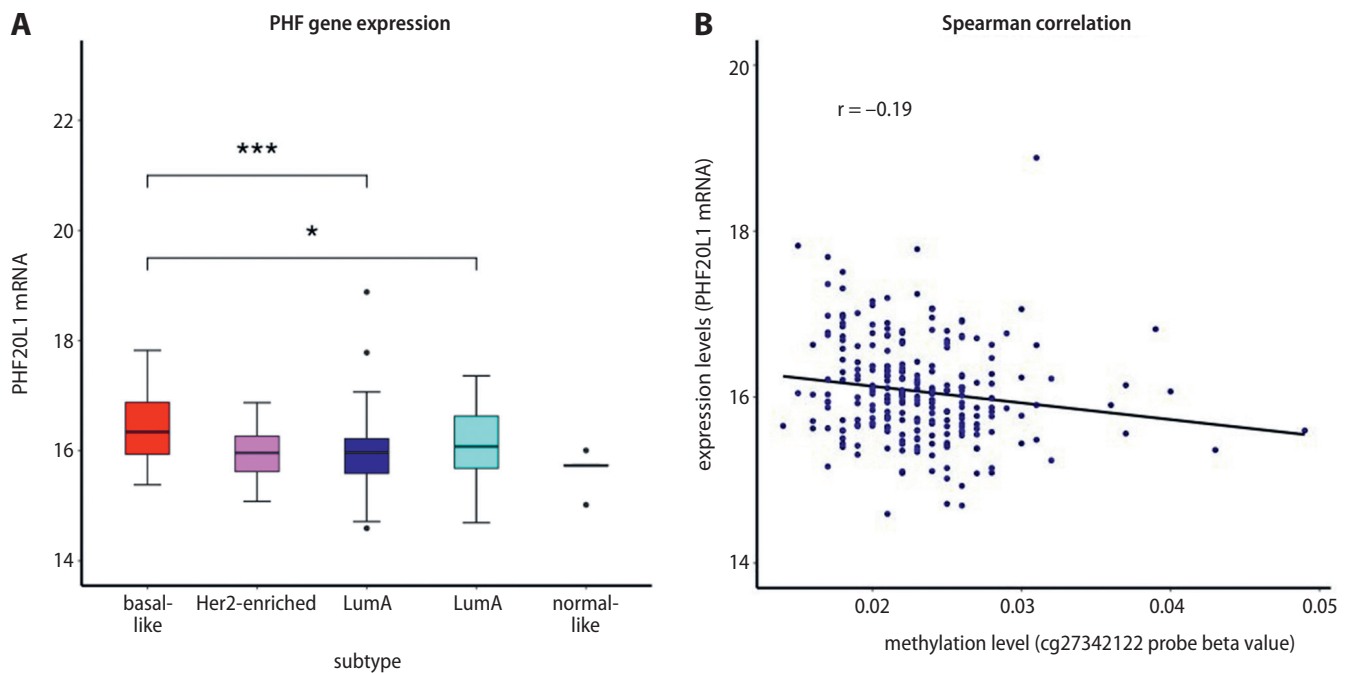
Fig. 2. Relationship between *PHF20L1* expression in BC and methylation. A. Box plot of mRNA expression based on the TCGA database (p < 0.0001); B. Correlation between cg27342122 methylation and *PHF20L1* expression. Spearman test showed a negative correlation between DNA methylation and *PHF20L1* transcription (r = −0.19, p < 0.001)

Table 1. Gene ontology analysis of gene expression. Functional annotation clustering (enrichment score 1.36-0.47)

Gene co-expressed	Category	Term/gene function	Count	%	p-value
N4BP2L2, PHF20L1, PNISR, YLPM1, ATG12, MFF, PON2, PRKRA, PIAS1, ZNF407	GOTERM_MF_DIRECT	alternative splicing	10	83.3	4.2E-2
N4BP2L2, PHF20L1, PNISR, YLPM1, ATG12, MFF, PON2, PRKRA, ZNF407	GOTERM_MF_DIRECT	splice variant	9	75	2.4E-2
PHF20L1, PNISR, STT3B, YLPM1, MFF, PRKRA, PIAS1, ZNF407, SMC5	GOTERM_MF_DIRECT	phosphoprotein	9	75	3.0E-2
N4BP2L2, PHF20L1, YLPM1, PON2, PIAS1, ZNF407, SMC5	GOTERM_CC_DIRECT	nucleus	7	58.3	7.3E-2
PNISR, YLPM1, PRKRA, PIAS1, SMC5	GOTERM_CC_DIRECT	nucleoplasm	5	41.7	7.3E-2
N4BP2L2, PNISR, YLPM1 MFF, SMC5	GOTERM_CC_DIRECT	coiled coil	5	41.7	6.6E-2

CC – cellular component; MF – molecular function.

(corroborated by miRDB), 190 miRNAs were predicted as regulators of *PHF20L1* gene expression, but only miR-96-5p, miR-9-5p and miR-182-5p were obtained using a very high score class for prediction (score ≥0.90). After searching in ONCOMINE, we found 12 genes co-expressed with *PHF20L1*. Next, we made a network with the miRNet tool in BC tissues, setting the cutoff degree on 1. We found 1 node with 442 miRNAs; this network included miRNAs predicted by mirDIP, including 79 miRNAs involved in breast neoplasms and triple-negative breast carcinoma (Fig. 3). Mirnetwork allowed us to observe that miRNAs predicted as *PHF20L1* regulators participate in cell differentiation, cell cycle and apoptosis (p = 0.006), and mir9-5p and mir-182-5p are involved in triple-negative breast carcinoma BC (p = 0.02), and mir-96-5p in breast neoplasms (p = 0.02).

PHF20L1 prognosis in breast cancer

The prognostic value of *PHF20L1* expression was examined with R software. The expression of *PHF20L1*

or the promoter methylation in cg5307234 and cg27342122 probe regions by subtype had no relation with overall survival (OS), but when we analyzed the methylation data from deceased patients alone, i.e., patients with shorter survival, we found that more hypomethylation of *PHF20L1* was observed in the basal-like subtype, with respect to the luminal A subtype, and methylation between the luminal A and luminal B subtypes (p < 0.01) was associated with survival (Fig. 4A). The Kaplan–Meier plotter platform was used to analyzed relapse-free survival (RFS) and distant metastasis-free survival (DMFS), which revealed that expression of *PHF20L1* is related with DMFS (p = 0.02) (Fig. 4B). Exploring the potential roles of genes co-expressed with *PHF20L1* in OS, RFS and DMFS, we obtained Kaplan–Meier survival curves from the Kaplan–Meier plotter platform. We found that expression of *ZNF407* and *PIAS1* were related with OS. Expression of all genes except *PHF20L1*, *STT3B*, *YLPM1*, and *MFF* was associated with RFS of BC, and *STT3B*, *PRKRA*, *ATG12*, and *PHF20L1* were associated with DMFS (Table 2).
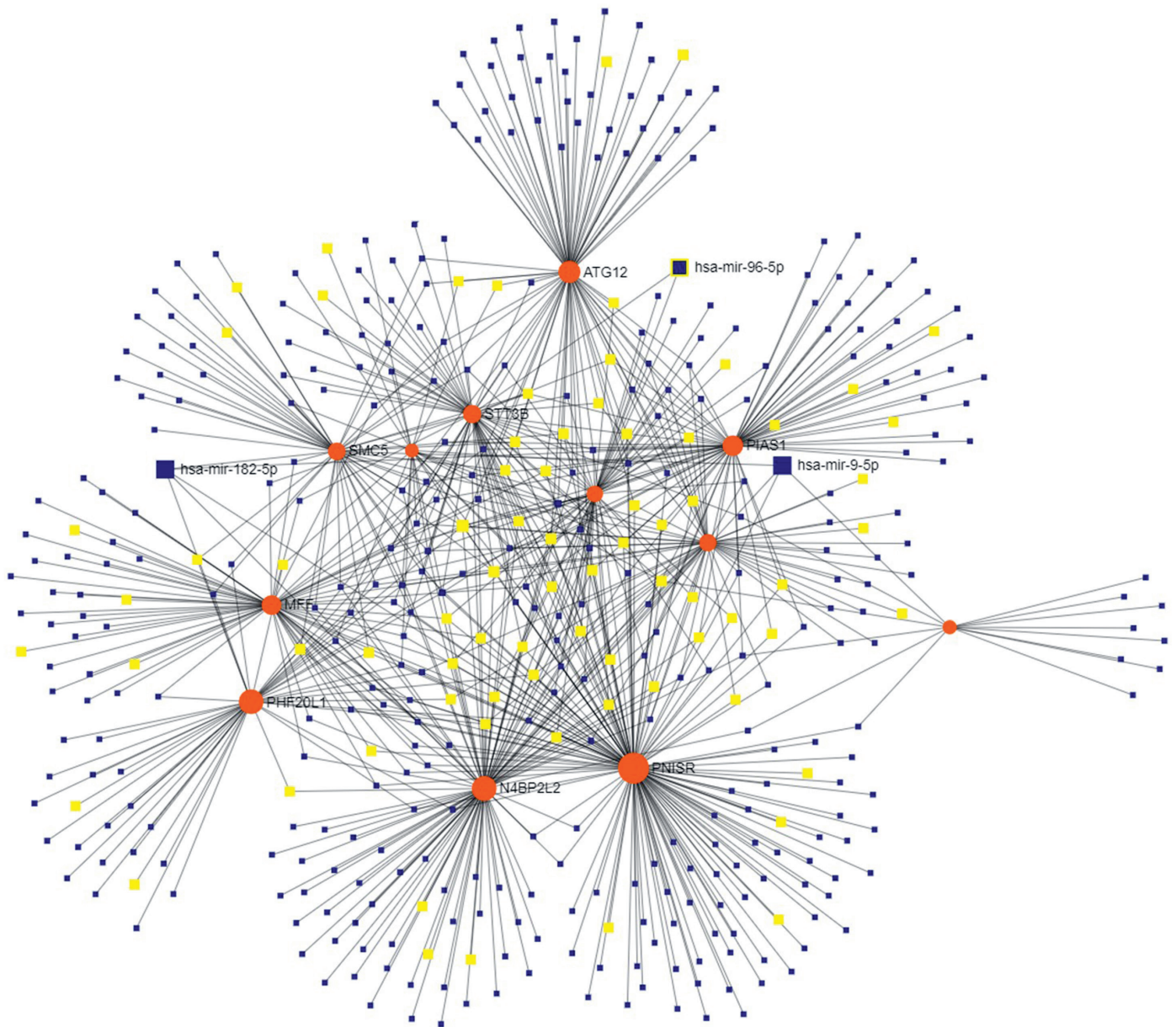
Fig. 3. Interaction miRNet of *PHF20L1* and co-expressed genes. The interactions among all co-expressed genes and associated miRNAs are shown. The red circles represent genes; the blue squares represent miRNAs. miRNAs predicted to regulate *PHF20L1* are larger squares and the yellow ones represent the miRNAs implicated in breast neoplasms (33 genes), triple-negative breast carcinoma (32 genes) or both (14 genes)

Discussion

Epigenetic readers contain diverse methyl–lysine binding motifs including PHD, chromo, Tudor, MBT, PWWP, Ank, BAH, WD40, ADD, and zn-CW domains.[25] *PHF20L1* is a reader that interacts with mono- and dimethylated lysine residues in *H3K4*, *H4K20*, *H3K27*, and *DNMT1*, due to its Tudor and PHD domains, and histone *H4K16* acetylation, due to its MYST (MOF) domain.[5,26] For example, *PHF20L1* is recruited to E2F-responsive promoters through pRb mono-methylated K810, which suggests that *PHF20L1* could participate in cell cycle progression mediating transcriptional repression.[27] *PHF20L1* is overexpressed in the aggressive subtypes basal-like and luminal B,

which have been strongly associated with shorter survival in patients with BC.[10] Thus, this gene could be a critical tethering factor regulating molecular mechanisms through methylation signals on both DNA and histones.[10] A growing body of evidence supports the epigenetic reprogramming of cancer cells as a key step in breast carcinogenesis. Teschendorff et al. found that genomic distribution of methylation is not random and is strongly enriched for binding sites of transcription factors specifying chromatin architecture.[28] We found differential methylation in *PHF20L1* promoter in the molecular subtypes basal-like and luminal A in 2 regions: -708 bp to TSS (cg5307234 probe) and -242 bp (cg27342122 probe). Basal-like, luminal A and luminal B subtypes have significant differences
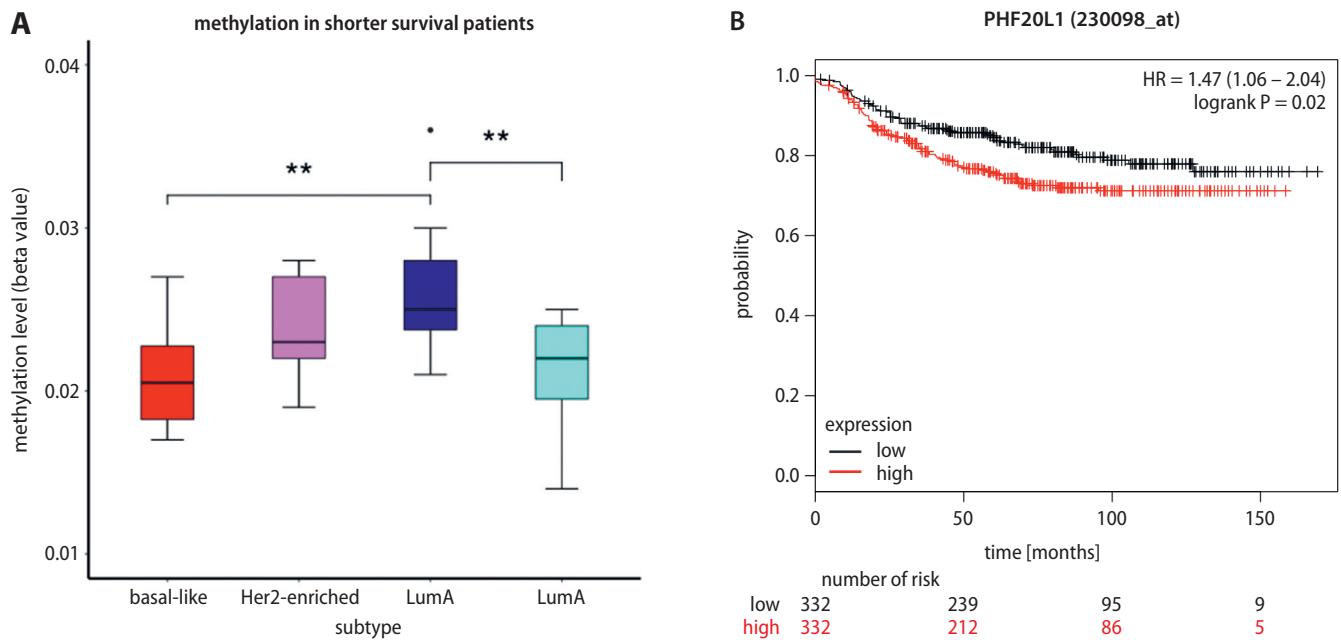
Fig. 4. Prognostic value of *PHF20L1* expression in survival. A. The relationship between mRNA expression of *PHF20L1* and survival by BC subtype (normal-like subtype was not included because it only included 1 patient); B. Kaplan–Meier distant metastasis-free survival analyses for *PHF20L1* expression in BC patients in Kaplan–Meier plotter. Value of p < 0.05, p-value was obtained from the log-rank test. See Table 2 for details of overall survival and relapse-free survival

Table 2. Prognostic value of genes co-expressed with PHF20L1 according to ONCOMINE

Gene	Location	Score*	OS p-value	RFS p-value	DMSF p-value
PHF20L1	8q24.22	–	0.24	0.88	0.02
STT3B	3p23	0.740	0.08	0.11	0.014
ZNF407	18q22.3	0.708	0.055	0.00042	0.073
PIAS1	15q23	0.654	0.008	0.002	0.18
YLPM1	14q24.3	0.654	0.09	0.081	0.94
MFF	2q36.3	0.654	0.33	0.59	0.18
PNISR	6q16.2	0.654	0.1	0.00053	0.37
PON2	7q21.3	0.654	0.2	0.021	0.077
PRKRA	2q31.2	0.654	0.95	0.026	0.042
N4BP2L2	13q13.1	0.654	0.22	0.0001	1
SMC5	9q21.12	0.631	0.9	0.0046	0.87
ATG12	5q22.3	0.631	0.62	2.9–E10	0.003

* score correlation ≥0.6; OS – overall survival; RSF – relapse free survival; DMSF – distant metastasis free survival.

in methylation in the promoter region. The methylation pattern was different inasmuch as region -708 to TSS was nearly methylated with a β value mean of 0.95 for luminal A and B subtypes, while in the -242 region both subtypes and basal-like were hypomethylated (β value of 0.023 and 0.020, respectively). Usually, promoters have sites for transcription factor binding. With aid from the TF2DNA database (http://fiserlab.org/tf2dna_db//index.html) and JASPAR CORE 2020 (http://jaspar.genereg.net/), we found that transcription factor EC (TFEC) binds to the cg5307234 region (-708 bp) and participates in regulating multiple cellular processes including survival, growth and differentiation.[29,30] The cg27342122 region (-242 bp) has sites for

binding of *GATA3*, *FOXP2* and *FOXP3* transcription factors. Of these, the transcription factor *GATA3* is relevant for its role in determination of cell identity. *GATA3* is expressed in mammary glands in the differentiated luminal epithelial cells.[31] So, differences in methylation pattern may affect the binding of transcription factors deregulating *PHF20L1* expression.

In our analysis, we found that *PHF20L1* overexpression was not related to OS in the analysis by cancer subtype except when the comparison was made only with patients with shorter survival. Similarly, hypomethylation was correlated with survival in these patients in the basal-like and luminal A and B subtypes. The luminal B subtype is distinguished

by a higher proliferative activity than luminal A and worse prognosis.[32] When we analyzed survival without grouping by subtypes and including the co-expressed genes, we found that overexpression of *PHF20L1*, *STT3B*, *PRKRA*, and *ATG12* was related to DMFS. We found that all genes overexpressed except *STT3B*, *YLPM1*, *MFF*, and *PHF20L1* are related to RSF. Interestingly, *PHF20L1* and many co-expressed genes are involved in key processes such as alternative splicing.

miRNAs have an important role in cellular regulation, and we found 3 miRNAs with a high probability to regulate *PHF20L1*: miR96-5p, miR9-5p and miR182-5p. miR96-5p may participate in epithelial–mesenchymal transition[33]; using miRNet, we found that this miRNA is involved in breast neoplasms. miR9-5p could enhance cancer stem cell-like traits of BC, but its role depends on the stage of BC, i.e., it could inhibit cell proliferation (tumor suppressor activity) or play an oncogenic role in metastasis.[34] On the other hand, miR182-5p is a key oncogenic miRNA that promotes cell proliferation and metastasis[35] and could be involved in epigenetic changes.[36] Therefore, these miRNAs might have an important role in methylation and expression changes of the *PHF20L1* gene contributing to its role in BC metastasis.

PHF20L1 is established as an important epigenetic reader whose loss could induce genome hypomethylation. For us, the use of public databases and bioinformatics tools was crucial to obtain a better picture of *PHF20L1* interactions particularly with miRNAs, which in turn are involved in a complex regulatory network affecting transcription.

Limitations

Our study has limitations. First, validation should be carried out both in vitro and in vivo to determine the clinical usefulness in patients with metastatic disease. The second limitation is the modest sample size for some analyses and the difference in our experimental approach to methylation analysis.

Conclusions

Our findings indicate that changes in methylation near TSS of the *PHF20L1* gene may influence its expression in BC subtypes and that *PHF20L1* gene overexpression affects distant metastasis-free survival in BC. Furthermore, the study suggests that miR96-5p, miR9-5p and miR182-5p target and regulate to *PHF20L1*. These results support participation of *PHF20L1* in the metastasis process.

Data availability

The database data supporting this research article is from previously reported studies and datasets, which have been cited. The data used to analyze with R software is available at the MEXPRESS website.

ORCID iDs

Jose Alfredo Sierra-Ramirez https://orcid.org/0000-0001-5060-5882
Emmanuel Seseña-Mendez https://orcid.org/0000-0002-9255-0231
Marycarmen Godinez-Victoria https://orcid.org/0000-0003-3317-7980
Marta Elena Hernandez-Caballero
　　https://orcid.org/0000-0003-4174-2118

References

1. Hamidi T, Singh AK, Chen T. Genetic alterations of DNA methylation machinery in human diseases. *Epigenomics*. 2015;7(2):247–265. doi:10.2217/epi.14.80
2. Kim Y, Tanner KG, Denu JM. A continuous, nonradioactive assay for histone acetyltransferases. *Anal Biochem*. 2000;280(2):308–314. doi:10.1006/abio.2000.4546
3. Carrozza MJ, Utley RT, Workman JL, Côté J. The diverse functions of histone acetyltransferase complexes. *Trends Genet*. 2003;19(6):321–329. doi:10.1016/S0168-9525(03)00115-X
4. Lee KK, Workman JL. Histone acetyltransferase complexes: One size doesn't fit all. *Nat Rev Mol Cell Biol*. 2007;8(4):284–295. doi:10.1038/nrm2145
5. Hou Y, Liu W, Yi X, et al. PHF20L1 as a H3K27me2 reader coordinates with transcriptional repressors to promote breast tumorigenesis. *Sci Adv*. 2020;6(16):eaaz0356. doi:10.1126/sciadv.aaz0356
6. Mendjan S, Taipale M, Kind J, et al. Nuclear pore components are involved in the transcriptional regulation of dosage compensation in *Drosophila*. *Mol Cell*. 2006;21(6):811–823. doi:10.1016/j.molcel.2006.02.007
7. Cui G, Park S, Badeaux AI, et al. PHF20 is an effector protein of p53 double lysine methylation that stabilizes and activates p53. *Nat Struct Mol Biol*. 2012;19(9):916–924. doi:10.1038/nsmb.2353
8. Wang Q, Yu M, Ma Y, et al. PHF20L1 antagonizes SOX2 proteolysis triggered by the MLL1/WDR5 complexes. *Lab Invest*. 2018;98(12):1627–1641. doi:10.1038/s41374-018-0106-8
9. Estève PO, Terragni J, Deepti K, et al. Methyllysine reader plant homeodomain (PHD) finger protein 20-like 1 (PHF20L1) antagonizes DNA (cytosine-5) methyltransferase 1 (DNMT1) proteasomal degradation. *J Biol Chem*. 2014;289(12):8277–8287. doi:10.1074/jbc.M113.525279
10. Jiang Y, Liu L, Shan W, Yang ZQ. An integrated genomic analysis of Tudor domain-containing proteins identifies PHD finger protein 20-like 1 (PHF20L1) as a candidate oncogene in breast cancer. *Mol Oncol*. 2016;10(2):292–302. doi:10.1016/j.molonc.2015.10.013
11. Lin S, Gregory RI. MicroRNA biogenesis pathways in cancer. *Nat Rev Cancer*. 2015;15(6):321–333. doi:10.1038/nrc3932
12. Borgonio-Cuadra VM, Miranda-Duarte A, Rojas-Toledo X, et al. Association between promoter hypermethylation of the DACT2 gene and tumor stages in breast cancer. *J BUON*. 2018;23(2):361–365. PMID:29745077
13. Li LC, Dahiya R. MethPrimer: Designing primers for methylation PCRs. *Bioinformatics*. 2002;18(11):1427–1431. doi:10.1093/bioinformatics/18.11.1427
14. R Core Team. R: A language and environment for statistical computing. https://www.r-project.org/. Accessed April 1, 2019.
15. Koch A, De Meyer T, Jeschke J, Van Criekinge W. MEXPRESS: Visualizing expression, DNA methylation and clinical TCGA data. *BMC Genomics*. 2015;16(1):636. doi:10.1186/s12864-015-1847-z
16. Hothorn T, Bretz F, Westfall P. Simultaneous inference in general parametric models. *Biometrical J*. 2008;50(3):346–363. doi:10.1002/bimj.200810425
17. Ogle DH, Wheeler P, Dinno A. FSA: Fisheries Stock Analysis. R package v. 0.8.25. 2019. https://github.com/droglenc/FSA. Accessed April 1, 2019.
18. Wickham H. *Ggplot2 Elegant Graphics for Data Analysis*. New York: Springer-Verlag; 2016. doi:10.1007/978-0-387-98141-3
19. Ahlmann-Eltze C. Package 'ggstatsplot'. https://www.rdocumentation.org/packages/ggsignif/versions/0.6.1. Accessed April 1, 2019.
20. Yuhao Chen XW. miRDB: An online database for prediction of functional microRNA targets. *Nucleid Acid Res*. 2020;48(D1):D127–D131. doi:10.1093/nar/gkz757
21. Tokar T, Pastrello C, Rossos AEM, et al. MirDIP 4.1: Integrative database of human microRNA target predictions. *Nucleic Acids Res*. 2018;46(D1):D360–D370. doi:10.1093/nar/gkx1144

22. Chang L, Zhou G, Soufan O, Xia J. miRNet 2.0: Network-based visual analytics for miRNA functional analysis and systems biology. *Nucleic Acids Res*. 2020;48(W1):W244–W251. doi:10.1093/nar/gkaa467

23. Therneau T. A Package for Survival Analysis in R. R package v. 3.2-7. https://CRAN.R-project.org/package=survival.

24. Györffy B, Lanczky A, Eklund AC, et al. An online survival analysis tool to rapidly assess the effect of 22,277 genes on breast cancer prognosis using microarray data of 1,809 patients. *Breast Cancer Res Treat*. 2010;123(3):725–731. doi:10.1007/s10549-009-0674-9

25. Musselman CA, Khorasanizadeh S, Kutateladze TG. Towards understanding methyllysine readout. *Biochim Biophys Acta Gene Regul Mech*. 2014;1839(8):686–693. doi:10.1016/j.bbagrm.2014.04.001

26. Avvakumov N, Côté J. The MYST family of histone acetyltransferases and their intimate links to cancer. *Oncogene*. 2007;26(37):5395–5407. doi:10.1038/sj.onc.1210608

27. Carr SM, Munro S, Sagum CA, Fedorov O, Bedford MT, La Thangue NB. Tudor-domain protein PHF20L1 reads lysine methylated retinoblastoma tumour suppressor protein. *Cell Death Differ*. 2017;24(12):2139–2149. doi:10.1038/cdd.2017.135

28. Teschendorff AE, Gao Y, Jones A, et al. DNA methylation outliers in normal breast tissue identify field defects that are enriched in cancer. *Nat Commun*. 2016;7:10478. doi:10.1038/ncomms10478

29. Zhao GQ, Zhao Q, Zhou X, Mattei MG, de Crombrugghe B. TFEC, a basic helix-loop-helix protein, forms heterodimers with TFE3 and inhibits TFE3-dependent transcription activation. *Mol Cell Biol*. 1993; 13(8):4505–4512. doi:10.1128/mcb.13.8.4505

30. Haq R, Fisher DE. Biology and clinical relevance of the micropthalmia family of transcription factors in human cancer. *J Clin Oncol*. 2011; 29(25):3474–3482. doi:10.1200/JCO.2010.32.6223

31. Asselin-Labat ML, Sutherland KD, Barker H, et al. Gata-3 is an essential regulator of mammary-gland morphogenesis and luminal-cell differentiation. *Nat Cell Biol*. 2007;9(2):201–209. doi:10.1038/ncb1530

32. Prat A, Pineda E, Adamo B, et al. Clinical implications of the intrinsic molecular subtypes of breast cancer. *Breast*. 2015;24(Suppl 2):S26–S35. doi:10.1016/j.breast.2015.07.008

33. Anderson O, Guttilla Reed IK. Regulation of cell growth and migration by miR-96 and miR-183 in a breast cancer model of epithelial-mesenchymal transition. *PLoS One*. 2020;15(5):e0233187. doi:10.1371/journal.pone.0233187

34. Li X, Zeng Z, Wang J, et al. MicroRNA-9 and breast cancer. *Biomed Pharmacother*. 2020;122:109687. doi:10.1016/j.biopha.2019.109687

35. Shah NR, Chen H. MicroRNAs in pathogenesis of breast cancer: Implications in diagnosis and treatment. *World J Clin Oncol*. 2014;5(2):48–60. doi:10.5306/wjco.v5.i2.48

36. Li Q, Zhu F, Chen P. MiR-7 and miR-218 epigenetically control tumor suppressor genes RASSF1A and claudin-6 by targeting HoxB3 in breast cancer. *Biochem Biophys Res Commun*. 2012;424(1):28–33. doi:10.1016/j.bbrc.2012.06.028

Crocin attenuates oxidative and inflammatory stress-related periodontitis in cardiac tissues in rats

Gulhan Kocaman[1,A,E,F], Eyup Altinoz[2,B–D], Mehmet Erman Erdemli[3,B,C], Mehmet Gul[4,C],
Zeynep Erdemli[3,C], Emrah Zayman[4,C], Harika Gozde Gozukara Bag[5,C], Tugba Aydın[6,E]

[1] Department of Periodontology, Faculty of Dentistry, Karabuk University, Turkey

[2] Department of Medical Biochemistry, Faculty of Medicine, Karabuk University, Turkey

[3] Department of Medical Biochemistry, Faculty of Medicine, Inonu University, Malatya, Turkey

[4] Department of Histology and Embryology, Faculty of Medicine, Inonu University, Malatya, Turkey

[5] Department of Biostatistics, Faculty of Medicine, Inonu University, Malatya, Turkey

[6] Department of Periodontology, Faculty of Dentistry, Ataturk University, Erzurum, Turkey

A – research concept and design; B – collection and/or assembly of data; C – data analysis and interpretation;
D – writing the article; E – critical revision of the article; F – final approval of the article

Abstract

Background. Periodontitis, a chronic inflammatory disease affecting the supporting tissues around the teeth, causes significant inflammatory and oxidative changes in cardiac tissue. Crocin is the active constituent of *Crocus sativus* (saffron) which has antioxidant properties and is protective against cardiovascular disturbances.

Objectives. The present study aimed to investigate the protective effects of crocin on periodontitis-induced oxidative/inflammatory cardiac degeneration in rats in vivo.

Materials and methods. Thirty female Sprague Dawley rats were randomly divided into 3 groups: control group, periodontitis group (PD) and periodonditis plus crocin group (PD+Cr). Experimental periodontitis was induced by placing silk ligatures on the maxillary second molar teeth for 30 days. Afterward, crocin (100 mg/kg body weight/day) was administered to the PD+Cr group and saline was administered to the PD group and the control group for 15 days. The subjects were sacrificed on the 45th day.

Results. Histological and biochemical analyses demonstrated that inducing periodontitis caused obvious damage to cardiac tissues which was significantly ameliorated by crocin ($p < 0.05$). Significant improvements in bone resorption parameters (cross-linked C-telopeptide of type I collagen and bone alkaline phosphatase) were also observed in the PD+Cr group ($p < 0.05$). In addition, crocin caused significant reductions of malondialdehyde levels and total oxidant score while antioxidant levels (glutathione, superoxide dismutase, total antioxidant score, and catalase) were significantly higher in PD+Cr group ($p < 0.05$).

Conclusions. This study reveals that periodontitis may cause oxidative damage in cardiac tissue and crocin improves periodontitis-induced degenerative changes in heart tissue, which is associated with its antioxidant properties.

Key words: periodontitis, inflammation, antioxidants, crocin, heart

Background

Oxidative stress results from changes in the balance between reactive oxygen species (ROS) and antioxidant capacity.[1] The ROS overproduction causes irreversible damage to biomolecules (such as membrane lipids, proteins and DNA) that are crucial to tissue and cellular function.[2] One of the most important health conditions affected by oxidative stress is cardiac failure. While myocardial antioxidants such as superoxide dismutase (SOD), catalase (CAT), glutathione peroxidase (GSH-Px), and vitamin E decrease in the heart tissue of patients with heart failure, free oxygen radicals and oxidative stress increase.[3] The ROS disrupt the contractile functions of the myocardium by directly affecting the proteins responsible for contraction–excitation coupling. They activate kinase signaling in hypertrophy and disrupt extracellular matrix remodeling by initiating matrix metalloproteases (MMPs).[4] Periodontal disease, associated with chronic inflammation, is characterized by high amounts of ROS, which cause increased oxidative damage in gingival tissue, periodontal ligaments and alveolar bone.[5]

The significant increase in cardiac oxidative stress caused by periodontitis is reportedly attributable to an excessive increase in ROS production rather than decreased antioxidant capacity. Moreover, cardiac oxidative stress associated with periodontitis may contribute to the pathological process leading to heart failure.[6] It has often been suggested that antioxidants limit oxidative damage in humans, thereby reducing the risk of some chronic health conditions, such as cardiovascular disease (CVD).[7]

Since ancient times, saffron (*Crocus sativus L.*) has been widely used as a spice, food colorant and alternative medicine to treat some diseases. In addition to the 3 main ingredients, crocin, crocetin and safranal, dried saffron contains almost 150 components including carotenoids, sugars, proteins, anthocyanins, vitamins, and minerals. Besides its strong antioxidant properties, saffron is used as a natural/traditional medicine for disease treatment due to its anti-inflammatory, anti-carcinogenic and antioxidant effects.[8] Carotenoids from saffron are free radical scavengers, especially against superoxide anions,[9] and could thus prevent oxidative damage. A considerable amount of evidence shows that crocin can effectively improve CVDs such as atherosclerosis, hyperlipidemia, hypertension, and myocardial injury.[10]

Experimental studies show that periodontitis, a chronic, systemic disease characterized by low-grade inflammation and oxidative stress, causes significant inflammatory and oxidative changes in cardiac tissue.[6,11] Although the cardioprotective effect of crocin is well known, information about its protective effects on periodontitis-related cardiac alterations is lacking.

Objectives

This study aimed to investigate the potential effects of periodontitis on the oxidative stress levels in cardiac tissue and the therapeutic activity of systemic crocin administration in such cases.

Materials and methods

Animals and experimental design

Thirty adult female Sprague Dawley rats weighing between 225 g and 250 g were used in this study. The rats were obtained from the Inonu University, Experimental Animals Production and Research Centre (INUTF-DEHUM), Malatya, Turkey. This study was authorized by the Inonu University Experimental Animals Ethics Committee. All experimental procedures were carried out at INUTF-DEHUM. The rats were housed in a room at 21°C, with 55–60% humidity and a 12 h light (08:00–20:00)–12 h dark (20:00–08:00) cycle. The rats consumed a soft diet ad libitum throughout the study period. Cage maintenance and drinking water changes were performed daily.

First, the experimental animals were deeply anesthetized by xylazine and ketamine to induce a periodontitis model. The maxillary right second molar teeth were enclosed with silk suture 5-0 and tied to the vestibule teeth. This ligature encompassing the molar teeth promoted bacterial accumulation, which led to inflammation and bone loss. After 30 days, the ligatures were discarded to permit a decrease in inflammation and allow healing. All rats were inspected for the development of periodontitis.[12]

The rats were randomly divided into 3 groups with 10 rats in each group. The control group received normal saline orally throughout the study. The periodontal disease (PD) group received normal saline orally following removal of the ligature. The periodontal disease plus crocin (PD+Cr) group received 100 mg/kg/day of crocin (Sigma-Aldrich, St. Louis, USA) orally following removal of the ligature.[13] The crocin was dissolved in normal saline and administered over 15 days to the rats in the PD+Cr group. Both the control and PD group received 1 mL of normal saline for 15 days. All animals were anesthetized with xylazine and ketamine, and heart tissue and 5 mL of blood were collected from their abdominal veins.

Samples

The heart tissue samples collected from all of the animals were used for biochemical and histological evaluations. The samples were washed with saline and divided into halves. The fragments of the 1st half were fixed in 10% formaldehyde, and those of the 2nd half were stored

at −80°C until biochemical analyses were performed. Serum samples were obtained from the blood samples via centrifuging at 600 × g for 20 min. Moreover, the right maxillary alveolar bones of the rats belonging to all groups were collected for histopathological examination to prove experimental periodontitis.

Biochemistry

Stored tissue samples were thawed and weighed just before the analyses. The tissues were mixed with phosphate buffer and homogenized for 1–2 min on ice at 12,000 rpm (IKA Ultra Turrax T-25 basic; IKA Labotechnik, Staufen, Germany) to procure 10% homogenates. Malondialdehyde (MDA) levels were measured in the homogenate, and the remaining was centrifuged at 600 × g for 30 min at 4°C to obtain a supernatant. All other biochemical analyses were conducted on the supernatant. Cross-linked C-telopeptide of type I collagen (CTx1), bone alkaline phosphatase (b-ALP), lactate dehydrogenase (LDH), and creatine kinase myocardial band (CK-MB) analyses were performed on the serum samples.

Measurement of tissue MDA levels

The MDA analyses were performed as described previously.[14] The tissue homogenate was mixed with 1% H_3PO_4 and 0.6% thiobarbituric acid, and the mixture was incubated in a boiling water bath for 45 min. Then, the mixture was extracted with n-butanol. The pink product was measured at 535 nm with a spectrophotometer (T80 UV/vis spectrometer; PG Instruments Ltd., Leicestershire, UK) and used to calculate the MDA level. The n-butanol was used as the blind, and tetramethoxypropane was used as the standard. The findings were noted as nM/g wet tissue (gwt).

Measurement of tissue glutathione levels

The glutathione (GSH) levels were measured as described previously.[15] 5,5'-dithiobis 2-nitrobenzoic acid (DTNB) was added to the supernatants, and a yellow-green color was observed. The colored product was measured at 410 nm and used to calculate the GSH level. Distilled water was used as the blank. The results were noted as nM/gwt.

Measurement of tissue SOD activity

The SOD activities were determined as described previously.[16] The supernatants were mixed with xanthine oxidase and an assay reagent mixture to expose the superoxide radicals to xanthine-xanthine oxidase, which generates a blue-colored formazan. Next, the SOD activities were measured at 560 nm and recorded as U/g protein.

Measurement of tissue CAT activity

The CAT activities were determined as previously described.[17] The supernatants were mixed with phosphate buffer (pH: 7.5 mM) containing H_2O_2. The CAT in the supernatant breaks down H_2O_2 into H_2O and O_2, which reduces the absorbance at 240 nm. The reduction in absorbance was observed for 1 min to calculate the enzyme activity. The CAT activities were noted as K/g protein.

Measurement of tissue total oxidant status

The total oxidant status (TOS) was ascertained using Erel's method.[18] A commercially-available TOS kit (Rel Assay Diagnostics, Gaziantep, Turkey) was utilized according to the manufacturer's instructions. An enzyme-linked immunosorbent assay (ELISA) reader was used to measure TOS at 25°C and 530 nm. The data were presented as μM H_2O_2 equiv/L.

Measurement of tissue total antioxidant status

The total antioxidant status (TAS) was ascertained using Erel's method.[19] A commercially-available TAS kit (Rel Assay Diagnostics) was utilized according to the manufacturer's instructions. Following preparation of the samples, absorptions were measured at 660 nm. The data were presented as mM Trolox equiv/L.

Measurement of serum CTx1 and b-ALP levels

Serum CTx1 and b-ALP concentrations were measured using a commercially-available, rat-specific CTx1 ELISA kit (Elabscience, Houston, USA) and a rat-specific b-ALP ELISA kit (Elabscience) according to the manufacturer's instructions at 37°C and 450 nm. The results were noted as ng/mL.

Measurement of serum CK-MB and LDH levels

Serum LDH and CK-MB were measured via commercially-available Architect c1600 automatic analyzer kits (Abbott, Abbott Park, USA). The results were noted as U/L.

Histopathology

For 48 h, the heart tissue samples were fixed in 10% neutral-buffered formaldehyde. The maxillary bone was fixed and decalcified in a 50% RDO (R) solution (Apex Engineering Products Corporation, Aurora, USA) for 12 h. Following dehydration in ethanol series (50–99%) and clearing

in xylene series, both tissues were embedded in paraffin wax. Five sections of 6 μm thickness each were taken from each paraffin block at 100 μm intervals. The sections were placed on slides and stained with hematoxylin and eosin (H&E). All of the sections were examined with ×20, ×40 and ×100 magnification objective lenses of light 203 microscopes (Nikon Eclipse Ni-U; Nikon Corp., Tokyo, Japan) with a camera attachment (Nikon DS-Fi2; Nikon Corp.), and 204 microscopic images were evaluated using an image analysis system (Nikon NIS-Elements Documentation 205 5.02; Nikon Corp.).

Histological alterations of the cardiomyocytes, in terms of order and integrity, vacuolization, hyalinization, and nuclear pyknosis, were scored on a semi-quantitative scale of 0–3 (normal – 0, minimal changes – 1, moderate changes – 2, and severe changes – 3). The prevalence of each degree of these findings was scored as "1" (<10%), "2" (11%–20%), "3" (21%–40%), or "4" (>40%). Total histologic damage scores were obtained by multiplying the scores of the histological alterations with the prevalence degree scores. The scoring system described by Ziebolz et al.[20] was modified and used. The maximum total score was 48.

Statistical analyses

Statistical analyses were performed using IBM SPSS Statistics for Windows v. 22.0 (IBM Corp., Armonk, USA). The Shapiro–Wilk test was used to assess data normality. The findings were summarized as the mean and standard deviation (SD). The homogeneity of the variances was analyzed using the Levene's test. Groups with homogeneous variances were evaluated with one-way analysis of variance (ANOVA) and the Tukey's honestly significant difference post hoc method. The Welch test and the Tamhane T2 pairwise comparison method were used for groups with heterogeneous variances. The histological scorings were presented as median, minimum and maximum values. The groups were compared with the Kruskal–Wallis test and the Conover pairwise comparison method. In all analyses, p-value <0.05 was considered significant.

Results

Biochemistry

The oxidant/antioxidant ratios within the heart tissues are listed in Table 1. The MDA level in rats with induced periodontitis showed an insignificant elevation compared to the control group. However, following the crocin treatment, the MDA levels decreased notably and were close to those in the control group (p < 0.05). Moreover, the TOS levels in the PD group were significantly elevated compared to those in the control group and the PD+Cr group (p < 0.05). On the other hand, the PD+Cr group showed significantly lower TOS levels compared to the PD group (p < 0.05). In contrast, non-enzymatic antioxidants, GSH levels, enzymatic antioxidants, and SOD and CAT enzyme activities were significantly reduced in the heart tissue of the rats with induced periodontitis compared to the tissues of both the control group and PD+Cr group (p < 0.05). Furthermore, the crocin treatment significantly elevated them compared to the corresponding value for the PD group (p < 0.05). While the TAS of the heart tissue was significantly decreased in both the PD and PD+Cr groups compared to the control groups (p < 0.05), it was significantly elevated in the PD+Cr compared to the PD group (p < 0.05).

The results of the biochemical analyses showing serum bone destruction and heart tissue injury indicators appear in Table 2. While periodontitis induction significantly elevated serum CTx1 levels in the control group and the PD+Cr group (p < 0.05), the serum b-ALP levels decreased significantly (p < 0.05). Following crocin treatment, both the CTx1 and b-ALP levels were significantly ameliorated compared to those of the PD group (p < 0.05). Moreover, while significant elevations were observed in the LDH and CK-MB levels of the PD group (p < 0.05) following the crocin treatment, they decreased slightly compared to the PD group.

Histopathology

The heart tissue sections of the control group were observed to have a normal histological structure. No

Table 1. Oxidant/antioxidant parameters of heart tissue

Group	MDA [nmol/gwt]	GSH [nmol/gwt]	SOD [U/g protein]	CAT [K/g protein]	TAS [mmol/L]	TOS [μmol/L]
Control	441.38 ±39.67[a,b]	1241.13 ±32.09[a]	71.01 ±5.00[a]	11.33 ±2.65[a]	2.21 ±0.08[a]	2.42 ±0.24[a]
PD	669.50 ±207.52[a]	1170.13 ±25.23[b]	24.92 ±3.86[b]	2.64 ±1.24[b]	1.24 ±0.03[b]	14.7 ±1.91[b]
PD+Cr	422.00 ±80.54[b]	1247.75 ±49.85[a]	60.20 ±5.59[c]	8.28 ±2.94[c]	1.55 ±0.10[c]	8.06 ±0.86[c]
p-value	0.032	0.001	<0.001	<0.001	<0.001	<0.001

Data are expressed as means ± standard deviation (SD) (n = 10). MDA – malondialdehyde; GSH – reduced glutathione; SOD – superoxide dismutase; CAT – catalase; TAS – total antioxidant status; TOS – total oxidant status; gwt – gram wet tissue. Groups: control group received normal saline solution, periodontitis (PD) group received normal saline solution and periodontitis plus crocin (PD+Cr) group received crocin. Statistically significant differences between groups are denoted with different superscript letters (p < 0.05).

Table 2. Biochemical analysis of serum markers related to bone resolution and cardiac injury

Groups	CTx1 [ng/mL]	b-ALP [ng/mL]	LDH [U/L]	CK-MB [U/L]
C	4.19 ±0.24[a]	1.72 ±0.25[a]	176.38 ±42.66[a]	191.84 ±40.69[a]
PD	8.53 ±1.08[b]	0.55 ±0.09[b]	345.50 ±154.25[b]	280.63 ±84.46[b]
PD+Cr	5.91 ±0.86[c]	1.04 ±0.20[c]	208.38 ±111.28[a,b]	251.00 ±67.86[a,b]
p-value	<0.001	<0.001	0.041	0.032

Data are expressed as means ± standard deviation (SD) (n = 10). CTx1 – cross-linked C-telopeptide of type I collagen; b-ALP – bone-specific alkaline phosphatase; LDH – lactate dehydrogenase; CK-MB – heart-specific creatine kinase. Groups: control group received normal saline solution, periodontitis (PD) group received normal saline solution and periodontitis plus crocin (PD+Cr) group received crocin. Statistically significant differences between groups are denoted with different superscript letters (p < 0.05).

cardiomyocyte damage was detected in the cardiac tissue sections of the control group rats. The cardiomyocytes in the heart tissue sections of these rats showed typical cardiomyocyte order and integrity upon microscopic examination (Fig. 1A–C).

The heart section evaluations of the PD group indicated different cardiomyocyte prevalence and degrees of disorganization and deformity, hyalinization, intracytoplasmic vacuolization, and nuclear pyknosis (Fig. 1D–F). The total histological damage score of this group was determined
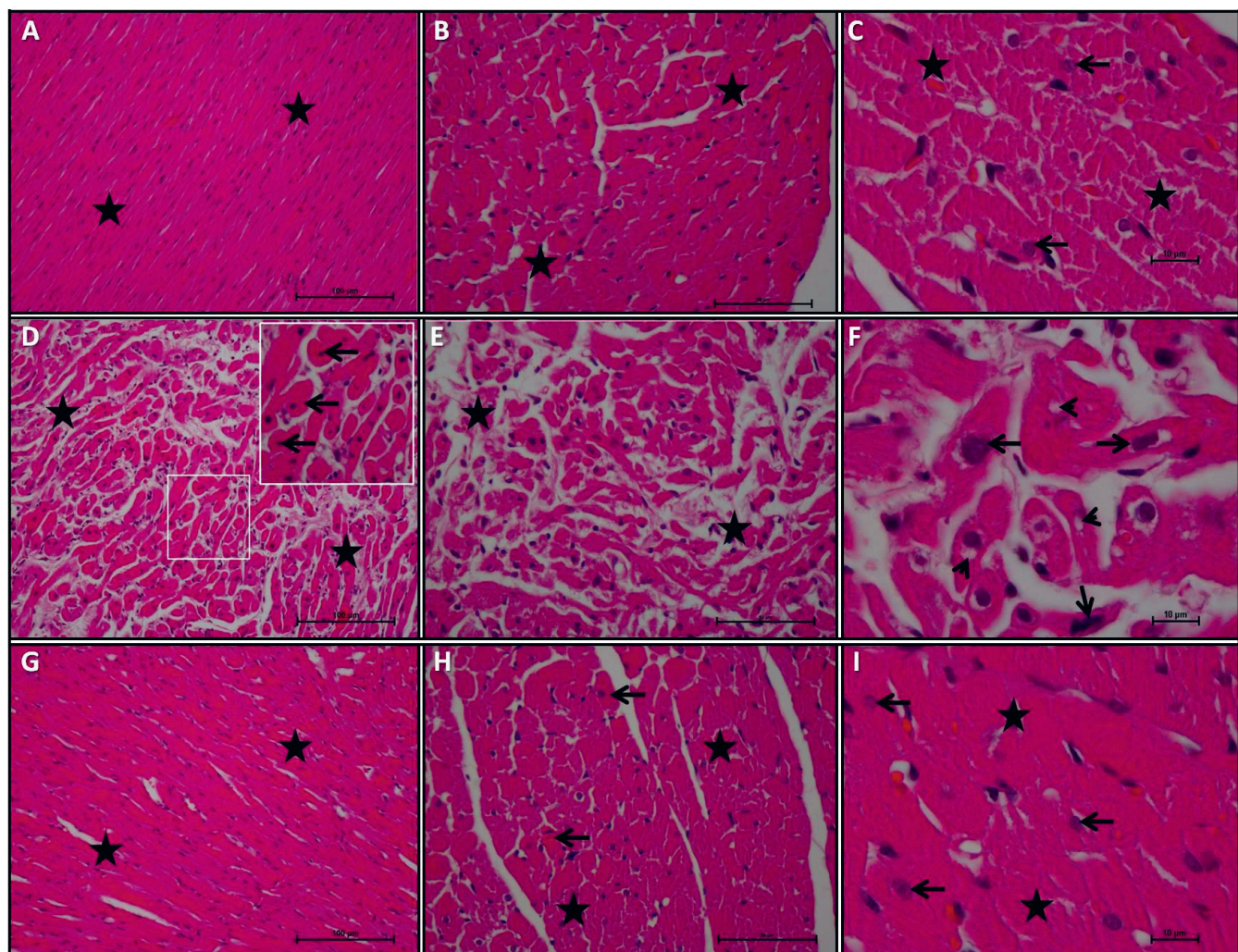
Fig. 1. Cardiac photomicrographs. A–C. Control group – myocardium layer. Cardiomyocytes with normal histological appearance at the transverse section plane (asterisk), cardiomyocyte nuclei (arrow). A. H&E staining, ×20 magnification; B: H&E staining, ×40 magnification; C: H&E staining, ×100 magnification. D–F. PD group – myocardium layer. Shape and organization disorder in cardiomyocytes (asterisk), pyknotic nuclei and hyalinization in cardiomyocytes (arrow), intracytoplasmic vacuoles in cardiomyocytes (arrowhead); D. H&E staining; large figure ×20 magnification, small figure ×40 magnification; E. H&E staining, ×40 magnification; F. H&E staining, ×100 magnification; G–I. PD+Cr group – myocardium layer at longitudinal section plane (asterisk), minimal cytoplasmic hyalinization and pyknotic nuclei in cardiomyocytes (arrow); G. H&E staining, ×20 magnification; H. H&E staining, ×40 magnification; I. H&E staining, ×100 magnification

Table 3. Cardiac tissue damage scores

Groups	Cardiomyocytes order and integrity	Intracytoplasmic vacuolization	Hyalinization	Nuclear pyknosis	Total scores
C	0 (0–0) [a]	0 (0–0) [a]	0 (0–0) [a]	0 (0–0) [a]	0 (0–0) [a]
PD	4 (2–6) [b]	4 (1–6) [b]	2 (1–4) [b]	2 (1–4) [b]	12 (7–15) [b]
PD+Cr	1 (0–2) [c]	0 (0–2) [c]	1 (0–2) [c]	1 (0–2) [c]	3 (2–4) [c]
p-value	<0.001	<0.001	0.0016	<0.001	<0.001

Data are expressed as min–max (n = 10). Groups: control group received normal saline solution, periodontitis (PD) group received normal saline solution and periodontitis plus crocin (PD+Cr) group received crocin. Statistically significant differences between groups are denoted with different superscript letters (p < 0.05).
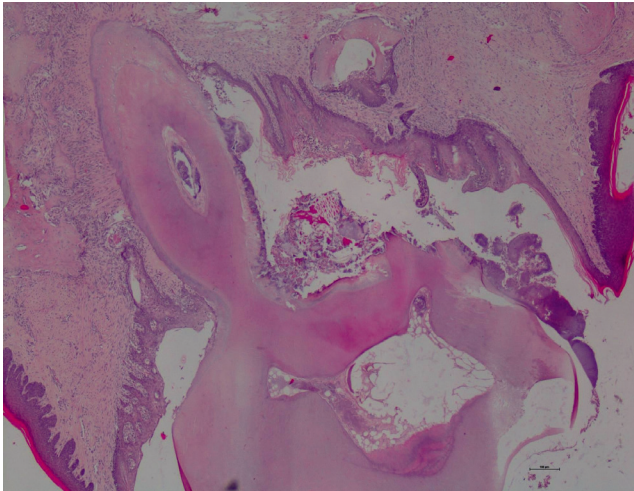
Fig. 2. Gingival photomicrograph

to be 12. The cardiac tissue damage scores are presented in Table 3.

The PD+Cr group showed significant decreases in all damage parameters compared to the PD group (Fig. 1G–I). The total histological damage score of the PD+Cr group was determined to be 3.

Figure 2 presents the histopathology of the gingiva tissue of a rat in the PD group. Inflammatory cell infiltration of the connective tissue epithelium and degeneration of the gingival epithelium were observed. Inflammatory cell infiltration in the fibrous connective tissue and degeneration sites in the periodontal ligament were defined. The cementum and alveolar bone surfaces were irregular due to several Howship's lacunae with differently-sized osteoclastic activity sites towards the periodontal ligament, and the histological images reflected increased bone resorption.

Discussion

The ROS, which play an important role in the pathogenesis of periodontitis, are caused either by the oral bacteria themselves or the stimulated immune response. Furthermore, polymorphonuclear leukocytes, the main protective cells against oral pathogenic bacteria, are responsible for the formation of ROS during phagocytosis.[5] In this study, bone resorption and inflammatory alterations were evaluated via a comparison of the serum CTx1 and b-ALP levels. Arabacı et al.[12] showed that serum b-ALP levels were significantly elevated in their periodontitis-induced group after melatonin treatment. Similarly, our study revealed that b-ALP levels, which reflect bone destruction induced by periodontitis, were significantly elevated following crocin treatment. The CTx1 released during bone resorption is one of the most widely studied and utilized bone resorption markers.[21] Some studies reported that an elevated serum CTx1 level in periodontitis is an indicator of bone destruction, and previous studies showed that serum CTx1 levels are higher in rats with periodontitis.[22,23] In this research, serum CTx1 levels were higher in the PD group compared to the control group and the PD+Cr group, which confirms the findings of previous research and suggests that elevated serum CTx1 levels are related to alveolar bone loss in periodontitis.[23] Moreover, the lower CTx1 level of the PD+Cr group compared to that of the PD group indicates that crocin exhibits its modulating effects on the bone cycle by repressing oxidative stress.

Periodontal disease is initiated by production of inflammatory mediators. These processes lead to loss of periodontal tissue structure and function. Pathogenic bacterial infections play a role in susceptibility to ROS and oxidative stress. Periodontal inflammation is a risk factor for systemic inflammation and eventually CVD. Therefore, 2 common hypotheses are proposed regarding the relationship between periodontitis and CVD: 1) bacteria may affect the vascular system directly[24]; or (2) local inflammation in the periodontal tissues may induce an inflammatory response in distant regions even without the dispersion of the infectious agent.[25] Prior findings support the latter hypothesis, and oxidative stress generated due to periodontitis may initiate the inflammatory damage that occurs in the early stages of atherosclerosis.[26] Furthermore, the systemic inflammation induced by periodontitis may accelerate atherosclerotic vascular damage and plaque rupture. Therefore, periodontitis, rather than a co-existing condition, is likely to cause CVD. Moreover, in this study, periodontal infection/inflammation may have directly or indirectly induced pathological alterations in the heart tissue and thus played a role in cardiac injury.

Neutrophils are responsible for the initiation of inflammation. The oxidative killing mechanisms of neutrophils

involve ROS production.[5] Although ROS essentially aim to eliminate bacteria, since they are dispersed to external tissues, they also destroy periodontal tissues. Moreover, they play a role in the pathogeneses of some inflammatory diseases, such as heart and vascular diseases.[27] Lipid peroxidation might play an important role in the onset of CVD, especially in the earliest periods.[28] A study on cardiac failure patients reported decreased serum GSH levels and increased serum MDA levels compared to a control group.[29] Conversely, while lipid peroxidation plays a role in CVD development, antioxidants protect against low-density lipoprotein (LDL) oxidation by clearing ROS.[30] Vitamin C may also contribute to the amelioration of atherosclerosis by reducing lipid peroxidation and elevating antioxidant levels. Moreover, another antioxidant, epigallocatechin gallate, reportedly improved the serum lipid profile and cardiac tissue antioxidant parameters in a rat atherosclerosis model.[31]

The most recent pharmacological studies provide some evidence on the potential of crocin as a therapeutic medicine due to its anti-tumoral, antioxidant and free-radical scavenging activities.[9] Antioxidants play a significant role in protecting against free radical-induced tissue injury by scavenging free radicals. Although the mechanism behind the free-radical scavenging effects of crocin as a water-soluble carotenoid is not clear, it is assumed that the mechanistic pathways may be similar to those of known carotenoids. Therefore, crocin may possibly modulate intracellular oxidative stress by regulating the enzymatic antioxidants of the organism when transported to the plasma. It is also reported to have a dose-dependent cytoprotective effect against the endothelial cell damage induced by H_2O_2.[32]

Some studies show that saffron has beneficial effects on CVD treatment.[10] Furthermore, the cardioprotective effects of saffron and its active constituents have been demonstrated in various models. Wang et al.[33] reported that crocin improves cardiac function after myocardial infarction, which in turn increases angiogenesis and myogenesis in the infarcted myocardium. The results of an in vivo rat study by Diana et al.[34] provided evidence that application of crocin is protective against cardiac dysfunction by exposure to cigarette smoke. Rahiman et al.[35] showed that crocin reduces ROS and protects against oxidative stress in H_2O_2-treated bovine aortic endothelial cells. Xu et al.[32] reported that crocin treatment inhibits atherosclerosis and regression by preventing cell apoptosis. Moreover, He et al.[36] used an animal atherosclerosis model to show that crocin treatment significantly decreases cholesterol, triglyceride and low-density lipoprotein (LDL) levels and restricts aortic plaque formation by decreasing endothelial cell apoptosis. Recently, crocin was found to have a protective effect on the vascular system against diazinon-related apoptosis via inhibition of caspase-dependent apoptosis in rat aortic tissue.[37] Oxidative stress and excessive free radical generation are the main stimuli

that induce apoptosis in some diseases, including CVDs. Feidantsis et al.[38] reported that crocin improved heart function in diabetic rats by enhancing the heat shock response, inhibiting apoptosis and normalizing autophagy in cells of the cardiac myocardium. Razavi et al.[39] showed that crocin decreases the Bax/Bcl-2 ratio, release of cytochrome c and caspase-3 activation, thereby demonstrating protective effects against diazinon-related cardiotoxicity by decreasing lipid peroxidation, histopathological alterations and apoptosis. The results of this study revealed that the elevated MDA and TOS levels in the heart tissue of rats with periodontitis can be lowered with crocin treatment. Moreover, crocin treatment following periodontitis induction ameliorated the decline in antioxidants (GSH, TAS, SOD, and CAT) within the heart tissue. The chemical and biological features of crocin manifest its antioxidant and free radical-scavenging properties.[8]

Limitations

The present study has some limitations. Firstly, the study results are not sufficient to suggest a direct relationship between human periodontitis and the short-term outcomes of an experimental periodontitis model. Secondly, study subjects are restricted to female-only rats; therefore, our results are insufficient to make a conclusion for both sexes. Thus, cardiac damage caused by periodontal inflammation and the damage-limiting effects of crocin should be studied more comprehensively and at the ventricular level in both sexes.

Conclusions

Periodontitis is a chronic systemic inflammatory disease and has the potential to increase the risk of cardiac damage/degeneration by causing a significant increase in oxidative damage markers in cardiac tissue. Crocin is an important adjunctive therapeutic agent to mitigate potential cardiac structural damage induced by periodontitis-related inflammation and oxidative damage.

ORCID iDs

Gulhan Kocaman https://orcid.org/0000-0002-8920-2391
Eyup Altinoz https://orcid.org/0000-0002-3991-9773
Mehmet Erman Erdemli https://orcid.org/0000-0003-4596-7525
Mehmet Gul https://orcid.org/0000-0002-5721-8778
Zeynep Erdemli https://orcid.org/0000-0002-9002-6604
Emrah Zayman https://orcid.org/0000-0002-6578-3371
Harika Gozde Gozukara Bag https://orcid.org/0000-0003-1208-4072
Tugba Aydın https://orcid.org/0000-0002-8497-7753

References

1. Chapple IL, Matthews JB. The role of reactive oxygen and antioxidant species in periodontal tissue destruction. *Periodontol 2000.* 2007;43:160–232. doi:10.1111/j.1600-0757.2006.00178.x
2. Chapple I, Brock G, Milward M, Ling N, Matthews J. Compromised GCF total antioxidant capacity in periodontitis: Cause or effect? *J Clin Periodontol.* 2007;34(2):103–110. doi:10.1111/j.1600-051X.2006.01029.x

3. Hill MF, Singal PK. Antioxidant and oxidative stress changes during heart failure subsequent to myocardial infarction in rats. *Am J Pathol*. 1996;148(1):291–300. PMID:8546218

4. Cadenas S. ROS and redox signaling in myocardial ischemia-reperfusion injury and cardioprotection. *Free Radic Biol Med*. 2018;117:76–89. doi:10.1016/j.freeradbiomed.2018.01.024

5. Wang Y, Andrukhov O, Rausch-Fan X. Oxidative stress and antioxidant system in periodontitis. *Front Physiol*. 2017;8:910. doi:10.3389/fphys.2017.00910

6. Köse O, Arabacı T, Gedikli S, et al. Biochemical and histopathologic analysis of the effects of periodontitis on left ventricular heart tissues of rats. *J Periodontal Res*. 2017;52(2):176–185. doi:10.1111/jre.12380

7. Neha K, Haider MR, Pathak A, Yar MS. Medicinal prospects of antioxidants: A review. *Eur J Med Chem*. 2019;178:687–704. doi:10.1016/j.ejmech.2019.06.010

8. Rios J, Recio M, Giner R, Manez S. An update review of saffron and its active constituents. *Phytother Res*. 1996;10(3):189–193. doi:10.1002/(SICI)1099-1573(199605)10:3<189::AID-PTR754>3.0.CO;2-C

9. Erben-Russ M, Michel C, Bors W, Saran M. The reaction of sulfite radical anion with nucleic acid components. *Free Radic Res Commun*. 1987;2(4–6):285–288. doi:10.3109/10715768709065293

10. Alavizadeh SH, Hosseinzadeh H. Bioactivity assessment and toxicity of crocin: A comprehensive review. *Food Chem Toxicol*. 2014;64:65–80. doi:10.1016/j.fct.2013.11.016

11. Köse O, Arabacı T, Yemenoglu H, et al. Influence of experimental periodontitis on cardiac oxidative stress in rats: A biochemical and histomorphometric study. *J Periodontal Res*. 2017;52(3):603–608. doi:10.1111/jre.12428

12. Arabacı T, Kermen E, Özkanlar S, et al. Therapeutic effects of melatonin on alveolar bone resorption after experimental periodontitis in rats: A biochemical and immunohistochemical study. *J Periodontol*. 2015;86(7):874–881. doi:10.1902/jop.2015.140599

13. Sugiura M, Shoyama Y, Saito H, Nishiyama N. Crocin improves the ethanol-induced impairment of learning behaviors of mice in passive avoidance tasks. *Proc Jpn Acad Ser B*. 1995;71(10):319–324. doi:10.2183/pjab.71.319

14. Ohkawa H, Ohishi N, Yagi K. Assay for lipid peroxides in animal tissues by thiobarbituric acid reaction. *Anal Biochem*. 1979;95(2):351–358. doi:10.1016/0003-2697(79)90738-3

15. Ellman GL. Tissue sulfhydryl groups. *Arch Biochem Biophys*. 1959;82(1):70–77. doi:10.1016/0003-9861(59)90090-6

16. Sun Y, Oberley LW, Li Y. A simple method for clinical assay of superoxide dismutase. *Clin Chem*. 1988;34(3):497–500. PMID:3349599

17. Aebi H. Catalase in vitro. *Methods Enzymol*. 1984;105:121–126. doi:10.1016/s0076-6879(84)05016-3

18. Erel O. A new automated colorimetric method for measuring total oxidant status. *Clin Biochem*. 2005;38(12):1103–1111. doi:10.1016/j.clinbiochem.2005.08.008

19. Erel O. A novel automated direct measurement method for total antioxidant capacity using a new generation, more stable ABTS radical cation. *Clin Biochem*. 2004;37(4):277–285. doi:10.1016/j.clinbiochem.2003.11.015

20. Ziebolz D, Rost C, Schmidt J, et al. Periodontal bacterial DNA and their link to human cardiac tissue: Findings of a pilot study. *Thorac Cardiovasc Surg*. 2018;7(1):83–90. doi:10.1055/s-0035-1564689

21. Hlaing TT, Compston JE. Biochemical markers of bone turnover: Uses and limitations. *Ann Clin Biochem*. 2014;51(2):189–202. doi:10.1177/0004563213515190

22. Foureaux RdC, Messora MR, de Oliveira LFF, et al. Effects of probiotic therapy on metabolic and inflammatory parameters of rats with ligature-induced periodontitis associated with restraint stress. *J Periodontol*. 2014;85(7):975–983. doi:10.1902/jop.2013.130356

23. Rodrigues W, Madeira M, Da Silva T, et al. Low dose of propranolol down-modulates bone resorption by inhibiting inflammation and osteoclast differentiation. *Br J Pharmacol*. 2012;165(7):2140–2151. doi:10.1111/j.1476-5381.2011.01686.x

24. Deshpande RG, Khan MB, Genco CA. Invasion of aortic and heart endothelial cells byporphyromonas gingivalis. *Infect Immun*. 1998;66(11):5337–5343. doi:10.1128/IAI.66.11.5337-5343.1998

25. Pouliot M, Clish CB, Petasis NA, Van Dyke TE, Serhan CN. Lipoxin A4 analogues inhibit leukocyte recruitment to *Porphyromonas gingivalis*: A role for cyclooxygenase-2 and lipoxins in periodontal disease. *Biochemistry*. 2000;39(16):4761–4768. doi:10.1021/bi992551b

26. Ekuni D, Tomofuji T, Sanbe T, et al. Vitamin C intake attenuates the degree of experimental atherosclerosis induced by periodontitis in the rat by decreasing oxidative stress. *Arch Oral Biol*. 2009;54(5):495–502. doi:10.1016/j.archoralbio.2009.02.006

27. Li H, Horke S, Förstermann U. Oxidative stress in vascular disease and its pharmacological prevention. *Trends Pharmacol Sci*. 2013;34(6):313–319. doi:10.1016/j.tips.2013.03.007

28. Steinberg D, Parthasarathy S, Carew TE, Khoo JC, Witztum JL. Beyond cholesterol: Modifications of low-density lipoprotein that increase its atherogenicity *N Engl J Med*. 1989;320(14):915–924. doi:10.1056/NEJM198904063201407

29. Tamer L, Sucu N, Polat G, et al. Decreased serum total antioxidant status and erythrocyte-reduced glutathione levels are associated with increased serum malondialdehyde in atherosclerotic patients. *Arch Med Res*. 2002;33(3):257–260. doi:10.1016/s0188-4409(01)00381-2

30. Jialal I, Vega GL, Grundy SM. Physiologic levels of ascorbate inhibit the oxidative modification of low density lipoprotein. *Atherosclerosis*. 1990;82(3):185–191. doi:10.1016/0021-9150(90)90039-I

31. Ramesh E, Elanchezhian R, Sakthivel M, et al. Epigallocatechin gallate improves serum lipid profile and erythrocyte and cardiac tissue antioxidant parameters in Wistar rats fed an atherogenic diet. *Fundam Clin Pharmacol*. 2008;22(3):275–284. doi:10.1111/j.1472-8206.2008.00585.x

32. Xu GL, Qian ZY, Yu SQ, Gong ZN, Shen XC. Evidence of crocin against endothelial injury induced by hydrogen peroxide in vitro. *J Asian Nat Prod Res*. 2006;8(1–2):79–85. doi:10.1080/10286020500044732

33. Wang Y, Wang Q, Yu W, Du H. Crocin attenuates oxidative stress and myocardial infarction injury in rats. *Int Heart J*. 2018;59(2):387–393. doi:10.1536/ihj.17-114

34. Dianat M, Radan M, Badavi M, Mard SA, Bayati V, Ahmadizadeh M. Crocin attenuates cigarette smoke-induced lung injury and cardiac dysfunction by anti-oxidative effects: The role of Nrf2 antioxidant system in preventing oxidative stress. *Respir Res*. 2018;19(1):58. doi:10.1186/s12931-018-0766-3

35. Rahiman N, Akaberi M, Sahebkar A, Emami SA, Tayarani-Najaran Z. Protective effects of saffron and its active components against oxidative stress and apoptosis in endothelial cells. *Microvasc Res*. 2018;118:82–89. doi:10.1016/j.mvr.2018.03.003

36. He SY, Qian ZY, Tang FT, Wen N, Xu GL, Sheng L. Effect of crocin on experimental atherosclerosis in quails and its mechanisms. *Life Sci*. 2005;77(8):907–921. doi:10.1016/j.lfs.2005.02.006

37. Razavi BM, Hosseinzadeh H, Abnous K, Khoei A, Imenshahidi M. Protective effect of crocin against apoptosis induced by subchronic exposure of the rat vascular system to diazinon. *Toxicol Ind Health*. 2016;32(7):1237–1245. doi:10.1177/0748233714555494

38. Feidantsis K, Mellidis K, Galatou E, Sinakos Z, Lazou A. Treatment with crocin improves cardiac dysfunction by normalizing autophagy and inhibiting apoptosis in STZ-induced diabetic cardiomyopathy. *Nutr Metab Cardiovasc Dis*. 2018;28(9):952–961. doi:10.1016/j.numecd.2018.06.005

39. Razavi BM, Hosseinzadeh H, Movassaghi AR, Imenshahidi M, Abnous K. Protective effect of crocin on diazinon induced cardiotoxicity in rats in subchronic exposure. *Chem Biol Interact*. 2013;203(3):547–555. doi:10.1016/j.cbi.2013.03.010

Silencing *Hoxa2* reverses dexamethasone-induced dysfunction of MC3T3-E1 osteoblasts and osteoporosis in rats

Yuan Liu[1,A–D], Le Wang[1,B,C], Youguo Yang[1,B,C], Jianbin Xiong[2,A,E,F]

[1] Department of Rheumatology, Liuzhou People's Hospital, Guangxi Medical University, China
[2] Department of Orthopedics, Liuzhou People's Hospital, Guangxi Medical University, China

A – research concept and design; B – collection and/or assembly of data; C – data analysis and interpretation;
D – writing the article; E – critical revision of the article; F – final approval of the article

Address for correspondence
Jianbin Xiong
E-mail: xjianbin56@163.com

Abstract

Background. Osteoporosis is damaging the health of women worldwide. Osteoporosis results from the imbalance between bone resorption and formation, which may be regulated by homeobox A2 (*Hoxa2*). However, the specific role and mechanism of *Hoxa2* in osteogenesis and dexamethasone (Dex)-induced osteoporosis remain unknown.

Objectives. The present study investigated the effect of *Hoxa2* on differentiation and osteoblastogenesis.

Materials and methods. Alkaline phosphatase staining and immunofluorescence staining were performed to evaluate the differentiation of MC3T3-E1 cells. Runt-related transcription factor 2 (*Runx2*), osteoprotegerin (OPG) and receptor activator of nuclear factor-kappa B ligand (RANKL) in Dex stimulated osteoblastic MC3T3-E1 cells, and Dex-induced osteoporotic rats were estimated using western blot and quantitative polymerase chain reaction (qPCR). Serum markers of bone turnover were determined using enzyme-linked immunosorbent assay (ELISA). Trabecular bones of femur tissues were observed using hematoxylin and eosin (H&E) staining.

Results. *Hoxa2* short hairpin RNA significantly promoted the differentiation of MC3T3-E1 cells and expression of *Runx2* and OPG in Dex-treated MC3T3-E1 cells and osteoporotic rats but inhibited the expression of RANKL. Furthermore, silencing *Hoxa2* resulted in the upregulation of bone alkaline phosphatase but suppressed the expression of tartrate-resistant acid phosphatase and C-terminal cross-linked telopeptides of type I collagen.

Conclusions. Silencing *Hoxa2* reversed the Dex-induced inhibition of osteoblastogenesis by modulating *Runx2* and RANK–RANKL–OPG axis.

Key words: homeobox A2, osteoblast, dexamethasone, osteogenesis

Background

The precise balance of bone turnover depends on the homeostasis of osteoblast-mediated bone formation and osteoclast-mediated bone resorption, which are mediated by a multitude of critical molecules working through various signaling pathways.[1] Osteoporosis occurs due to the imbalance of bone formation and resorption, with excess resorption leading to reduced bone mass and increased bone fragility. The proliferation and differentiation of osteoblasts from undifferentiated mesenchymal cells play important roles in bone formation.[2] Glucocorticoid-induced osteoporosis is regarded as the most common form of secondary osteoporosis and involves a reduction in osteoblastogenesis[3]; thus, Dex-treated osteoblast and animal models have been widely accepted as in vitro and in vivo models of osteoporosis.[4,5] Although osteoporosis treatments based on the inhibition of bone resorption and promotion of bone formation are widely used, prolonged administration of these agents, such as bisphosphonates or estrogen receptor modulator, can lead to several adverse effects such as mandibular necrosis, venous thrombosis, cardiac arrhythmia, and renal inadequacy.[6] Thus, more effective therapeutic strategies with fewer adverse reactions are urgently needed. To date, there is still considerable need for illustrating the effects of critical regulatory factors of osteoblastogenesis and for therapeutic targets associated with osteoporosis.

Currently, several signaling pathways and factors involved in osteoporosis have been determined.[7] For instance, *Runx2*, which can act as a transcriptional regulator of bone metabolism, participates in the differentiation and formation of osteoblasts as well as signal transduction of specific pathways, including the osteoprotegerin (OPG)/receptor activator of nuclear factor κB ligand (RANKL) pathway.[8,9] Notably, a combination treatment with RANKL and receptor activator of nuclear factor κB (RANK) promotes the differentiation and proliferation of osteoclasts, and OPG has been found to inhibit osteoclast activation by competitively combining with RANK. Thus, both OPG and RANK are key molecules in bone formation and reconstruction.[10] Bone formation is largely dependent on the proliferation and differentiation of osteoblasts.[11–13] The ALP production is regarded as an indicator of osteogenesis, to a certain extent, reflecting the degree of osteoblast differentiation.[14] MC3T3-E1 cells display developmental, sequential gene expression similar to that of osteoblasts during bone formation in vivo, which are considered a well-established model for studying osteoblast proliferation and differentiation.[15,16]

Homeobox A2 (*Hoxa2*), a unique transcription factor of the homeobox family, regulates many growth and development processes. Knockout of *Hoxa2* in mice has been found to promote expression of the cartilage and bone-specific gene *Runx2*, which regulates the expression of bone-specific markers.[17] Previous research has shown that *Hoxa2* inhibits osteoblast differentiation by negatively regulating

the osteogenic transcription factor *Runx2*.[18] Moreover, downregulation of *Hoxa2* via miR-135 facilitates the differentiation of adipose-derived stem cells (ADSCs) into osteoblasts via the *Runx2* pathway.[19] Osteoblast formation per se upregulates the Hoxa gene cluster expression, particularly of mid-cluster genes, and downregulates the expression of *Hoxa7* and *Hoxa10*, differences of which in expression appear related to promoter methylation. Hoxa expression is profoundly regulated during osteoblast differentiation through canonical methylation-dependent mechanisms.[20] However, the molecular mechanisms by which *Hoxa2* influences differentiation and regeneration of osteoblasts, especially in glucocorticoid-induced osteoporosis, require further investigation to clarify whether *Hoxa2* is essential for these processes and whether it is a suitable target for a gene therapy-based approach to osteoporosis.

Objectives

The aim of this study was to identify the precise role of *Hoxa2* in glucocorticoid-induced suppression of osteogenesis. Dex-induced MC3T3-E1 osteoblasts and osteoporotic rats were respectively transfected and administrated with adenovirus-packaged *Hoxa2* short hairpin RNA (shRNA) in vitro and in vivo to observe the effect of *Hoxa2* on the differentiation of osteoblasts, as well as osteoporosis in rats.

Materials and methods

Construction of recombinant adenovirus-delivered *Hoxa2* shRNA

Two shRNA sequences targeting *Hoxa2* (*Hoxa2* shRNA#1: 5'-CCCACTGTTCCTAACTGCTTGTCAA-3' and *Hoxa2* shRNA#2: 5'-GCTCCCTGGACAGTCCTGTAGATA-3') were designed according to GenBank accession number (SEQ ID: nM_010451.2). The scrambled shRNA (5'-GCTGCTGGATTTGACCGAGAGACAA-3') was used as a negative control (Sangon Biotechnology, Shanghai, China). These shRNAs were packaged with adenovirus vector pHBAd-U6-GFP. The fluorescent intensity of cells was analyzed using a fluorescence microscope (Carl Zeiss, Jena, Germany) or a flow cytometer (FACS Calibur; Becton Dickinson, Franklin Lakes, USA).

Cell culture and transfection

The mouse osteoblastic cell line MC3T3-E1 was purchased from American Type Cell Culture (ATCC, Manassas, USA) and maintained in α-Minimal Essential Medium (Gibco BRL, Rockville, USA) supplemented with 10% fetal bovine serum (FBS), 100 U/mL of penicillin (Hyclone, Logan, USA) and 100 U/mL of streptomycin at 37°C in a 5% CO_2 atmosphere. The cells were passaged upon

reaching 70% fusion using 0.25% trypsin, and cells of passages 2 through 4 were used for experiments.

MC3T3-E1 cells were divided into 5 groups and seeded at a density of 2×10^5 cells/well in six-well plates. The Dex group was pretreated with 100 nM Dex for 72 h (Sigma-Aldrich, St. Louis, USA). MC3T3-E1 cells in the blank group were cultured with normal saline, and the Dex+scrambled shRNA group was treated with 100 nM Dex for 24 h followed by transfection with scrambled shRNA for 48 h. The Dex+*Hoxa2* shRNA#1 group and Dex+*Hoxa2* shRNA#2 groups were treated with 100 nM Dex for 24 h followed by transfection with *Hoxa2* shRNA#1 or *Hoxa2* shRNA#2 for 48 h, respectively.

Cell viability assay

The commercially available Cell Counting Kit-8 (CCK-8) assay (Sigma-Aldrich) was used to assess cell viability according to the manufacturer's instructions. Cells in the logarithmic growth phase were seeded in 96-well culture plates at 3×10^3 cells/well. Then, 10 μL 0f CCK-8 solution was added to each well for 2 h at 5 h, 24 h, 48 h, and 72 h after cultivation. The absorbance at 450 nm in each well was measured using a microplate reader (BioTek, Winooski, USA), and experiments were performed in triplicate.

ALP staining

MC3T3-E1 cells were washed twice with phosphate-buffered saline (PBS) and fixed with 4% paraformaldehyde for 15 min, followed by washing with 25 mM Tris-Cl (pH 9.0). Then, cells were stained with ALP dye solution containing 8 mM $MgCl_2$, 0.4 mg/mL of α-naphthyl phosphate, and 1 mg/mL of Fast Red TR (Sigma-Aldrich) for 30 min and rinsed with PBS to terminate the reaction. The ALP-positive cells (stained red) were counted under a fluorescence microscope (Carl Zeiss).

Immunofluorescence staining

MC3T3-E1 cells were seeded in Petri dishes and washed with PBS, and then cells were fixed in 4% formaldehyde for 30 min at room temperature. MC3T3-E1 cells were subsequently permeabilized with 0.5% Triton X-100 solution for 10 min and sealed with FBS for 30 min. After that, the cells were incubated with the following primary antibodies: mouse anti-bone alkaline phosphatase (BALP) monoclonal antibody (1 : 100; Abcam, Cambridge, USA), and mouse anti-PICP monoclonal antibody (1 : 50; Abcam) at 4°C overnight. After washed with PBS, the secondary goat-anti-mouse IgG-fluorescein isothiocyanate (FITC; 1 : 500; Abcam) was added to incubate cells for 1 h, and nuclei were counterstained with DAPI (4′, 6-diamidino-2-phenylindole dihydrochloride). Finally, fluorescence staining was observed using a laser confocal fluorescence microscope (Carl Zeiss).

Animal administration

A total of 30 male Wistar rats (body weight 250–300 g, 12 weeks old) were maintained under a standard pathogen-free environment at 22–25°C and 45–55% humidity with a 12 h light/dark cycle. The rats had free access to water and a standard rodent diet. After acclimatization for 1 week, rats were randomly divided into 5 groups: control group (administered with normal saline); Dex group (daily subcutaneous injection with 0.1 mg/kg Dex for 6 weeks); Dex+scramble shRNA group; Dex+*Hoxa2* shRNA#1 group; and Dex+*Hoxa2* shRNA#2 group (6 weeks of subcutaneous injection of 0.1 mg/kg of Dex plus an intravenous injection of 1×10^9 pfu/mL of scramble shRNA or *Hoxa2* shRNA#1 or *Hoxa2* shRNA#2 once every 2 days for 4 weeks). The serum and right femurs were collected from the sacrificed animals at the endpoint. The animal experiment was performed in accordance with the protocol approved by the Ethics Committee of Liuzhou People's Hospital 2020 (China; approval No. KY-E-14-d).

RT-qPCR

Gene expression in MC3T3-E1 cells and proximal femoral tissues was assessed using quantitative polymerase chain reaction (qPCR). Total RNA extraction was performed using TRIzol® reagent (Invitrogen, Carlsbad, USA) according to the manufacturer's instructions. The RNA concentration and purity were verified using the Nanodrop 2000 (Thermo Fisher Scientific, Rockford, USA). For reverse transcription, cDNA was synthesized chemically with 2 μg of total RNA using the RevertAid First Strand cDNA Synthesis Kit (MBI Fermentas, Vilnius, Lithuania). The qPCR was performed with the SYBR Green PCR kit (Qiagen, Crawley, UK) using an ABI quantitative PCR 7300 system (Applied Biosystems, Foster City, USA). The amplification conditions for PCR were 95°C for 5 min followed by 40 cycles of 10 s of denaturation at 95°C, 20 s of annealing at 60°C and 30 s of extension at 72°C. The following primers were used: *Hoxa2*, forward: 5'-CTGTGGAGCTGGCCTAAACA-3' and reverse: 5'-GCAAAGCCACCTGGTCAAAG-3'; *Runx2*, forward: 5'-GACTGTGGTTACCGTCATGGC-3' and reverse:5'-ACTTGGTTTTTCATAACAGCGGA-3'; OPG, forward: 5'-AAAGCACCCTGTAGAAAACA-3' and reverse: 5'-CCGTTTTATCCTCTCTA CACTC-3'; RANKL, forward: 5'-TATGATGGAAGGCTCATGGT-3' and reverse: 5'-TGTCCTGAACTTTGAAAGCC-3'; *GAPDH*, forward: 5'-TGGCCTTCCGTGTTCCTAC-3' and reverse: 5'-GAGTTGCTGTTGAAGTCGCA-3'. Upon completion of the reaction, the amplification curve and melting curve were assessed. The relative expression of each mRNA was compared to that of *GAPDH* and calculated using the $2^{-\Delta\Delta Ct}$ method.

528

Y. Liu et al. Role of *Hoxa2* in Dex-induced osteoporosis

Western blot

Protein was extracted using lysis buffer containing 1 mM phenylmethane sulfonyl fluoride (PMSF; Applygen, Beijing, China), and the total protein concentration was measured using a BCA assay kit (Sigma-Aldrich). Protein samples were separated with 10% sodium dodecyl sulfate polyacrylamide gel electrophoresis (SDS-PAGE) and transferred to nitrocellulose membranes (Applygen). Non-specific binding was blocked by adding 5% fat-free milk in Tris-buffered saline containing 0.1% Tween-20 (TBST). Membranes were then incubated at 4°C overnight with primary antibodies against *GAPDH* (1 : 500; Santa Cruz Biotechnology, Santa Cruz, USA), rabbit anti-*Hoxa2* polyclonal antibodies (1 : 300; Abcam), mouse anti-*RANKL* monoclonal antibody (1 : 500; Abcam), rabbit anti-*Runx2* monoclonal antibody (1 : 500; Cell Signaling Technology, Danvers, USA), and rabbit anti-OPG polyclonal antibody (1 : 800; Abcam). The membranes were washed with TBST and then incubated with goat anti-mouse/rabbit secondary antibodies (1 : 1000; Santa Cruz Biotechnology) at room temperature for 1 h. Protein bands were visualized using enhanced chemiluminescence (ECL) reagent (Thermo Fisher Scientific), and GAPDH was used as an endogenous protein for normalization.

Histopathological analysis

The femur was fixed with 4% neutral buffered formalin for 7 days at 4°C and decalcified in 5% ethylenediamine-tetraacetic acid (EDTA) for 3 weeks. The tissues then were embedded in paraffin wax and cut into 5 μm sections, which were stained with hematoxylin and eosin (H&E). The histopathological changes of bone cortex and trabecula were observed under a light microscope (model IX53; Olympus Corp., Tokyo, Japan).

ELISA

Serum biomarkers for bone turnover, including BALP, tartrate-resistant acid phosphatase 5b (TRAP5b) and carboxy-terminal of type I collagen cross-links (CTX-I), were assessed using enzyme-linked immunosorbent assay (ELISA) kits (Immunodiagnostic Systems, Fountain Hills, USA) according to the manufacturer's instructions.

Statistical analysis

Data are presented as mean ± standard error of the mean (SEM). One-way analysis of variance (ANOVA) was used to assess the differences in variables among multiple groups, and comparisons within groups were made using post hoc tests. In addition, data obtained from multiple measurements of the same dependent variable at different time points were compared using repeated-measures ANOVA. The statistical significance was defined by a value

of $p < 0.05$. All statistical comparisons were performed using SPSS v. 17.0 (SPSS Inc., Chicago, USA).

Results

The upregulated *Hoxa2* induced by Dex in MC3T3-E1 cells was overturned by *Hoxa2* shRNA

The sequences of *Hoxa2* shRNA and scrambled shRNA are presented in Fig. 1A. MC3T3-E1 cells were transfected with scrambled shRNA, *Hoxa2* shRNA#1 and *Hoxa2* shRNA#2, respectively. Green fluorescence was observed post-transfection, indicating that shRNAs were transfected into cells successfully (Fig. 1B,C). The silencing effects of *Hoxa2* shRNAs were evaluated using RT-PCR and western blot analysis. Results showed that Dex promoted the level of *Hoxa2* at both mRNA and protein levels. However, the mRNA expression of *Hoxa2* in MC3T3-E1 cells transfected with *Hoxa2* shRNA#1 or *Hoxa2* shRNA#2 was significantly decreased, consistent with the downregulation of *Hoxa2* protein level. The scrambled shRNA did not affect *Hoxa2* expression (Fig. 1D,E). These findings demonstrated that the level of *Hoxa2* was increased in Dex-induced MC3T3-E1 cells, and the *Hoxa2* shRNAs were effective.

Knockdown of *Hoxa2* attenuated the inhibitory effect of Dex on osteoblast differentiation in MC3T3-E1 cells

The cell viability was determined using the CCK-8 assay. The viability of MC3T3-E1 cells exposed to Dex was drastically weakened compared to the blank group at 24 h, 48 h and 72 h, whereas *Hoxa2* shRNA#1 and *Hoxa2* shRNA#2 elevated the cell viability, hinting that the important role of *Hoxa2* in MC3T3-E1 cell viability (Fig. 2A). BALP and PICP, which reflect activity of the osteoblasts,[21,22] were selected to determine the differentiation and function of osteoblasts. The enrichment of BALP and PICP expressions was observed in untreated MC3T3-E1 cells, and their levels were greatly reduced following treatment with Dex. Moreover, *Hoxa2* shRNAs rescued the expressions of BALP and PICP partly compared with the Dex+scrambled shRNA group (Fig. 2B,C). Collectively, these results suggested that *Hoxa2* affected the viability of MC3T3-E1 cells, and the inhibitory effect of Dex on osteoblast differentiation was reversed by silencing *Hoxa2*.

Hoxa2 knockdown alleviated the inhibitory effect of Dex on osteogenesis in MC3T3-E1 cells

The ALP is regarded as an indicator of osteogenesis, to a certain extent, reflecting the degree of osteoblast differentiation.[23] Results showed that the number of positive
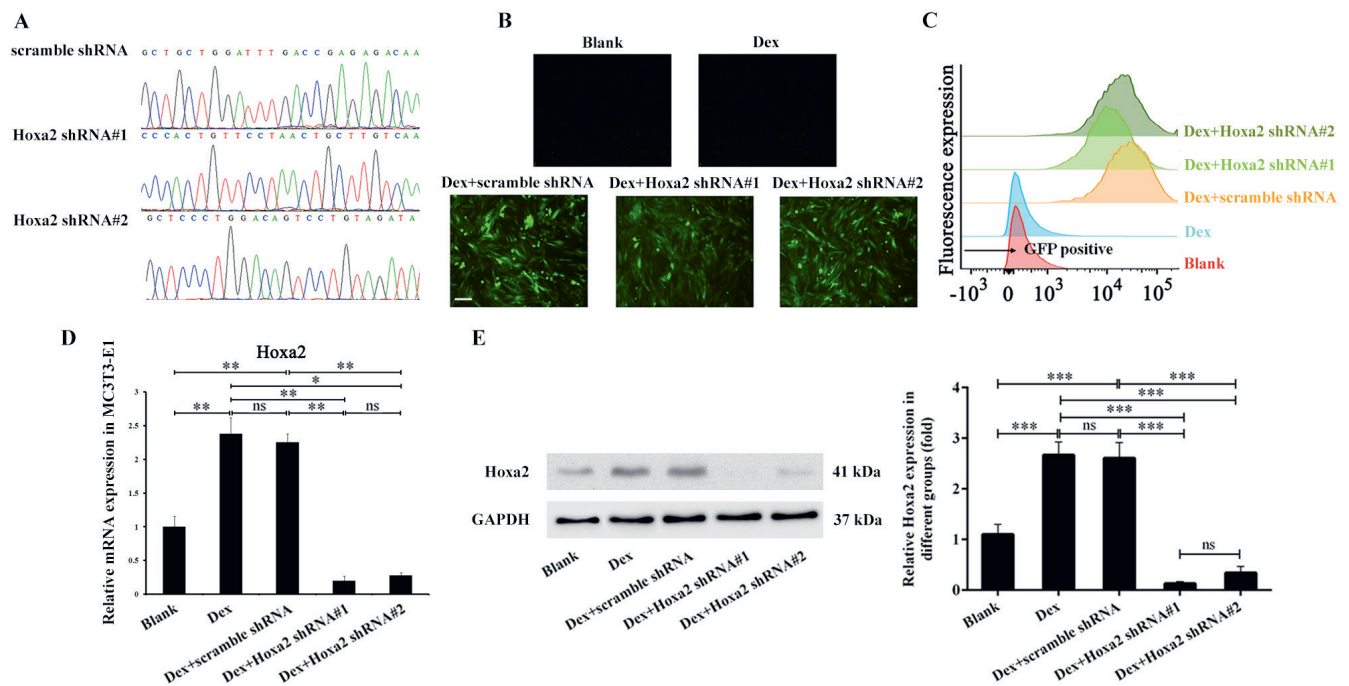
Fig. 1. The upregulated *Hoxa2* induced by Dex in MC3T3-E1 cells was overturned by *Hoxa2* shRNA. A. Gene sequencing was used to identify recombinant adenoviruses for *Hoxa2* shRNA1 and shRNA2; B. Fluorescence microscopy was used to examine the expression of green fluorescence in MC3T3-E1 cells after transfection with the control shRNA and 2 *Hoxa2* shRNAs. Scale bar: 50 μm; C. The transfection efficiency of *Hoxa2* shRNA in MC3T3-E1 cells was determined with flow cytometry after the treatment of cells with dexamethasone (Dex); D and E. Silence effect of *Hoxa2* shRNA in MC3T3-E1 cells was confirmed with real-time PCR (RT-PCR) and western blot

*p < 0.05; **p < 0.01; ***p < 0.001; ns – not significant.

ALP-positive cells (red staining) was reduced after Dex stimulation. In contrast, numerous ALP-positive cells were observed following transfection of *Hoxa2* shRNA#1 or *Hoxa2* shRNA#2 (Fig. 3A). To further confirm the role of *Hoxa2* in Dex-induced osteogenesis dysfunction, we analyzed the expression levels of several transcriptional factors and signaling molecules known to be involved in the regulation of osteogenesis, including *Runx2*, OPG, and RANKL.[23–25] Dex treatment decreased the mRNA expressions of osteoblastogenic molecules *Runx2* and OPG in MC3T3-E1 cells compared with the blank group (Fig. 3B,C). In contrast, the mRNA expression of the negative osteogenesis regulator RANKL was significantly higher in the Dex group than in the blank group (Fig. 3D). Similar results were observed in the protein expression of these molecules (Fig. 3E). Furthermore, *Hoxa2* shRNA resulted in an increase of *Runx2* and OPG at both mRNA and protein expression, but also in a decrease of RANKL expression compared with the Dex+scrambled shRNA group (Fig. 3B–E). The above findings suggested that *Hoxa2* shRNA counteracted the inhibitory effects of Dex on osteogenesis.

Hoxa2 shRNA inhibited Dex-induced bone loss

Adenovirus-packaged *Hoxa2* shRNA#1 was selected for in vivo experiments. As shown in Fig. 4A, strong green fluorescence in femur tissues was observed after administration of scramble shRNA and *Hoxa2* shRNA#1, suggesting that the adenovirus-packaged shRNAs were successfully injected into rats. The mRNA level of *Hoxa2* in rat right femurs was significantly increased following Dex treatment, while *Hoxa2* shRNA#1 markedly inhibited the expression of *Hoxa2* (Fig. 4B). Given the potential role of *Hoxa2* in Dex-induced osteoporosis, we further evaluated the histological changes of femur tissues in response to *Hoxa2* knockdown. As shown in Fig. 4D, trabecular bones of femur tissues appeared rupture and reduction in Dex-induced osteoporotic rats compared to the control group, indicating the validity of the osteoporotic rat model. However, *Hoxa2* shRNA administration increased bone mass and improved structure to a comparable level with the normal group.

Hoxa2 was required for the osteogenesis and bone resorption regulated by Dex

In addition, the mRNA levels of *Runx2* and OPG in femur tissues were both reduced following Dex treatment. However, *Hoxa2* shRNA#1 reversed the downregulation of *Runx2* and OPG induced by Dex (Fig. 4A,B). Dex promoted the expression of RANKL in femur tissues, while it was significantly decreased after administration of *Hoxa2* shRNA#1 (Fig. 4C). The protein levels of *Runx2*, OPG and RANKL in each group were consistent with mRNA
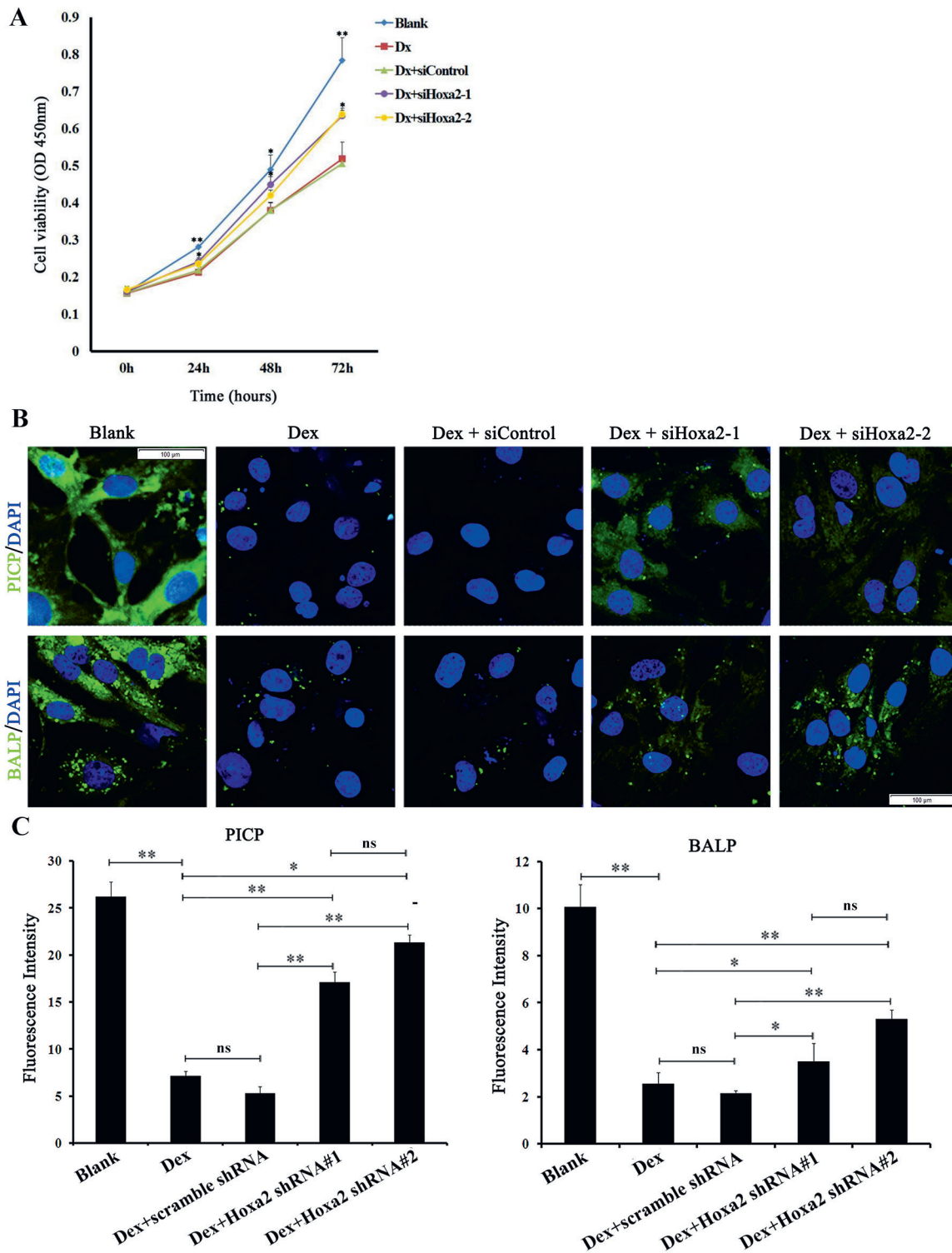
Fig. 2. Knockdown of *Hoxa2* attenuated the inhibitory effect of Dex on osteoblast differentiation in MC3T3-E1 cells. A. MC3T3-E1 cells viability after stimulation with Dex and *Hoxa2* shRNA; B and C. The expressions BALP and PICP in osteoblasts were determined with immunofluorescence staining. DAPI (blue) was used as a nuclear stain, and the expression of bone turnover markers is represented by green staining. Scale bar: 10 μm. Immunofluorescence staining of BALP and PICP was quantified using Image Pro Plus 4.5 software (Media Cybernetics, Silver Spring, USA)

levels (Fig. 4D). These results indicated that silencing *Hoxa2* rescued the expressions of osteogenetic molecules in vivo. Compared with the control group, serum markers of bone resorption, including TRAP5b and C-terminal cross-linked telopeptides of type I collagen (CTX-1), were

significantly increased in the Dex groups. However, Dex reduced the levels of bone formation marker BALP in comparison with the control group (Fig. 4E–G). Consistent with the beneficial effects on histological changes, *Hoxa2* shRNA administration resulted in a reduction of serum
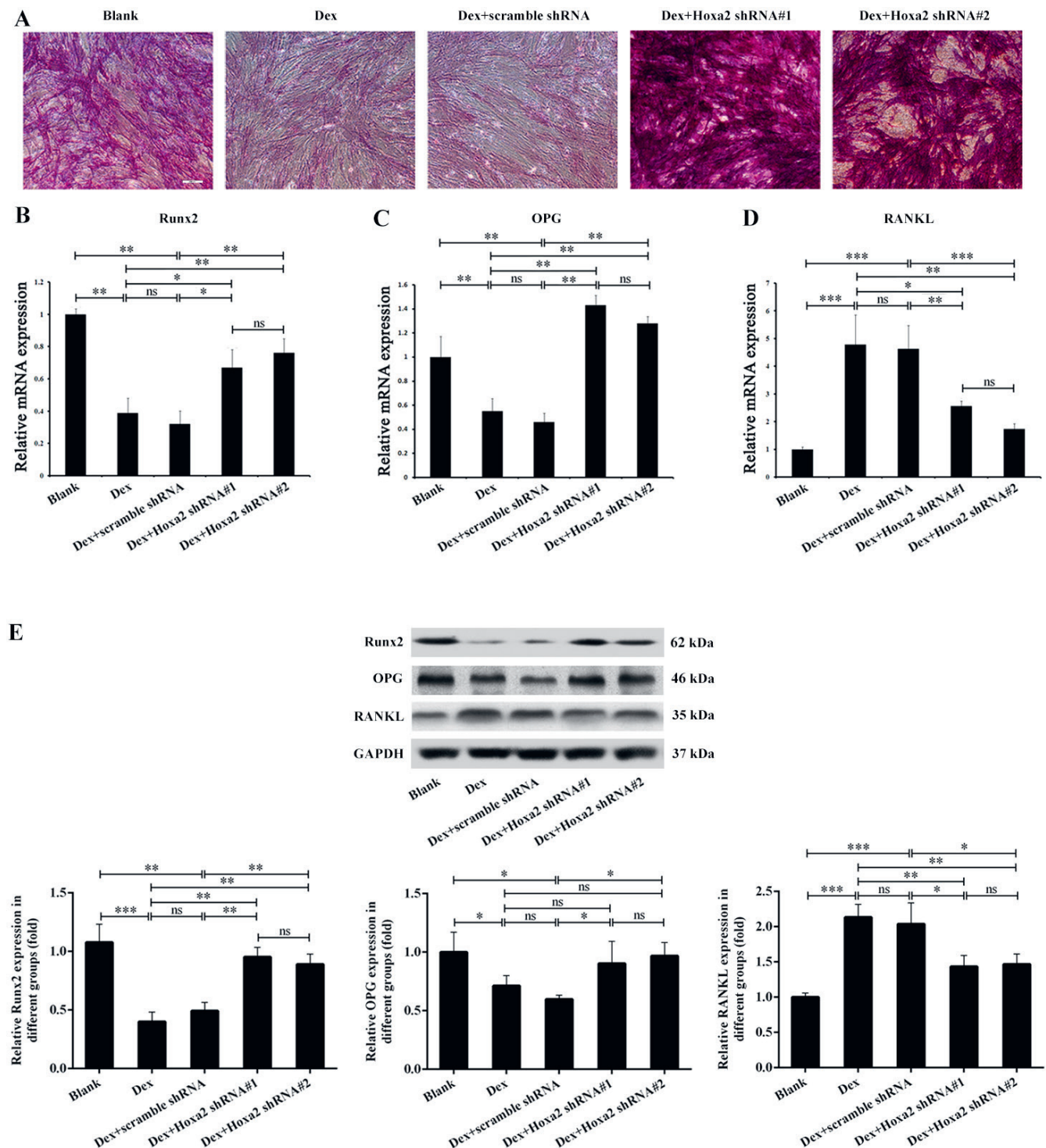
Fig. 3. *Hoxa2* knockdown alleviated the inhibitory effect of Dex on osteogenesis in MC3T3-E1 cells. A. Differentiation of MC3T3-E1 cells was evaluated with ALP staining. The degree of red staining represented the number of ALP-positive cells and the extent of differentiation. Scale bar: 100 µm; B–D. RT-qPCR results show the effect of *Hoxa2* shRNA on mRNA levels of *Runx2*, OPG and RANKL; E. Western blot showing the effect of *Hoxa2* shRNA on protein levels of *Runx2*, OPG and RANKL

*p < 0.05; **p < 0.01; ***p < 0.001; ns – not significant.

TRAP5b and CTX-1, and an increase of BALP expression compared to the Dex group (Fig. 4E–G). The comprehensive results suggested that silencing *Hoxa2* could reverse the Dex-mediated bone resorption and trabecular bone reduction.

Discussion

The normal process of bone metabolism is maintained by collaboration between osteoblasts and osteoclasts. Proliferation and differentiation of osteoblasts are responsible for
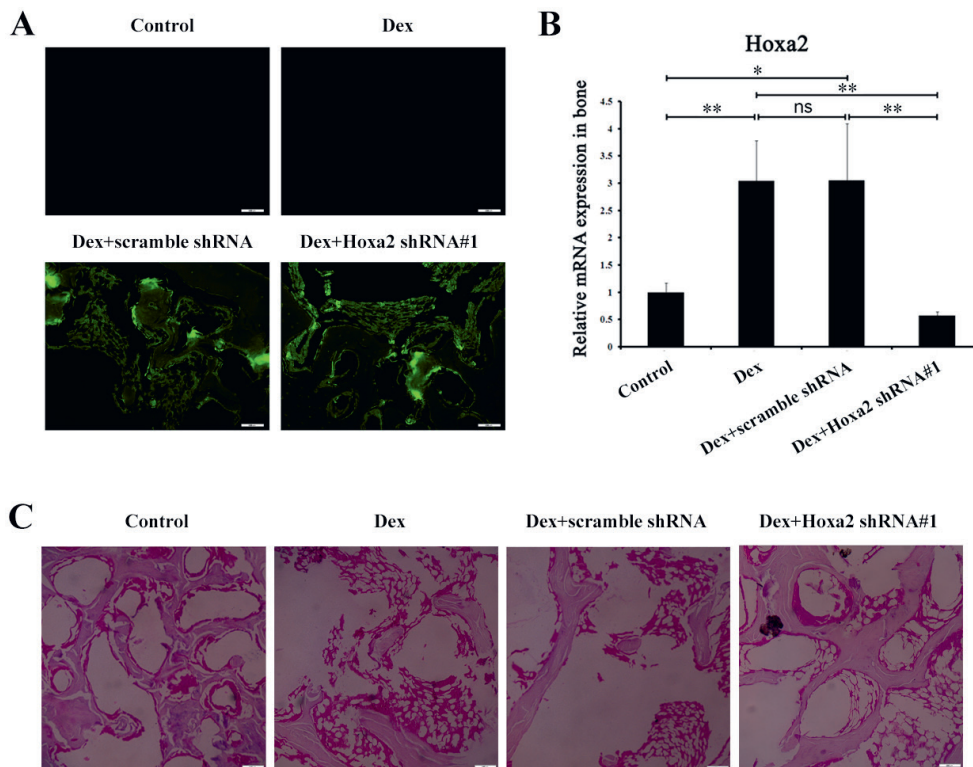
Fig. 4. *Hoxa2* shRNA inhibited Dex-induced bone loss. A. Tissue targeting of *Hoxa2* shRNA#1 in rats. Scale bar: 100 µm; B. Silence effect of *Hoxa2* shRNA#1 in bone tissue was confirmed with RT-qPCR; C. Histopathological changes of femur tissue in rats from a different group at the endpoint of the experiment; scale bar 100 µm.

*p < 0.05; **p < 0.01; ns – not significant.

bone formation.[26,27] To the best of our knowledge, MC3T3-E1 cells are a commonly used model for studying the function of osteoblasts.[15,16] *Hoxa2* is one of the Hox homeodomain family transcription factors and has been found to regulate bone metabolism and skeletal morphogenesis.[17] Gersch et al. demonstrated that *Hoxa-2* was upregulated in active osteoblasts during bone regeneration, and Dobreva et al. also reported higher expression of *Hoxa2* in SATB2$^{-/-}$ osteoblasts.[28,29] In view of the previous study, in which *Hoxa2* was shown to play a separate role in antagonizing bone formation,[30] we sought to explore the potential effect of *Hoxa2* on Dex-induced osteoporosis. Osteoporosis animal models were successfully developed in Dex-induced rats, with disease manifesting itself in pathological changes of the femur.[31] Consistent with previous findings, we confirmed that *Hoxa2* was overexpressed in mouse osteoblast-like MC3T3-E1 cells and bone tissue of rats. Besides, Dex promoted *Hoxa2* mRNA and protein expression. The above results promoted the hypothesis that *Hoxa2* could be involved in the Dex-induced osteoblasts dysfunction and osteoporosis.

Another study has provided evidence that osteoblasts exposed to Dex display significant reductions in Col-I expression and ALP activity.[32] Dex suppressed the osteogenic differentiation of bone marrow-derived mesenchymal stem cells and let-7f-5p expression, which could be reversed by the downregulation of TGFBR1.[33] This data was consistent with our findings showing that the expression of BALP and PICP was decreased in Dex-treated MC3T3-E1 cells. Notably, the expression of BALP and PICP was restored partially after *Hoxa2* knockdown. The homeostasis between osteoblasts and osteoclasts is mediated by various

signaling molecules, including *Runx2*[34,35] and the RANK–RANKL–OPG axis, imbalance of which leads to bone metabolism dysfunction.[1] Franceschetti et al. found that RANKL effects on bone differentiation required PI3 kinase using computational analyses of several pathways in RANKL-driven differentiation of murine bone marrow osteoclast precursors.[36] PI3K was shown to mediate BMP2 induction of osteogenic differentiation.[37] PI3K is involved in osteoblast adhesion to extracellular matrix and titanium.[38] In our study, silencing *Hoxa2* in Dex-induced osteoblasts and osteoporotic rats resulted in the upregulation of *Runx2* and OPG as well as downregulation of RANKL. In line with its promotional effect on osteoblasts differentiation, *Hoxa2* regulating osteogenesis may be related to the *Runx2* and RANK–RANKL–OPG axis. Thus, these findings revealed the underlying mechanism of *Hoxa2* in osteoporosis. In addition, RANKL effects on bone differentiation were regulated by PI3K, and *Hoxa2* affected the osteoblasts differentiation by downregulating the RANKL. Whether *Hoxa2* requires modulation of PI3 kinase activity warrants further investigation.

In Dex-induced osteoporotic rats, bone turnover biomarkers BALP, TRAP5b and CTX-1 have been identified to predict the activity and function of osteoblasts during the metabolic process.[39] However, bone turnover biomarker expression varies throughout different metabolic statuses.[12] The serum TRAP5b and CTX-1 were markedly reduced by the administration of *Hoxa2* shRNA, while the BALP showed a significant increase compared to the Dex group, indicating that *Hoxa2* shRNA inhibited osteoclasts activity and bone resorption.
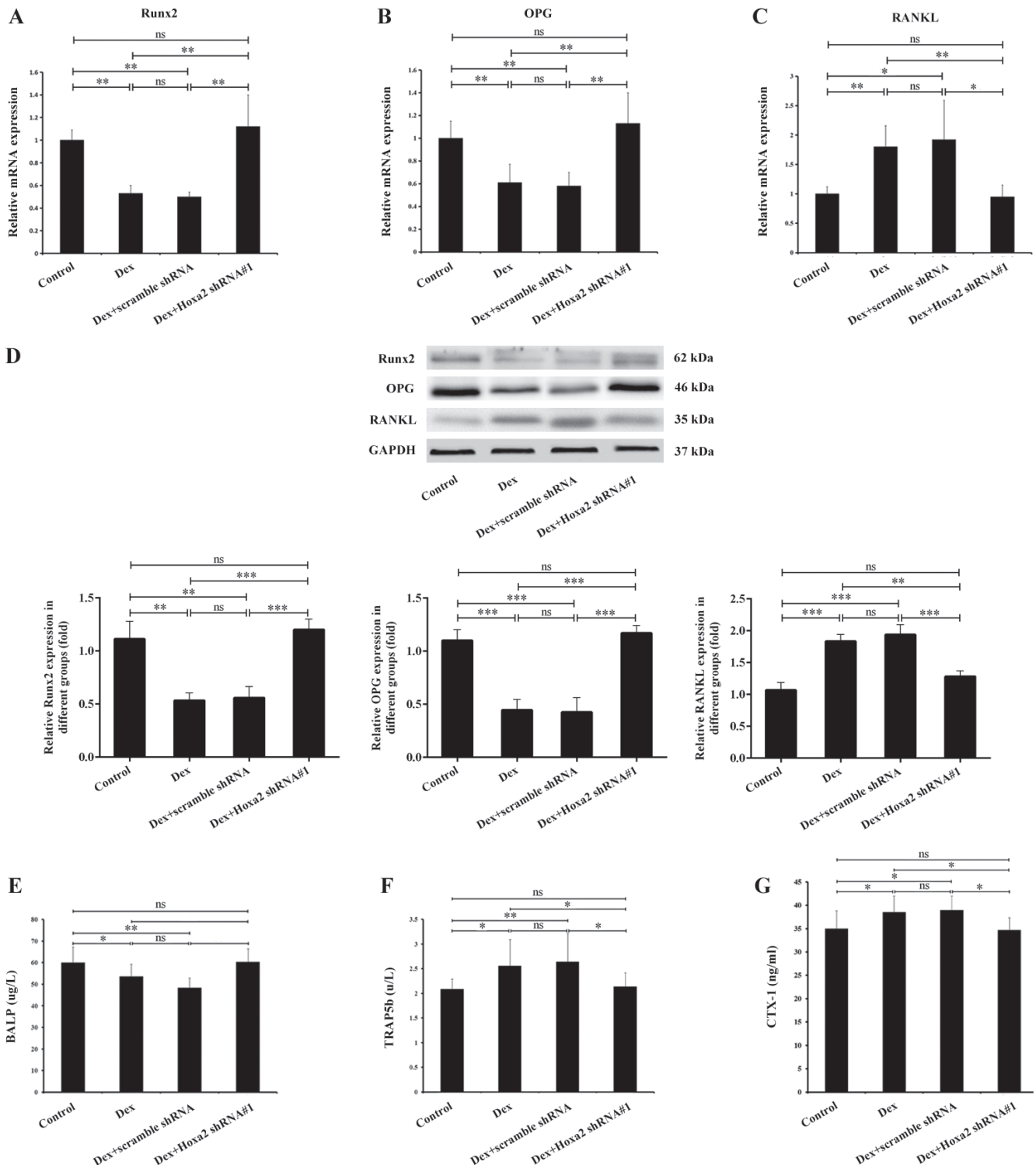
Fig. 5. *Hoxa2* was required for the osteogenesis and bone resorption regulated by Dex. A–D. RT-qPCR and western blot showing the effect of *Hoxa2* shRNA#1 on mRNA and protein levels of *Runx2*, OPG and RANKL in Dex-induced osteoporotic rats; E–G. Bone turnover markers, including BALP, TRAP5b and CTX-1, in the serum of rats were evaluated using ELISA

$*p < 0.05$; $**p < 0.01$; $***p < 0.001$; ns – not significant.

Conclusions

These findings provided evidence that *Hoxa2* was involved in the differentiation and osteogenesis of MC3T3-E1 osteoblasts. *Hoxa2* knockdown relieved Dex-regulated osteoporosis via modulating the *Runx2* and the RANK–RANKL–OPG axis. Our research provided an experimental basis for investigating a potential mechanism of bone metabolism in glucocorticoid-induced osteoporosis. Further studies are expected to reveal the complete regulatory

mechanisms of *Hoxa2* in the pathogenesis of osteoporosis and its potential as a gene therapy target for the treatment of osteoporosis.

ORCID iDs

Yuan Liu   https://orcid.org/0000-0002-3913-0588
Le Wang   https://orcid.org/0000-0003-4426-9717
Youguo Yang   https://orcid.org/0000-0001-7215-8585
Jianbin Xiong   https://orcid.org/0000-0002-3946-0616

References

1. Huang W, Yang S, Shao J, Li YP. Signaling and transcriptional regulation in osteoblast commitment and differentiation. *Front Biosci*. 2007;12:3068–3092. PMID:17485283
2. Pittenger MF, Mackay AM, Beck SC, et al. Multilineage potential of adult human mesenchymal stem cells. *Science*. 1999;284(5411):143–147. doi:10.1126/science.284.5411.143
3. Adami G, Saag KG. Glucocorticoid-induced osteoporosis update. *Curr Opin Rheumatol*. 2019;31(4):388–393. doi:10.1097/BOR.0000000000000608
4. Chen Z, Xue J, Shen T, Ba G, Yu D, Fu Q. Curcumin alleviates glucocorticoid-induced osteoporosis by protecting osteoblasts from apoptosis in vivo and in vitro. *Clin Exp Pharmacol Physiol*. 2016;43(2):268–276. doi:10.1111/1440-1681.12513
5. Shi C, Qi J, Huang P, et al. MicroRNA-17/20a inhibits glucocorticoid-induced osteoclast differentiation and function through targeting *RANKL* expression in osteoblast cells. *Bone*. 2014;68:67–75. doi:10.1016/j.bone.2014.08.004
6. Yamauchi M, Sugimoto T. Status and issues of medical treatment for osteoporosis [in Japanese]. *Nihon Rinsho*. 2015;73(10):1621–1627. PMID:26529921
7. Iñiguez-Ariza NM, Clarke BL. Bone biology, signaling pathways, and therapeutic targets for osteoporosis. *Maturitas*. 2015;82(2):245–255. doi:10.1016/j.maturitas.2015.07.003
8. Chen D, Zhao M, Mundy GR. Bone morphogenetic proteins. *Growth Factors*. 2004;22(4):233–241. doi:10.1080/08977190412331279890
9. Gaur T, Lengner CJ, Hovhannisyan H, et al. Canonical WNT signaling promotes osteogenesis by directly stimulating *Runx2* gene expression. *J Biol Chem*. 2005;280(39):33132–33140. doi:10.1074/jbc.M500608200
10. Khosla S. Minireview: The OPG/RANKL/RANK system. *Endocrinology*. 2001;142(12):5050–5055. doi:10.1210/endo.142.12.8536
11. Butler JS, Queally JM, Devitt BM, Murray DW, Doran PP, O'Byrne JM. Silencing *Dkk1* expression rescues dexamethasone-induced suppression of primary human osteoblast differentiation. *BMC Musculoskelet Disord*. 2010;11:210. doi:10.1186/1471-2474-11-210
12. Camassa JA, Diogo CC, Bordelo JPA, et al. Tartrate-resistant acid phosphate as biomarker of bone turnover over the lifespan and different physiologic stages in sheep. *BMC Vet Res*. 2017;13(1):239. doi:10.1186/s12917-017-1170-9
13. Ducy P, Zhang R, Geoffroy V, Ridall AL, Karsenty G. Osf2/Cbfa1: A transcriptional activator of osteoblast differentiation. *Cell*. 1997;89(5):747–754. doi:10.1016/s0092-8674(00)80257-3
14. Taylor LM, Turksen K, Aubin JE, Heersche JN. Osteoclast differentiation in cocultures of a clonal chondrogenic cell line and mouse bone marrow cells. *Endocrinology*. 1993;133(5):2292–2300. doi:10.1210/endo.133.5.7691585
15. Fu C, Xu D, Wang CY. Alpha-lipoic acid promotes osteoblastic formation in H_2O_2-treated MC3T3-E1 cells and prevents bone loss in ovariectomized rats. *J Cell Physiol*. 2015;230(9):2184–2201. doi:10.1002/jcp.24947
16. Quarles LD, Yohay DA, Lever LW, Caton R, Wenstrup RJ. Distinct proliferative and differentiated stages of murine MC3T3-E1 cells in culture: An in vitro model of osteoblast development. *J Bone Miner Res*. 1992;7(6):683–692. doi:10.1002/jbmr.5650070613
17. Kanzler B, Kuschert SJ, Liu YH, Mallo M. Hoxa-2 restricts the chondrogenic domain and inhibits bone formation during development of the branchial area. *Development*. 1998;125(14):2587–2597. PMID:9636074
18. Hu R, Liu W, Li H, et al. A Runx2/miR-3960/miR-2861 regulatory feedback loop during mouse osteoblast differentiation. *J Biol Chem*. 2011;286(14):12328–12339. doi:10.1074/jbc.M110.176099
19. Xie Q, Wang Z, Zhou H, et al. The role of miR-135-modified adipose-derived mesenchymal stem cells in bone regeneration. *Biomaterials*. 2016;75:279–294. doi:10.1016/j.biomaterials.2015.10.042
20. da Silva RA, Fuhler GM, Janmaat VT, et al. HOXA cluster gene expression during osteoblast differentiation involves epigenetic control. *Bone*. 2019;125:74–86. doi:10.1016/j.bone.2019.04.026
21. Naylor K, Eastell R. Bone turnover markers: Use in osteoporosis. *Nat Rev Rheumatol*. 2012;8(7):379–389. doi:10.1038/nrrheum.2012.86
22. Takahashi S. Bone metabolic markers for evaluation of bone metastases [in Japanese]. *Clin Calcium*. 2013;23:391–400. PMID:23445893
23. Komori T. Regulation of osteoblast differentiation by transcription factors. *J Cell Biochem*. 2006;99(5):1233–1239. doi:10.1002/jcb.20958
24. Martin TJ. Historically significant events in the discovery of RANK/RANKL/OPG. *World J Orthop*. 2013;4(4):186–197. doi:10.5312/wjo.v4.i4.186
25. Martin TJ, Sims NA. RANKL/OPG: Critical role in bone physiology. *Rev Endocr Metab Disord*. 2015;16(2):131–139. doi:10.1007/s11154-014-9308-6
26. Lane NE, Kelman A. A review of anabolic therapies for osteoporosis. *Arthritis Res Ther*. 2003;5(5):214–222. doi:10.1186/ar797
27. Marx RE, Garg AK. Bone structure, metabolism, and physiology: Its impact on dental implantology. *Implant Dent*. 1998;7:267–276. doi:10.1097/00008505-199807040-00004
28. Gersch RP, Lombardo F, McGovern SC, Hadjiargyrou M. Reactivation of Hox gene expression during bone regeneration. *J Orthop Res*. 2005;23(4):882–890. doi:10.1016/j.orthres.2005.02.005
29. Dobreva G, Chahrour M, Dautzenberg M, et al. *SATB2* is a multifunctional determinant of craniofacial patterning and osteoblast differentiation. *Cell*. 2006;125(5):971–986. doi:10.1016/j.cell.2006.05.012
30. Ellies DL, Krumlauf R. Bone formation: The nuclear matrix reloaded. *Cell*. 2006;125(5):840–842. doi:10.1016/j.cell.2006.05.022
31. Yang X, Jiang T, Wang Y, Guo L. The role and mechanism of *SIRT1* in resveratrol-regulated osteoblast autophagy in osteoporosis rats. *Sci Rep*. 2019;9(1):18424. doi:10.1038/s41598-019-44766-3
32. Liu P, Baumgart M, Groth M, et al. Dicer ablation in osteoblasts by Runx2 driven cre-loxP recombination affects bone integrity, but not glucocorticoid-induced suppression of bone formation. *Sci Rep*. 2016;6:32112. doi:10.1038/srep32112
33. Shen GY, Ren H, Shang Q, et al. Let-7f-5p regulates *TGFBR1* in glucocorticoid-inhibited osteoblast differentiation and ameliorates glucocorticoid-induced bone loss. *Int J Biol Sci*. 2019;15(10):2182–2197. doi:10.7150/ijbs.33490
34. Bruderer M, Richards RG, Alini M, Stoddart MJ. Role and regulation of *RUNX2* in osteogenesis. *Eur Cell Mater*. 2014;28:269–286. doi:10.22203/ecm.v028a19
35. Pratap J, Galindo M, Zaidi SK, et al. Cell growth regulatory role of *RUNX2* during proliferative expansion of preosteoblasts. *Cancer Res*. 2003;63(17):5357–5362. PMID:14500368
36. Franceschetti T, Dole NS, Kessler CB, Lee SK, Delany AM. Pathway analysis of microRNA expression profile during murine osteoclastogenesis. *PLoS One*. 2014;9:e107262. doi:10.1371/journal.pone.0107262
37. Baker N, Sohn J, Tuan RS. Promotion of human mesenchymal stem cell osteogenesis by PI3-kinase/Akt signaling, and the influence of caveolin-1/cholesterol homeostasis. *Stem Cell Res Ther*. 2015;6:238. doi:10.1186/s13287-015-0225-8
38. Baroncelli M, Fuhler GM, van de Peppel J, et al. Human mesenchymal stromal cells in adhesion to cell-derived extracellular matrix and titanium: Comparative kinome profile analysis. *J Cell Physiol*. 2019;234(3):2984–2996. doi:10.1002/jcp.27116
39. Chapurlat RD, Confavreux CB. Novel biological markers of bone: From bone metabolism to bone physiology. *Rheumatology (Oxford)*. 2016;55(10):1714–1722. doi:10.1093/rheumatology/kev410

Arbutin inhibits inflammation and apoptosis by enhancing autophagy via SIRT1

Chaoting Ma[A–F], Dandan Zhang[A–C,E,F], Qiuyan Ma[A–C,F], Yu Liu[A–C,F], Yingxin Yang[A–C,E,F]

Department of Ophthalmology, Beijing Hospital of Traditional Chinese Medicine, Capital Medical University, China

A – research concept and design; B – collection and/or assembly of data; C – data analysis and interpretation;
D – writing the article; E – critical revision of the article; F – final approval of the article

Address for correspondence
Yingxin Yang
E-mail: yingxingyxy@163.com

Abstract

Background. SIRT1 plays a protective role against diabetic retinopathy as it regulates inflammation, apoptosis and autophagy of cells.

Objectives. This study was designed to investigate the effects of arbutin and to identify a potential mechanism of action. Adult human retinal pigment epithelial (ARPE-19) cells were exposed to high glucose (HG) or treated with different concentrations of arbutin.

Materials and methods. The protein levels of pro-inflammatory cytokines, like tumor necrosis factor-α (TNF-α), interleukin (IL)-1β, IL-6, and p65 were assessed using enzyme-linked immunosorbent assay (ELISA). The expression of NF-κB p65 and cyclooxygenase-2 (COX-2) was detected with western blot assay. Cell apoptosis was analyzed with TUNEL assay, and expression levels of Bcl2, BAX, cleaved caspase-3, cleaved PARP, LC3II, LC3I, and beclin1 were detected with western blot assay. Autophagy levels were detected using LC3II immunofluorescence staining.

Results. Arbutin treatment markedly enhanced viability and autophagy mediators, decreased pro-inflammatory proteins and reduced apoptosis in ARPE cells under HG exposure, while increasing SIRT1 protein level. This could be blocked by Sirtinol treatment. Additionally, 3MA treatment significantly reduced the efficacy of arbutin against inflammatory markers and apoptosis in ARPE cells exposed to HG.

Conclusions. Arbutin suppressed inflammation and apoptosis of ARPE cells induced by HG by promoting autophagy via SIRT1. A potential target, SIRT1, was identified for the treatment of DR, and new effects of and action mechanisms for arbutin were found and confirmed.

Key words: arbutin, SIRT1, p65, autophagy, diabetic retinopathy

Background

Diabetic retinopathy (DR) is a serious complication of diabetes.[1,2] It begins with macular edema, which ruptures the blood–retina barrier and eventually leads to the formation of a hard exudate. Chronic hyperglycemia is the basis of DR pathogenesis.[3] Retinal pigment epithelium, located between the neuroretina and choroid, is an important dense pigment layer in the retina. It plays an important role in maintaining the structural and functional integrity of the retina,[4] as well as a crucial role in the pathogenesis of DR.[5,6]

Arbutin is a natural soluble glycosylated phenol with the molecular structure $C_{12}H_{16}O$. It exhibits a wide range of pharmacological activities, including anti-inflammatory and antioxidant effects.[7–10] Studies have shown that arbutin can protect HK-2 cells from damage induced by high glucose (HG),[11] and reduce H_2O_2-induced damage to optic ganglion cells.[12] However, whether arbutin can inhibit retinal damage induced by HG remains to be investigated. Studies have shown that arbutin can inhibit the effect of lipopolysaccharide-induced lung injury by activating silent mating type information regulator 2 homolog 1 (SIRT1).[13] The SIRT1, which is a NAD+-dependent class III histone deacetylase, plays a wide range of roles in retinal injury induced by HG, which could mediate the regulation of NF-κB signaling. It has been shown to regulate the cell apoptosis pathway in HG-treated cells.[14–20]

Objectives

The purpose of this study was to explore the mechanism of arbutin in reducing inflammation and apoptosis of retinal cells induced by HG.

Materials and methods

Cell line

Adult human retinal pigment epithelial (ARPE-19) were purchased from American Type Culture Collection (ATCC, Manassas, USA). The ARPE-19 cells were cultured in DMEM/F12 medium (Hyclone, Logan, USA) containing 10% fetal bovine serum (FBS; Gibco, Waltham, USA), in a cell incubator at a constant temperature of 37°C, containing 5% CO_2. The cell status was observed daily, and the medium was changed every 2 days.

MTT assay

The ARPE-19 cells at logarithmic growth phase were seeded into 96-well plates with a cell density of 1×10^4/mL (200 μL of cell suspension; Corning Inc., Corning, USA). After the cells fully adhered to the well, the culture medium was removed and replaced with a high-sugar treatment; for the control group, this comprised normal culture medium, while the rest of the treatment groups, medium was used with a glucose concentration of 50 mmol/L. Cells were cultured for 24 h or 48 h. The medium was removed and MTT was added. Cells were cultured at 37°C for 4 h, then dimethyl sulfoxide (DMSO) was added to fully dissolve the crystals. The optical density (OD) at 490 nm was detected using a microplate reader (SpectraMax M5; Thermo Fisher Scientific, Waltham, USA).

ELISA

The ARPE-19 cells (5×10^4/mL) at logarithmic growth phase were seeded into cell culture flask. Twenty-four hours after adherent fusion, the cells were treated with different concentrations of arbutin for 24 h or 48 h. The culture medium was collected and centrifuged at 3000 rpm for 10 min to obtain the supernatant. The protein levels of pro-inflammatory cytokines, like TNF-a, IL-1β, IL-6, and p65 were assessed using ELISA assay. The expression of NF-κB p65 and cyclooxygenase-2 (COX-2) was detected with western blot assay. The absorbance at 450 nm was detected using a microplate reader (SpectraMax M5).

Western blot

The ARPE-19 cells in each group were collected and digested using RIPA Lysis Buffer containing phenylmethylsulfonyl fluoride (PMSF; 80 μL) for 30 min. The supernatant was collected in a high-speed bench refrigerated centrifuge. The concentration of protein was detected using the BCA method. After SDS-PAGE electrophoresis, the protein was transferred to a polyvinylidene difluoride (PVDF) membrane, which was blocked using bovine serum albumin (BSA) for 1 h and then washed with Tris-buffered saline with Tween (TBST) 3 times. The primary antibody (NF-κB p65, ab32536, 1 : 30; COX-2, ab169782, 1 : 2000; Bcl-2, ab32124, 1 : 1000; Bax, ab182733, 1 : 2000; cleaved caspase-3, ab32042, 1 : 500; *GADPH*, ab8245, 1 : 2000; all from Abcam, Cambridge, UK; and cleaved PARP, #9541, 1 : 1000; Cell Signaling Technology, Inc., Danvers, USA) was produced using the corresponding dilutions detailed above, added to the membrane and incubated at 4°C overnight. The membrane was then washed with TBST 3 times on the 2nd day. The secondary antibody conjugated with horseradish peroxidase (HRP; ab7090, ab97040, 1 : 10000; Abcam) was then added and incubated with the membrane in a shaker at room temperature for 1 h. *GAPDH* was used as an internal reference.

TUNEL assay

Apoptotic cells were stained with FITC-labeled dUTP using terminal deoxynucleotidyl transferase as a catalyst. The experiment was performed using a TUNEL kit (Roche, Basel, Switzerland) according to the manufacturer's

protocol. DAPI was used to stain the nucleus, and results were observed under a fluorescence microscope (Olympus Corp., Tokyo, Japan).

Immunofluorescence assay

The cells were fixed with 100% methanol for 5 min at room temperature and then permeabilized with Triton X-100 (3 g/L) for 30 min. The primary antibody (anti-LC3II; Abcam) was used with cells overnight at 4°C. Next, the secondary antibody (an Alexa Fluor® 488 goat anti-rabbit secondary antibody; Abcam) was added for incubation for 30 min at room temperature. DAPI was used to stain the nucleus. Anti-fluorescent quenching agent was added to mount the sections. The cells were observed under a fluorescence microscope (Olympus Corp.).

Statistical analyses

Summary results were expressed as mean ± standard deviation (SD). Each experiment was repeated 3 times or more within each group. Data comparing more than 2 groups were analyzed with one-way analysis of variance (ANOVA), followed by Tukey's test. Each experiment was repeated at least 3 times. A value of $p < 0.05$ indicated that differences between groups were statistically significant. Statistical analysis was performed using Graph Pad Prism v. 8.0 software (GraphPad Software, San Diego, USA).

Results

The effects of arbutin on APRE19 cell viability following HG exposure

Retinal pigment epithelial cells are regarded as the most important cells implicated in DR. A MTT assay was used to detect the effects of different concentrations of arbutin (25 µm, 50 µm or 100 µm) on the cell viability of APRE19 cells. Results showed that there was no statistically significant difference in the viability of APRE19 cells treated with 25 µm, 50 µm or 100 µm arbutin after 24 h or 48 h compared with the control group (0 µm) (Fig. 1A). When the cells were pretreated with 25 µm, 50 µm or 100 µm arbutin for 1 h and then treated with HG (30 mM), the activity of ARPE-19 cells was significantly higher than that of the HG group in a dose-dependent manner (Fig. 1B).

The effects of arbutin on the NF-κB pathway

As shown in Fig. 2A, the expression levels of TNF-a, IL-1β and IL-6 in the APRE19 cell supernatant treated with 30 mmol/L HG for 24 h were significantly higher than those of the control group. After pretreatment with arbutin, APRE19 cells were cultured in a high-sugar environment,
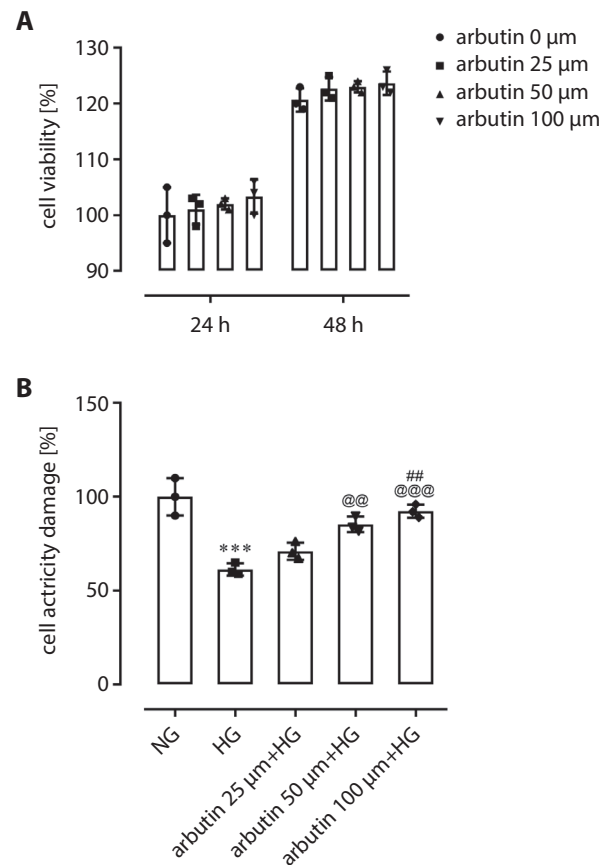
Fig. 1. A. After APRE19 cells were treated with arbutin at different concentrations (0 µm, 25 µm, 50 µm, or 100 µm) for 24 h or 48 h, there was no significant change in the viability of APRE19 cells;
B. Arbutin pre-treatment markedly increased the viability of APRE19 cells under HG conditions. Results are expressed as mean ±SD

***$p < 0.001$ compared to NG group; @@$p < 0.01$ and @@@$p < 0.001$ compared to HG group; ##$p < 0.01$ compared to arbutin 25 µM+HG group.

and TNF-α, IL-1β, and IL-6 levels in the cell supernatant were significantly reduced in a dose-dependent manner. The protein expression levels of NF-κB p65 and COX-2 in APRE19 cells were assessed using western blotting assay. The expression levels of NF-κB p65 and COX-2 were significantly increased by different modes (25 µm, 50 µm or 100 µm) of arbutin treatment (Fig. 2B,C).

Arbutin inhibition of apoptosis in APRE19 cells under HG exposure

A TUNEL assay was used to detect the effects of different concentrations of arbutin (25 µm, 50 µm or 100 µm) on apoptosis in APRE19 cells. Compared with the HG group, APRE19 cells treated with arbutin showed gradually decreasing apoptosis levels with increasing arbutin concentration (Fig. 3A). To identify the potential mechanism by which arbutin suppressed cell apoptosis, levels of Bcl2, BAX, cleaved caspase-3 and cleaved PARP were detected through western blotting assay (Fig. 3B,C). The results show that arbutin led to a significant reduction in the expression of BAX, cleaved caspase-3 and cleaved PARP

A

B

C
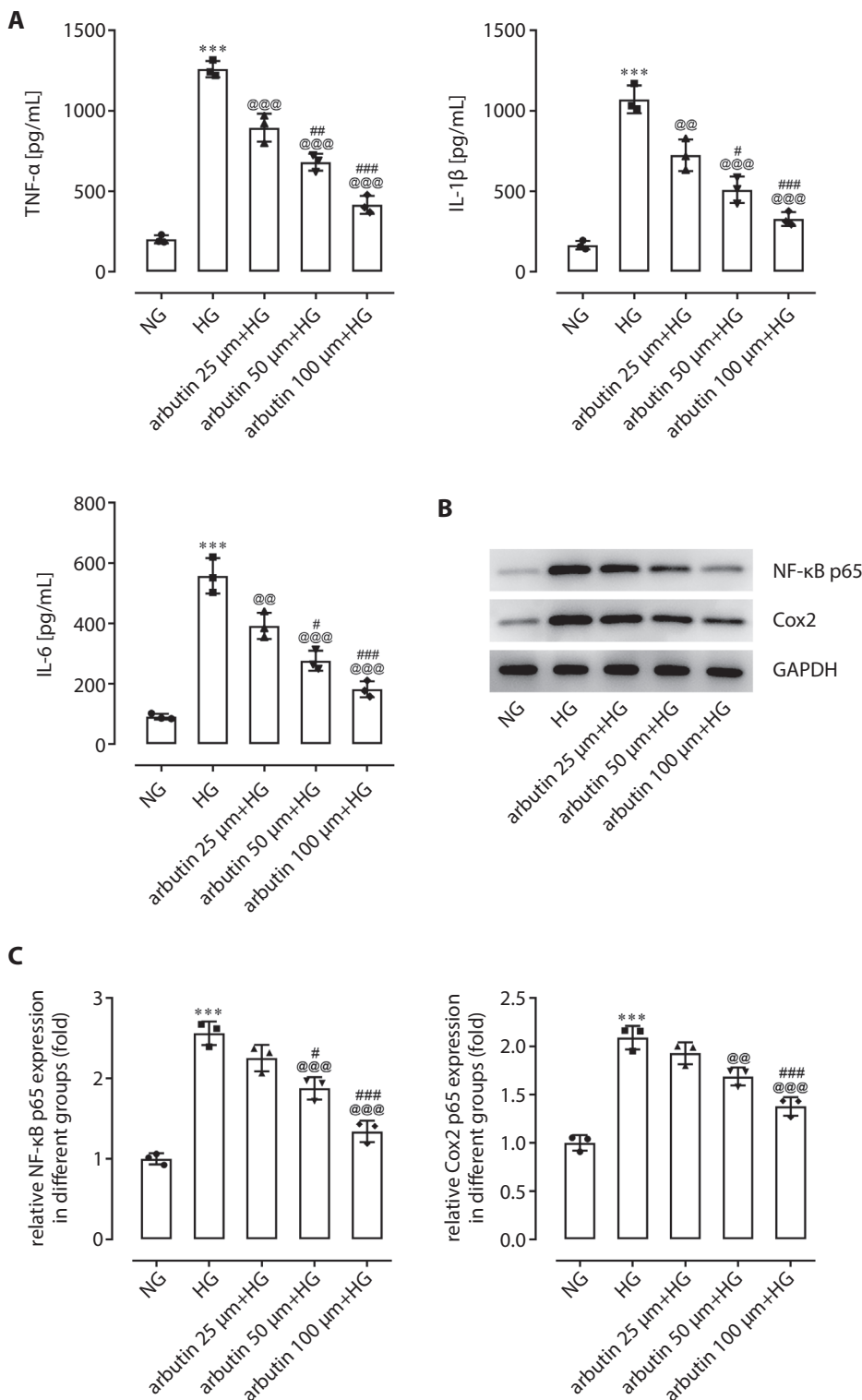
Fig. 2. A. TNF-a, IL-1β and IL-6 expression levels in APRE19 under HG stimulation after pretreatment with different concentrations of arbutin (25 μm, 50 μm or 100 μm) were determined using ELISA;
B and C. The effect of arbutin on NF-κB p65 and COX-2 expression in APRE19 cells quantified with western blot. Results are expressed as mean ±SD

***$p < 0.001$ compared to NG group; @@$p < 0.01$ and @@@$p < 0.001$ compared to HG group; #$p < 0.05$, ##$p < 0.01$ and ###$p < 0.001$ compared to arbutin 25 μM+HG group.

in APRE19 cells compared with the HG group. On the contrary, the expression of Bcl2 was increased.

SIRT1 inhibition interferes with arbutin suppression of autophagy

The above results fully demonstrated that arbutin could suppress both the activity and levels of inflammatory mediators, and cell apoptosis caused by HG. However, the exact mechanism of the action of arbutin was unknown. A study has suggested that SIRT1 can reduce inflammation and apoptosis of cardiomyocytes by promoting autophagy.[21] Therefore, we investigated whether SIRT1 could mediate the effects of arbutin on the inflammation and apoptosis of APRE19 cells. Western blotting was used to detect the changes of SIRT1 protein expression
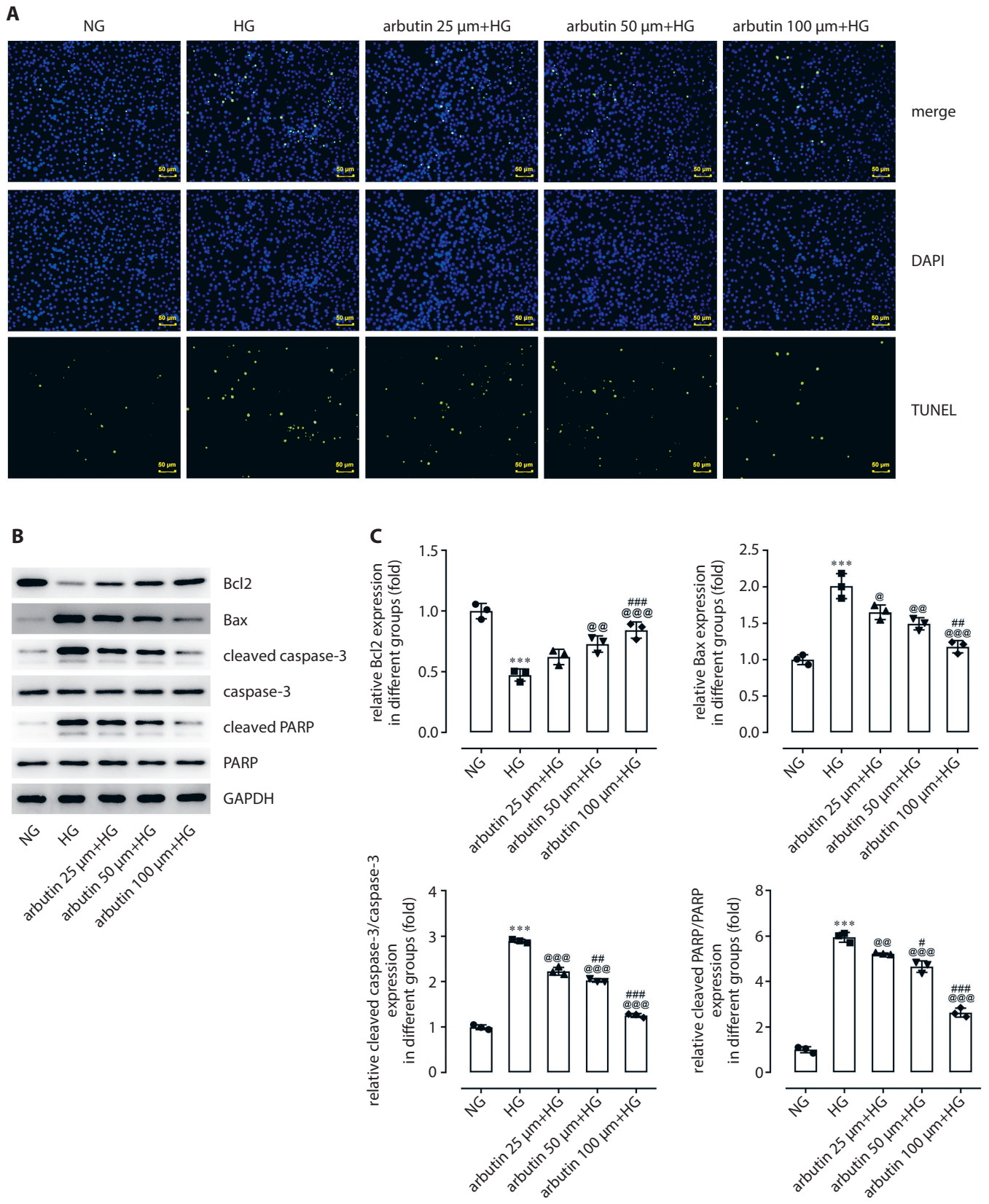
Fig. 3. A. TUNEL assay was used for the analysis of cell apoptosis in HG-induced APRE19 cells; B and C. Apoptosis-related protein levels quantified using ELISA assay. Results are expressed as mean ±SD

***p < 0.001 compared to NG group; @p < 0.05, @@p < 0.01 and @@@p < 0.001 compared to HG group; ##p < 0.01 and ###p < 0.001 compared to arbutin 25 μM+HG group.
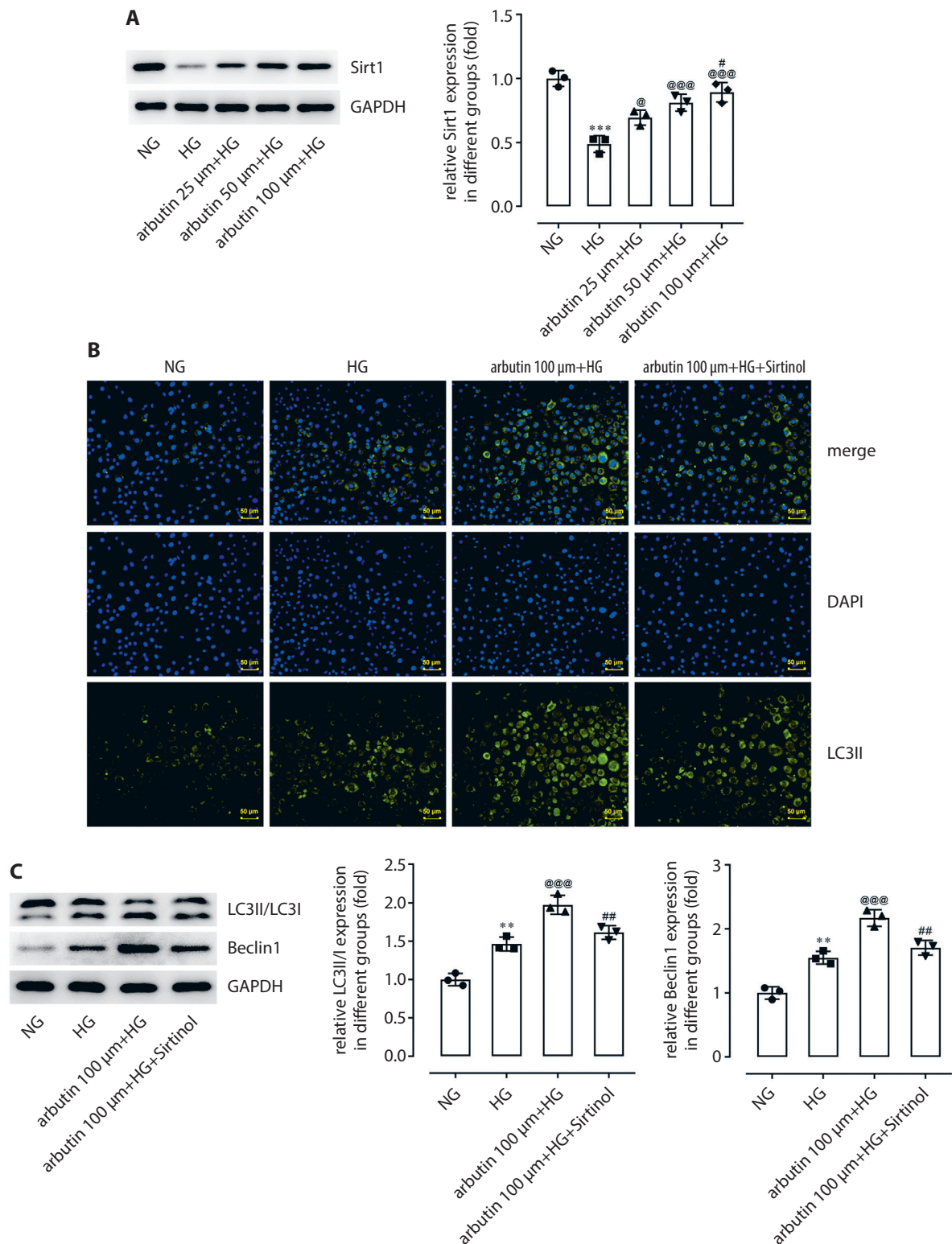
Fig. 4. A. SIRT1 expression quantified using western blot following HG or arbutin treatment; B. Immunofluorescence staining of LC3II; C. Expression levels of beclin 1, LC3II and LC3I quantified using western blot. Results are expressed as mean ±SD

**p < 0.01 and ***p < 0.001 compared to NG group; @p < 0.05 and @@@p < 0.001 compared to HG group. #p < 0.05 and ##p < 0.01 compared to arbutin 25 μM+HG group.

in APRE19 cells after arbutin treatment at different concentrations (25 μm, 50 μm or 100 μm). The HG exposure significantly reduced the relative protein level of SIRT1 in APRE19 cells when compared to the normal glucose

(NG) group (Fig. 4A). Additionally, compared to the HG group, the expression level of SIRT1 in APRE19 cells significantly increased in response to increased arbutin concentration (Fig. 4A).
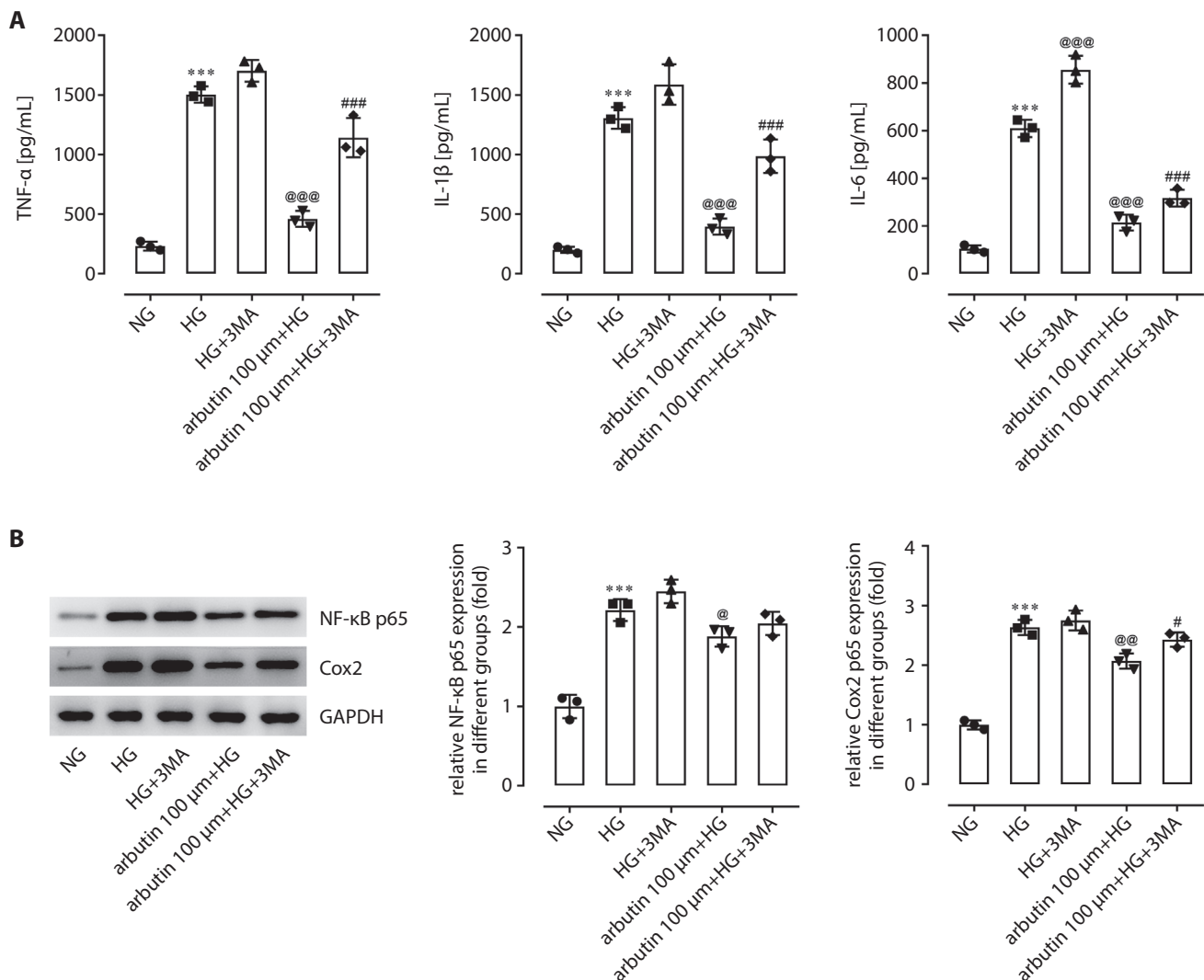
Fig. 5. A. 3MA suppresses the effects of arbutin on the expression of TNF-a, IL-1β and IL-6 in APRE19 cell supernatant under HG stimulation; B. 3MA suppresses the effects of arbutin on the expression of NF-KB p65 and COX-2 in APRE19 cell supernatant under HG stimulation. Results are expressed as mean ±SD

***p < 0.001 compared to NG; @p < 0.05, @@p < 0.01 and @@@p < 0.001 compared to HG; #p < 0.05 and ###p < 0.001 compared to arbutin 25 μM+HG group.

Sirtinol (100 μm), an inhibitor of SIRT1, was used to pretreat APRE19 cells for 1 h, after which APRE19 cells underwent a combination treatment of HG and arbutin (100 μm) for 24 h. The immunofluorescence results showed that expression of LC3ll in the HG group was higher than expression in the normal group (Fig. 4B). LC3ll expression was further increased by co-treatment with arbutin and HG. Surprisingly, sirtinol significantly suppressed the effects of arbutin.

Western blot results showed that the expression level of beclin 1 and the ratio of LC3II/LC3I were both significantly higher in the HG group than that in the control group. Beclin-1 is an autophagy-related protein necessary for the formation of autophagosomes, which has increased expression in the retinas of diabetic rats.[22] Arbutin treatment led to a further significant increase in the expression of beclin 1 and in the ratio of LC3II/LC3I, which was lessened by addition of sirtinol (Fig. 4C).

Autophagy blocking suppresses the anti-inflammatory effects of arbutin

Following pretreatment for 1 h with 3-methyladenine (3MA), an autophagy inhibitor, and culture in a HG environment, the levels of TNF-a, IL-1β and IL-6 in cell supernatant were significantly higher than those cultured in a HG environment alone (Fig. 5A). Moreover, 3MA pretreatment markedly blocked the effects of arbutin on these pro-inflammatory mediators, implying that the inflammation of APRE19 cells induced by HG may have been suppressed by arbutin via autophagy enhancement. Furthermore, we observed a similar action mechanism of arbutin in decreasing NF-KB p65 and COX-2 expression (Fig. 5B).

A

B

C
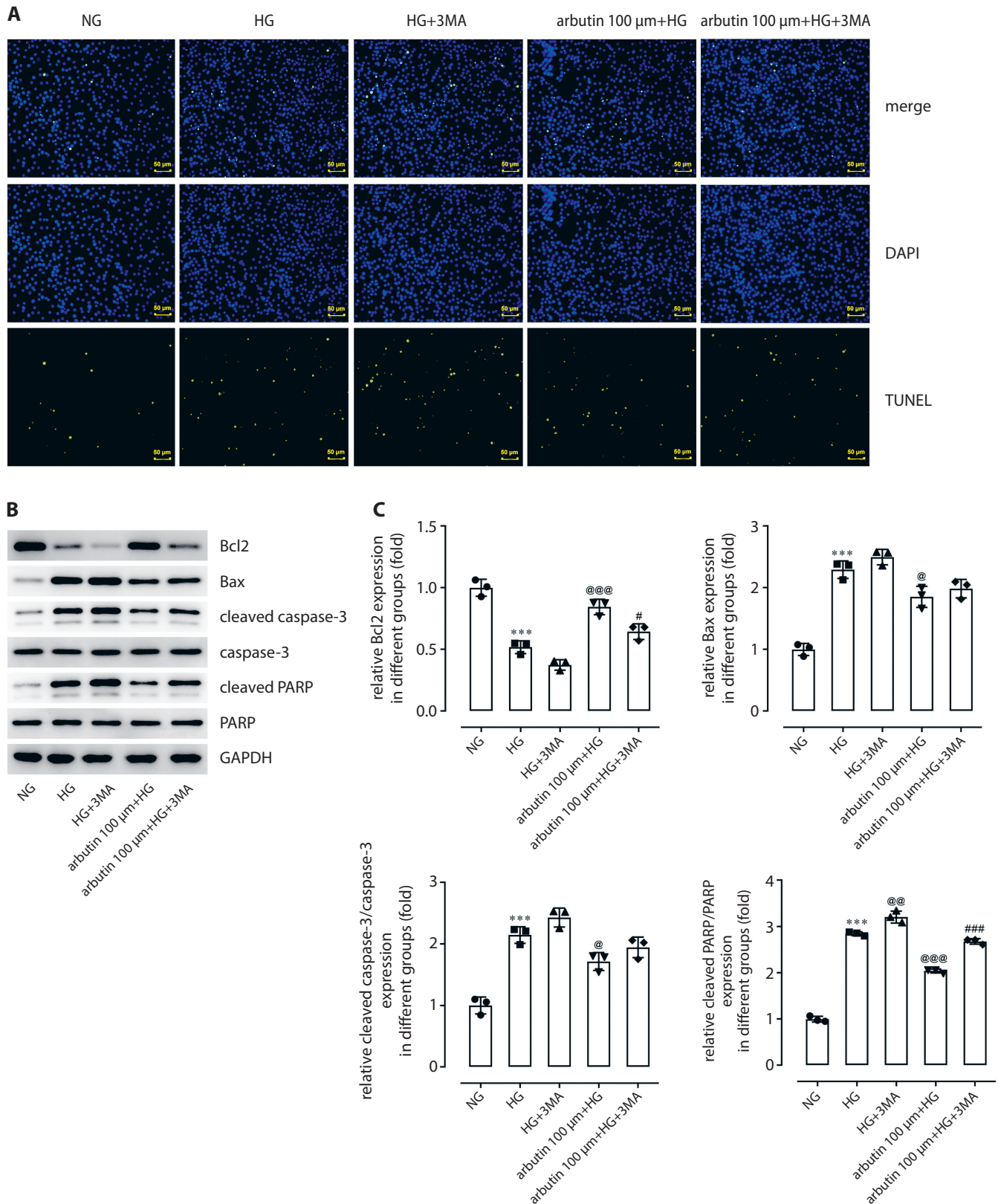
Fig. 6. A. APRE19 cell apoptosis visualized with TUNEL staining; B and C. Quantification of Bcl2, BAX, cleaved caspase-3, and cleaved PARP expression using western blot. Results are expressed as mean ±SD

***$p < 0.001$ compared to NG group. @$p < 0.05$, @@$p < 0.01$ and @@@$p < 0.001$ compared to HG group; #$p < 0.05$ and ##$p < 0.01$ compared to arbutin 25 µM+HG group.

Inhibition of autophagy cancels out the anti-apoptotic effects of arbutin

Pretreatment with 3MA for 1 h increased the apoptosis level of APRE19 cells stimulated by HG in comparison with the HG group (Fig. 6A). Expression levels of BAX, cleaved caspase-3 and cleaved PARP in the APRE19 cells were also elevated by 3MA while Bcl2 was decreased (Fig. 6B,C). Furthermore, 3MA could reverse the influence of arbutin on the cellular behaviors brought about by HG induction, suggesting the involvement of autophagy in the inhibition of apoptosis by arbutin. Based on the abovementioned results, we drew the conclusion that arbutin produced inhibitory effects on inflammation and apoptosis by enhancing autophagy via SIRT1.

Discussion

Arbutin is commonly used as a protective agent, with no toxic effects to cells, and in vitro studies have shown that the activity of cells is not significantly affected by high concentrations of arbutin.[23] Our findings are similar, in that ARPE19 cell viability was not significantly affected by an increase in arbutin concentration. Furthermore, arbutin markedly enhanced the viability of ARPE19 cells exposed to HG, suggesting that arbutin could protect these cells from HG-induced injury.

The presence of hyperglycemia in DR affects multiple biochemical pathways, such as the polyol, late glycosylated end-product and protein kinase C (PKC) pathways, the activation of which can lead to oxidative stress, inflammation and leucocyte stagnation, and induce the secretion of growth factors and cytokines, apoptosis and autophagy.[20,22,24–26] Previous studies found that some inflammatory factors, such as IL-1β, IL-6 and TNF-α, are strongly correlated with the severity of DR.[27–29]

Inflammatory cytokines in RPE can be promoted in a HG environment,[30] and high levels of TNF-α, IL-1β, and IL-6 were observed in APRE19 cells when induced by HG stimulation. These were significantly decreased by arbutin treatment in a dose-dependent manner. Hyperglycemia causes inflammation of the retina, which in turn leads to apoptosis.[31] In addition to the inhibition of cell apoptosis by arbutin, the protein levels of Bcl2, BAX, cleaved caspase-3, and cleaved PARP were significantly downregulated in APRE19 cells treated with arbutin, indicating regulation of the apoptosis pathway, mediated by mitochondria. Cleaved PARP plays an important role in DNA damage repair and apoptosis, as a cleaving substrate of caspase and a core component of the apoptosis pathway.[32,33]

The regulation of autophagy is closely connected to the progression of DR. Basal autophagy exerted anti-inflammatory effects, as recently reviewed.[34] Under HG stimulation, increased autophagy levels may be insufficient to balance protein and organelle turnover.[22,34] We observed elevated autophagy levels in ARPE cells induced by HG, which were further enhanced by arbutin addition. It is surprising that sirtinol, as an inhibitor of SIRT1, significantly blocked the enhancement of autophagy by arbutin, although previously some studies have shown regulation of autophagy via SIRT1.

In our subsequent experiments, the inhibition of autophagy by 3MA could significantly hinder the regulatory effects of arbutin on HG-triggered ARPE19 cell behaviors that we confirm in this study. SIRT1 has been implicated in regulating inflammation and apoptosis processes in DR,[35] and showed increased levels following arbutin treatment. The NFκB pathway regulates the expression of COX-2, through initiating transcription of the *PTGS2* gene, which encodes COX-2.[36] SIRT1 has been reported to suppress NF-κB activities, which are closely correlated with the expression of IL-1β, IL-6 and TNF-α, reduce COX-2 expression and play a vital role in inflammation.[35,37] Therefore, in the present study, arbutin could suppress inflammation by upregulating SIRT1 via inhibition of the NF-κB pathway. However, this needs to be confirmed by much deeper research. In RPE cells, SIRT1 could produce anti-apoptotic effects and reduce mitochondrial damage.[38] Based on these experimental results, mitochondria-mediated apoptosis induced by HG could be suppressed through enhancement of SIRT1 expression by arbutin.

Limitations

There is still lack of in vivo evidence supporting the positive effects of arbutin on DR. Additionally, how arbutin promoted the expression of Sirt1 requires further deeper studies.

Conclusions

Arbutin treatment protected ARPE cells from inflammation and apoptosis induced by HG induction. The mechanism for this was autophagy enhancement via SIRT1. The present study provides novel insight into the treatment of DR and identifies a new molecular target for the development of therapy.

ORCID iDs

Chaoting Ma https://orcid.org/0000-0003-3682-8312
Dandan Zhang https://orcid.org/0000-0003-3040-7007
Qiuyan Ma https://orcid.org/0000-0003-3450-7195
Yu Liu https://orcid.org/0000-0001-7990-8983
Yingxin Yang https://orcid.org/0000-0002-3089-0273

References

1. Moldogazieva NT, Lutsenko SV, Terentiev AA. Reactive oxygen and nitrogen species-induced protein modifications: Implication in carcinogenesis and anticancer therapy. *Cancer Res*. 2018;78(21):6040–6047. doi:10.1158/0008-5472.CAN-18-0980

2.   Lin LM, Peng F, Liu YP, et al. Coadministration of VDR and RXR agonists synergistically alleviates atherosclerosis through inhibition of oxidative stress: An in vivo and in vitro study. *Atherosclerosis*. 2016;251: 273–281. doi:10.1016/j.atherosclerosis.2016.06.005

3.   Jeffrey BG, Weisinger HS, Neuringer M, Mitchell DC. The role of docosahexaenoic acid in retinal function. *Lipids*. 2001;36(9):859–871. doi:10.1007/s11745-001-0796-3

4.   Strauss O. The retinal pigment epithelium in visual function. *Physiol Rev*. 2005;85(3):845–881. doi:10.1152/physrev.00021.2004

5.   Ponnalagu M, Subramani M, Jayadev C, Shetty R, Das D. Retinal pigment epithelium-secretome: A diabetic retinopathy perspective. *Cytokine*. 2017;95:126–135. doi:10.1016/j.cyto.2017.02.013

6.   Grigsby J, Betts B, Vidro-Kotchan E, Culbert R, Tsin A. A possible role of acrolein in diabetic retinopathy: Involvement of a VEGF/TGFβ signaling pathway of the retinal pigment epithelium in hyperglycemia. *Curr Eye Res*. 2012;37(11):1045–1053. doi:10.3109/02713683.2012.713152

7.   Ebrahim-Tabar F, Nazari A, Pouramir M, Ashrafpour M, Pourabdolhossein F. Arbutin improves functional recovery and attenuates glial activation in lysolecethin-induced demyelination model in rat optic chiasm. *Mol Neurobiol*. 2020;57(7):3228–3242. doi:10.1007/s12035-020-01962-x

8.   Nakamura Y, Torikai K, Ohto Y, Murakami A, Tanaka T, Ohigashi H. A simple phenolic antioxidant protocatechuic acid enhances tumor promotion and oxidative stress in female ICR mouse skin: Dose-and timing-dependent enhancement and involvement of bioactivation by tyrosinase. *Carcinogenesis*. 2000;21(10):1899–1907. doi:10.1093/carcin/21.10.1899

9.   Safari H, Zabihi Z, Pouramir M, et al. Decrease of intracellular ROS by arbutin is associated with apoptosis induction and downregulation of IL-1β and TNF-α in LNCaP prostate cancer. *J Food Biochem*. 2020:e13360. doi:10.1111/jfbc.13360

10. Ahmadian SR, Ghasemi-Kasman M, Pouramir M, Sadeghi F. Arbutin attenuates cognitive impairment and inflammatory response in pentylenetetrazol-induced kindling model of epilepsy. *Neuropharmacology*. 2019;146:117–127. doi:10.1016/j.neuropharm.2018.11.038

11. Lv L, Zhang J, Tian F, Li X, Li D, Yu X. Arbutin protects HK-2 cells against high glucose-induced apoptosis and autophagy by up-regulating microRNA-27a. *Artif Cells Nanomed Biotechnol*. 2019;47(1):2940–2947. doi:10.1080/21691401.2019.1640231

12. Zhao W, Wang S, Qin T, Wang W. Arbutin attenuates hydrogen peroxide-induced oxidative injury through regulation of microRNA-29a in retinal ganglion cells. *Biomed Pharmacother*. 2019;112:108729. doi:10.1016/j.biopha.2019.108729

13. Ye J, Guan M, Lu Y, Zhang D, Li C, Zhou C. Arbutin attenuates LPS-induced lung injury via Sirt1/Nrf2/NF-κBp65 pathway. *Pulm Pharmacol Ther*. 2019;54:53–59. doi:10.1016/j.pupt.2018.12.001

14. Manna P, Achari AE, Jain SK. Vitamin D supplementation inhibits oxidative stress and upregulate SIRT1/AMPK/GLUT4 cascade in high glucose-treated 3T3L1 adipocytes and in adipose tissue of high fat diet-fed diabetic mice. *Arch Biochem Biophys*. 2017;615:22–34. doi:10.1016/j.abb.2017.01.002

15. Qu B, Gong K, Yang H, et al. SIRT1 suppresses high glucose and palmitate-induced osteoclast differentiation via deacetylating p66Shc. *Mol Cell Endocrinol*. 2018;474:97–104. doi:10.1016/j.mce.2018.02.015

16. Luo J, He T, Yang J, Yang N, Li Z, Xing Y. SIRT1 is required for the neuroprotection of resveratrol on retinal ganglion cells after retinal ischemia-reperfusion injury in mice. *Graefes Arch Clin Exp Ophthalmol*. 2020;258(2):335–344. doi:10.1007/s00417-019-04580-z

17. Mortuza R, Feng B, Chakrabarti S. SIRT1 reduction causes renal and retinal injury in diabetes through endothelin 1 and transforming growth factor β1. *J Cell Mol Med*. 2015;19(8):1857–1867. doi:10.1111/jcmm.12557

18. Zeng Y, Yang K, Wang F, et al. The glucagon like peptide 1 analogue, exendin-4, attenuates oxidative stress-induced retinal cell death in early diabetic rats through promoting Sirt1 and Sirt3 expression. *Exp Eye Res*. 2016;151:203–211. doi:10.1016/j.exer.2016.05.002

19. Zhang TH, Huang CM, Gao X, Wang JW, Hao LL, Ji Q. Gastrodin inhibits high glucose-induced human retinal endothelial cell apoptosis by regulating the SIRT1/TLR4/NF-κBp65 signaling pathway. *Mol Med Rep*. 2018;17(6):7774–7780. doi:10.3892/mmr.2018.8841

20. Tong P, Peng QH, Gu LM, Xie WW, Li WJ. LncRNA-MEG3 alleviates high glucose induced inflammation and apoptosis of retina epithelial cells via regulating miR-34a/SIRT1 axis. *Exp Mol Pathol*. 2019;107:102–109. doi:10.1016/j.yexmp.2018.12.003

21. Luo G, Jian Z, Zhu Y, et al. Sirt1 promotes autophagy and inhibits apoptosis to protect cardiomyocytes from hypoxic stress. *Int J Mol Med*. 2019;43(5):2033–2043. doi:10.3892/ijmm.2019.4125

22. Lopes de Faria JM, Duarte DA, Montemurro C, Papadimitriou A, Consonni SR, Lopes de Faria JB. Defective autophagy in diabetic retinopathy. *Invest Ophthalmol Vis Sci*. 2016;57(10):4356–4366. doi:10.1167/iovs.16-19197

23. Jurica K, Brčić Karačonji I, Mikolić A, Milojković-Opsenica D, Benković V, Kopjar N. In vitro safety assessment of the strawberry tree (*Arbutus unedo* L.) water leaf extract and arbutin in human peripheral blood lymphocytes. *Cytotechnology*. 2018;70(4):1261–1278. doi:10.1007/s10616-018-0218-4

24. Zhou P, Xie W, Meng X, et al. Notoginsenoside R1 ameliorates diabetic retinopathy through PINK1-dependent activation of mitophagy. *Cells*. 2019;8(3):213. doi:10.3390/cells8030213

25. Chen P, Miao Y, Yan P, Wang XJ, Jiang C, Lei Y. MiR-455-5p ameliorates HG-induced apoptosis, oxidative stress and inflammatory via targeting SOCS3 in retinal pigment epithelial cells. *J Cell Physiol*. 2019; 234(12):21915–21924. doi:10.1002/jcp.28755

26. Stitt AW, Curtis TM, Chen M, et al. The progress in understanding and treatment of diabetic retinopathy. *Prog Retin Eye Res*. 2016;51:156–186. doi:10.1016/j.preteyeres.2015.08.001

27. Ozturk BT, Bozkurt B, Kerimoglu H, Okka M, Kamis U, Gunduz K. Effect of serum cytokines and VEGF levels on diabetic retinopathy and macular thickness. *Mol Vis*. 2009;15:1906–1914. PMID:19784389

28. Maier M, Weger M, Haller-Schober EM, et al. Multiplex bead analysis of vitreous and serum concentrations of inflammatory and proangiogenic factors in diabetic patients. *Mol Vis*. 2008;14:637–643.

29. Koleva-Georgieva DN, Sivkova NP, Terzieva D. Serum inflammatory cytokines IL-1beta, IL-6, TNF-alpha and VEGF have influence on the development of diabetic retinopathy. *Folia Med (Plovdiv)*. 2011; 53(2):44–50. doi:10.2478/v10153-010-0036-8

30. Zhang W, Liu H, Rojas M, Caldwell RW, Caldwell RB. Anti-inflammatory therapy for diabetic retinopathy. *Immunotherapy*. 2011;3(5):609–628. doi:10.2217/imt.11.24

31. Tangvarasittichai O, Tangvarasittichai S. Oxidative stress, ocular disease and diabetes retinopathy. *Curr Pharm Des*. 2018;24(40):4726–4741. doi:10.2174/1381612825666190115121531

32. Adki KM, Kulkarni YA. Potential biomarkers in diabetic retinopathy. *Curr Diabetes Rev*. 2020;16(9):971–983. doi:10.2174/1573399816666200217092022

33. Luo DW, Zheng Z, Wang H, et al. UPP mediated diabetic retinopathy via ROS/PARP and NF-κB inflammatory factor pathways. *Curr Mol Med*. 2015;15(8):790–799. doi:10.2174/1566524015666150921110500

34. Rosa MD, Distefano G, Gagliano C, Rusciano D, Malaguarnera L. Autophagy in diabetic retinopathy. *Curr Neuropharmacol*. 2016;14(8): 810–825. doi:10.2174/1570159x14666160321122900

35. Karbasforooshan H, Karimi G. The role of SIRT1 in diabetic retinopathy. *Biomed Pharmacother*. 2018;97:190–194. doi:10.1016/j.biopha.2017.10.075

36. Wyatt GL, Crump LS, Young CM, et al. Cross-talk between SIM2s and NFκB regulates cyclooxygenase 2 expression in breast cancer. *Breast Cancer Res*. 2019;21(1):131. doi:10.1186/s13058-019-1224-y

37. Mendes KL, Lelis DF, Santos SHS. Nuclear sirtuins and inflammatory signaling pathways. *Cytokine Growth Factor Rev*. 2017;38:98–105. doi:10.1016/j.cytogfr.2017.11.001

38. Bhattacharya S, Chaum E, Johnson DA, Johnson LR. Age-related susceptibility to apoptosis in human retinal pigment epithelial cells is triggered by disruption of p53-Mdm2 association. *Invest Ophthalmol Vis Sci*. 2012;53(13):8350–8366. doi:10.1167/iovs.12-10495

Ultrasound irradiation inhibits proliferation of cervical cancer cells by initiating endoplasmic reticulum stress-mediated apoptosis and triggering phosphorylation of JNK

Juan Qin[1,B–D,F], Guolin Song[2,B–D,F], Yan Wang[3,A,B,E,F], Qin Liu[1,B,C,E,F], Hong Lin[1,B,C,F], Jinyun Chen[3,A,C,E,F]

[1] Department of Gynecology, Guiyang Maternal and Child Health Care Hospital, China

[2] Guizhou University of Traditional Chinese Medicine, Guiyang, China

[3] State Key Laboratory of Ultrasound in Medicine and Engineering, College of Biomedical Engineering, Chongqing Key Laboratory of Biomedical Engineering, Chongqing Medical University, China

A – research concept and design; B – collection and/or assembly of data; C – data analysis and interpretation;
D – writing the article; E – critical revision of the article; F – final approval of the article

Address for correspondence
Jinyun Chen
E-mail: qinjuan2019@sina.com

Abstract

Background. Cervical cancer is the 2nd most frequently diagnosed gynecological cancer. Therefore, it is clinically significant to discover an effective anti-cancer approach.

Objectives. This study aimed to investigate the effects of low-intensity ultrasound irradiation (USI) on cervical cancer cells and associated mechanisms of cell death.

Materials and methods. Normal human cervical HaCaT cells and cervical cancer cell lines C33A, Hela and Siha were cultured and γ-rays applied at a dosage of 2.0 Gy/min. The MTT assay was then used to assess viability (proliferation) of HaCaT, C33A, Hela, and Siha cells. Small interfering RNA (siRNA) sequences that silence the glucose-related protein (*GRP78*) gene were synthesized. Structural changes to cells exposed to USI were observed with scanning electron microscopy. Immunocytochemistry and western blotting were utilized to examine *GRP78*, C/EBP-homologous protein (CHOP), phosphorylated JNK (p-JNK), and caspase-12 expression in cervical cancer cells.

Results. Ultrasound irradiation reduced the viability of cervical cancer cells and increased apoptosis, compared to untreated tumor cells ($p < 0.05$). This effect was not apparent on HaCaT cells. Ultrasound irradiation also induced formation of apoptotic bodies compared to untreated tumor cells ($p < 0.05$), and activated endoplasmic reticulum (ER) stress-associated apoptosis compared to untreated tumor cells ($p < 0.05$), by triggering *GRP78*, CHOP and caspase-12 expression. Moreover, USI triggered ER stress by upregulating *GRP78* expression. Remarkably, USI triggered phosphorylation of JNK compared to untreated tumor cells ($p < 0.05$). Ultrasound irradiation initiated phosphorylation of JNK by increasing *GRP78* expression. Silencing of *GRP78* further enhanced the effect of USI on tumor cells.

Conclusions. Ultrasound irradiation significantly inhibited proliferation and induced apoptosis of cervical cancer cells by initiating ER stress associated with apoptosis signaling pathways and triggering phosphorylation of JNK.

Key words: apoptosis, cervical cancer, ER stress, ultrasound irradiation

Background

Cervical cancer is the 2nd most frequently diagnosed gynecological cancer and the 4th leading cause of tumor-associated death for females worldwide.[1,2] About 275,100 women are diagnosed with cervical cancer and die every year, which accounts for 9% of all cancer-associated female mortality.[3] Among the deaths from cervical cancer, approx. 85% occurs in developing countries,[4] where patients lack the effective therapy resources for cervical cancer treatment. Therefore, it is clinically significant to discover an effective anti-cancer approach and clarify the associated mechanisms of cervical cancer proliferation.

According to previous investigations,[5,6] non-invasive surgery for cancer treatment that induces cancer cell apoptosis, is an effective approach for killing the cancer cells. In recent years, ultrasound irradiation (USI) has been proven to induce apoptosis of some tumor cell lines, such as human leukemia, ovarian carcinoma and lung cancer cells.[7–9] Actually, low-intensity USI exhibits great potential to induce apoptosis as it is easily applied, and therefore should be considered to be the optimal ultrasound for cancer treatment in clinic.[10] As low-intensity USI triggers apoptosis in various cancers, it could be employed as a promising strategy to eliminate tumor cells.[11] Meanwhile, a study by Yang et al.[12] also reported that USI induced apoptosis in numerous cancer cells by activating different apoptotic signaling pathways, including endoplasmic reticulum (ER) stress-associated and mitochondrial pathways.

Objectives

By considering the potential effects of USI on cancer cell apoptosis, we hypothesized that the USI treatment might play a critical role for inducing cervical cancer cell apoptosis. Thus, the present research aimed to clarify the effects of low-intensity USI on apoptosis of cervical cancer cell lines and the apoptosis-associated mechanisms.

Materials and methods

Cell culture

The human normal cervical cell line (HaCaT) and the cervical cancer cell lines C33A, Hela and Siha were cultured in Dulbecco's modified Eagle's medium (DMEM; Gibco, Grand Island, USA) supplemented with 10% fetal bovine serum (FBS; Gibco) and 1% penicillin-streptomycin (Beyotime, Shanghai, China) in the humidified atmosphere with 5% CO_2 at 37°C.

Ultrasound irradiation administration and trial grouping

The C33A, Hela and Siha groups were subdivided into HaCaT group (only referring to the MTT and flow cytometry assay), untreated tumor cells (i.e., tumor cells not treated with USI) group, tumor cells exposed to USI and then cultured for 6 h (6 h group), tumor cells exposed to USI and then cultured for 12 h (12 h group), and tumor cells exposed to USI and then cultured for 24 h (24 h group). The USI was conducted using the JC200 Haifu ultrasound system (Chongqing Haifu Medical Technology Co. Ltd., Chongqing, China). The USI processes were assigned based on a previous study.[13] Cells were treated with USI at a transducer frequency of 10.0 MHz and with mechanical index (power) of 0.25 W/cm^2 for 10 s.

MTT assay

Suspensions of HaCaT, C33A, Hela, and Siha cells were seeded into 96-well cell culture plates (Corning-Costar, Corning, USA) at a dosage of 1×10^6 cells/mL and cultured for 6–24 h at 37°C. In order to evaluate the cell viability (cell proliferation), 20 μL of MTT solution (5 mg/mL in phosphate-buffered saline (PBS; Beyotime) was added to each well and cultured for another 4 h at 37°C. After the incubation of MTT, a total of 200 μL of dimethyl sulfoxide (DMSO; Amresco Inc., Solon, USA) was added to the wells for 10 min to dissolve any formed formazan crystals. Finally, the absorbance of each well was examined at wavelength of 490 nm using a Multiskan Mk3 microplate reader (Thermo Scientific Pierce, Shanghai, China).

Flow cytometry assay

Apoptosis of cervical cancer cells, including HaCaT, C33A, Hela, and Siha, were assessed with Annexin V-PE/7-AAD Apoptosis Detection regent (Cat. No. 559763; Becton Dickinson Biosciences, San Jose, USA) based on the manufacturer's protocol. Briefly, cells were collected and treated with Annexin V-PE for 15 min and then propidium iodide (PI) for 15 min in the dark at 25°C. Next, cells were analyzed using a FACS Vantage SE (Becton Dickinson Biosciences) flow cytometer, using the 546/647 band-pass filter (for monitoring PI signals) and the 530/578 band-pass filter (for monitoring Annexin-V signals), and the data were analyzed with the Cell Quest software v. 5.1 (Becton Dickinson Biosciences).

Small interfering RNA synthesis and identification

The Small interfering RNA (siRNA) synthesis was conducted according to a previous study.[14] The candidate sequences for the siRNA synthesis, and the optimal siRNA sequences for silencing the glucose-related protein

Table 1. siRNA sequences for *GRP78* gene silencing and primer for PCR assay

Genes or siRNAs	Sense/anti-sense	Sequences
GRP78-homo-731	sense	5'-GAGGCUUAUUUGGGAAAGATT-3'
	anti-sense	5'-UCUUUCCCAAAUAAGCCUCTT-3'
GRP78-homo-1081	sense	5'-GGGCAAAGAUGUCAGGAAATT-3'
	anti-sense	5'-UUUCCUGACAUCUUUGCCCTT-3'
GRP78-homo-1548	sense	5'-GAGGUGUCAUGACCAAACUTT-3'
	anti-sense	5'-AGUUUGGUCAUGACACCUCTT-3'
Negative control	sense	5'UUCUCCGAACGUGUCACGUTT-3'
	anti-sense	5'-ACGUGACACGUUCGGAGAATT-3'
GRP78	forward	5'-AGACGGGCAAAGATGTCAGG-3'
	reverse	5'-GAGTCGAGCCACCAACAAGA-3'

(*GRP78*) gene identified using quantitative real-time polymerase chain reaction (qRT-PCR) analysis with specific primer for *GRP78* are listed in Table 1. The siRNA was transfected into the above cell lines using Lipofectamine 2000 regent (Invitrogen/Life Technologies, Carlsbad, USA). Briefly, RNAs in all tumor cells were extracted using Trizol kits (Beyotime). Complementary DNAs (cDNAs) were then synthesized with the cDNA Synthesis Kit (Cat. No. 18080200; Thermo Fisher Scientific, Rockford, USA) following the manufacturer's protocol. The mRNA levels of *GRP78* gene were determined with SYBR-Green I PCR system, purchased from Western Biotech (Chongqing, China), using specific primers (Table 1). Amplified products for *GRP78* gene were analyzed using GDS8000 Gel-Scanning equipment (UVP, Sacramento, USA) based on equipment instructions. Finally, the *GRP78* gene expression was calculated and analyzed using $2^{-\Delta\Delta ct}$ method.

Scanning electron microscopy

The structural changes of the cervical cancer cells when exposed to USI were observed using scanning electron microscopy. Briefly, cervical cancer cells were adjusted to the concentration of 10^6 cells/well on six-well plates and cultured for 24 h to confirm adhesion. Cells were washed with PBS and the suspensions were dropped onto glass coverslips for 30 min and then incubated using 4% formalin (Beyotime) for 5 min. Then, cells were fixed using the 1% osmic acid (Beyotime) for 30 min, washed with ice-cold PBS solution and then soaked in 2% tannin (Beyotime) overnight at 4°C. Finally, cervical cancer cells were coated with a vacuum spray-plating equipment and the image was captured using scanning electron microscope S-3000N (Hitachi, Tokyo, Japan).

Immunocytochemistry assay

All cells were cultured onto slides and fixed with 4% paraformaldehyde (Beyotime) at room temperature for 10 min. Cells were washed with PBS and endogenous peroxidase inactivated using 3% hydrogen peroxide (Beyotime) at 25°C for 5 min. Cells were subsequently blocked using 5% bovine serum albumin solution (BSA; Beyotime) at 25°C for 15 min, then incubated with rabbit anti-human *GRP78* monoclonal antibody (1 : 3000, Cat. No. ab108615; Abcam Cambridge, USA), rabbit anti-human C/EBP-homologous protein (CHOP) polyclonal antibody (1 : 3000, Cat. No. MBS000292; MyBioSource, Vancouver, Canada), rabbit anti-human phosphorylated C-Jun N-terminal kinase (p-JNK) monoclonal antibody (1 : 3000, Cat. No. ab124956; Abcam), and rabbit anti-human caspase-12 polyclonal antibody (1 : 2000, Cat. No. ab62484; Abcam) overnight at 4°C. Subsequently, cells were washed using PBS and incubated using Biotin-labeled goat anti-rabbit antibody (1 : 1000, Cat. No. ab6720; Abcam) for 60 min at 37°C. Finally, cells were observed and images captured using a professional CKX41 inverted fluorescence microscope (Olympus Corp., Tokyo, Japan).

Western blot assay

The cervical cancer cells were lysed with RIPA buffer (Beyotime) according to manufacturer's protocol. Cell lysates were then separated using 15% SDS-PAGE (Beyotime) and electrotransferred onto polyvinylidene fluoride (PVDF) membranes (Bio-Rad, Hercules, USA). The membrane was blocked using PBS solution containing 5% skim milk and supplementing with 0.05% Tween-20 (Beyotime). Subsequently, PVDF membrane was treated with rabbit anti-human *GRP78* monoclonal antibody (1 : 3000; Abcam), rabbit anti-human CHOP polyclonal antibody (1 : 2000; MyBioSource), rabbit anti-human p-JNK monoclonal antibody (1 : 3000; Abcam), rabbit anti-human caspase-12 polyclonal antibody (1 : 2000; Abcam), and rabbit anti-human β-actin polyclonal antibody (1 : 2000; Abcam) overnight at 4°C. Subsequently, PVDF membranes were treated with horseradish peroxidase (HRP)-labeled goat anti-rabbit antibody (1 : 2000; Abcam). The western blot band signals for the isolated proteins were visualized and imaged with ECL Western Blotting Substrate (Cat. No. 32106, Thermo

Fisher Scientific). Finally, the images were captured using GDS8000 Gel Scanning System (UVP).

Statistical analyses

Our data were analyzed using IBM SPSS v. 19.0 software (IBM Corp., Armonk, USA). All data are presented as mean ± standard deviation (SD). The statistical differences between 2 groups were analyzed using the Student's t test. The differences among multiple groups were also analyzed using the Tukey's post hoc test-validated analysis of variance (ANOVA). A p-value <0.05 represented a significant difference. At least 6 repeats were conducted for all tests or experiments.

Results

Ultrasound irradiation reduced viability and increased apoptosis of cervical cells

In order to observe effects of USI on the proliferation of HaCaT, C33A cells, Hela cells, and Siha cells, an MTT assay was conducted. The MTT results indicated that cell viabilities were significantly reduced at 6 h, 12 h and 24 h post-treatment compared with the untreated cells (Fig. 1A, p < 0.05). Meanwhile, the apoptosis of cervical cancer cells was measured with flow cytometry. Our findings showed that cell apoptosis rates were significantly increased at 6 h, 12 h and 24 h post-treatment compared with untreated cells (Fig. 1B, p < 0.05).
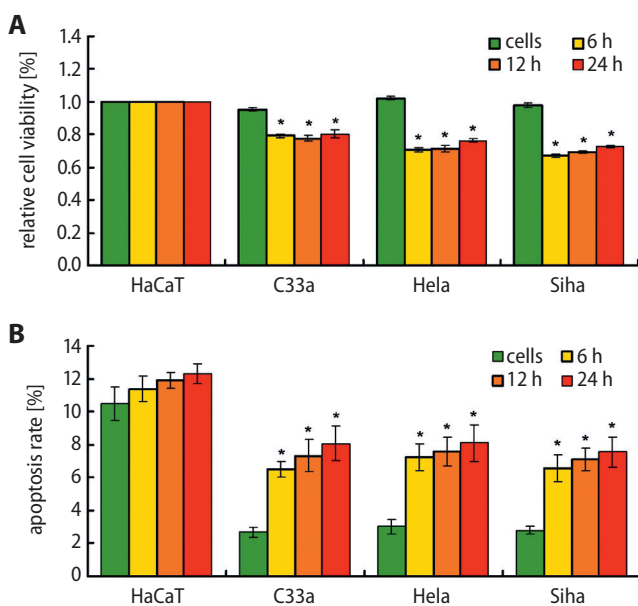

Fig. 1. Evaluation for cell viability and cell apoptosis of normal cervical cells and cervical cancer cells. A. Statistical analysis for cell viability of normal cervical cell (HaCaT) and cervical cancer cell lines C33A, Hela and Siha cells at 6 h, 12 h and 24 h post-USI; B. Statistical analysis for cell apoptosis of normal cervical cell HaCaT and cervical cancer cell lines C33A, Hela and Siha cells at 6 h, 12 h and 24 h post-USI; *p < 0.05 compared to untreated cells (HaCaT, C33A, Hela, and Siha)

USI induced the formation of apoptotic body

To confirm the reason that USI caused cervical cancer cell death, apoptotic bodies were evaluated in Hela cells. The results indicated that there were no apoptotic bodies present in the untreated cells (Hela cells) (Fig. 2). However, apoptotic bodies in the 6-hours treatment group and 12-hours treatment group were visibly more compared to that in untreated cells (Fig. 2). Meanwhile, both C33A and Siha cells displayed numerous apoptotic bodies (data not shown).

Ultrasound irradiation activated ER stress-associated apoptosis

The ER stress-associated apoptotic signaling molecules,[15] including *GRP78*, CHOP and caspase-12, were examined with immunocytochemistry analysis. Our findings demonstrated that USI significantly increased caspase-12 expression in C33A cells, Hela cells and Siha cells, compared with the untreated cells (Fig. 3 p < 0.05). Furthermore, USI significantly upregulated CHOP expression in C33A cells, Hela cells and Siha cells, compared with the untreated cells (Fig. 4, p < 0.05). Finally, compared with the untreated cells, *GRP78* levels were also significantly enhanced in the C33A cells, Hela cells and Siha cells undergoing the USI treatment (Fig. 5, p < 0.05).

Ultrasound irradiation phosphorylation of JNK

The phosphorylation of the JNK molecule could reflect apoptosis occurring within cancer cells. Therefore, we examined the expression of p-JNK in C33A, Hela and Siha cells. The present findings showed that USI significantly increased phosphorylation of JNK in both C33A and Siha cells, compared to that in the untreated tumor cells at 6 h, 12 h and 24 h post-treatment (Fig. 6, p < 0.05). However, the effects of USI on p-JNK were not found in Hela cells (Fig. 6).

Ultrasound irradiation triggered ER stress by modulating *GRP78* expression

In this study, we synthesized 3 siRNA sequences, and found that the siRNA sequence *GRP78*-homo-1548 exhibited the best silencing effects on *GRP78* expression (Fig. 7), and was therefore used for subsequent studies in cervical cancer cells.

To determine specific mechanisms associated with USI-triggered ER stress, the stress-regulatory protein *GRP78* was detected with western blotting analysis (Fig. 8A). Our findings demonstrated that USI significantly increased caspase-12 (Fig. 8B), CHOP (Fig. 8C) and *GRP78* (Fig. 8D) protein expression in Hela cells at all time points
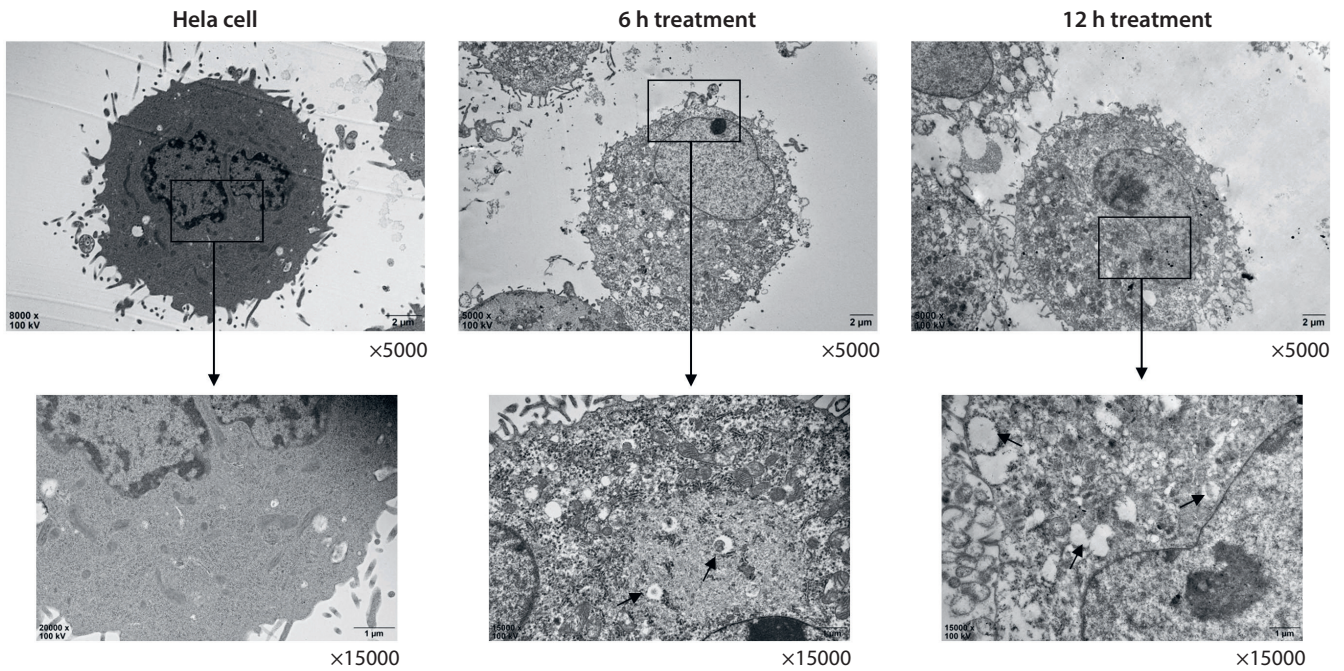
Fig. 2. Observation of structural changes of normal cervical cells and cervical cancer cells exposed to USI using scanning electron microscopy. The black arrows represent the apoptotic bodies
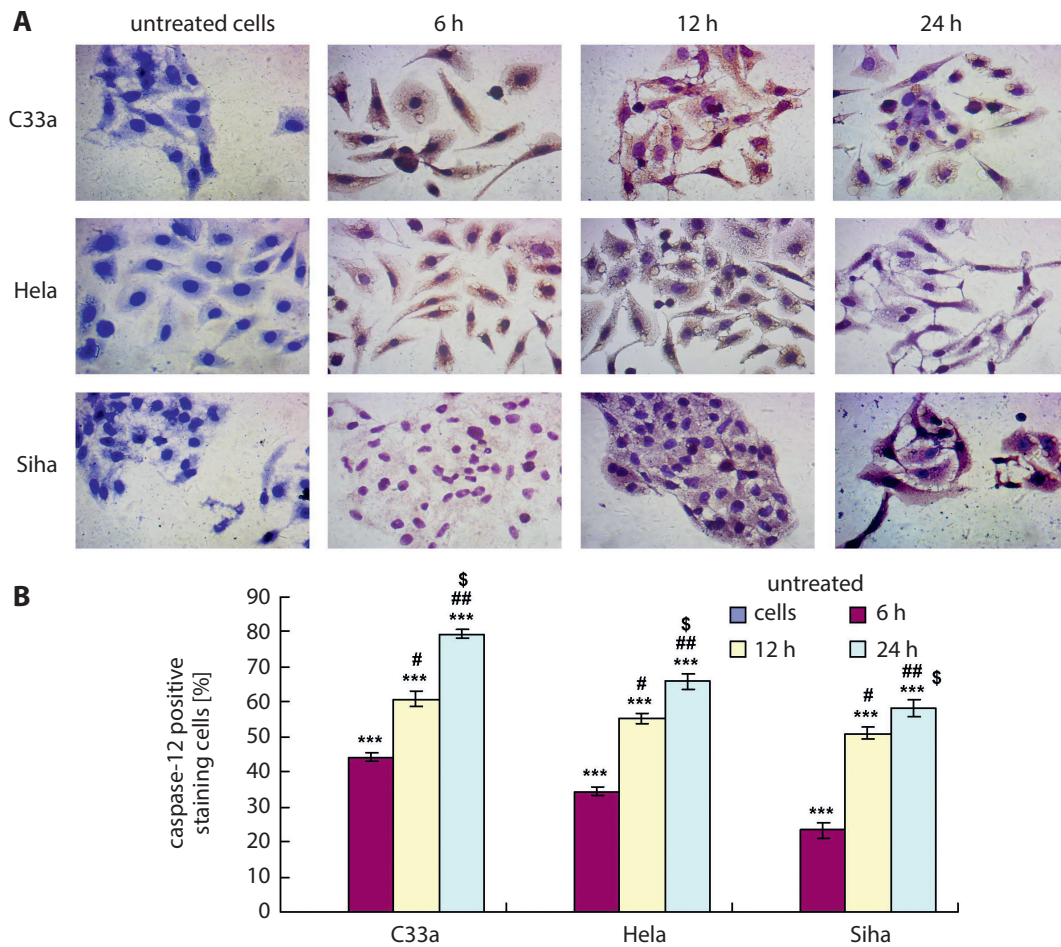
Fig. 3. Examination for caspase-12 expression in cervical cancer cells using immunocytochemistry assay. A. Immunocytochemistry images of caspase-12 expression in C33A, Hela and Siha cells; B. Statistical analysis of the expression of caspase-12 in cells; ×200 magnification; ***$p < 0.001$ compared to untreated cells; #$p < 0.05$ and ##$p < 0.01$ compared to 6 h USI administration group; $$p < 0.05$ compared to 12 h USI administration group

A
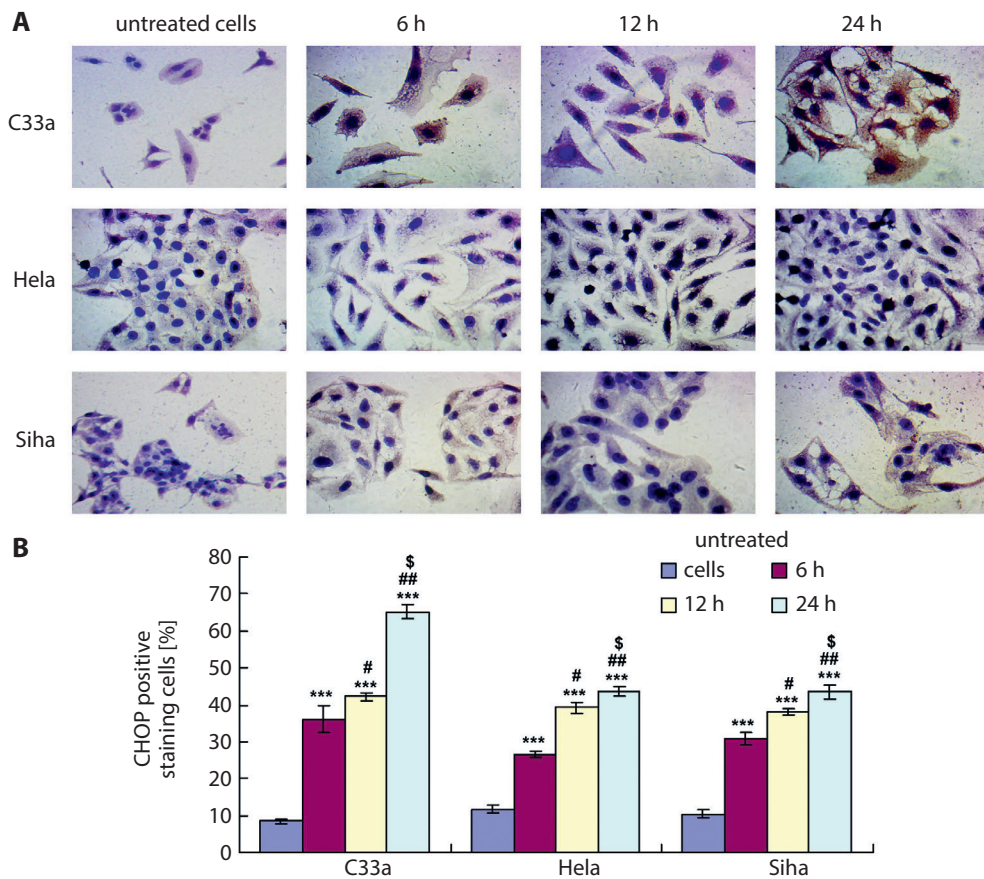
Fig. 4. Evaluation of CHOP expression in cervical cancer cells with immunohistochemistry assay. A. Immunohistochemistry images for CHOP expression in C33A, Hela and Siha cells; B. Statistical analysis of the CHOP expression in cells; ×200 magnification; ***p < 0.001 compared to untreated cells group; #p < 0.05 and ##p < 0.01 compared to 6 h USI administration group; $p < 0.05 compared to 12 h USI administration group

B

A
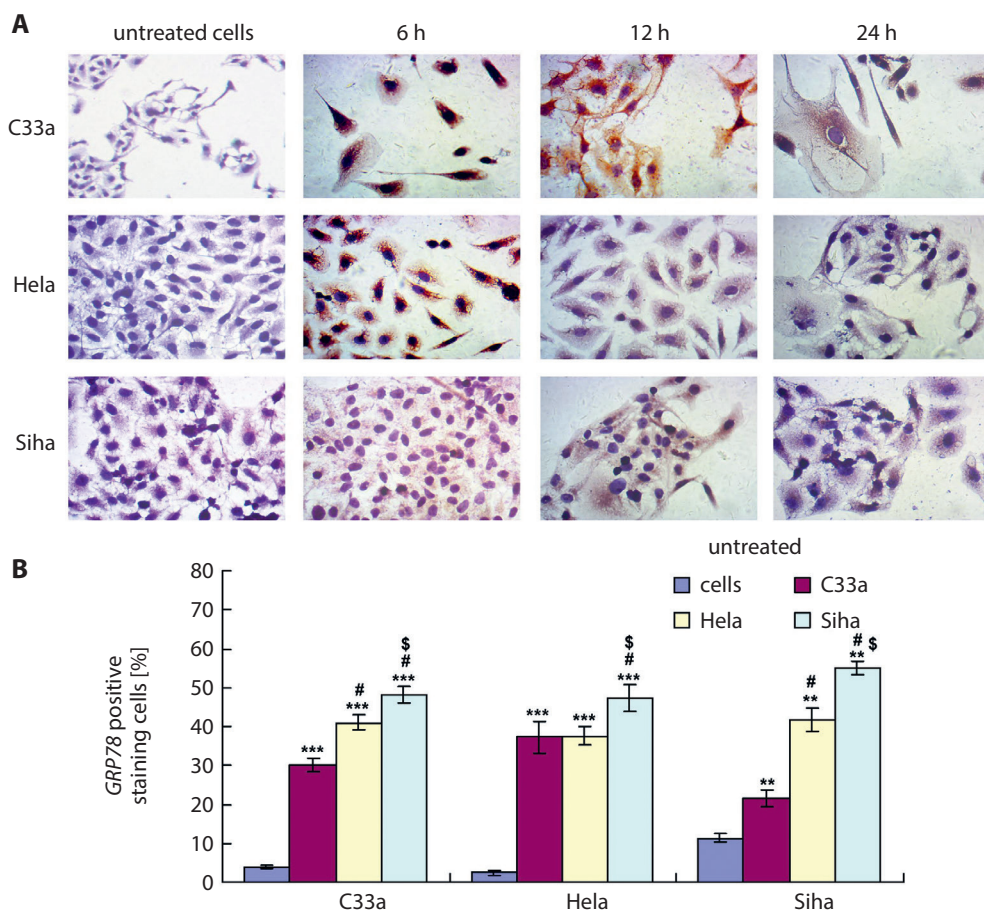
Fig. 5. Determination of *GRP78* expression in cervical cancer cells with immunohistochemistry analysis. A. The images for the immunohistochemistry assay for expression of *GRP78* in C33A, Hela and Siha cells; B. Statistical analysis for expression of *GRP78* in cells; ×200 magnification; **p < 0.01 and ***p < 0.001 compared to untreated cells group; #p < 0.05 compared to 6 h USI administration group; $p < 0.05 compared to 12 h USI administration group

B

A

B
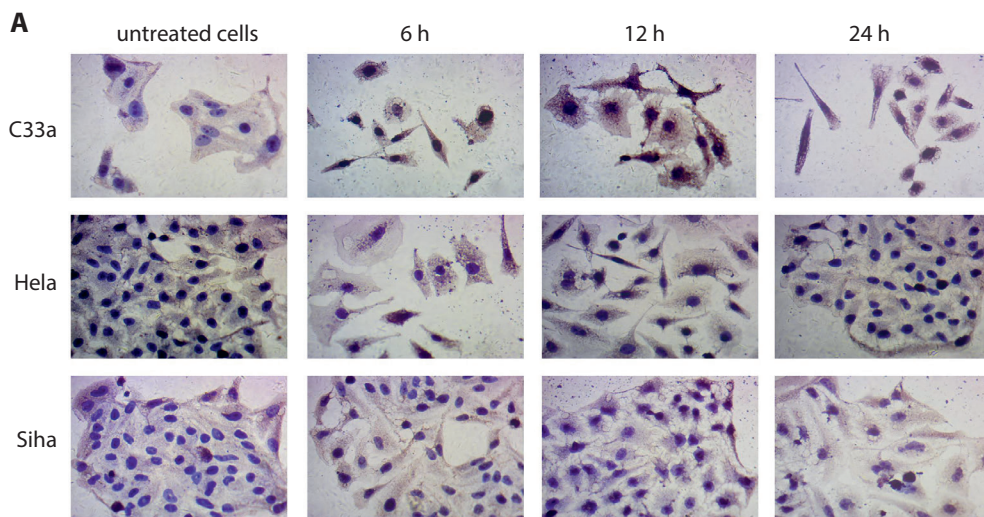
Fig. 6. Determination for *GRP78* expression in cervical cancer cells with the immunohistochemistry analysis. A. The images for the immunohistochemistry for expression of *GRP78* in C33A, Hela and Siha cells; B. Statistical analysis of the expression of *GRP78* in cells; ×200 magnification; *p < 0.05 compared to untreated cells group

A

B
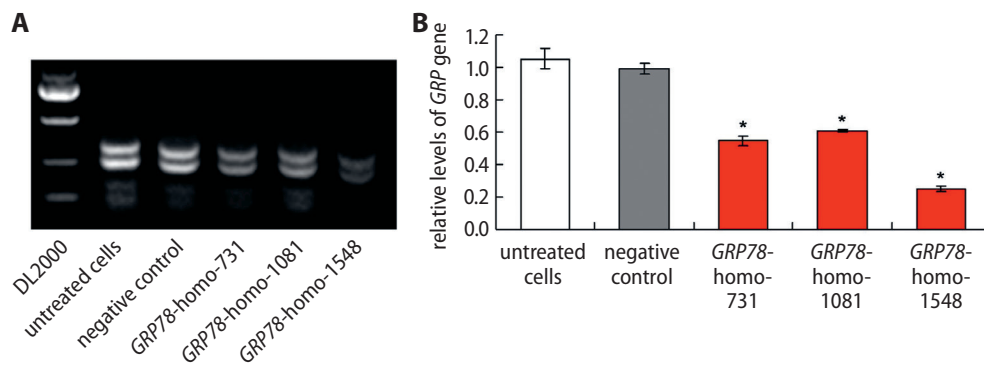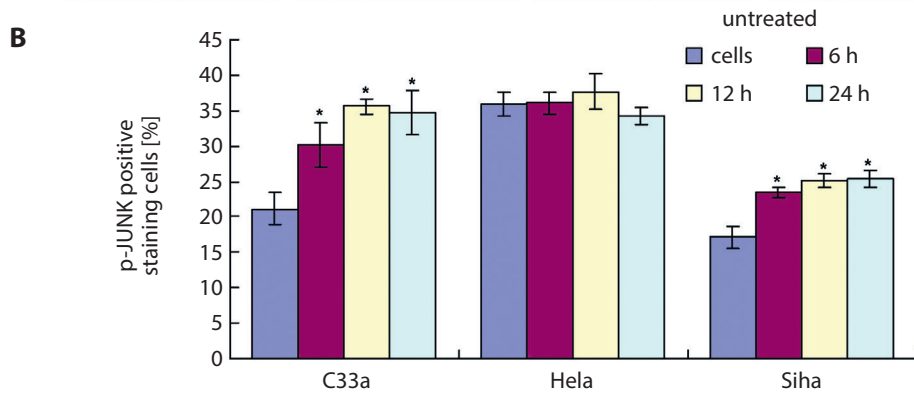
Fig. 7. Identification and screening for *GRP78* silencing siRNA sequences. A. Gel image for the *GRP78* siRNA sequences; B. Statistical analysis for the levels of GRP sequences; *p < 0.05 compared to untreated cells group

post-treatment, compared to that of the untreated cells (p < 0.05). Meanwhile, inhibition of *GRP78* (siRNA treatment) also significantly enhanced the expression of caspase-12 (Fig. 8B, 12 h post-USI administration), CHOP (Fig. 8C, at 6 h, 12 h and 24 h post-USI treatment) and reduced GRP78 (Fig. 8D, at 6 h, 12 h and 24 h post-USI treatment) proteins in Hela cells compared to that in the untreated tumor cells (p < 0.05) at 6 h, 12 h and 24 h post-USI treatment.

Finally, suppression of *GRP78* also significantly increased the expression of caspase-12, CHOP and decreased GRP78 proteins in C33A and Siha cells compared to that in the untreated tumor cells at 6 h, 12 h and 24 h post-treatment (data not shown).

Ultrasound irradiation enhanced phosphorylation of JNK by downregulating *GRP78* expression

The results showed that suppression of *GRP78* enhanced the ratio of JNK p-JNK/JNK in Hela cells compared to that in the untreated tumor cells at 6 h, 12 h and 24 h post-treatment (Fig. 8E, p < 0.05). Moreover, inhibition of *GRP78* also significantly increased expression of p-JNK in C33A cells and Siha cells compared to that in untreated tumor cells (data not shown).
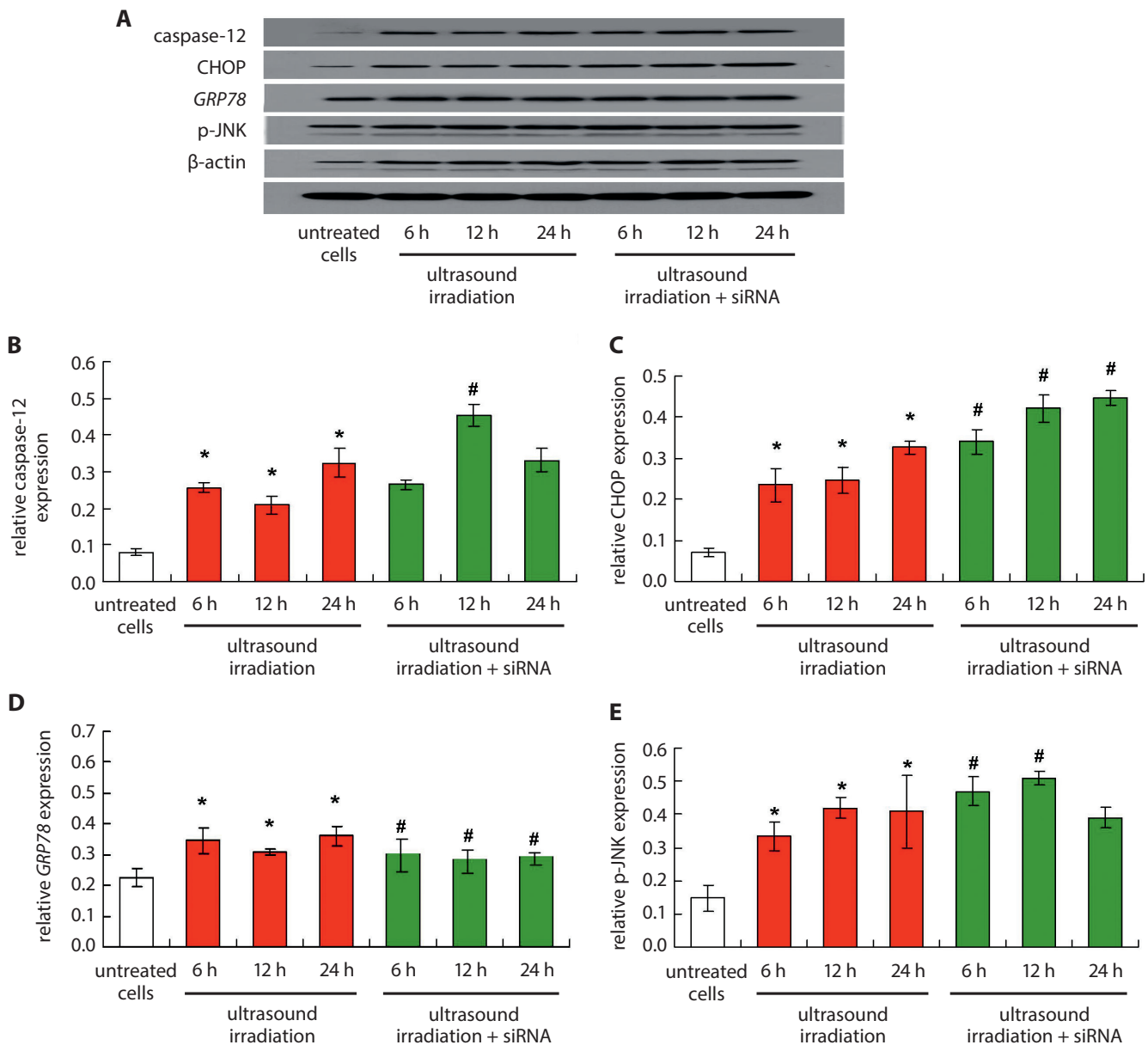
Fig. 8. Evaluation for caspase-12, CHOP, *GRP78*, and p-JNK expression in cervical cancer cells using western blotting assay. A. Images of western blotting assays and bands; B. The statistical analysis of expression of caspase-12; C. The statistical analysis of expression of CHOP; D. The statistical analysis of expression of *GRP78*; E. The statistical analysis of the ratio of p-JNK/JNK; *p < 0.05 compared to untreated cells group; #p < 0.05, ##p < 0.01 compared to untreated cervical cancer cells at the same time points

Discussion

Cervical cancer is considered to be a leading cause of cancer-associated death worldwide for women.[16] It is usually diagnosed clinically as advanced or moderate stages; however, the efficacy of traditional therapy is relatively poor.[17] Therefore, there is a significant and urgent need to establish an effective and safe therapeutic strategy for cervical cancer. Although USI could induce apoptosis in both cancer cells and normal cells, the cancer cells are more sensitive to the treatment and more easily killed compared to normal cells.[18,19] Meanwhile, Lagneaux et al.[20] reported that cancer cells are more susceptible to the USI

due to higher cell apoptotic rates. Therefore, USI that can cause apoptosis might be of clinical importance as a novel therapeutic approach.

In this study, we first examined cell viability and apoptosis in both a normal cervical cell line (HaCaT cells) and cervical cancer cell lines (C33A, Hela and Siha). The MTT assay results showed that USI significantly reduced the cell viability of all cancer cells at 6 h, 12 h and 24 h post-treatment. The flow cytometry assay findings indicated that USI triggered significant amounts of apoptosis in all cervical cancer cells at 6 h, 12 h and 24 h post-treatment. However, USI demonstrated no effects on the cell viability and apoptosis of normal cervical cells. Therefore, we believed that USI treatment is safe for normal cervical cells, and

only the cervical cancer cells were utilized in the following experiments for exploring mechanisms of cell viability and apoptosis.

Apoptosis, a process of programmed cell death, can maintain tissue homeostasis and eliminate dead cells from both normal and cancer tissues.[21] Previous studies have reported that there are 2 main categories of apoptosis, including mitochondria-mediated[22,23] and ER stress-mediated apoptosis.[14,24] Ultrasound irradiation-induced apoptosis of cancer cells has previously been demonstrated to use the mitochondria-associated pathway[25]; therefore, this aspect is not discussed. In the present study, we investigated whether USI caused apoptosis by verifying the biomarker expression of ER stress-mediated apoptosis, including *GRP78*, CHOP and caspase-12.[26] Our results showed that all of these ER stress biomarkers were significantly upregulated following USI in treated cervical cancer cells compared to untreated tumor cells. This suggests that USI induced cancer cell death (decreased cell viabilities) and apoptosis (formed apoptotic bodies) via the ER-mediated signaling pathway.

A previous study[27] demonstrated that p-JNK is associated with cell apoptosis, and therefore we also evaluated the levels of p-JNK in USI-treated cervical cancer cells. Our results indicated that USI triggered a significant increase in p-JNK in both C33A cells and Siha cells. This result suggests that USI induced apoptosis in cervical cancer cells also via activating p-JNK, which is consistent with the previous study.[28]

The GRP78 protein plays critical roles in regulating ER-mediated apoptosis in cancer cells.[29] When cancer cells are suffering from the stimuli, *GRP78* is overexpressed to regulate any misfolded proteins, and in this way, silencing of the *GRP78* gene might initiate ER stress.[30] In this study, we designed the siRNA sequence of *GRP78*-homo-1548 to downregulate *GRP78* expression and to clarify the role of this key molecule in USI-mediated apoptosis. The results indicated that silencing of *GRP78* significantly upregulated caspase-12 and CHOP expression, which increases ER stress-mediated apoptosis of Hela cells. Meanwhile, p-JNK expression was also activated in Hela cells undergoing *GRP78* silencing. These findings suggest that the *GRP78* molecule might participate in apoptosis in USI-treated cervical cancer cells.

Limitations

Although this study received a few interesting findings, there are also some limitations.

This study mainly focused on ER stress-induced apoptosis; however, we did not discuss the classical apoptosis pathway. Actually, some previous studies[31–34] have explored the classical pathways or molecules involved in USI-induced apoptosis of cancer cells. Xu et al.[31] reported that ultrasound could induce apoptosis in cervical cancer cells via regulating Bcl-2 and Bax proteins.

Xiao et al.[32] found that ultrasound demonstrated a wider application in the clinical treatment of cervical cancer through modulating cleaved caspase-9. Chen et al.[33] proved that ultrasound remarkably downregulated Bax and caspase-3 expression in cervical cancer cells. Finally, Tang et al.[34] discovered that caspase-8 is also involved in the apoptosis in ultrasound-treated cancer cells. However, the intrinsic apoptosis pathway (involving tumor necrosis factor α (TNF-α), TRAIL and FAS-L molecule) and extrinsic apoptosis pathway (involving mitochondria-mediated molecules) have not been fully clarified herein, which is a limitation of our study.

Conclusions

The present findings indicated that USI could significantly inhibit the proliferation and induce apoptosis of cervical cancer cells. Ultrasound irradiation-induced cervical cell apoptosis was mediated by initiating the ER stress-associated signaling pathway and triggering the phosphorylation of JNK in cervical cancer cells. These results might provide the experimental insight for the therapeutic intervention of USI in cervical cancer therapy. In the future, we would investigate the effects of USI on tumor growth of xenografted mice. Moreover, we would also combine USI and ER stress inducers for enhancing the regression of tumors with the minimum off-target effects.

ORCID iDs

Juan Qin ⓘ https://orcid.org/0000-0002-1358-1663
Guolin Song ⓘ https://orcid.org/0000-0001-7104-2708
Qin Liu ⓘ https://orcid.org/0000-0003-2243-7839
Hong Lin ⓘ https://orcid.org/0000-0001-9968-1405
Yan Wang ⓘ https://orcid.org/0000-0003-1984-7597
Jinyun Chen ⓘ https://orcid.org/0000-0002-6818-7145

References

1. Siegel RL, Miller KD, Jemal A. Cancer statistics, 2017. *CA Cancer J Clin*. 2017;67(1):7–30. doi:10.3322/caac.21387
2. Zielecka-Debska D, Blaszczyk J, Blaszczyk D, et al. The effect of the population-based cervical cancer screening program on 5-year survival in cervical cancer patients in Lower Silesia. *Adv Clin Exp Med*. 2019;28(10):1377–1383. doi:10.17219/acem/109759
3. Feraly J, Shin HR, Bray F, Forman D, Mathers C, Parkin DM. Estimates of worldwide burden of cancer in 2008: GLOBOCAN 2008. *Int J Cancer*. 2010;127(12):2893–2917. doi:10.1002/ijc.25516
4. Bhat S, Kabekkodu SP, Noronha A, Satyamoorthy K. Biological implications and therapeutic significance of DNA methylation regulated genes in cervical cancer. *Biochimie*. 2016;121:298–311. doi:10.1016/j.biochi.2015.12.018
5. Fulda S, Debatin KM. Apoptosis pathways in neuroblastoma therapy. *Cancer Lett*. 2003;197(1–2):131–135. doi:10.1016/s0304-3835(03)00091-0
6. Wang SY, Li Y, Jiang YS, Li RA. Investigation of serum miR-411 as a diagnosis and prognosis biomarker for non-small cell lung cancer. *Eur Rev Med Pharmacol Sci*. 2017;21(18):4092–4097. PMID:29028091
7. Feril LB, Kondo T, Zhao QL, et al. Enhancement of ultrasound-induced apoptosis and cell lysis by echo-contrast agents. *Ultrasound Med Biol*. 2003;29(2):331–337. doi:10.1016/s0301-5629(02)00700-7
8. Yu T, Wang Z, Mason TJ. A review of research into the uses of low level ultrasound in cancer therapy. *Ultrason Sonochem*. 2004;11(2):95–103. doi:10.1016/S1350-4177(03)00157-3

9. Tian ZM, Wan MX, Lu MZ, Wang XD, Wang L. The alteration of protein profile of Walker 256 carinosarcoma cells during the apoptotic process induced by ultrasound. *Ultrasound Med Biol*. 2005;31(1):121–128. doi:10.1016/j.ultrasmedbio.2004.09.008

10. Liu B, Luo Y, Luo D, et al. Treatment effect of low intensity pulsed ultrasound on leukopenia induced by cyclophosphamide in rabbits. *Am J Transl Res*. 2017;9(7):3315–3325. PMID:28804549

11. Shi M, Liu B, Liu G, et al. Low intensity-pulsed ultrasound induced apoptosis of human hepatocellular carcinoma cells in vitro. *Ultrasounds*. 2016;64:43–53. doi:10.1016/j.ultras.2015.07.011

12. Yang F, Yu X, Li T, et al. Exogenous H_2S regulates endoplasmic reticulum-mitochondria cross-talk to inhibit apoptotic pathways in STZ-induced type I diabetes. *Am J Physiol Endocrinol Metab*. 2017;312(3): E199–E203. doi:10.1152/ajpendo.00196.2016

13. Wang L, Zhang M, Tan K, Kim S, Lee SH. Preparation of nanobubbles carrying androgen receptor siRNA and their inhibitory effects on androgen-independent prostate cancer combined with ultrasonic irradiation. *PLoS One*. 2014;9(5):e96586. doi:10.1371/journal. pone.0096586

14. Yun S, Han YS, Lee JH. Enhanced susceptibility to 5-Fluorouracil in human colon cancer cells by silencing *GRP78*. *Anticancer Res*. 2017; 37(6):2975–2984. doi:10.21873/anticanres.11651

15. Zou L, Li X, Wu N, Jia P, Liu C, Jia D. Palmitate induces myocardial lipotoxic injury via the endoplasmic reticulum stress-mediated apoptosis pathway. *Mol Med Rep*. 2017;16(5):6934–6939. doi:10.3892/ mmr.2017.7404

16. Einstein MH, Schiller JT, Viscidi RP, et al. Clinician's guide to human papillomavirus immunology: Knowns and unknowns. *Lancet Infect Dis*. 2009;9(6):347–356. doi:10.1016/S1473-3099(09)70108-2

17. Heijkoop ST, Nout RA, Quint S, Mens JWM, Heijmen BJM, Hoogeman MS. Dynamics of patient reported quality of life and symptoms in the acute phase of online adaptive external beam radiation therapy for locally advanced cervical cancer. *Gynecol Oncol*. 2017;147(2):439–449. doi:10.1016/j.ygyno.2017.08.009

18. Feng Y, Tian ZM, Wan MX, Zheng ZB. Low intensity ultrasound-induced apoptosis in human gastric carcinoma cells. *World J Gastroenterol*. 2008;14(31):4873–4879. doi:10.3748/wjg.14.4873

19. Li H, Liu J, Chen M. Therapeutic evaluation of radiotherapy with contrast-enhanced ultrasound in non-resectable hepatocellular carcinoma patients with portal vein tumor thrombosis. *Med Sci Monit*. 2018;24:8183–8189. doi:10.12659/MSM.911073

20. Lagneaux L, de Meulenaer EC, Delforge A, et al. Ultrasound low-energy treatment: A novel approach to induce apoptosis in human leukemic cells. *Exp Hematol*. 2002;30(11):1293–1301. doi:10.1016/s0301-472x (02)00920-7

21. Wang Q, Xu H, Zhao X. Baicalin inhibits human cervical cancer cells by suppressing protein kinase C/signal transducer and activator of transcription (PKC/STAT3) signaling pathway. *Med Sci Monit*. 2018; 23:1955–1961. doi:10.12659/msm.909640

22. Huang LH, Li J, Gu JP, Qu MX, Yu J, Wang ZY. Butorphanol attenuates myocardial ischemia reperfusion injury through inhibiting mitochondria-mediated apoptosis in mice. *Eur Rev Med Pharmacol Sci*. 2018;22(6):1819–1824. doi:10.26355/eurrev_201803_14601

23. Zhang H, Zhang Y, Hu S. Melatonin protects cardiac microvasculature against ischemia/reperfusion injury via suppression of mitochondrial fission-VDAC1-HK2-mPTP-mitophagy axis. *J Pineal Res*. 2017;63(1):12413. doi:10.1111/jpi.12413

24. Zhu P, Hu S, Jin Q. Ripk3 promotes ER-stress-induced necroptosis in cardiac IR injury: A mechanism involving calcium overload/XO/ ROS/mPTP pathway. *Redox Biol*. 2018;16:157–168. doi:10.1016/j.redox. 2018.02.019

25. Xu XM, Zhang Y, Qu D, Jiang TS, Li SQ. Osthole induces G2/M arrest and apoptosis in lung cancer A549 cells by modulating PI3K/Akt pathway. *J Exp Clin Cancer Res*. 2011;30(1):33. doi:10.1186/1756-9966-30-33

26. Yin ZC, Xiong WH, Pang QJ. CXCR3 mediates chondrocyte injury through regulating nitric oxide. *Eur Rev Med Pharmacol Sci*. 2018;22(8): 2454–2460. doi:10.26355/eurrev_201804_14839

27. Nadel G, Yao Z, Ben-Ami I, Naor Z, Seger R. Gg-induced apoptosis is mediated by AKT inhibition that leads to PKC-induced JNK activation. *Cell Physiol Biochem*. 2018;50(1):121–135. doi:10.1159/000493963

28. Deng B, Zhang S, Miao Y, Wen F, Guo K. Down-regulation of Frizzled-7 expression inhibits migration, invasion and epithelial-mesenchymal transition of cervical cancer cell lines. *Med Oncol*. 2015;32(4):102. doi:10.1007/s12032-015-0552-8

29. Luo C, Fan W, Jiang Y, Zhou S, Cheng W. Glucose-related protein 78 expression and its effects on cisplatin-resistance in cervical cancer. *Med Sci Monit*. 2018;23:2197–2209. doi:10.12659/MSM.906413

30. van Lidth de Jeude JF, Meijer BJ, Wielenga MCB, et al. Induction of endoplasmic reticulum stress by deletion of Grp78 depletes Apc mutant intestinal epithelial stem cells. *Oncogene*. 2017;36(24):3397–3405. doi:10.1038/onc.2016.326

31. Xu T, Nie Y, Bai J, et al. Suppression of human 8-oxoguanine DNA glycosylase (OGG1) augments ultrasound-induced apoptosis in cervical cancer cells. *Ultrasonics*. 2016;72:1–14. doi:10.1016/j.ultras.2016.07.005

32. Xiao X, Zhang Y, Lin Q, Zhong K. The better effects of microbubble ultrasound transfection of miR-940 on cell proliferation inhibition and apoptosis promotion in human cervical cancer cells. *Onco Targets Ther*. 2019;12:6813–6824. doi:10.2147/OTT.S209692

33. Chen ZY, Liang K, Lin Y, Yang F. Study of the UTMD-based delivery system to induce cervical cancer cells apoptosis and inhibit proliferation with shRNA targeting survivin. *Int J Mol Sci*. 2013;14(1):1763–1777. doi:10.3390/ijms14011763

34. Tang W, Liu Q, Wang X, et al. Involvement of caspase 8 in apoptosis induced by ultrasound-activated hematoporphyrin in sarcoma 180 cells in vitro. *J Ultrasound Med*. 2009;27(4):645–656. doi:10.7863/ jum.2008.27.4.645

Exenatide regulates inflammation and the production of reactive oxygen species via inhibition of S1PR2 synthesis

Yunyun Yang[A–E], Qingyi Zhao[A–C,E–F]

Department of Ophthalmology, Zhangjiagang TCM Hospital (affiliated to Nanjing University of Chinese Medicine), China

A – research concept and design; B – collection and/or assembly of data; C – data analysis and interpretation;
D – writing the article; E – critical revision of the article; F – final approval of the article

Address for correspondence
Yunyun Yang
E-mail: zhaoqingyi77@126.com

Abstract

Background. Microvascular dysfunction is one of the most serious complications of diabetic retinopathy (DR). As a novel treatment drug for type 2 diabetes, exenatide possesses protective properties against retinal neurodegeneration. Sphingosine-1-phosphate receptor 2 (S1PR2) could regulate blood glucose in diabetes, and inhibition of S1PR2 is involved in the treatment of diabetes. However, the mechanism of exenatide in human retinal vascular endothelial cells (hRVECs) has not been fully defined.

Objectives. We tested the hypothesis that S1PR2 plays a vital role in high glucose (HG)-induced hRVECs, and that exenatide could ameliorate HG-induced hRVEC injury by regulating S1PR2 production.

Materials and methods. The hRVECs underwent HG-stimulation. Quantitative real-time polymerase chain reaction (RT-qPCR) and western blot were performed to examine the expression of S1PR2. Oxidative stress levels, inflammatory markers and cell apoptosis were detected using reactive oxygen species (ROS) staining, enzyme-linked immunosorbent assay (ELISA) kits and TUNEL staining.

Results. High glucose increased the level of S1PR2 in hRVECs and reduced the expression of glucagon-like peptide-1 receptor (GLP1R) compared to the control group. Exenatide decreased the level of S1PR2 induced by HG. Sphingosine-1 blocked the effects of exenatide, alleviating the ROS and cell apoptosis induced by HG. JTE-013 treatment protected hRVECs from injury by HG. The inhibitory effects of exenatide on S1PR2 expression lessened HG-induced hRVEC injury.

Conclusions. The results demonstrate a possible mechanism of exenatide mediated inhibition of S1PR2 synthesis, and support S1PR2 as a novel target for treating DR.

Key words: diabetic retinopathy, high glucose, exenatide, SIPR2

Background

Diabetic retinopathy (DR) is a common complication of diabetes mellitus, which can lead to blindness in severe cases. The primary source of damage to retinal microvessels is peroxide damage caused by high glucose (HG).[1] Exenatide, a novel type 2 diabetes treatment drug, can simulate the activity of endogenous glucagon-like peptide-1 (GLP-1) while resisting degradation by dipeptidyl peptidase IV. Studies have shown that exenatide shows similar effects to GLP-1. For example, exenatide stimulates insulin secretion in a glucose-dependent manner, reduces plasma glucagon levels, inhibits gastric emptying and food intake, reduces body weight, and delays β-cell dysfunction to a certain extent.[2]

Regulators of GLP-1/GLP-1 receptor (GLP-1R) signaling could also have parallel roles in S1P/sphingosine-1-phosphate receptor 2 (S1P/S1PR2) signaling.[3,4] Human retinal S1PR2 is reported to be expressed in vascular endothelial cells.[5] In a high-sugar environment, increased S1P activates S1PR2, and, in turn, the intracellular signaling pathway, which plays important roles in cell proliferation, inflammation regulation and angiogenesis.[6] The S1PR2 antagonist JTE-013 can prevent cell damage and inhibit the elevation of blood glucose in diabetic mice due to its glucose reducing activity.[7,8] Sphingosine-1 may also regulate Akt-eNOS signaling in lung endothelial cells and affect vascular barrier functions in vivo.[5] Therefore, the targeted inhibition of S1PR2 is important for the treatment of diabetes.

Inflammation has been reported to be a cause of diabetic retinal damage in the early stages of DR.[9] Therefore, we also analyzed the effect of exenatide on inflammation. Reactive oxygen species (ROS) are greatly increased in the body during inflammation, which can lead to direct damage to lipid proteins and chromosomal nucleic acids, triggering cell apoptosis and the occurrence and development of the disease. Hyperglycemia causes the overproduction of ROS through various mechanisms, along with the imbalance of normal physiological functions of cells.[10,11] There appears to be a vicious positive feedback cycle involving ROS, inflammation and cell apoptosis.[12] However, whether the long-lasting ligand GLP-1R is also involved in retinal vascular endothelial cell injury induced by HG through targeted inhibition of S1PR2 still needs to be confirmed. Preliminary experiments have shown that exenatide decreases S1PR2 levels in retinal vascular endothelial cells when induced by HG.

Objectives

This study explores whether exenatide reduces retinal vascular endothelial cell injury by targeting S1PR2 expression.

Materials and methods

Cell line

Human retinal vascular endothelial cells (hRVECs) were purchased from Shanghai Cell Bank, Chinese Academy of Sciences, Shanghai, China. They are adherent cells that can be passed on at a confluence rate of 80~90% in low-glucose Dulbecco's modified Eagle's medium (L-DMEM; Gibco, Waltham, USA) containing 10% fetal bovine serum (FBS), 100 U/mL of penicillin and 100 U/mL of streptomycin (Sigma-Aldrich, St. Louis, USA). The hRVECs at logarithmic growth stage were digested with pancreatin, and resuspended to a concentration of 3×10^4 cells/mL in L-DMEM medium containing 1% FBS. The cells were then divided into a control group (normal saline), mannitol group (MG, 25 mmol/L), HG group (HG, 25 mmol/L), MG+exenatide group, HG+exenatide group, HG+exenatide+S1P (1 μm) group, and HG+JTE-013 (0.1 μm) group. Exenatide, S1P or JTE-013 were added to the cells as soon as the hyperglycemia cell model was established. After treatment for 48 h, further experiments were performed.

RT-qPCR

After 48 h of treatment, the total RNA of each group was extracted with Trizol reagent (Trizol, Waltham, USA), and reverse-transcribed into cDNA (TaKaRa, Tokyo, Japan). The synthesized cDNA was used as a template for quantitative experiments on an ABI 7100 quantitative fluorescence polymerase chain reaction (PCR) instrument (Applied Biosystems, Waltham, USA). The reaction system for RNA amplification was prepared as follows: RNase-free deionized water (10 μL), cDNA (1 μL), upstream and downstream primers (0.5 μL, respectively), and SYBR Premix (8 μL). *GAPDH* mRNA was used as an internal reference. The relative levels of S1PR1, S1PR2, S1PR3, and S1PR4 mRNA were calculated using the $2^{-\Delta\Delta Ct}$ method.

ELISA

The hRVECs were seeded into six-well plates. Cells were cultured as indicated above. After transfection for 48 h, cells were collected to detect the contents of tumor necrosis factor α (TNF-α), interleukin (IL)-1β and IL-6 protein in each group, using TNF-α, IL-1β and IL-6 enzyme-linked immunosorbent assay (ELISA) kits provided by Thermo Fisher Scientific (Waltham, USA).

ROS staining

Intracellular ROS were detected using dichloro-dihydrofluorescein (DCFH) fluorescent probe (Nanjing Jiancheng Bioengineering Institute, Nanjing, China). The hRVECs were seeded into six-well plates and 20 μmol of DCFH

fluorescence probes were added to all cells except for the negative control group. The samples were incubated in darkness for 45 min, washed with phosphate-buffered saline (PBS) 3 times, then observed under an inverted fluorescence microscope (Nikon Eclipse Ti; Nikon Corp., Tokyo, Japan) and photographed. The fluorescence intensity was detected through a fluorescence microplate (Bio-Rad, Hercules, USA). The utilized excitation wavelength was 488 nm and the emission wavelength was 525 nm.

TUNEL staining

Apoptotic cells were stained according to the instructions for the TUNEL kit (Beyotime, Shanghai, China). Cells were washed with PBS and then fixed with 4% paraformaldehyde. Phosphate-buffered saline with 0.1% Triton X-100 was added for incubation in an ice bath for 2 minutes. The TUNEL solution was prepared and added to cell sections. The tablets were sealed with anti-fluorescence quenching solution and observed under a fluorescence microscope (Olympus Corp., Tokyo, Japan).

Western blot

Total hRVEC protein was extracted, and SDS polyacrylamide gel was prepared after routine quantitative and denaturation. Routine sampling, electrophoresis, membrane transfer, and sealing were performed. The primary antibodies and *GAPDH* primary antibody (Abcam, Cambridge, UK) were added and incubated at 4°C overnight. Tris-buffered saline with Tween (TBST) was used to wash the membrane 3 times; then, the membrane was incubated with secondary antibody for 1 h. The membrane was washed using TBST 3 times. Electrochemiluminescence (ECL) solution was added for 20 s in a dark room. The grey value was analyzed using ImageJ software (National Institutes of Health, Bethesda, USA).

Statistical analyses

GraphPad Prism v. 6.0 (GraphPad Software, San Diego, USA) was used for statistical analyses of the data. Comparison among multiple groups of samples was performed using one-way analysis of variance (ANOVA), followed by Tukey's test. All experiments were repeated at least 3 times. A value of $p < 0.05$ was considered as statistically significant.

Results

Exenatide regulates the expression of GLP-1R and S1PR2 in hRVECs

High glucose stimulated S1PR2 levels in hRVECs (Fig. 1A). In contrast to the control group, S1PR1, S1PR3 and S1PR4 levels showed only slight increases after HG

induction (Fig. 1A). Mannitol had no effect on levels of S1PR1, S1PR2, S1PR3, or S1PR4.

We examined whether exenatide affected the production of S1PR2 protein. The levels of S1PR2 protein and S1PR2 mRNA in hRVECs stimulated by HG were both substantially higher than in the control group (Fig. 1B). Mannitol was used as an osmotic pressure control. In the MG group, exenatide did not affect either S1PR2 protein or S1PR2 mRNA levels. However, exenatide markedly reduced S1PR2 protein and S1PR2 mRNA levels in hRVECs stimulated by HG, relative to the HG group (Fig. 1C). Exenatide, as an agonist of GLP-1R, exerted positive effects on GLP-1R expression in hRVECs. These findings suggest that exenatide reduced S1PR2 production in HG-stimulated hRVECs.

Exenatide decreased inflammatory marker levels through S1PR2 regulation

Inflammatory cytokines, such as IL-1β and TNF-α, are highly expressed in the retinas of DR patients, leading to an inflammatory response and damage to the blood–retinal barrier, and thereby promoting the development of DR. We analyzed pro-inflammatory markers to assess inflammatory response induced HG in hRVECs. In contrast to the control group, HG markedly increased TNF-α, IL-1β and IL-6 expression (Fig. 2). Significantly, inhibitory effects on these pro-inflammatory factors were observed when hRVECs were treated with both exenatide and HG (Fig. 2), which indicated a possible protective effect of exenatide against the inflammatory response. In addition, S1P, an agonist of S1PR2, counteracted the inhibition of inflammation mediators by exenatide. We also found that hRVECs in the HG+JTE-013 group exhibited similar responses to those in the HG+exenatide group. These data implied that exenatide could decrease the inflammatory response induced by HG through regulation of S1PR2 protein activity.

Exenatide reduces ROS levels through S1PR2

Disruption of the balance between the formation and clearance rates of free radicals can produce oxidative stress and cell damage. Therefore, we analyzed the effects of exenatide on ROS and explored the regulation mechanism, using either S1P or JTE-013, an effective and selective S1PR2 antagonist. Exenatide reduced ROS levels, as revealed through ROS staining and the detection of fluorescence intensity (Fig. 3), whereas S1P counteracted exenatide-mediated ROS downregulation in HG-stimulated hRVECs. When JTE-013 was utilized to block the functions of S1PR2, ROS levels were significant decreased in HG-stimulated hRVECs relative to the HG group. The results were consistent with the reported effects of exenatide. These observations implied that exenatide decreased ROS levels through downregulation of S1PR2 production.
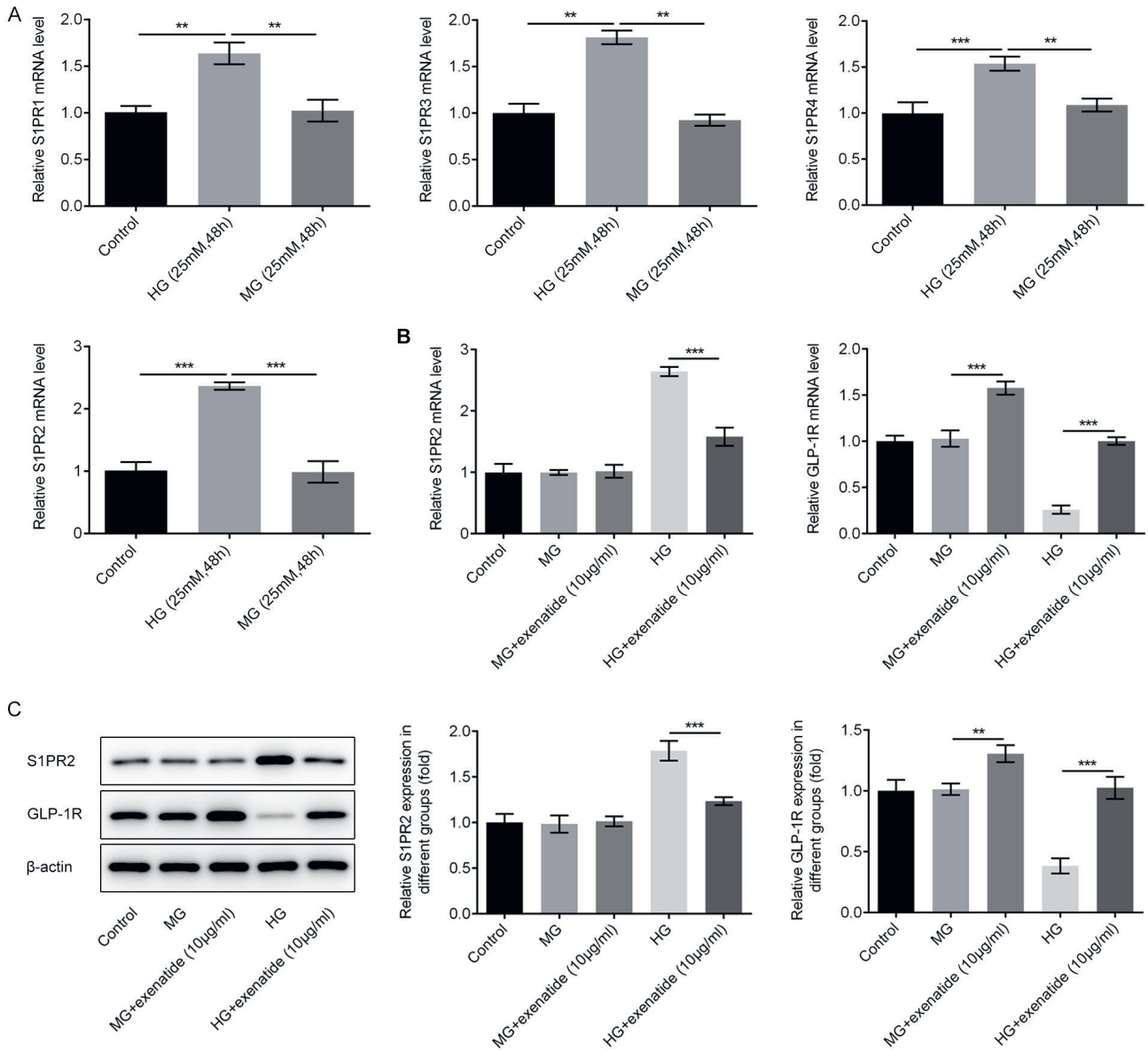
Fig. 1. A. Treatment with HG (25 mM) for 48 h stimulated S1PR2 production in hRVECs, as seen with RT-qPCR and western blot; B and C. Exenatide (10 µg/mL) stimulated a decrease in S1PR2 production in hRVECs with HG. All results are presented as mean ±SD percentage of the control level, based on 3 independent tests

**p < 0.01; ***p < 0.001.
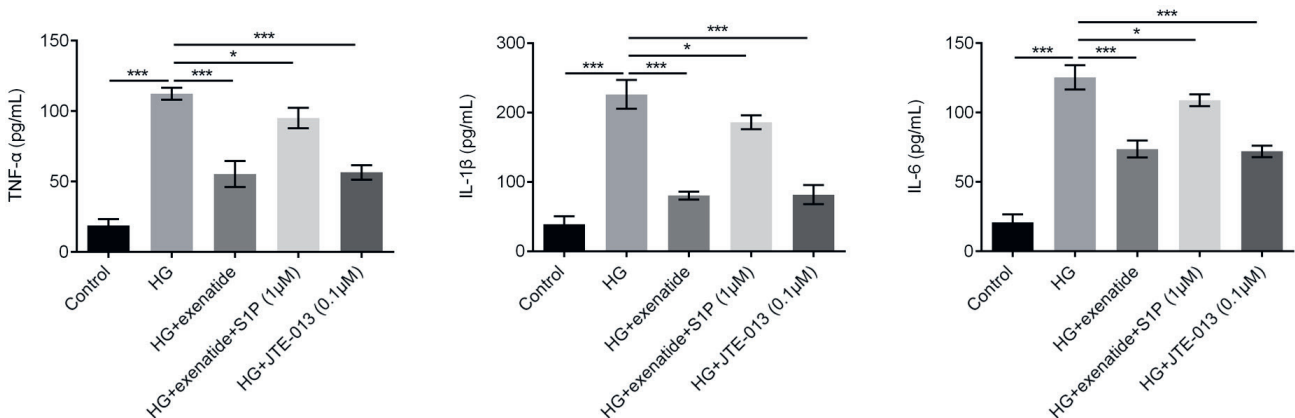
Fig. 2. Exenatide (10 µg/mL) reduced TNF-a, IL-1β and IL-6 expression through regulation of S1PR2. The results are expressed as mean ±SD of the mean

*p < 0.05; ***p < 0.001.
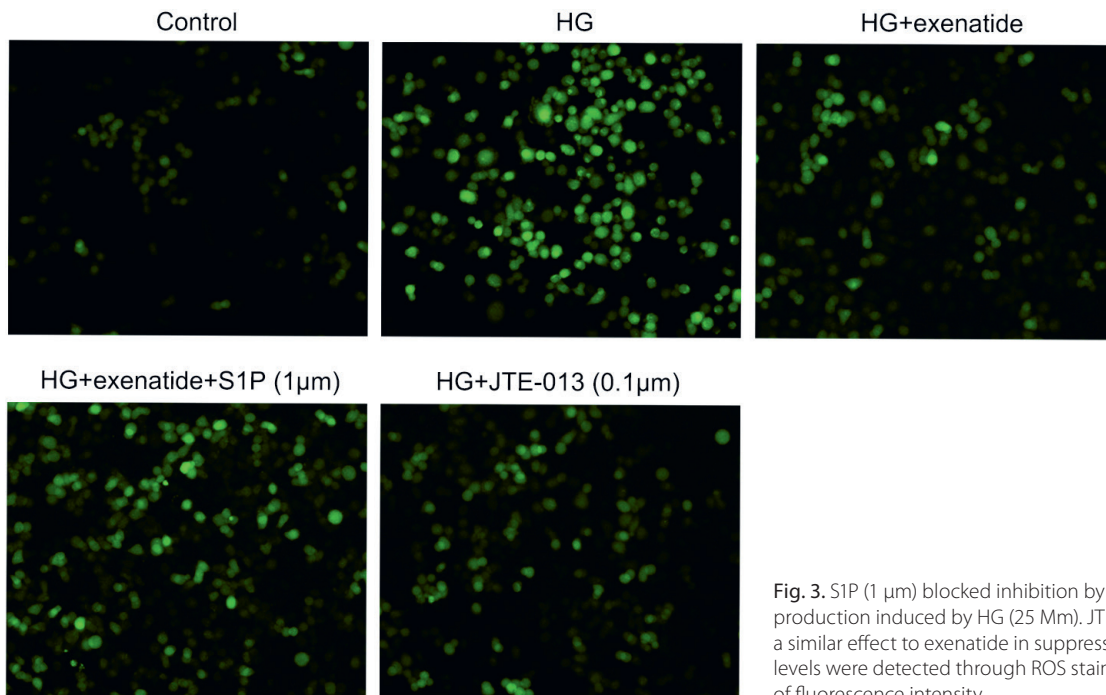
Fig. 3. S1P (1 μm) blocked inhibition by exenatide of ROS production induced by HG (25 Mm). JTE-013 (0.1 μm) presented a similar effect to exenatide in suppressing ROS. The ROS levels were detected through ROS staining and the analysis of fluorescence intensity

Exenatide lessened cell apoptosis triggered by HG through S1PR2

TUNEL staining was performed to assess cell apoptosis levels, which revealed a dramatic increase of cell apoptosis in hRVECs exposed to HG (Fig. 4A,B). Simultaneously, exenatide treatment reduced HG-induced cell apoptosis, which could be blocked by addition of S1P. The S1PR2 antagonist markedly decreased apoptosis in hRVECs compared with the HG group. These results indicated that exenatide protected hRVECs from apoptosis induced by HG through S1PR2. Next, we explored how exenatide regulated cell apoptosis caused by HG. The expression of a panel of established apoptosis-related proteins was analyzed using western blot assay. As shown in Fig. 4C, exenatide induced an increase of Bcl2, as well as a reduction of Bax, cleaved caspase-3 and cleaved caspase-9.

Discussion

The present study provides evidence that exenatide protects cells against ROS injury, inflammatory damage and apoptosis, based on composite results obtained in HG-induced hRVECs. Our research also reveals the mechanisms underlying the protective effect of exenatide, whereby exenatide reduces S1PR2 expression. Our study identified the novel mechanism of action of exenatide, and the involvement of S1PR2 in HG-induced hRVEC injury. These provide the molecular basis for further investigation of exenatide functions and might show a potential new target for treating DR.

The effects of exenatide on HG-induced hRVECs was investigated through analyzing ROS, inflammatory markers and cell apoptosis in the present study. Our data shows that exenatide reduced the protein levels of inflammation-related markers IL-1β, TNF-α and IL-6, ROS levels and cell apoptosis. These observations were consistent with a previous study implicating exenatide in the regulation of inflammation, apoptosis and oxidative stress.[13] Reactive oxygen species production is a part of the defense mechanism of the body, with a maintained balance between production and elimination. However, under certain pathological conditions, the antioxidant defense ability of the body decreases, and thus its oxidation capabilities exceed its antioxidant capabilities. Oxidative stress is considered to play a key role in DR development, which could destroy the integrity of the cell membrane, promote cell apoptosis and cause microvascular damage.[14,15] In DR, hyperglycemia leads to abnormal production of ROS, which further contributes to local inflammation and cell apoptosis.[12] Furthermore, there is a vicious cycle of positive feedback involving ROS, inflammation and cell apoptosis that is closely correlated with the development of DR. The present study reveals that overproduction of ROS caused by HG induction was decreased by exenatide, and that this repression was counteracted by S1P, an agonist of S1PR2. Moreover, JTE-013, an antagonist of S1PR2, also exhibited an inhibitory effect on ROS production. These observations show the involvement of S1PR2 in exenatide-decreased ROS levels.

The S1PR2 has been reported to regulate phosphorylation of Akt and endothelial nitric oxide synthase (eNOS),[5] and AKT can also activate eNOS in endothelial cells,[16] suggesting S1PR2 could regulate Akt-eNOS, as 1 study
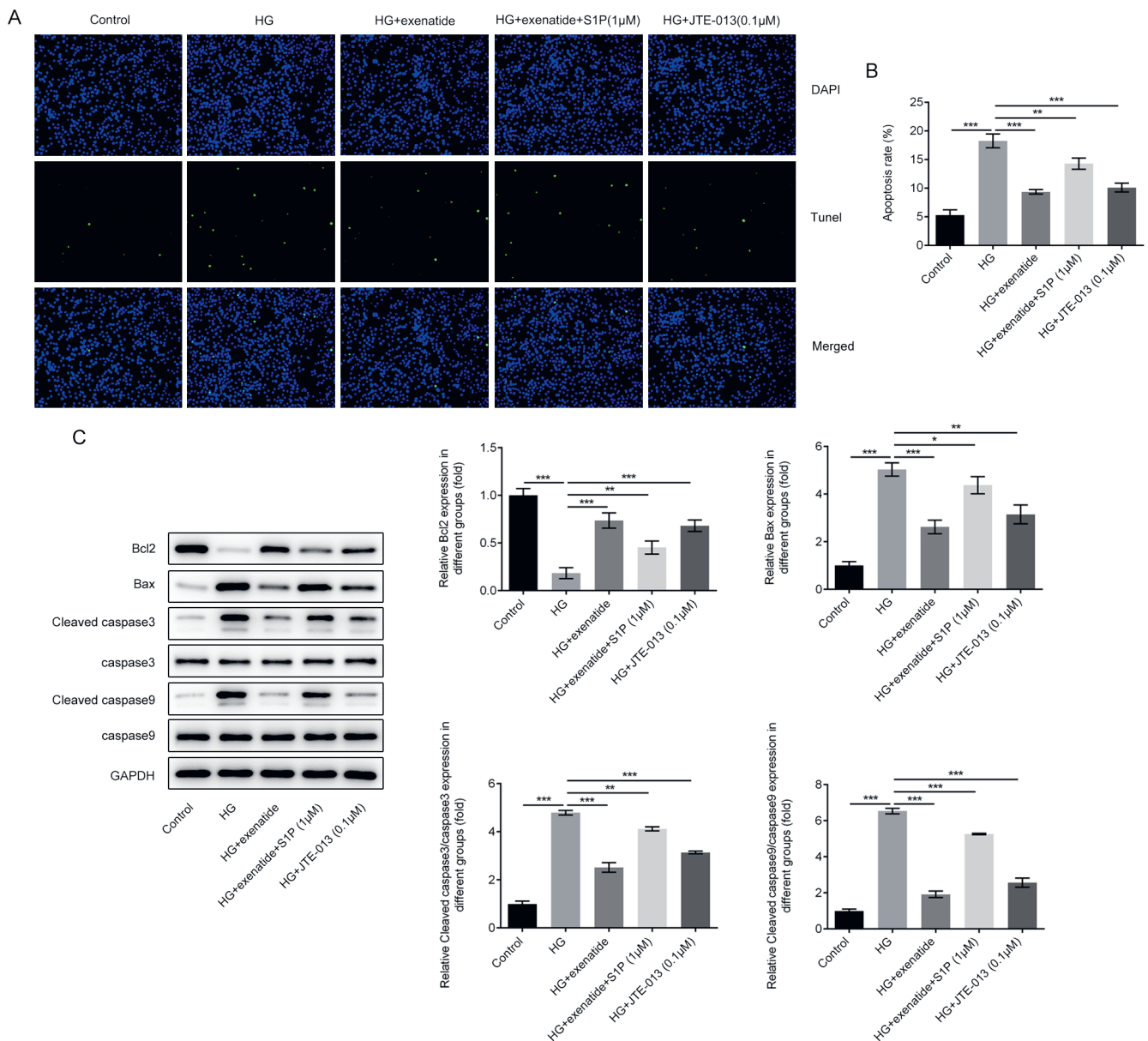
Fig. 4. A and B. TUNEL staining was utilized to analyze cell apoptosis levels; C. Changes in apoptosis-related protein levels (Bcl-2, Bax, cleaved caspase-3, caspase-3, cleaved caspase-9, and caspase-9) after different treatments was visualized using western blot analysis. The results are shown as mean ±SD percentage of the control level based on 3 independent tests

*p < 0.05; **p < 0.01; ***p < 0.001.

has indicated.[5] The modulation of AKT signals is involved in the regulation of ROS and apoptosis in retinal endothelial cells under HG exposure.[17] Therefore, the effect of exenatide reducing S1PR2 expression, and in turn inhibiting ROS, inflammatory makers and cell apoptosis, might be mediated by the involvement of AKT signals, which requires further study.

A previous study demonstrated protective roles of GLP-1 receptor agonists in preventing retinal neurodegeneration, including neural apoptosis.[18] The GLP-1 receptor agonists reduce Bax expression and upregulate caspase-8 levels, while also increasing BCLxl levels.[18] In addition, exenatide has been reported to protect retinal ganglion cells from HG-induced injury.[19] Our study demonstrates that

exenatide can also regulate Bcl2, Bax, cleaved caspase-3, and cleaved caspase-9 levels in hRVECs, which could be blocked by S1P. Similar results were also observed in HG-treated hRVECs after JTE-013 treatment. Therefore, we conclude that exenatide reduced HG-activated apoptosis in hRVECs through suppression of S1PR2 production. The pro-apoptotic role of S1PR2 has been investigated in several studies.[20–22]

Limitations

The study of the regulatory role of S1PR2 was limited to in vitro hRVECs model of DR; in vivo models of DR still require further study.

Conclusions

Presently, the main strategy for DR treatment is to protect retinal microvasculature from injury resulting from diabetes. Our study implies a possible mechanism for exenatide and presents a S1PR2 as a novel molecular target for delaying DR progression.

ORCID iDs

Yunyun Yang https://orcid.org/0000-0001-5593-0086
Qingyi Zhao https://orcid.org/0000-0002-2303-6546

References

1. Yamagishi S, Fukami K, Matsui T. Crosstalk between advanced glycation end products (AGEs)-receptor RAGE axis and dipeptidyl peptidase-4-incretin system in diabetic vascular complications. *Cardiovasc Diabetol*. 2015;14:2, doi:10.1186/s12933-015-0176-5

2. Kahn SE, Haffner SM, Hesse MA, et al. Glycemic durability of rosiglitazone, metformin, or glyburide monotherapy. *N Eng J Med*. 2006; 355(23):2427–2443. doi:10.1056/NEJMoa066224

3. Huang S, Ma S, Ning M, et al. TGR5 agonist ameliorates insulin resistance in the skeletal muscles and improves glucose homeostasis in diabetic mice. *Metabolism*. 2019;99:45–56. doi:10.1016/j.metabol. 2019.07.00

4. Yang Z, Xiong F, Wang Y, et al. TGR5 activation suppressed S1P/S1P2 signaling and resisted high glucose-induced fibrosis in glomerular mesangial cells. *Pharmacol Res*. 2016;111:226–236. doi:10.1016/j. phrs.2016.05.035

5. Cui H, Okamoto Y, Yoshioka K, et al. Sphingosine-1-phosphate receptor 2 protects against anaphylactic shock through suppression of endothelial nitric oxide synthase in mice. *J Allergy Clin Immunol*. 2013; 132(5):1205–1214.e1209. doi:10.1016/j.jaci.2013.07.026.

6. Obinata H, Hla T. Sphingosine 1-phosphate in coagulation and inflammation. *Semin Immunopathol*. 2011;34(1):73–91. doi:10.1007/ s00281-011-0287-3

7. Japtok L, Schmitz EI, Fayyaz S, Krämer S, Hsu LJ , Kleuser B. Sphingosine 1-phosphate counteracts insulin signaling in pancreatic β-cells via the sphingosine 1-phosphate receptor subtype 2. *FASEB J*. 2015; 29(8): 3357–3369. doi:10.1096/fj.14-263194

8. Imasawa T, Koike K, Ishii I, Chun J, Yatomi Y. Blockade of sphingosine 1-phosphate receptor 2 signaling attenuates streptozotocin-induced apoptosis of pancreatic beta-cells. *Biochem Biophys Res Commun*. 2010;392(2):207–211. doi:10.1016/j.bbrc.2010.01.016

9. Wang W, Lo ACY. Diabetic retinopathy: Pathophysiology and treatments. *Int J Mol Sci*. 2018;19(6):1816. doi:10.3390/ijms19061816

10. Madsen-Bouterse SA, Kowluru RA. Oxidative stress and diabetic retinopathy: Pathophysiological mechanisms and treatment perspectives. *Rev Endocr Metab Disord*. 2008;9(4):315–327. doi:10.1007/s11154-008-9090-4

11. Osborne NN, Casson RJ, Wood JPM, et al. Retinal ischemia: Mechanisms of damage and potential therapeutic strategies. *Prog Retin Eye Res*. 004;23(1):91–147. doi:10.1016/j.preteyeres.2003.12.001

12. Wu MY, Yiang GT, Lai TT, Li CJ. The oxidative stress and mitochondrial dysfunction during the pathogenesis of diabetic retinopathy. *Oxid Med Cell Longev*. 2018;2018:3420187. doi:10.1155/2018/3420187

13. Fang J, Tang Y, Cheng X, et al. Exenatide alleviates adriamycin-induced heart dysfunction in mice: Modulation of oxidative stress, apoptosis and inflammation. *Chem Biol Iinteract*. 2019;304:186–193. doi:10.1016/j.cbi.2019.03.012

14. Madsen-Bouterse SA, Zhong Q, Mohammad G, Ho YS, Kowluru RA. Oxidative damage of mitochondrial DNA in diabetes and its protection by manganese superoxide dismutase. *Free Radical Res*. 2010;44(3): 313–321. doi:10.3109/10715760903494168

15. Bonnefont-Rousselot D. Glucose and reactive oxygen species. *Curr Opin Clin Nutr Metab Care*. 2002;5(5):561–568. doi:10.1097/00075197-200209000-00016

16. Huang W, Yan Z, Li D, Ma Y, Zhou J, Sui Z. Antioxidant and anti-inflammatory effects of blueberry anthocyanins on high glucose-induced human retinal capillary endothelial cells. *OxidMed Cell Longev*. 2018; 2018:1862462. doi:10.1155/2018/1862462

17. Xie W, Zhou P, Qu M, et al. Ginsenoside Re attenuates high glucose-induced RF/6A injury via regulating PI3K/AKT inhibited HIF-1α/VEGF signaling pathway. *Front Pharmacol*. 2020;11:695. doi:10.3389/fphar. 2020.00695

18. Hernández C, Bogdanov P, Corraliza L, et al. Topical administration of GLP-1 receptor agonists prevents retinal neurodegeneration in experimental diabetes. *Diabetes*. 2016;65(1):172–187. doi:10.2337/ db15-0443

19. Hao M, Kuang HY, Fu Z, Gao XY, Liu Y, Deng W. Exenatide prevents high-glucose-induced damage of retinal ganglion cells through a mitochondrial mechanism. *Neurochem Int*. 2012;61(1):1–6. doi:10. 1016/j.neuint.2012.04.009

20. Webster CR, Anwer MS. Hydrophobic bile acid apoptosis is regulated by sphingosine-1-phosphate receptor 2 in rat hepatocytes and human hepatocellular carcinoma cells. *Am J Physiol Gastrointest Liver Physiol*. 2016;310(10):G865–G873. doi:10.1152/ajpgi.00253.2015

21. Hendley AM, Wang YJ, Polireddy K, et al. p120 catenin suppresses basal epithelial cell extrusion in invasive pancreatic neoplasia. *Cancer Res*. 2016;76(11):3351–3363. doi:10.1158/0008-5472.can-15-2268

22. Liu K, Cui K, Feng H, et al. JTE-013 supplementation improves erectile dysfunction in rats with streptozotocin-induced type I diabetes through the inhibition of the rho-kinase pathway, fibrosis, and apoptosis. *Andrology*. 2020;8(2):497–508. doi:10.1111/andr.12716

Intestinal amyloidosis:
Clinical manifestations and diagnostic challenge

Renata Talar-Wojnarowska[1,A–D,F], Krzysztof Jamroziak[2,A,D–F]

[1] Department of Digestive Tract Diseases, Medical University of Lodz, Poland
[2] Department of Hematology, Transplantation and Internal Medicine, University Clinical Center of the Medical University of Warsaw, Poland

A – research concept and design; B – collection and/or assembly of data; C – data analysis and interpretation;
D – writing the article; E – critical revision of the article; F – final approval of the article

Address for correspondence
Renata Talar-Wojnarowska
E-mail: r-wojnarowska@wp.pl

Abstract

Amyloidosis is a heterogeneous group of diseases in which the extracellular deposition of abnormal fibrillar proteins disrupts tissue structure and function. Intestinal involvement is a very rare manifestation of amyloidosis compared to the most affected organs, the heart and kidneys. Damage of the gastrointestinal tract may be the only manifestation of amyloidosis, or – more often – is a component of the involvement of several organs in systemic amyloidosis. Any part of the digestive tract can be involved; however, the small bowel is the most affected part, followed by the colon. Intestinal amyloidosis is characterized by a heterogeneous clinical picture, with weight loss, chronic diarrhea, abdominal pain, intestinal bleeding, or pseudo-obstruction. Endoscopic findings are characterized by a fine granular appearance, erosions, ulcerations, mucosal friability, multiple protrusions, or tumor-like lesions. Pathologic examination allows for a definitive diagnosis using Congo red staining and a positive sample with apple-green birefringence. The disease can easily be misdiagnosed with several other diseases of the digestive tract and lead to diagnostic challenges in clinical practice. Further, the amyloid colonic deposition may mimic inflammatory bowel disease, malignancy, ischemic colitis, and collagenous colitis. Therefore, gastroenterologists need to include amyloidosis in their diagnostic work-up.

Key words: differential diagnosis, symptoms, intestinal amyloidosis

Introduction

Amyloidosis is a heterogeneous group of diseases, characterized by the extracellular deposition of different abnormal fibrillar proteins, which disrupt tissue structure and function. Amyloidosis can either be acquired or hereditary, systemic or localized. The most affected organs include the kidneys, heart, nervous system, or gastrointestinal tract. The current recommended terminology of amyloidosis, represented in the classification of the International Society of Amyloidosis, is based on the structure of the chemical precursors of the amyloid fibril deposits.[1] While many proteins have the potential to form amyloid fibrils, the most frequent is the immunoglobulin light chain (AL amyloidosis), transthyretin amyloidosis (ATTR), serum amyloid A (AA amyloidosis), and Aβ2 amyloid (hemodialysis – associated amyloidosis).[2–4]

The AL amyloidosis is a malignant condition in which monoclonal immunoglobulin light chains, lambda or less commonly kappa, are produced by a relatively small population of plasma cell clones in the bone marrow. These monoclonal immunoglobulin light chains are deposited extracellularly in the form of misfolded, insoluble protein-complexes known as amyloid.[2] The AL amyloidosis is the most common type of amyloidosis, with an estimated annual incidence of 10–12 cases per million people. The median age of the patients diagnosed with AL amyloidosis was 63 years.[5] The clinical presentation of AL amyloidosis depends on the type and number of organs affected. The heart and the kidneys are affected most, followed by the autonomic nervous system, liver and gastrointestinal tract. The plasma cell clones in AL amyloidosis share phenotypic alterations with those observed in multiple myeloma clones.[2,5] Another type of amyloidosis, AA amyloidosis, is associated with infectious, neoplastic or inflammatory disorders, among which rheumatoid arthritis is one of the most commonly observed. The amyloidogenic fibrils are composed of serum amyloid A protein (SAA) which are hepatic acute phase reactants.[6] Transthyretin amyloidosis (ATTR), a less common type of amyloidosis, is a hereditary disease caused by a transthyretin gene mutation or is acquired as an amyloid disease in the elderly.[7]

Gastrointestinal tract-specific damage may be the only manifestation of the disease, or – more often – is a component of the involvement of several organs in systemic amyloidosis. The digestive tract is affected in 3–28% of diagnosed patients, apart from cardiac, renal or neurological injuries.[8–10] Most types of amyloidosis may be manifested with intestinal involvement without any specific endoscopic characteristics. According to published data, AL amyloidosis is the most diagnosed form of amyloidosis based on gastrointestinal biopsies (52.8–83.3%), followed by AA (1.5–16.2%) and ATTR amyloidosis (4.2–12.5%).[9,11,12]

Intestinal amyloidosis can be easily misdiagnosed and confused with several other digestive tract diseases, and can introduce diagnostic challenges in clinical practice.

The deposition of amyloid within the colon mimics other diseases, such as inflammatory bowel disease (IBD), malignancy, ischemic colitis, or collagenous colitis.[9,10] The misdiagnosis rate of amyloidosis is high because its clinical manifestations are complex and lack specificity. These obstacles often result in a delay of diagnosis and a deleterious effect for patients. The clinical manifestations of intestinal amyloidosis may vary from asymptomatic to serious forms, including intestinal mass or spontaneous perforation. Patients typically present with weakness, fatigue and unintentional weight loss. Moreover, they suffer from abdominal pain, early satiety, nausea, vomiting, diarrhea, fecal incontinence, constipation, and gastrointestinal bleeding.[13,14] Therefore, it is important that both general practitioners (GPs) and gastroenterologists need to include amyloidosis in their diagnostic workup for disease confirmation and more effective treatment.

Objectives

This review aims to comprehensively discuss current amyloidosis literature to elucidate the clinical manifestations, diagnosis, as well as diagnostic challenges associated with intestinal amyloidosis.

Clinical manifestations

Diarrhea

Described in 11–46% of patients, chronic diarrhea is one of the most common symptoms of intestinal amyloidosis.[8,9,13,15] In patients with unexplained diarrhea, weight loss, malabsorption, or protein loss, amyloidosis must be considered. The clinical experience of patients is not characteristic but usually the diarrhea is prolonged (longer than 4 weeks), postprandial, and may be accompanied by fecal incontinence or malnutrition.[13,16] Some patients present with watery diarrhea, with no blood, mucus or pus. Less often, patients present with bloody diarrhea associated with fever and abdominal pain or cramping.[17–19] Recurrent diarrhea may be associated with muscle weakness, electrolyte disturbances, or peripheral paresthesia in the lower extremities.[16]

Differential diagnosis requires the exclusion of infectious and parasitic causes of diarrhea, including *Salmonella, Shigella, Campylobacter,* and toxin A for *Clostridium difficile* analysis. In digestive tract amyloidosis, fecal calprotectin may be indicative of mild intestinal inflammation.[20,21] Radiological examinations are non-specific; however, abdominal computed tomography (CT) scans may show edematous wall thickening of the small bowel and colon.[21] The results of ileocolonoscopy are non-specific, either with an accentuated vascular pattern along the colon, diffusely distributed petechial mucosal suggillations, or shallow erosions in the colon and terminal ileum.[12,16,22] In some patients,

the presence of diffuse ulcerations with necrotic and hemorrhagic materials in the colon were observed.[19] In all described cases, the deposition of amorphous hyaline material infiltrating the submucosa wall in the colon was verified using hematoxylin and eosin (H&E) staining. Additionally, Congo red staining allowed for the confirmation of amyloidosis by the detection of green birefringence on amyloid depositions in the lamina propria of the colonic mucosa.[16,18,19]

The mechanism behind the presentation of diarrhea in patients with amyloidosis is not fully understood. It is generally suggested that diarrhea arises due to motility disturbances of the gastrointestinal tract which are caused by autonomic neuropathy and intestinal inflammation.[13] Moreover, abnormal small intestinal motility facilitates the bacterial contamination of the small intestine. Bacterial contamination is a common underlying cause of diarrhea and should be routinely tested for. Further, if diarrhea is observed, treatment with antibiotics should be considered.[23] Moreover, the malabsorption of bile acid, commonly associated with abnormal motility, also contributes to worsened neuropathological symptoms.[24] The treatment of chronic diarrhea in patients with amyloidosis is non-specific and is mostly aimed at controlling the symptoms. In some cases, octreotide and steroids can be used in refractory diarrhea with protein-losing enteropathy.[25] Causal treatment for intestinal involvement is available only in some types of amyloidosis. For example, in AA amyloidosis, the treatment should be focused on the therapy of the underlying disease. For the most common type of amyloidosis, AL amyloidosis, its treatment is best accomplished through high-dose chemotherapy followed by autologous stem-cell transplantation in patients qualifying for such an intensive approach, and by conventional chemotherapy in the remainder of cases. Further, treatment must be implemented after the final confirmation of the diagnosis and should be carried out in a reference center by a multidisciplinary team consisting of a hematologist, cardiologist, nephrologist, neurologist, and gastroenterologist.

Malnutrition and unintentional weight loss

Large clinical studies assessing the manifestations of amyloidosis have reported unintentional weight loss to be the most reported symptom of this disease.[9,26,27] The nutritional disorder is prevalent among patients with intestinal amyloidosis and is undoubtedly underdiagnosed. It is hypothesized that malnutrition is associated with asthenia and lack of appetite. Typical laboratory results, including ferropenic anemia, folic acid, and vitamin B_{12} deficiency or hypoalbuminemia, have highlighted these factors as potentially significant contributors to malnutrition in amyloidosis.[28] Additionally, there is a significant correlation between malnutrition, poor quality of life, as well as a shorter survival time in patients with amyloidosis.[27]

The pathogenesis of weight loss is multifactorial. Furthermore, it may be observed in patients with amyloidosis even before the onset of any other symptoms.[13,29] Amyloid deposition probably contributes to weight loss through an increased metabolism due to enhanced inflammatory reactions and oxidative stress.[13] Moreover, in patients with intestinal amyloidosis, chronic diarrhea, malabsorption, nausea, and vomiting, or the feeling of early satiety could be contributing factors that negatively affect the patients' energy intake. In a study analyzing the clinical features of patients with AL amyloidosis, the symptoms associated with weight loss were reduced appetite (43%), altered taste of food (27%), early satiety (25%), or fatigue (21%).[27] Such data infers that amyloidosis should always be considered as a possible cause of unintentional weight loss, especially in older patients. Lobo et al.[30] reported jejunal biopsy data which showed that, in patients over 65 years of age with suspicion of intestinal malabsorption, amyloidosis was one of the most diagnosed causes of malnutrition besides the villous atrophy, intestinal lymphangiectasia, unspecific jejunitis, and Whipple's disease.[30]

In AA amyloidosis, the management of weight loss in intestinal amyloidosis is focused on establishing an accurate, final diagnosis and the subsequent treatment of the underlying disease. Dietary advice must be considered early in the course of the disease and should include small-volume meals with low soluble fiber and fat content. Patients with weight loss, nausea or vomiting due to intestinal dysmotility can be treated with nutritional support, especially with fat-soluble vitamins, and medications such as prokinetics and antiemetics. For severe malabsorption, total parenteral nutrition may be useful if dysmotility-related symptoms are disabling, and the patient becomes malnourished.[31]

Intestinal bleeding

Intestinal amyloidosis may also manifest with upper or lower gastrointestinal hemorrhage. Patients may complain of coffee-ground emesis or melena as a sign of bleeding from the duodenum. Additionally, they may present with hematochezia, indicative by the passage of bright red blood primarily from the lower digestive tract.[32,33] Intestinal bleeding occurs as a symptom in 4–36% of patients with digestive tract amyloidosis and may be caused by erosions, ulcerations or generalized oozing without a particular source.[15,33–35] The initial diagnosis is made using endoscopic examination and is confirmed with biopsy and histopathologic analysis of amyloid deposits. Endoscopic features of amyloidosis also include punctate, erythematous lesions that appeared scalloped, ulcerated and hemorrhaged on contact.[12,36]

Several mechanisms have been reported by which amyloidosis can induce intestinal hemorrhage. One of the possible explanations is the association between AL amyloidosis and coagulation abnormalities, which can increase the risk of intestinal hemorrhage. Mumford et al. examined 337 patients with AL amyloidosis.[34] Their data indicated that the most common coagulation abnormalities were

prolongation of the thrombin time associated with hepatic amyloid infiltration, proteinuria and hypoalbuminemia, and followed by a prolongation of the prothrombin time.[34] Other well-defined mechanisms for amyloidosis hemorrhage involve localized intestinal ischemia, which occurs when all layers of the intestine and blood vessel walls are infiltrated. This may lead to diffuse mucosal oozing with necrosis and amyloid deposition in the vessel walls. Together, these factors induce fragility and subsequent hemorrhage.[36]

The diagnosis of amyloidosis is important after the initial bleeding has been controlled, as there are treatment options available that can have a significant impact on the disease course. The intestinal hemorrhage may stop spontaneously without intervention; however, the bleeding caused by amyloidosis tends to relapse and endoscopic or surgical procedures may be needed.[33,36]

Intestinal dysmotility and pseudo-obstruction

When the patient has no predisposing factors, physicians may not suspect intestinal amyloidosis as a cause of dysmotility and the pseudo-obstruction of the small or large intestine.[35,37] The delayed transit time in intestinal amyloidosis is similar to that seen in other systemic diseases, e.g., scleroderma. Patients usually present with chronic obstructive symptoms such as constipation and acute phases of pseudo-obstruction. Further, their symptoms may include severe colicky pain, an inability to pass feces and flatus, and progressive abdominal distension. In patients with intestinal amyloidosis, plain abdominal radiographs have shown a markedly diffuse dilatation of the small or large intestine with different air-fluid levels.[38] Clinical manifestations and radiological findings are very suggestive of acute mechanical obstruction that mimics the indication for surgical intervention. The final confirmation of amyloidosis may be achieved through the biopsy of the colon. It is reported that deposits of pink amorphous material stained with Congo red and displayed the typical apple-green birefringence are indicative of intestinal amyloidosis. Moreover, the recognition of intestinal amyloidosis in patients with unexplained etiologies of luminal obstruction is important to avoid laparotomy, which would be of no benefit.[39]

The reasons for intestinal dysmotility in amyloidosis patients are not fully understood. However, the malfunction of the autonomic and enteric nervous systems, including the depletion of intestinal neuroendocrine cells, seems to be of importance. The underlying mechanisms are myopathic and induce neuromuscular dysfunctions due to the deposition of amyloid within the smooth muscle of the intestine or infiltration of amyloid into the myenteric plexus which causes pressure-induced atrophy of the adjacent fibers.[37] The intestinal dysmotility in amyloidosis patients is likely a sequential process that starts with the deposition of amyloid in the vasculature, followed by the involvement of the muscular layers, and potentially affects the myenteric plexus. This final stage is accompanied by clinical symptoms of severe intestinal dysmotility.[40]

Perforation

Perforation is a very rare complication of intestinal amyloidosis; however, it may be the first sign of this disease and usually requires surgical intervention.[41,42] In such cases, patients suddenly develop severe pain with abdominal wall tenderness and peritoneal signs. An abdominal radiograph or CT may reveal extraluminal free air and stool around the perforated colon. An emergency exploratory laparotomy should be performed based on the preoperative diagnoses of intestine perforation and acute generalized peritonitis. In 1 patient, a perforation 4 cm in diameter that was accompanied by a surrounding hematoma and necrotic tissue at the mesenteric site of the sigmoid colon was visible.[43] In another patient, a section of the sigmoid colon having 26 cm in length and showing focal mucosal ulceration with perforation, and the surrounding serosal reaction was removed.[44] In all cases, histological examination revealed vascular wall thickening which stained positive with the Congo red stain, and vascular lumen stenosis with ischemic changes in the small intestine.[43,44]

The mechanism behind intestinal perforation is based on massive amyloid deposits which seem to induce vascular lumen stenosis and result in intestinal ischemic changes. In most cases, the submucosal blood vessels are the earliest and most frequent site of amyloid deposition. Amyloid fibrils gradually accumulate in both the vessels and intestinal wall, causing mucosal impairment as well as ischemic changes due to vascular involvement.[45] This can lead to blood vessel occlusion with resulting infarction or perforation.[43,44]

Amyloidomas

Tumor-like lesions (amyloidomas) are detected in 3.5% of patients with amyloidosis, not only in the digestive tract but also in the lungs, urinary bladder, prostate, epipharynx, and anterior mediastinum.[3] From a gastroenterological point of view, there may be single or multiple lesions, localized in all parts of the digestive tract; however, these lesions are observed most often in the small bowel and colon. Amyloidomas of the small bowel, without extraintestinal manifestations, are rare and are typically diagnosed after resection because of potential complications including stricture and hemorrhage, or the difficulty in discriminating malignant lesions.

Patients with colon amyloidomas complain of constipation, progressive abdominal distention and discomfort with dilatation of colonic segments shown in the abdominal X-ray. Some patients manifest recurrent bleeding

and the amyloid deposition in the vascular walls in areas adjacent to the tumor is visible under pathologic examination.[3,46]

Amyloidomas are characterized in colonoscopy as circumferential tumor-like lesions, which resemble colon cancer.[47] In all cases, a differential diagnosis with intestinal lymphoma, adenocarcinoma and gastrointestinal stromal tumors should be carefully assessed.[28] Multiple biopsies, not only from obviously abnormal lesions but also from normal-appearing intestinal mucosa, are recommended for the definitive confirmation of the diagnosis. In addition, the results of analysis of dysplastic gland proliferation and neoplastic infiltration in amyloidomas should be negative. Surgical treatment is often prescribed for undiagnosed amyloidomas; however, conservative strategies can also facilitate an improvement in tumor treatment. For example, in the clinical case reported by Ando et al., the tumor was completely diminished after one month of observed bowel rest.[47]

Although the mechanism underlying the development of such tumor-like lesions is unclear, the involvement of the amyloid deposits in the vascular wall appears to lead to ischemic changes which induce nodular elevations that resemble colon neoplasms. The extensive amyloid deposits affect the entire wall thickness, destroy the mucosa, and allow for the deep infiltration of amyloid into the muscularis propria, which induces luminal narrowing of the blood vessels.[48,49]

Diagnosis of intestinal amyloidosis

Without a known history of amyloidosis, the clinical diagnosis of intestinal involvement is very difficult. Endoscopic findings of intestinal amyloidosis are not specific and are characterized by fine granular appearance, erosions, ulcerations, mucosal friability, or multiple protrusions. Further, the type of symptoms does not predict endoscopic findings; however, the histopathological results partially correlate to the different types of amyloid fibril protein. The gold standard for diagnosing amyloidosis is a tissue biopsy of an affected organ which is then stained with Congo red stain. A positive sample demonstrates a green birefringence under polarized light. In patients with AA amyloidosis, amyloid deposits mainly in the lamina propria mucosae and perivascular walls in the submucosa of the gastrointestinal tract. Therefore, tissue with a fine granular appearance and mucosal friability may be observed endoscopically in some patients with AA amyloidosis. Conversely, in patients with AL amyloidosis, amyloid tends to massively deposit in the muscularis mucosa, submucosa and muscularis propria. Endoscopically, multiple polypoid protrusions and thickening of the folds are slightly more characteristic of AL amyloidosis.[12,50]

As systemic amyloidosis often affects the gastrointestinal tract from the early phase of illness, even without clinical symptoms, the digestive tract is the preferential site for biopsy with regard to procedural safety and sensitivity. Examinations of biopsies from the upper gastrointestinal tract revealed higher positive rates of a biopsy of the stomach and duodenum (91.3%) relative to those taken from the stomach only (62.1%). Additionally, the high sensitivity of the duodenum biopsies was consistent with the findings that the small intestine is mostly occupied during amyloidosis.[8] However, apart from the duodenum and distal part of the ileum, the small intestine is relatively difficult to access with endoscopic examinations. In some patients, push enteroscopy or capsule endoscopy are helpful to detect lesions that are limited to the jejunum. Endoscopic ultrasonography of these lesions may reveal the hypoechoic thickening of the mucous and the submucosal layers.[51] Barium enema or CT findings are non-specific and are characterized by regular thickening of the folds, jejunalization of the ileum and granular mucosal pattern In the case of colonic involvement, luminal narrowing and the loss of colonic haustrations are also characteristic of observations made using CT.[52]

The diagnosis of amyloidosis is based on histopathological findings; however, neither endoscopic imaging nor the Congo red staining is sufficient to distinguish the amyloidosis subtype. Amyloid typing is essential to make a correct diagnosis and initiate the appropriate treatment. Currently, the best methods to discern the amyloid type are immunohistochemistry, immunoelectron microscopy or mass spectrometry (the highest specificity and sensitivity, but available in very few health centers worldwide).[5,53] It is worth emphasizing that there are no specific biomarkers to diagnose or predict amyloidosis; however, N-terminal pro-brain natriuretic peptide (NT-proBNP) is increased during the early stages of cardiac involvement. Additionally, proteinuria may be the first symptom of renal amyloidosis.[5] In all patients, serum-free light chain (FLC) and serum and urine immunofixation electrophoresis should be performed. In any case of amyloidosis, the infiltration of other organs, especially the heart and kidneys, should be assessed using both laboratory and imaging methods. The prudent use of invasive tests is recommended and peripheral tissue biopsy with abdominal fat aspirate is preferred. The biopsy of involved organs, such as the kidneys or liver, is characterized by high sensitivity but also by a risk of complications, and should be performed only when other methods fail to confirm the diagnosis of amyloidosis.[2,5]

Diagnostic challenge

Intestinal amyloidosis can easily be misdiagnosed and confused with several other diseases of the digestive tract, especially with IBD. Jean et al. reported a clinical case of a family with hereditary lysozyme amyloidosis who had clinical manifestations limited to the gastrointestinal tract.[54] Three members of the family had the initial

diagnosis of IBD with a history of abdominal pain, diarrhea and rectal hemorrhage. Further, pancolitis was also observed using colonoscopy. Finally, in addition to inflammatory lesions, amyloid deposits were detected in rectocolic biopsies as well as biopsies taken from the stomach and duodenum. One patient presented with ileal ulcers, as confirmed with lower endoscopy, which suggested the diagnosis of IBD; however, colon biopsies revealed amyloid deposits without inflammatory infiltration.[54] Additionally, the same patients had non-specific IBD symptoms and partially responded to standard treatment of inflammatory colitis. In other reported cases, amyloidosis was only considered when a patient with an initial diagnosis of IBD presented with heart failure and restrictive cardiomyopathy.[55] Some patients may also have symptoms of systemic amyloidosis, such as macroglossia or proteinuria, which are characteristic of kidney involvement. These observations can lead to the final diagnosis of amyloidosis.[8,15] However, it is much more difficult to recognize the disease with the isolated involvement of 1 organ. Together, these data indicate that a high degree of clinical suspicion is needed to make an early diagnosis of amyloidosis in patients with non-specific symptoms.

The prevalence of secondary amyloidosis among IBD patients is 0.53–2.0%; however, epidemiological data suggest that secondary amyloidosis may be under-diagnosed. IBD patients with AA amyloidosis are significantly associated with proteinuria and cardiac comorbidities, including cardiomyopathy, heart failure, or atrial fibrillation.[56,57] Therefore, these patients should be routinely screened for kidney and heart diseases. Physicians and gastroenterologists involved in the treatment of IBD patients should be aware of these complications and be vigilant in identifying the early signs and symptoms of amyloidosis. The phenotype most frequently associated with amyloidosis is males with aggressive and extensive Crohn's disease (CD), fistulizing behavior and perianal disease; or with the development of proteinuria and renal failure.[58] The incidence of amyloidosis is significantly higher in patients with small and large bowel involvement and with a long duration of the disease with a cumulative incidence of 1.0% at 10 years and 5.7% at 20 years after CD onset.[57]

It is known that the clinical and endoscopic imaging of amyloidosis may be very similar to other intestinal diseases and that a final diagnosis is possible only after pathologic examination. Recently, a 61-year-old patient with Behçet disease (BD) and massive hematochezia was described.[58] In that case, the colonoscopy showed multiple, small, round-shaped ulcers extending from the ascending to the transverse colon. A biopsy revealed amorphous eosinophilic extracellular deposits in the vascular wall. The deposits stained positive on Congo red staining and showed apple-green birefringence under polarized light. Moreover, immunohistochemistry revealed that the deposits were positive for the lambda light chain. These lines of evidence led to an additional diagnosis

of AL amyloidosis. In this case, the endoscopic images differed from those typically observed in BD in which multi-segmented and diffuse colonic involvement is rare as the images portrayed a visual combination of the endoscopic features of BD disease and intestinal AL amyloidosis.[58,59]

Conclusions

In conclusion, since the clinical presentation of intestinal amyloidosis is frequently non-specific, establishing an accurate diagnosis requires careful endoscopic, radiologic and histopathological evaluation. Gastroenterologists must become confident with imaging findings of intestinal amyloidosis to make a correct differential diagnosis. These competencies will facilitate both proper diagnostic and therapeutic management. Intestinal amyloidosis may present with more varieties of clinical symptoms than previously thought. The final diagnosis requires a confirmation based on biopsy with histopathological confirmation and subtype assessment. The use of endoscopy with pathological examinations should be actively considered as early as possible, as the several types of amyloidosis are currently treatable, and the best results can be achieved in the initial phase of the disease. To conclude, amyloidosis is a rare, complex disease, and its proper diagnosis requires the cooperation of physicians of many different disciplines.

ORCID iDs

Renata Talar-Wojnarowska   https://orcid.org/0000-0003-3887-2712
Krzysztof Jamroziak   https://orcid.org/0000-0001-7207-8534

References

1. Sipe JD, Benson MD, Buxbaum JN, et al. Amyloid fibril proteins and amyloidosis: Chemical identification and clinical classification. International Society of Amyloidosis 2016 Nomenclature Guidelines. *Amyloid*. 2016;23(4):209–213. doi:10.1080/13506129.2016.1257986
2. Wechalekar AD, Gillmore JD, Hawkins PN. Systemic amyloidosis. *Lancet*. 2016;387(10038):2641–2654. doi:10.1016/S0140-6736(15)01274-X
3. Matsuda M, Katoh N, Ikeda S. Clinical manifestations at diagnosis in Japanese patients with systemic AL amyloidosis: A retrospective study of 202 cases with a special attention to uncommon symptoms. *Intern Med*. 2014;53(5):403–412. doi:10.2169/internalmedicine.53.0898
4. Merlini G, Bellotti V. Molecular mechanisms of amyloidosis. *N Engl J Med*. 2003;349(6):583–596. doi:10.1056/NEJMra023144
5. Fotiou D, Dimopoulos MA, Kastritis E. Systemic AL amyloidosis: Current approaches to diagnosis and management. *Hemasphere*. 2020;10; 4(4):e454. doi:10.1097/HS9.0000000000000454
6. Wiland P, Wojtala R, Goodacre J, Szechinski J. The prevalence of subclinical amyloidosis in Polish patients with rheumatoid arthritis. *Clin Rheumatol*. 2004;23(3):193–198. doi:10.1007/s10067-003-0842-y
7. Sekijima Y. Transthyretin (ATTR) amyloidosis: Clinical spectrum, molecular pathogenesis and disease-modifying treatments. *J Neurol Neurosurg Psychiatry*. 2015;86(9):1036–1043. doi:10.1136/jnnp-2014-308724
8. Okuda Y, Yamada T, Ueda M, Ando Y. First nationwide survey of 199 patients with amyloid A amyloidosis in Japan. *Intern Med*. 2018;57(23): 3351–3355. doi:10.2169/internalmedicine.1099-18
9. Lim AY, Lee JH, Jung KS, et al. Clinical features and outcomes of systemic amyloidosis with gastrointestinal involvement: A single-center experience. *Korean J Intern Med*. 2015;30(4):496–505. doi:10.3904/kjim.2015.30.4.496

10. Yen T, Chen FW, Witteles RM, Liedtke M, Nguyen LA. Clinical implications of gastrointestinal symptoms in systemic amyloidosis. *Neurogastroenterol Motil*. 2018;30(4):e13229. doi:10.1111/nmo.13229

11. Freudenthaler S, Hegenbart U, Schönland S, Behrens HM, Krüger S, Röcken C. Amyloid in biopsies of the gastrointestinal tract: A retrospective observational study on 542 patients. *Virchows Arch*. 2016; 468(5):569–577. doi:10.1007/s00428-016-1916-y

12. Hokama A, Kishimoto K, Nakamoto M, et al. Endoscopic and histopathological features of gastrointestinal amyloidosis. *World J Gastrointest Endosc*. 2011;3(8):157–161. doi:10.4253/wjge.v3.i8.157

13. Nakov R, Sarafov S, Nakov V, et al. Gastrointestinal manifestations in hereditary transthyretin amyloidosis associated with Glu89Gln mutation. *J Gastrointestin Liver Dis*. 2019;28(4):421–426. doi:10.15403/jgld-362

14. James DG, Zuckerman GR, Sayuk GS, Wang HL, Prakash C. Clinical recognition of AL type amyloidosis of the luminal gastrointestinal tract. *Clin Gastroenterol Hepatol*. 2007;5(5):582–588. doi:10.1016/j.cgh.2007.02.038

15. Shimazaki C, Hata H, Iida S, et al. Nationwide survey of 741 patients with systemic amyloid light-chain amyloidosis in Japan. *Intern Med*. 2018;57(2):181–187. doi:10.2169/internalmedicine.9206-17

16. Asakura K, Yanai S, Nakamura S, et al. Endoscopic findings of small-bowel lesions in familial amyloid polyneuropathy: A case report. *Medicine (Baltimore)*. 2016;95(11):e2896. doi:10.1097/MD.0000000000002896

17. Zhang J, Shao C, Zhu J, Tu C, Lv X. Abdominal distension and diarrhea as the main symptoms of primary amyloidosis: A case report and literature review. *Exp Ther Med*. 2016;11(5):1809–1811. doi:10.3892/etm.2016.3093

18. Meira T, Sousa R, Cordeiro A, Ilgenfritz R, Borralho P. Intestinal amyloidosis in common variable immunodeficiency and rheumatoid arthritis. *Case Rep Gastrointest Med*. 2015;2015:405695. doi:10.1155/2015/405695

19. Kim SH, Kim JH, Gu MJ. Secondary intestinal amyloidosis presenting intractable hematochezia: A case report and literature review. *Int J Clin Exp Pathol*. 2014;15;7(4):1805–1808. PMID:24817984

20. Nakov R, Sarafov S, Nakov V, et al. Transthyretin amyloidosis with gastrointestinal manifestation: A case report. *J Gastrointestin Liver Dis*. 2019;28(3):359–361. doi:10.15403/JGLD-422

21. Kim YJ, Kim HS, Park SY, et al. Intestinal amyloidosis with intractable diarrhea and intestinal pseudo-obstruction. *Korean J Gastroenterol*. 2012;60(3):172–176. doi:10.4166/kjg.2012.60.3.172

22. Azzam A, Balasubramaniam R, Safa S, McIvor C, Mollee P. Malabsorption secondary to gout-induced amyloidosis. *ACG Case Rep J*. 2017;4:e32. doi:10.14309/crj.2017.32

23. Obici L, Suhr OB. Diagnosis and treatment of gastrointestinal dysfunction in hereditary TTR amyloidosis. *Clin Auton Res*. 2019;29(Suppl 1): 55–63. doi:10.1007/s10286-019-00628-6

24. Wixner J, Suhr OB, Anan I. Management of gastrointestinal complications in hereditary transthyretin amyloidosis: A single center experience over 40 years. *Expert Rev Gastroenterol Hepatol*. 2018;12(1):73–81. doi:10.1080/17474124.2018.1397511

25. Shin JK, Jung YH, Bae MN, et al. Successful treatment of protein: Losing enteropathy due to AA amyloidosis with octreotide in a patient with rheumatoid arthritis. *Mod Rheumatol*. 2013;23(2):406–411. doi:10.1007/s10165-012-0675-0

26. Cowan AJ, Skinner M, Seldin DC, et al. Amyloidosis of the gastrointestinal tract: A 13-year, single-center, referral experience. *Haematologica*. 2013;98(1):141–146. doi:10.3324/haematol.2012.068155

27. Sattianayagam PT, Lane T, Fox Z, et al. A prospective study of nutritional status in immunoglobulin light chain amyloidosis. *Haematologica*. 2013;98(1):136–140. doi:10.3324/haematol.2012.070359

28. Mainenti PP, Segreto S, Mancini M, et al. Intestinal amyloidosis: Two cases with different patterns of clinical and imaging presentation. *World J Gastroenterol*. 2010;16(20):2566–2570. doi:10.3748/wjg.v16.i20.2566

29. Wixner J, Mundayat R, Karayal ON, Anan I, Karling P, Suhr OB; THAOS investigators. THAOS: Gastrointestinal manifestations of transthyretin amyloidosis – common complications of a rare disease. *Orphanet J Rare Dis*. 2014;9:61. doi:10.1186/1750-1172-9-61

30. Lobo B, Casellas F, de Torres I, Chicharro L, Malagelada JR. Usefulness of jejunal biopsy in the study of intestinal malabsorption in the elderly. *Rev Esp Enferm Dig*. 2004;96(4):259–264. doi:10.4321/s1130-01082004000400005

31. Park SW, Jee SR, Kim JH, et al. Duodenal amyloidosis secondary to ulcerative colitis. *Intest Res*. 2018;16(1):151–154. doi:10.5217/ir.2018.16.1.151

32. Shiratori Y, Fukuda K, Ikeya T, Takagi K, Nakamura K. Primary gastrointestinal amyloidosis with gastrointestinal hemorrhage and intestinal pseudo-obstruction: A report of a rare case. *Clin J Gastroenterol*. 2019;12(3):258–262. doi:10.1007/s12328-018-00929-9

33. Ali MF, Patel A, Muller S, Friedel D. Rare presentation of primary (AL) amyloidosis as gastrointestinal hemorrhage without systemic involvement. *World J Gastrointest Endosc*. 2014;6(4):144–147. doi:10.4253/wjge.v6.i4.144

34. Mumford AD, O'Donnell J, Gillmore JD, et al. Bleeding symptoms and coagulation abnormalities in 337 patients with AL amyloidosis. *Br J Haematol*. 2000;110(2):454–460. doi:10.1046/j.1365-2141.2000.02183.x

35. Leong RY, Nio K, Plumley L, Molmenti E, Klein JD. Systemic amyloidosis causing intestinal hemorrhage and pseudo-obstruction. *J Surg Case Rep*. 2014;2014(9):rju087. doi:10.1093/jscr/rju087

36. Spier BJ, Einstein M, Johnson EA, Zuricik AO 3rd, Hu JL, Pfau PR. Amyloidosis presenting as lower gastrointestinal hemorrhage. *WMJ*. 2008; 107(1):40–43. PMID:18416369

37. Tada S, Iida M, Yao T, Kitamoto T, Yao T, Fujishima M. Intestinal pseudo-obstruction in patients with amyloidosis: Clinicopathologic differences between chemical types of amyloid protein. *Gut*. 1993;34: 1412–1417. doi:10.1136/gut.34.10.1412

38. Georgiades CS, Neyman EG, Barish MA, Fishman EK. Amyloidosis: Review and CT manifestations. *Radiographics*. 2004;24(2):405–416. doi:10.1148/rg.242035114

39. Wetwittayakhlang P, Sripongpun P, Jandee S. Primary gastrointestinal amyloidosis: An unusual cause of acute intestinal pseudo-obstruction. *Case Rep Gastroenterol*. 2019;13(3):462–467. doi:10.1159/000503897

40. den Braber-Ymker M, Heijker S, Lammens M, Croockewit S, Nagtegaal ID. Intestinal involvement in amyloidosis is a sequential process. *Neurogastroenterol Motil*. 2018;30(12):e13469. doi:10.1111/nmo.13469

41. Ussia A, Vaccari S, Lauro A, et al. Colonic perforation as initial presentation of amyloid disease: Case report and literature review. *Dig Dis Sci*. 2020;65(2):391–398. doi:10.1007/s10620-019-05948-1

42. Shaulov A, Avivi I, Cohen Y, Duek A, Leiba M, Gatt ME. Gastrointestinal perforation in light chain amyloidosis in the era of novel agent therapy: A case series and review of the literature. *Amyloid*. 2018;25(1):11–17. doi:10.1080/13506129.2017.1416350

43. Harada K, Ichikawa D, Konishi H, et al. Perforation of the sigmoid colon and massive ischemia of the small intestine caused by amyloidosis associated with multiple myeloma: A case report. *Int Surg*. 2014;99(6):685–690. doi:10.9738/INTSURG-D-14-00058.1

44. Parks RW, O'Rourke D, Bharucha H, Wilson BG. Perforation of the sigmoid colon secondary to localised amyloidosis. *Ulster Med J*. 2002; 71(2):144–146. PMID:1251301

45. Madsen LG, Gimsing P, Schiødt FV. Primary (AL) amyloidosis with gastrointestinal involvement. *Scand J Gastroenterol*. 2009;44: 708–711. doi:10.1080/00365520902783717

46. Egeli T, Sokmen S, Akarsu M, Gurel D. Mechanical bowel obstruction due to localized extensive amyloidotic involvement in the left colon. *Indian J Surg*. 2015;77(Suppl 1):94–96. doi:10.1007/s12262-014-1175-6

47. Ando K, Fujiya M, Ito T, et al. Atypical tumour-like involvement of the colon in secondary systemic amyloidosis which vanished after 1 month of observation. *BMJ Case Rep*. 2011;2011:bcr0120113775. doi:10.1136/bcr.01.2011.3775

48. Peny MO, Dobengnie JC, Haot J, Van Gossum A. Localized amyloid tumor in small bowel. *Dig Dis Sci*. 2000;45(9):1850–1853. doi:10.1023/a:1005536901678

49. Saindane AM, Losada M, Macari M. Focal amyloidoma of the small bowel mimicking adenocarcinoma on CT. *AJR Am J Roentgenol*. 2005; 185(5):1187–1189. doi:10.2214/AJR.04.1134

50. Tada S, Iida M, Yao T, et al. Endoscopic features in amyloidosis of the small intestine: Clinical and morphologic differences between chemical types of amyloid protein. *Gastrointest Endosc*. 1994;40(1): 45–50. doi:10.1016/s0016-5107(94)70008-7

51. Choi JH, Ko BM, Kim C, et al. A case of localized amyloid light-chain amyloidosis in the small intestine. *Intest Res*. 2014;12(3):245–250. doi:10.5217/ir.2014.12.3.245

52. Özcan HN, Haliloğlu M, Sökmensüer C, Akata D, Özmen M, Karçaaltıncaba M. Imaging for abdominal involvement in amyloidosis. *Diagn Interv Radiol*. 2017;23(4):282–285. doi:10.5152/dir.2017.16484

53. Gertz M, Adams D, Ando Y, et al. Avoiding misdiagnosis: Expert consensus recommendations for the suspicion and diagnosis of transthyretin amyloidosis for the general practitioner. *BMC Fam Pract*. 2020;23;21(1):198. doi:10.1186/s12875-020-01252-4

54. Jean E, Ebbo M, Valleix S, et al. A new family with hereditary lysozyme amyloidosis with gastritis and inflammatory bowel disease as prevailing symptoms. *BMC Gastroenterol*. 2014;14:159. doi:10.1186/1471-230X-14-159

55. Rahman N, Toqeer M, Hawley I, et al. Primary systemic amyloidosis presenting as idiopathic inflammatory colitis. *BMJ Case Rep.* 2011; 2011:bcr0820114596. doi:10.1136/bcr.08.2011.4596

56. Tosca Cuquerella J, Bosca-Watts MM, Tejedor Alonso S, Mora De Miguel F, Minguez Perez M. Amyloidosis in inflammatory bowel disease: A systematic review of epidemiology, clinical features, and treatment. *J Crohns Colitis*. 2016;10(10):1245–1253. doi:10.1093/ecco-jcc/jjw080

57. Miyaoka M, Matsui T, Hisabe T, et al. Clinical and endoscopic features of amyloidosis secondary to Crohn's disease: Diagnostic value of duodenal observation and biopsy. *Dig Endosc*. 2011;23(2):157–165. doi:10.1111/j.1443-1661.2010.01069.x

58. Sato S, Yashiro M, Matsuoka N, et al. Behçet disease associated with gastrointestinal amyloidosis manifested as hematochezia: A case report. *Medicine (Baltimore)*. 2018;97(26):e11153. doi:10.1097/MD.0000 000000011153

59. Skef W, Hamilton MJ, Arayssi T. Gastrointestinal Behçet's disease: A review. *World J Gastroenterol*. 2015;21(13):3801–3812. doi:10.3748/ wjg.v21.i13.3801